論文 / 著書情報
Article / Book Information

題目(和文)	
Title(English)	Study on accurate flowrate measurement downstream of the double bent pipe using ultrasonic velocity profile method
著者(和文)	TreenusonWeeracho
Author(English)	Weerachon TREENUSON
出典(和文)	学位:博士(工学), 学位授与機関:東京工業大学, 報告番号:甲第9476号, 授与年月日:2014年3月26日, 学位の種別:課程博士, 審査員:木倉　宏成,齊藤　正樹,高橋　実,赤塚　洋,加藤　之貴
Citation(English)	Degree:Doctor (Engineering), Conferring organization: Tokyo Institute of Technology, Report number:甲第9476号, Conferred date:2014/3/26, Degree Type:Course doctor, Examiner:,,,,
学位種別(和文)	博士論文
Type(English)	Doctoral Thesis

STUDY ON ACCURATE FLOWRATE MEASUREMENT DOWNSTREAM OF THE DOUBLE BENT PIPE USING ULTRASONIC VELOCITY PROFILE METHOD

Doctoral Dissertation by

Weerachon TREENUSON

for the degree of

Doctor of Engineering

Tokyo Institute of Technology

March, 2014

CONTENTS

NOMENCLATURES

D	Inner pipe diameter
r	Radius position in a pipe
V_{TX}	Velocity component along ultrasound beam path
V_{axial}	Velocity component along streamwise direction
θ	Incidence or refraction angle of ultrasound
c_f	Sound speed in fluid
f_0	Frequency of ultrasound emitted from transducer
f_d	Doppler shift frequency
t_f	Traveling time of ultrasound pulse
L_f	Distance from transducer to particle
ϕ	Circumferential angle
α	Out-of-plane angle

LIST OF TABLES AND FIGURES

Chapter 1

Chapter 2

Chapter 3

Chapter 4

Chapter 5

Chapter 6

Fig. 6-30 FFT’s results of each Circumferential velocity profile at 5D of out of plane angle 16 degree double bent pipe.

CHAPTER 1

INTRODUCTION

1.1 BACKGROUND

World electricity generation rose at an average annual rate of 3.6% from 1971 to 2009, greater than the 2.1% growth in total primary energy supply. This increase was largely due to more electrical appliances, the development of electrical heating in several developed countries and of rural electrification programs in developing countries.

The share of electricity production from fossil fuels has gradually fallen, from just under 75% in 1971 to 67% in 2009. This decrease was due to a progressive move away from oil, which fell from 20.9% to 5.1%.

Oil for world electricity generation has been displaced in particular by dramatic growth in nuclear electricity generation, which rose from 2.1% in 1971 to 17.7% in 1996. However, the share of nuclear has been falling steadily since then and represented 13.4% in 2009. The share of coal remained stable, at 40-41% while that of natural gas increased from 13.3% to 21.4%. The share of hydro-electricity decreased from 22.9% to 16.2%. The share of new and renewable energies, such as solar, wind, geothermal, biofuels and waste increased. However, these energy forms remain of limited importance: in 2009, they accounted for only 3.3% of total electricity production for the world as a whole **[1-1]**. Therefore, the totally rising of electricity power influences energy supplier to increase power level to support this demand.

The maximum power level at which a commercial nuclear power plant may operate. This power level is used, with other data, in many of the licensing analyses that demonstrate the safety of the plant. This power level is included in the license and technical specifications for the plant. In the United States, Nuclear Regulatory Commission (NRC) controls any change to a license or technical specification, and the licensee may only change these documents after NRC approves the licensee's application for change. The process of increasing the maximum power level at which a commercial nuclear power plant may operate is called a power uprate **[1-1]**.

There are many factors present today that support the resurgence of nuclear power throughout the world. Such factors include the increasing reliance on global oil sources, the increasing price of oil and gas as fuel sources, and the need for generating power that is environmentally clean. In the United States, which has not seen a new nuclear power station begin commercial operation since

1993, the opportunity for new nuclear build has gained significant momentum. During the interim (1993 to present) you would have been surprised if you saw a newspaper headline that stated, "U.S. Builds Three 1362 MWe Nuclear Power Plants to Support Nation's Energy Needs." Although this never occurred, the U.S. Nuclear Regulatory Commission (US-NRC) has approved new generation via power uprate projects at existing nuclear power plants. In fact, power uprates have contributed over 4000 MWe of new generation in the U.S. since 1993, with another 2600 MWe expected by 2010. This is equivalent to five large nuclear power stations. Power uprates have also been successfully implemented in other parts of the world, primarily Europe, where the focus has been on plant modernization. Power uprates will never compete fully with the capacity of a new build, but they are an important component of an existing utility's strategy for a safe, clean and reliable energy future **[1-2]**.

Utilities have been using power uprates since the 1970s as a way to increase the power output of their nuclear plants. To increase the power output of a reactor, typically more highly enriched uranium fuel and/or more fresh fuel is used. This enables the reactor to produce more thermal energy and therefore more steam, driving a turbine generator to produce electricity. In order to accomplish this, components such as pipes, valves, pumps, heat exchangers, electrical transformers and generators, must be able to accommodate the conditions that would exist at the higher power level. For example, a higher power level usually involves higher steam and water flow through the systems used in converting the thermal power into electric power. These systems must be capable of accommodating the higher flows.

In some instances, licensees will modify and/or replace components in order to accommodate a higher power level. Depending on the desired increase in power level and original equipment design, this can involve major and costly modifications to the plant such as the replacement of main turbines. All of these factors must be analyzed by the licensee as part of a request for a power uprate, which is accomplished by amending the plant's operating license. The analyses must demonstrate that the proposed new configuration remains safe and that measures continue to be in place to protect the health and safety of the public. These analyses, which span many technical disciplines and may be complex, are reviewed by the NRC's technical and legal staffs and NRC management before a request for a power uprate is approved **[1-3]**.

1.2 TYPES OF POWER UPRATES

1.2.1 Measurement uncertainty recaptures (MUR) uprate.

A term applied to the regulatory process of reducing certain emergency core cooling system (ECCS) assumptions regarding reactor power measurement uncertainty from a standard assumption (typically 2–3%) to a specific value based on the use of more accurate feedwater flow measurement devices. The reduction in the uncertainty assumption can result in an increase in reactor licensed thermal power of 1.2–1.7% above currently licensed thermal power **[1-4]**.

- 34 American pressurized water reactors (PWRs), 5 European PWRs and 2 Asian PWRs **[1-5]**

1.2.2 Stretch power uprate (SPU).

A term describing an uprate that uses the original plant designs excess margin to accommodate an increase in reactor thermal power. Conceptually, such an uprate would not require significant plant modifications since it is ostensibly using existing design margin in the plant equipment. In the USA, the Nuclear Regulatory Commission (NRC) has defined a stretch power uprate as any uprate less than 7% of the originally licensed thermal power of the plant **[1-4]**.

- 42 American PWRs, 2 European PWRs and 4 Asian PWRs **[1-5]**

1.2.3 Extended power uprate (EPU).

EPUs represent the most challenging power uprate due to the wide range of design and licensing basis impacts and the need for plant modifications. However, the larger payback from an EPU in terms of MWe has resulted in 13 approvals in the U.S., adding over 1500 MWe of nuclear capacity since 1998 **[1-4]**. It requires significant modifications to major balance-of-plant (BOP) equipment (e.g., high-pressure turbines, condensate pumps and motors, main generators and/or transformers). The non-safety systems, structures and components (SCCs) of an NPP these are usually referred to as the power production side of the power plant **[1-5]**.

- 13 American PWRs and 10 European PWRs

1.3 MEASUREMENT UNCERTAINTY RECAPTURE POWER UPRATE OF FEEDWATER SYSTEM

Measurement uncertainty recapture power uprate applications request that the NRC amend the operating license for a plant to increase core thermal power by a value less than 2 percent of the licensed power level. Licensees typically achieve such uprates by implementing enhanced techniques for calculating reactor power. This involves the use of state-of-the-art devices that reduce the degree of uncertainty associated with measuring feedwater flow and, in turn, allow for more accurate power calculations.

The applications for power uprates that are based on improved feedwater measurement techniques should have a limited effect on plant analyses and equipment. When licensees submit applications for this type of power uprate, the staff intends to focus its review on the affected areas. (For purposes of this guidance, "affected areas" are those areas for which existing analyses of record do not bound plant operation at the proposed power level and, as a result, new analyses or evaluations should be performed to provide a basis for operation at the proposed power level. Similarly, "affected equipment" includes equipment for which existing analyses of record for capacities and/or design, actual design, and/or operational or licensing functional requirements should be modified to support operation at the proposed power level.)

The NRC staff has typically completed its review of measurement uncertainty recapture power uprate applications in 6 to 8 months. The duration of the staff's review strongly depends on the quality and completeness of licensees' applications and the staff's needs for additional information. The duration of staff reviews of quality applications for which the staff does not need additional information in order to complete its review could be reduced by 2 to 3 months. **These time estimates are for applications that reflect the use of approved flow measurement devices and do not include other requests or changes.** If a power uprate application includes other requests or changes, the staff will apply the agency's existing timeliness goals for completing its review of the application (i.e. completing reviews of 95 percent of licensing applications within 1 year and 100 percent within 2 years.) [1-4].

On August 23, 2001, the NRC held a public workshop to discuss the draft guidance. The staff evaluated feedback received during the workshop and modified the draft guidance based on this staff

evaluation. Attachment 2 to this RIS summarizes the staff's evaluation of the feedback. Attachment 2 is organized by guidance section. This organization was utilized to simplify the use (cross-referencing) of the guidance. Licensees may wish to use Attachments 1 and 2 together to ensure that they clearly understand the staff's intent in the guidance.

For further guidance on the level of detail necessary for the staff's review, licensees may refer to the corresponding sections in NUREG-0800, "Standard Review Plan for the Review of Safety Analysis Reports for Nuclear Power Plants," the NRC's Standard Review Plan (SRP). The reference to the SRP was not intended to indicate that the SRP will be used in place of plant-specific licensing bases to assess the acceptability of an application. The SRP is referenced here solely to provide guidance regarding an appropriate level of detail; it is not intended that licensees need to conform to the guidance in the SRP. Applicability of the SRP to a plant is determined on a plant-specific basis, consistent with the licensing basis of the plant. In addition, where the NRC has approved a specific methodology (e.g., topical report) for the type of measurement uncertainty recapture power uprate being requested, licensees should follow the format prescribed for that specific methodology and provide the information called for in that methodology and the NRC's letter and safety evaluation approving the methodology.

The staff will update the attached guidance as necessary to reflect lessons learned from staff reviews. The staff may use the NRC's Web site to post updates and other information related to power uprates. Licensees are encouraged to notify the staff of areas where they believe efficiencies may be gained (e.g., areas where generic dispositions are possible) [1-5].

Accurate flowrate measurement is very important for many industrial facilities. For example, accurate flowrate measurement can manage existing light water reactors (LWRs) of nuclear power plants. It is very important to increase the core thermal power of the plants to the highest or full capacity and efficiency. In addition, the accurate flowrate measurement in feed water systems is essential for the calculation of the core thermal power.

1.4 REVIEW OF PREVIOUS WORKS

1.4.1 Differential Pressure Flowmeter

Differential pressure flow measurement is old and reliable. With the aid of microprocessor technology now discharge coefficient calculations can be done in real time. Even more, properties of the fluid can be stored on the instrument and measuring temperature and absolute pressure allows to correct fluid parameters such as density and viscosity and then to obtain the mass flow rate. This are called multivariable mass flow meters. By other side years of research and experiments had been done obtaining better characterization of typical differential pressure devices (nozzles, orifice plate, etc.) as shown in **Fig. 1-1**

$$Q_M = p_1 \cdot v_1 = p_2 \cdot v_2 \qquad \textbf{(1-1)}$$

where Q_M is Mass flow rate along the pipe, units are e.g. Kg/second. A_2, A_1 are Up and down stream cross sectional area of the pipe.
Difference between the (static) pressures measured at the wall pressure tappings, one of which is on the upstream side and the other of which is on the downstream side of a primary device (or in the throat for a Venturi tube) inserted in a straight pipe through which flow occurs, when any difference in height between the up-stream and downstream tappings has been taken into account.

Differential pressure flow meters using such as orifice, venture and nozzle have been usually used because of their cost and usefulness. However, their measurement accuracy is influenced by changes in flow conditions which result from, for example, metal deposition, corrosion and surface wear inside the pipes. Maintenance and overhaul are necessary to cope with the aging **[1-1]**.

The other limitation of differential pressure flow meters is the requirement of the inlet length of upstream pipe which is long enough to form the stable flow as fully developed turbulent flow. However, the space for piping in real plants is very limited **[1-2]**. There are many bents in piping systems, and flow behavior in the complicated pipe system will become very complicated. It is difficult to measure accurate flowrate of the complicated flow. However, if the accurate flow rate can be measured at or close to the bent, the size of the pipe systems will be reduced.

1.4.2 Ultrasonic Flowmeter

In the late 1990's several developments spurred renewed interest in power uprates and resulted in an increased rate of plant projects to take advantage of the economic benefits of power uprates. **State-of-the-art ultrasonic feedwater flow measurement** devices were developed and installed at numerous nuclear power plants to provide a more accurate determination of reactor thermal power, which is important to safety analysis. Since reactor power uncertainty is often a dominant parameter in many safety analyses, the use of reduced uncertainties allows operation with increased operational margin to plant and fuel design limits and a small increase in the licensed thermal power. The first MUR uprate was approved by the US-NRC in 1999 and since then over 30 MUR uprates have been approved resulting in an additional 500 MWe of capacity **[1-2]**.

The performance of the velocity distribution in a pipe is changing the paradigm of flow metering. In the past, the process is based on a principle of Heron and said to be 2,000 years old **[1-3]**. Heron's principle states: "… it does not suffice to determine the section of flow, to know the quantity of water …. It is necessary to find the velocity of the current…". Namely, the volume flow rate was and still is estimated as an average flow velocity time cross-sectional area: $Q=Av$. A paradigm shift has occurred to use the first principle of flow rate as an integral of the total volume or mass flux passing a cross section of the pipe, which corresponds to the integral of velocy distribution over an area **[1-4] [1-5]**

K., Tezuka, M., Mori, T., Suzuki and Y., Takeda "Calibration tests of pulse-Doppler flow meter at national standard loops." Flow Measurement and Instrumentation 19 (2008) 181–187 Calibration tests of UdFlow, the ultrasonic pulse-Doppler flowmeter manufactured by the Tokyo Electric Power Company, were conducted at the national standard loop in Mexico, CENAM (The Centro National de Metrologia), in order to evaluate the accuracy of the flowmeter. Four ultrasonic transducers were mounted circumferentially on the surface of 100 and 200 mm stainless steel pipes to measure four velocity profiles. Flow rates can be obtained by integrating each measuring line and averaging them. Air was injected upstream of the measuring point to provide bubbles as ultrasonic reflectors. Tests were conducted at five different flow rates with Reynolds numbers from 200,000 to 1,200,000. Tests were repeated six times at each flow rate to evaluate repeatability. In addition, a take-off and put-back test was carried out on the 100 mm pipe at a flow rate of 3000 L/min to evaluate reproducibility. The values of the CENAM loop are based on the average of weighing time while

those of the ultrasonic-Doppler flow velocity-profile flowmeter are based on the time average of instantaneous values. The calibration tests found a deviation of less than 0.3% between the two devices in terms of the average of the values recorded in six rounds of measurement. Measurement at a different Reynolds number showed that the overall average deviation between the two devices was less than 0.3%.

Calibration tests of UDF were conducted at four national standard loops: NIST in the United States, NMIJ in Japan, NMI in the Netherlands, and CENAM in Mexico, to evaluate the accuracy of this new type of flow-metering system. The velocity profiles at NIST, NMIJ, and NMI showed deviations within ~0.5%. Following improvements to the UDF system, the maximum spreads in individual MF test results in the mean values from the UDF are from −0.17% to +0.14% for 100 mm diameter pipe and from −0.18% to +0.23% for 200 mm diameter pipe over the range of Reynolds numbers tested at CENAM. At CENAM the short-term stability (repeatability) and longer-term stability (reproducibility) are both considered good, i.e., better than 0.3% under these test conditions. Further testing will be needed to better quantify reproducibility characteristics. The expanded uncertainty for the UDF meter factor in these tests at CENAM is bounded by ±0.26% as a worst case for 100 mm pipe and by ±0.19% as a worst case for 200 mm pipe. These values are computed for 95% confidence levels with a coverage factor k of 2.57. The air bubble injection used for these tests had a negligible effect on the CENAM primary standard measurements.

A new flow metering system has been developed using the ultrasonic Doppler method that can be a solution to the limitations of the conventional flow meters **[1-6]**. The most famous type of Ultrasonic flowrate meter is the time of flight (TOF) type which is partly used, in nuclear power plants not only in US but also worldwide **[1-7]**. The ultrasonic TOF method uses a different time between the ultrasonic transmission and reception by the ultrasound transmitter and ultrasound receiver. The advantage of this method is the prolong running without any maintenance compared to orifice flowmeters and venture nozzles. It is because of the locating of transducers are set on the outer surface of the pipes.

However, this TOF type has some limitations about the calibration of the flowrate calculation. If the flow becomes complicated, many velocity profiles are needed to obtain accurate flowrate. For this reason, the ultrasonic velocity profile (UVP) method which is able to measure velocity profiles directly has been developed for accurate measurement. The only requirement for this UVP method is

that sufficient number of particles must be dispersed in the fluid as ultrasound reflectors **[1-8]**.

M. Mori et al. have confirmed about the accuracy of flowrate measurement for fully developed flow in a straight pipe using UVP method **[1-9]**. The results showed that the difference between the averaged values of ultrasonic Doppler method and NIST gravimetric measurement were about 0.18%. Y. Inoue et al. also applied this method to measure the flowrate of metallic pipe **[1-1]**.

Tezuka, K., Mori, M., Suzuki, T., Aritomi, M., Kikuru, H., & Takeda, Y., "Assessment of Effects of Pipe Surface Roughness and Pipe Elbows on the Accuracy of Meter Factors Using the Ultrasonic Pulse Doppler Method" Journal of NUCLEAR SCIENCE and TECHNOLOGY, Vol. 45, No. 4, p. 304–312 (2008). The velocity profile of the flow in a pipe and its influence on the profile factor used with conventional flow meters were investigated with ultrasonic pulse Doppler measurements. From the measured velocity profiles, the influences of surface roughness and Reynolds number were characterized qualitatively and quantitatively. As pipe surface roughness changes during plant operation, the velocity profile changes, producing a change in the profile factor. Variation in the Reynolds number also influences the change in the profile factor. Experiments were conducted at high temperature and pressure to evaluate the ultrasonic pulse Doppler method for measuring the flow of nuclear plant cooling water. Helium gas bubbles provided sufficiently persistent ultrasonic reflectors when injected into high-pressure water, permitting the velocity profile of the flow to be obtained under high-temperature and high-pressure conditions using this method.

The influences of surface roughness and Reynolds number were characterized qualitatively and quantitatively using an ultrasonic pulse-Doppler flowmeter. The flow velocity profiles measured in the present experiments were obviously affected by surface roughness. A larger inner surface roughness results in a steeper velocity profile, the trend of which corresponds to theoretical expectations. The correction factors used in time-of-flight ultrasonic flowmeters change by approximately 1.5% as the inner surface roughness changed in these experiments. This does not necessarily correspond to actual plant conditions, but it points to the possibility that the effect of pipe inner surface roughness in operating power plants, where wall roughness actually changes with time (as noted in the paper), should be taken into consideration to obtain flow rate measurements accurate to within a few percent. The results at high pressure indicate the possibility that a pulse Doppler system can be used to measure the velocity profile under the high-temperature and high-pressure conditions of nuclear feed water.

However, turbulent flow will quickly appear if pipe is bent or there is other equipment on the pipe, i.e. strainers, valves and so on. Promoted turbulence can cause swirling effect within the pipe **[1-10]**. The effect can rapidly distort velocity profiles, degrading the flow meter's accuracy and reliability. This is the reason why flow meters require long and straight pipes for upstream and downstream to be installed **[1-11]**.

To solve this difficulty, UVP has some advantages compared with conventional flow measurement techniques. It can measure and obtain the instantaneous velocity profile from outside of pipe changing its measurement line. It allows to make two-dimensional flow velocity map and to calculate accurate flowrate from the map. However, UVP measurement can measure only velocity profiles in line and multiple measurement lines are necessary to make two-dimensional velocity map. S. Wada et al. studied about the flowrate measurement after a single bent pipe of upward flow where just below a bend and sudden expansion pipe employing three measurement lines. They reported that the errors were less than 1% **[1-12]**. R. Kotze et al. studied about the flowrate measurement using UVP measurement with multiple measurement lines for the accurate flowrate measurement in the complex flow such as in the valve **[1-13]**. However, the errors in the case were quite high as more than 10% because of insufficient of the number of measurement lines. Nevertheless, the complex bent pipe systems are usually used in general plants. Therefore, UVP should be applied to measure the accurate flowrate of complicated flow near the bent pipe.

Takeda, Y., "Development of an ultrasound velocity profile monitor", Nuclear Engineering and Design 126, 277-284 (1991). An ultrasound velocity profile (UVP) monitor has been developed. It utilities a pulsed echographic ultrasound technique and can instantaneously measure a velocity profile along one line in a vector form. The principle and characteristics of the method and the developed systems are described. The results of confirmation experiments have proved that the method measures the velocity profile to high accuracy (5% for velocity and 1% for position). Applications in various configurations demonstrate its efficiency for obtaining spatial information about flow structures as well as its effectiveness in measuring flow in liquid metals.

An ultrasound velocity profile monitor has been developed, which can instantaneously measure a velocity profile along one line in a vector form. The method and the system developed showed that a velocity profile can be obtained with high accuracy: 5% for velocity and 1% for position.

Application to the various configurations demonstrated here confirmed the method to be very efficient for obtaining spatial information about flow structures, and to be effective for liquid metals as well. Since the measurement is made instantaneously, it could replace a conventional flow visualisation in many cases.

The complicated flow behavior is realized using the double bent pipe system in this study. UVP measurements with multiple measurement lines are executed for disturbed flow after the double bent. The flowrate is calculated by circumferential interpolation of obtained velocity profiles by UVP with multiple measurement lines. The results of velocity profiles and flowrates obtained are compared those of CFD. The usefulness of our experiments has been confirmed. The theoretical analysis to estimate the optimal number of measurement lines and the minimum inlet length or measurement position base on sampling rate theorem and Fast Fourier Transform (FFT) are also applied to confirm the results theoretically. Accordingly, development of an accurate flowrate measurement using multiple measurement lines is investigated with UVP method.

Wada, S., Kikura, H, Aritomi, M., Mori, M., & Takeda, Y., “Development of Pulse Ultrasonic Doppler Method for Flow Rate Measurement in Power Plant Multilines Flow Rate Measurement on Metal Pipe” Journal of NUCLEAR SCIENCE and TECHNOLOGY, Vol. 41, No. 3, p. 339–346 (March 2004) Ultrasonic Doppler method for a flow metering system has been developed. The method has the capability to obtain instantaneous velocity profiles along the ultrasonic beam. Our purpose is to apply the ultrasonic Doppler method to a flow rate measurement of feed- or recirculation- water in power plants. The principle of the flow measurement method is based on the integration of an instantaneous velocity profile over a pipe diameter. Hence, it is expected to eliminate installation problems such as entry length, also to follow transient flow rate precisely by increasing ultrasonic transducers.

In this paper, we report that the errors are less than 1% just below a bend and sudden expansion pipe employing three measuring lines. And then, for constructing a basic system of a flow rate measurement in power plants, a transmission of ultrasound through a metallic wall is investigated, at first. Afterward, since there is no ultrasonic reflectors in the feedwater in power plants, cavitation bubbles are induced as ultrasonic reflectors and the results are appeared that cavitation bubbles are effective when the pipe material is metallic.

Flow metering system using ultrasonic Doppler method has been developed. In the present study, we reported the results of multilines flow rate measurement employing this method. The laboratory experiments appeared that for fully developed flow condition an accurate measurement of flow rate was achievable using only a single measuring line, and additionally, for non-developed flow which is located just below the bend pipe the multilines method was successfully applied and the errors were less than 1%.

The reflector of ultrasound was obtained very efficiently using ultrasonic cavitation bubbles. Even for the metallic wall pipe, it was appeared that cavitation bubbles were available to measure the instantaneous velocity profile and the flow rate accurately compared with using nylon powder.
As mentioned above, it is indicated that the present multilines flow metering system by using ultrasonic Doppler method has very high accuracy under non-ideal flow conditions such as non-developed flow or non-axis-symmetric flow. And we constructed the basic system of a flow rate measurement in power plants using metallic pipes and cavitation bubbles as ultrasound reflectors.

1.4.3 Computational fluid dynamics (CFD)

Y., Eguchi, T., Murakami, M., Tanaka, H., Yamano “A finite element LES for high-Re flow in a short-elbow pipe with undisturbed inlet velocity”, Nuclear Engineering and Design 241, 4368-4378 (2011) The paper is concerned with a large-eddy simulation (LES) for a high-Reynolds-number flow in a short elbow pipe, which can potentially be employed in the primary piping system of the Japan Sodium-cooled Fast Reactor (JSFR). The basic performance of the LES is studied for an elbow pipe flow without turbulence at inlet boundary at Re = 1.2×10^6 by comparison with a flow observed in a 1/3-scale water experiment, where the flow disturbance at the pipe inlet is small. In setting up the computational conditions, special care was taken to ensure that the mesh subdivision was suitable for the simulation of the pipe flow through a theoretical consideration. We discuss the effects of the turbulence model (Smagorinsky model, WALE model) and the inlet velocity profile on the results. The mechanism of the pressure fluctuation and the origin of the fluid force are also discussed with the aid of spectral analysis and the visualization of essential hydraulic quantities.

The flow in a short-elbow pipe at Re = 1.2×106 was solved using a finite element LES code, SMART-fem, with the Smagorinsky model and the WALE (wall-adapting local eddy viscosity) model for three different inlet velocity profiles without inlet turbulence. The finite element mesh was

designed so that the flow structure in the boundary layer could be resolved with a non-slip wall condition. It has been revealed that the inlet velocity profile has a considerable impact on the flow separation features at the elbow, even though the inlet velocity did not contain fluctuational components in the present computations. That is, the thicker the boundary layer at the inlet, the smaller the flow separation region. The reason for this tendency was explained by the instability induced by the Tollmien–Schlichting wave near the pipe wall, which tends to grow above a certain Reynolds number based on the boundary layer thickness. Such a disturbance near the wall would enable the flow to attach to the elbow and to reduce the flow separation region.

The basic fluctuational features of the computed pressure were analyzed with a spectrum diagram, which showed the consistency with the experimental data in terms of the predominant non-dimensional frequency (Strouhal number). A comparison of the computational results and data in the literature have also demonstrated that the root-mean-square value of pressure fluctuation at the elbow exit is larger than that of a straight pipe by almost two orders of magnitude. The wall forces are computed by surface integration, which indicated that the wall force in the out-of-pipe plane direction is well correlated to the pressure fluctuation at the elbow exit on the intrados side. The visualization of the pressure fluctuations and flow separation suggested that the Dean vortices destabilized by the oscillatory flow separation may be the primary cause of the pressure and force fluctuations. Our future work is to implement a scheme for generating inlet disturbances in the code and to examine the effect of inlet disturbances on the flow separation at the elbow.

E. Mandard, D. Kouam´e, R. Battault, J.-P. Remenieras and F. Patat, “Ultrasonic Symposium Access of asymmetric fluid velocity profile in high precision ultrasonic velocimetry” IEEE 2006, A transit time ultrasonic flowmeter is a very accurate tool to measure the volumetric flowrate of a fluid flowing in a pipe. To estimate the flowrate, the fluid velocity averaged over the cross-section of the pipe has to be estimated from the fluid velocities averaged over the paths of the flowmeter. That is the reason why the velocity profile of the fluid, which depends on not only the Reynolds number but also on the upstream and downstream pipe configuration, is of great interest in transit time flowmetering. In this work, we propose to reconstruct the fluid velocity profile by using the measures of a 18 paths flowmeter measures to offer an in situ diagnostic tool of the flow. We first test tomography methods: filtered back-projection and then an iterative one, the Algebraic Reconstruction Technique (ART).

These methods are not really appropriate to our context of incomplete data. We have previously [1] defined a theoretical parametric model of the velocity profile which allows to in situ detect and characterize the asymmetry of the flow. We defined in this work a new parametric model which has a flowrate function of the asymmetry of the profile. It also has the advantage of determining the parameters of the symmetric term of the model in taking into account the asymmetric part of the profile. This new profile is a promising way in increasing the accuracy of the flowmeter in disturbed flow condition by taking into account the additional information provided by the velocity profile reconstruction.

To develop an in situ diagnostic tool of the flow, we reconstruct the fluid velocity profile thanks to the path velocities measured by a transit time ultrasonic flowmeter. We first test tomography methods: filtered back-projection and an iterative one, the Algebraic Reconstruction Technique (ART). These methods are not actually appropriate to our context of incomplete data. We have previously defined a theoretical parametric model which allows to in situ detect and characterize the asymmetry of the flow profile [1]. The new model proposed here has the advantage of having a flowrate which is function not only of the parameters of the symmetric term of the parametric model but also of the parameters of the asymmetric terms. It has an additional advantage that is the fact that the parameters of the term in Power law $V0$ and n are determined as function of the asymmetry of the profile. This new model is a promising way to increase the accuracy of the flowmeter in disturbed flow conditions by taking into account the additional information provided by the velocity profile reconstruction.

Hilgenstock and R. Erns, “Analysis of installation effects by means of computational fluid dynamics CFD vs experiments”, Flow measurement instruments. Vol. I, No. 314, pp. 161-171, 1996 0 1997 Elsevier Science Ltd Installation effects were considered with the help of computational fluid dynamics (CFD). The information obtained by numerical simulation was much more extensive than in experimental investigations. Using standard turbulence models, reasonable agreement with experimental data was achieved. The use of advanced turbulence models improves the agreement drastically but needs far more computer resources. Visualization of calculated flows was performed with the aid of an advanced graphic system. The assessment of the validation procedure was found to be dependent on various aspects which are discussed in detail. The influence of flow disturbances on various ultrasonic flow meters was numerically investigated.
Answers to the asked questions:

1. What can we learn from CFD that we do not get from experiments?

- In contrast to the experiment, CFD predicts flow disturbances in pipe systems and installation effects as a complete three-dimensional flow field.
- The phenomenological structure of the flow is clearly visible in the CFD-solution.
- The decay-process of flow disturbances can be investigated in detail.

2. Is the accuracy of the numerical solution acceptable?

When using advanced turbulence models the numerical data agree very well with experimental findings at least for the double bend out-of-plane.

More validation work is necessary for other pipe configurations.

For industrial applications the accuracy of numerical results is in the same order of magnitude as the accuracy in real testing rig experiments. Thus, CFD is a good and effective basis to investigate installation effects and flow disturbances.

3. Is it possible to replace experiments?

Numerical and experimental approaches have both advantages and disadvantages depending on the intention of the investigation (such as influence of flow disturbances on turbine meters and ultrasonic flow meters).

In the near future it will not be possible to replace experiments by CFD simulations, but it is important to note that experiments and CFD must supplement each other.

Regarding the simulation of the ultrasonic flow meters, based on numerical flow simulations the following conclusions may be drawn. Here, CFD can help:

- to investigate the influences of disturbances on different ultrasonic flow meters,
- to investigate the performance of different path configurations,
- to calibrate ultrasonic flow meters numerically even under disturbed flow conditions,
- to reduce the costs of developing ultrasonic flowmeters.

M. Pellegrini, H., Endo, and H., Ninokata “Numerical investigation of bent pipe flows at transitional Reynolds number”, Progress in Nuclear Energy 53, 916-920 (2011). **[1-..]** The correct evaluation of flows at transitional Reynolds number in nuclear reactors is gaining higher importance in relation to the accident analysis for buoyancy-driven flows which dominate the heat decay removal process. In the present paper a comparative study of different turbulence modeling and wall treatment for the evaluation of a fluid flow in transitional Reynolds number, is presented employing computational fluid dynamics (CFD). The relative performance of the models is assessed through benchmarking of fully developed pipe flow at Reynolds number 4900 and of a 90° bend pipe at Reynolds number

5000. Predictions of velocity profiles at different locations are compared to both experimental and accurate numerical simulations.

It has been found that the predictions between the models can vary considerably in particular in relation to the different wall treatment employed on the wall. The results show the concerns about the employment of the available turbulence models and wall treatments in low Reynolds number flow regimes and explanation is provided in relation to their formulation.

Two benchmarks for the evaluation of transitional flows were analyzed through comparison with experiments and accurate numerical solutions. The fully developed pipe flow shows that damping functions, employed with k-ε models, predict a laminar flow which does not satisfy the turbulent characteristics found both experimentally and numerically (DNS). On the other hand the employment of a two layer approach on the wall assures the reproduction of the turbulent profile even though some discrepancies for the evaluation of the u_τ are introduced. Turbulent profile but with unpredicted normalized velocity is then shown for the k-ω model also.

The 90° bent pipe evaluations instead shows how the anisotropic models (k-ε cubic and RST) are able to predict with reasonable accuracy the behavior of the secondary flows which influence the velocity profile downstream the bend. The presence of the anisotropic model seems to be the main feature to be able to predict the phenomenon. These considerations are validated by the behavior of the SST model which, independently from the accurate inlet conditions, provides not accurate results for the downstream velocity profile and secondary flow predictions.

The study shows that for the state of art turbulence models the one which shows a high generality of application in case of bent pipes in transitional turbulence seems to be the k-ε model together with the employment of two layer approach for the wall treatment which, even though underestimating the profile of the fully developed flow, is able to capture the main characteristics of the flow downstream an elbow with strong curvature.

As a final remark the authors would add that the employment of low Reynolds number k-ε model, despite the achieved results in Section 2.1.2, is regarded to be potentially generic and able to improve the general predictions of the flow, such as the prediction of the instability which is not accessed via two layer treatment of the wall. The reasons of its failure are to be imputed to the

applied damping functions which show a not proper behavior out of their range of applicability.
This work points out the deficiencies and the strength points of the available turbulence modeling, representing a starting point for a possible development of a more general approach which could combine application to high Reynolds number and transitional flows [1-].

1.5 OBJECTIVES AND OUTLINE OF THE THESIS

This thesis presents a study on ultrasonic measurement technique for the complicated flow as downstream of the double bent pipe. The main purposes are development of ultrasonic velocity profile (UVP) method with multiple ultrasound transducers.

To achieve this, methodology is designed start from the fundamental of UVP. Firstly, the ultrasonic characteristics are investigated. Ultrasonic velocity profiles (UVP) utilize a pulse ultrasonic beam and the scattering of ultrasonic waves on tracer particles to obtain instantaneous velocity profiles. **Chapter 2** summarized basic characteristics of ultrasonic waves, their propagations, diffractions, inflections; reflection and the mode of transformations between longitudinal and transversal (shear) waves. Appreciation of the characteristics of ultrasound waves and their behavior in various media is essential to understanding the use of diagnostic ultrasound in clinical medicine. During the propagation of an ultrasound wave, the molecules of the medium vibrate over very short distances in a direction parallel to the longitudinal wave. One of the most important factor of ultrasound flow measurement is the measurement of **sound velocity** in water is very important because it will be one of the most important parameter to measure the velocity of fluid in pipe flow in **sect. 2.1**. **Acoustic impedance** is important in the determination of acoustic transmission and reflection at the boundary of two materials having different acoustic impedances the design of ultrasonic transducers assessing absorption of sound in a medium in **sect. 2.2**. In **section 2.3**, the arrangement of **the incident angle** can avoid the reflection from the pipe wall. The reflections and refraction angle of ultrasound wave accord with the Snell's law. Therefore, the decided of incident angle is the first step to set up the experiment in velocity profiles which suitable to obtain good results. In **section 2.4**, UVP measurement obtains velocity profile from just after the emission of ultrasound to a setting value. Thus, the profile includes unnecessary profile, i.e. profile in **pipe wall**, as well as the necessary velocity profile of the flow.

Chapter 3. Flowrate measurement on the double bent pipe. Flow rate in the transient conditions downstream of double 90º bent was measured to investigate the accuracy of the flow rate measurement using this multi-lines method. Many ultrasonic transducers can be used when more accurate flowrate is desired or the flow is asymmetric flow. Flowrate using multiple flow profiles can be calculated by using the interpolation of each velocity profile. When flowrate near the bent pipe is measured by UVP method, many measurement lines are necessary to make two- or

three-dimensional velocity profile mapping due to its asymmetric flow.

Chapter 4. UVP measurement can obtain only velocity profiles in line. Usual Particle Image Velocimetry (PIV) gives two-dimensional velocity mapping; however, PIV cannot obtain the flow distribution instantaneously. Hence, it is difficult to obtain fully three-dimensional velocity profile experimentally. To evaluate this limitation of experimental method, the numerical simulations using Computational Fluid Dynamics (CFD) were conducted. Numerical simulation calculation can give fully three-dimensional velocity profiles. In these days, computers are well developed, and numerical simulation becomes very popular and useful method to obtain velocity profiles because of its costs compare to the real experimental. Thus, simulation calculation was performed for the experimental condition, and the numerical result was compared with the experimental one as velocity profiles along the measuring lines. It can confirm both experimental and numerical results.

Chapter 5. The estimation of the number of measurement line using a new analytical method for in plane double bent pipe. Fourier analysis is a mathematical method used to break down and transform a periodic function i.e., a mathematical relationship between a quantity and a variable or variables whose relative values consistently repeat over some regular period of time into a set of simpler functions which can then be summed and transformed back into the original form. Today, it has been applied to a wider variety of problems in the physical and natural sciences. Improved, expanded upon, and the core of what has come to be known as the field of harmonic analysis, Fourier analysis has evolved and progressed to include the study of more abstract and general phenomena. Then, in this study, it was applied to estimate the largest number of waves, and necessary numbers of transducers for each position are indicated analytically by using sampling rate theorem.

Chapter 6. The estimation of measurement lines is important to measure accurate flowrate effectively. From this aspect, the number of velocity profiles was optimized experimentally to calculate the flowrate in former chapter. However, necessary number of sensors can be calculated analytically by regarding velocity profiles as a kind of wave. Sampling rate theorem for waves can indicate the necessary number of the sensors. To apply the theorem to this kind of measurement by UVP method, the velocity profiles on the radial measurement lines must be converted into circumferential profile(s). Therefore, multiple measurements changing circumferential angle by 10° were examined and observed profiles on line were accumulated for conversion into circumferential velocity profiles on concentric circles. Every velocity profile shows harmonic wave [6-1] that the

horizontal axis means the transducer circumferential position of transducer, while the vertical axis means the time-averaged velocity normalized by the mean velocity. From each harmonic wave, we can verify the circumferential position where peaks of waves occur. Then, it is simply to set the position of measurement line.

REFERENCES

[1-1] Energy Balances of non-OECD Countries 2013, *International Energy Agency*, OECD, , ISBN : 9789264203075 (2013)

[1-2] Watford, G., Plant Modifications Assisting the Global Energy Demand, World Nuclear Association, Annual Symposium (2005)

[1-3] United State Nuclear Regulatory Commission (US.NRC), Operating Reactor Licensing, Power Uprating, (2013)

[1-4] Power uprate in nuclear power plants: guidelines and experience, prepared within the framework of the Technical Working Group on Life Management of Nuclear Power Plants. International Atomic Energy Agency (IAEA nuclear energy series, ISSN 1995-7807; no. NP-T-3.9), ISBN 978–92–0–111610–9, (2011)

[1-5] Uprating Programs, Nuclear Services/ Engineering Services, *Westinghouse Electric Company*, NS-ES-0020, (2011)

[1-6] Inoue, Y., Kikura, H., Murakawa, H., Aritomi, M. & Mori, M., A Study of Ultrasonic Propagation for Ultrasonic Flow Rate Measurement, *Flow Measurement Instruments*, Vol. 19, pp. 223-232 (2008)

[1-7] Takeda, Y., Development of an Ultrasound Velocity Profile Monitor, *Nuclear Engineering Design*, Vol. 126 pp. 277-284, (1991)

[1-8] Bud, R. & Warner D.J., Instruments of science: an historical encyclopedia, *Science Museum*, London, pp.245 (1998)

[1-9] Mori, M., Takeda, Y, Taishi, T., Furuichi, N., Aritomi, M & Kikura, H., Development of a novel flow metering system suing ultrasonic velocity profile measurement, *Experiment of Fluids* 32, pp. 153-160 (2002)

[1-10] Yakeda, Y., Ultrasonic Doppler Velocity Profiler for Fluid Flow, *Springer*, Japan, (2012)

[1-11] Estrada, H., Hauser, E. & Phillips, J., Precision Flow Measurement for Continuous Power Cycle Efficiency Monitoring, *Proc.9th Topical Meeting on Nuclear Thermal-Hydraulics, Operation and Safety (NUTHOS)*, Taiwan, (2012)

[1-12] Sawchuk, B. D. and Peck, B.: Flow Conditioning for Natural Gas Measurement, *CGA Gas Measurement School*, (1998)

[1-13] Takeda, Y., Furuichi, N., Mori, M., Aritomi, M. & Kikura, H.: Development of a New Flow Metering System Using UVP. Preliminary performance assessments using NIST flow standards, *ASME Fluids Engineering Division Summer Meeting*, (2000)

[1-14] Mori, M., Takeda, Y., Taishi, T., Furuichi, N., Aritomi, M., & Kikura, H., Development of a Novel Flow Meter System Using Ultrasonic Velocity Profile Measurement, *Experiments in Fluids*, **32**-2, pp. 153-160 (2002)

[1-15] Steenbergen, W., Turbulent Pipe Flow with Swirl, *Thesis of Eindhoven University of Technology*, (1995)

[1-16] Tunstall, M. J. & Harvey, J. L., On the Effect of a Sharp Bend in a Fully Developed Turbulent Pipe Flow, *Journal of Fluid Mechanics.*, vol.34 535 (1968)

[1-17] Wada, S., Tezuka, K., Treenuson, W., Tsuzuki, N. & Kikura, H., Study on the Optimal Number of Transducers or Pipe Flow Rate Measurement Downstream of a Single Elbow Using the Ultrasonic Velocity Profile Method, *Science and Technology of Nuclear Installations*, (2012)

[1-18] Kotze, R., Wiklund, J., Haldenwang, R. & Fester, V., Measurement and Analysis of Flow Behaviour in Complex Geometries Using Ultrasonic Velocity Profiling (UVP) Technique, *Flow Measurement Instruments*, vol. 22 (2011), 110-119.

[1-19] Malcolm J. & Povey, W., Ultrasonic Techniques for Fluids Characterization, *Academic Press* (1997)

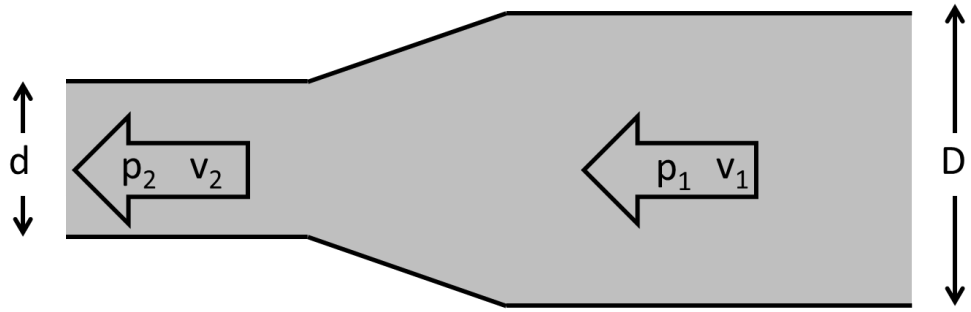

Fig. 1-1 Principle of differential pressure flowrate calculation

CHAPTER 2

SET UP CONDITIONS OF UVP MEASUREMENT

2.1 INTRODUCTIONS

Ultrasound is a mechanical disturbance that moves as a pressure wave through a medium. When the medium is a patient, the wavelike disturbance is the basis for use of ultrasound as a diagnostic tool. Appreciation of the characteristics of ultrasound waves and their behavior in various media is essential to understanding the use of diagnostic ultrasound in clinical medicine. During the propagation of an ultrasound wave, the molecules of the medium vibrate over very short distances in a direction parallel to the longitudinal wave. It is this vibration, during which momentum is transferred among molecules, that causes the wave to move through the medium. The basical level of sound is shown in **Table 2-1**.

2.2 MEASUREMENT OF SOUND VELOCITY IN WATER

The measurement of sound velocity in water is very important because it will be one of the most important parameter to measure the velocity of fluid in pipe flow. The velocity of sound will be able to measure with many methods using basic principle from the technique of Colladon and Sturm (1827) in Lake Geneva. This technique is variously known as pitch and catch, pulse-echo time of flight or "Acoustic Time of Flight Measurement" (AToM).

The time variation is characterized by the frequency f and the spatial variation by the wavelength λ.Both frequency and the spatial variable wavelength are related through the velocity of sound, which is given by;

$$v = f\lambda \qquad \textbf{(2-1)}$$

The accuracy and errors of ultrasonic velocity measurement becomes significant of the flowrate measurement. The other error factor come from the precise of timer which important to calculate the duration of period.

The temperature is important, because the path length can vary with temperature and because the velocity of sound in water is strongly depend on temperature. Since the velocity of sound in water varies by approximately 3 (m/s)/°C at 20°C an error in temperature of 0.1°C will produce an error in the velocity of 0.3 m/s **[2-1]**

2.3 DIFFERENT OF LIGHT WAVE AND ULTRASOUND WAVES

Light and sound have many similarities because of their common wave/particle duality. However, they have fundamentally different origins. There are two main differences between sound waves and light waves **[2-2]**. The first difference is in velocity. Sound waves travel through air at the speed of approximately 1,100 feet per second; light waves travel through air and empty space at a speed of approximately 186,000 miles per second. The second difference is that sound is composed of longitudinal waves (alternate compressions and expansions of matter) and light is composed of transverse waves in an electromagnetic field. Although both are forms of wave motion, sound requires a solid, liquid, or gaseous medium; whereas light travels through empty space. The opposite is true of light. Light travels approximately one-third slower in water than in air. Sound travels through all substances, but light cannot pass through opaque materials. Frequency affects both sound and light. A certain range of sound frequencies produces sensations that you can hear. A slow vibration (low frequency) in sound gives the sensation of a low note. A more rapid sound vibration (higher frequency) produces a higher note. Likewise, a certain range of light frequencies produces sensations that you can see. Violet light is produced at the high-frequency end of the light spectrum, while red light is produced at the low-frequency end of the light spectrum. A change infrequency of sound waves causes an audible sensation a difference in pitch. A change in the frequency of a light wave causes a visual sensation a difference in color.

Table 2-1 illustrates the properties of sound compare to the light. Light radiation can be polarized whereas compression sound cannot. In solids it is possible to produce a mode of sound called *"shear"* which can be polarized, but only fluids, in which the shear mode of propagation is highly attenuated, are considered in this work. It is easier to control both phase and frequency in an ultrasound signal, making this an ideal form of radiation to investigate poorly understood features of wave phenomena such as wave propagation under conditions of strong scattering.

2.4 ACOUSTIC IMPEDANCE

Ultrasound is the mechanic wave which there are four main properties such as reflection refraction absorption and insertion. The refection and Transmission at multiple interface is necessary to consider. When an acoustic wave propagates perpendicularly to the interface, reflection and transmission occur at the boundaries between material 1 and plate (material 2), and again at plate

and material 1. Describing the impedance ration between the materials as

$$m = Z_1/Z_2 \qquad \textbf{(2-2)}$$

Sound travels through materials under the influence of sound pressure. Because molecules or atoms of a solid are bound elastically to one another, the excess pressure results in a wave propagating through the solid. The acoustic impedance (Z) of a material is defined as the product of its density (p) and acoustic velocity (V).

$$Z = pV \qquad \textbf{(2-3)}$$

Acoustic impedance is important in the determination of acoustic transmission and reflection at the boundary of two materials having different acoustic impedances the design of ultrasonic transducers assessing absorption of sound in a medium **[2-3]**. The following applet can be used to calculate the acoustic impedance for any material, so long as its density (*p*) and acoustic velocity (*V*) are known. The applet also shows how a change in the impedance affects the amount of acoustic energy that is reflected and transmitted. The values of the reflected and transmitted energy are the fractional amounts of the total energy incident on the interface **[2-4]**.

2.5 INCIDENT ANGLE OF TRANSDUCER SETUP

Among ultrasonic techniques pulse-echo method is the most commonly used in industry, mainly due to its simplicity and efficiency. However, the accurate measurement of defects perpendicular to the inspection surface is one of the limitations of pulse-echo technique **[2-5]**. To calculate the axial velocity of fluid flow, we need incident angle to receive the echo wave which reflecting from the surface of particle to calculate the Doppler frequency as form from the different phase shifts and finally we can calculate the velocity of fluid flow. If we don't have incident angle, we cannot calculate the axial velocity profile. The reflection and refraction angle of ultrasound wave accord with the Snell's law (**Eq. (2-4**)) which explains relationship between the sound velocity in each medium and the angle of wave path in each medium from the Snell's law as follows:

$$\frac{\sin\theta_1}{C_1} = \frac{\sin\theta_2}{C_2} = \frac{\sin\theta_3}{C_3} \qquad \textbf{(2-4)}$$

where C is the sound velocity in the different medium, subscribe i means the kind of medium as shown in **Fig. 2-4**. θ_i are the inclined angle in the mediums as well. From this equation, if medium 1 and medium 3 are same kind of medium that means sound velocity of both media have equal value, then the reflection angle in the medium will also same.

The arrangement of the incident angle can avoid the reflection from the pipe wall which affecting the experimental results. To solve this effect, the most suitable incident angle should be defined to obtain the accurate results of these conditions. The transmission ratio of ultrasound can be calculated as following: To design the incident angle, we need to consider about the constraint that is,

-Transmission of ultrasound in the medium as the consideration of the power of ultrasound when it pass through the difference interface of material. In theoretical using, the refraction will effect for the power of ultrasound, to reduce this effect, we design to use the water box which contain the water to be the first medium which same as the fluid flow. From Snell's laws, we can assure that the refraction angle in fluid flow will similar with the setup angle of transducer on the pipe wall.

-The effect of vortex in measurement line. At near the double bent pipe, the flow is very complicated especially vicinity close to the outlet of double bent pipe. This is because the centrifugal force which spread from the center of bent pipe the outer of pipe and recirculate back to the inner side of pipe again it mean the vortex. The direction of stream line show the shape as circle. It is difficult to measure velocity profile in the recirculation area or vortex. From this reason, we must avoid the effect of vortex.

$$\frac{A_{t2}}{A_{i0}} = \frac{4\lambda_0\mu_1 l_0 l_1 (1+l_0)(s_1^{\,2}-1)(s_1^{\,4}-1)}{F_1 F_2} \quad \textbf{(2-5)}$$

$$F_1 = \lambda_0 l_1 (1+l_0^{\,2})(1+s_1^{\,2}) + \mu_1 l_0 \{(s_1^{\,2}-1) + 4 l_1 s_1\} \quad \textbf{(2-6)}$$

$$F_2 = \lambda_2 l_1 (1+l_2^{\,2})(1+s_1^{\,2}) + \mu_1 l_2 \{(s_1^{\,2}-1) + 4 l_1 s_1\} \quad \textbf{(2-7)}$$

$$l_0 = \cot\theta_{l0} \quad \textbf{(2-8)}$$

$$l_1 = \cot\theta_{l1} \quad \textbf{(2-9)}$$

$$s_0 = \cot\theta_{s0} \quad \textbf{(2-10)}$$

$$s_1 = \cot\theta_{s1} \quad \textbf{(2-11)}$$

where *A* is the amplitude of the ultrasound pulse, subscribe *t* and *i* are transmitted and incident wave in medium, λ and μ are the Lame constants of the medium, θ is the incident or refracted angle of the ultrasonic pulse, *l* is longitudinal wave in different media, *s* is shear wave in media. A is the character of power of ultrasound wave. The power of ultrasound can show as amplitude which comes in the form of sound pressure (Kg/m2s). When a sound wave is incident on an interface between two interface, part of it is reflected back into the original medium as the reflection wave. Its' amplitude will decrease when pass thought the interface of different medium. The amount of energy reflected back depends on impedance. The greater the difference in impedance between the medium is forming the interface the greater the amount of energy that is reflected back.

As mention before, A is the amplitude or the power of ultrasound wave. The power of ultrasound can show as amplitude which come in the form of sound pressure (Kg/m2s). The subscription i is incident angle of ultrasound wave. t is the subscription of transmission wave when ultrasound wave pass through different medium. 0, 1 and 2 are subscription of 3 different medium. 0 is the first medium which ultrasound pass thought directly from the head of transducer. The pulse ultrasonic wave was emitted through the second medium and the third medium are the subscription as 1 and 2 respectively.

In solids, sound waves can propagate in four principle modes that are based on the way the particles oscillate. Sound can propagate as longitudinal waves, shear waves, surface waves, and in thin materials as plate waves. Longitudinal and shear waves are the two modes of propagation most widely used in ultrasonic testing. In longitudinal waves, the oscillations occur in the longitudinal direction or the direction of wave propagation. Since compressional and dilatational forces are active in these waves, they are also called pressure or compressional waves. They are also sometimes called density waves because their particle density fluctuates as they move. Compression waves can be generated in liquids, as well as solids because the energy travels through the atomic structure by a series of compressions and expansion (rarefaction) movements. In the transverse or shear wave, the particles oscillate at a right angle or transverse to the direction of propagation. Shear waves require an acoustically solid material for effective propagation, and therefore, are not effectively propagated in materials such as liquids or gasses. Shear waves are relatively weak when compared to longitudinal waves. In fact, shear waves are usually generated in materials using some of the energy from longitudinal waves.

2.6 DETERMINATION OF PIPE WALL IN VELOCITY PROFILE

At near pipe wall, the UVP measurements usually have error from the different space of measuring volume which their space was in different medium between the pipe wall and fluid. Consequently, the average velocity is very low at the close area of transducer because of the small size of measuring volume. On the other hand at the opposite side wall, the average velocity is high because of the large measuring volume. At the close area of transducer the measuring volume is smaller than the area where is far from the transducer as the opposite side of pipe wall. There are the errors of the measurement near the pipe wall. The size of wave fronts are expending from the starting point where nearly the transducer to the long distance from the transducer along the wave propagating direction. The effect of beam spread property influence in the far field of the transducer which is the farther pipe wall. Nevertheless, the calculation of flowrate using only first half of the velocity profile to integrate around the center of pipe. From this reason, we can avoid the effect of the area near the pipe wall.

UVP measurement obtains velocity profile from just after the emission of ultrasound to a setting value. Thus, the profile includes unnecessary profile, i.e. profile in pipe wall, as well as the necessary velocity profile of the flow. **Figure 2-9** illustrates location of transducer, pipe wall, following area and measurement volume. Measurement volume is a space where pulse waves transmit and able to measure the velocity of the particles in the medium. The length of measurement volume is 0.74 mm. *N* means a number named for each measurement volume where pulse ultrasound can hit the particle and echo signal reflected back to the same transducer. Subscript *PW1* means the measurement volume at the vicinity of the near side pipe wall, and subscript *PW2* means that of the farther pipe wall. N_R means the number of measurement volumes which exists between the volume *PW1* and the center of the pipe. When the flow is fully developed stable and axially symmetric, N_R, N_{PW1} and N_{PW2} can be calculated regarding velocity magnitude as the center of pipe using **Eqs. (6) - (8)**.

$$N_R = \{(R_p) / (\cos \theta_w)\}/\Delta N \qquad \textbf{(2-12)}$$

$$N_{PW1} = N_{Vmax} - N_R \qquad \textbf{(2-13)}$$

$$N_{PW2} = N_{Vmax} + N_R \qquad \textbf{(2-14)}$$

where R_p is the inner radius of the pipe. Subscript V_{max} means a measurement volume at the position of maximum velocity in the velocity profile. θ_w is incident angle. ΔN means channel width. Velocity profile before N_{PW1} and after N_{PW2} is unnecessary for flow observation. In order to indicate this, an experiment using long straight pipe was executed in experimental apparatus as shown in **Fig. 2-10**. Flowrate was controlled by using ball valve and bypass system and setup by electromagnetic flowmeter. Flow conditioner was used to clear the swirl flow. Test section was set in water box which used for the reduction of reflection. The overflow cylinder was used to keep the stable pressure in system. **Table 2-3** shows the experimental conditions for this preliminary experiment. The distance from the flow conditioner to the measuremet point was set approximately 50 D. Reynolds number was around 60,000. Temperature of the fluid was kept with cooling system at 25°C. Channel width (ΔN) is 0.74.

2.7 RESULTS AND DISCUSSIONS

Figure 2-5 shows the refractions of ultrasound occur by difference of acoustic impedances of the media at the interface. Only longitudinal wave (l_2) can pass in fluid (gas and liquid) phases because the energy can travel through the atomic structure by a series of compressions and expansions rarefactions movements. In longitudinal wave, the oscillations occur in the longitudinal direction of the direction of the wave propagation. Since compression and dilation forces are active in these waves, they are also sometimes called density waves because their particle density fluctuates as they more.

Figure 2-6 illustrates the ultrasonic transmission ratio from acrylic resin to water against the incident angle. Total transmission rate from the transducer to water strongly depends on the incident angle and also longitudinal and shear wave. However, shear vertical wave can pass into solid phase like longitudinal wave with different refractive angle from longitudinal one due to different sound speed. Then, shear vertical waves and longitudinal waves generate multiple wave paths into the flow field. Echo signals of other wave path become only noises when one major path is used for the measurement and they decrease the accuracy[11)]. When considering this reason, adopting incident angle of 45° with strongest shear vertical wave is preferable for flowrate measurements in pipes because the transmission ratio into water is strongest and forms a single wave path. The critical angle of longitudinal wave which can transmit with only small incident angle from water to acrylic pipe is approximately 32º, as shown in **Fig.2-7**.

Figure 2-7 shows the results from the experiment. The flowrate errors from many incident angles from 0° to 90° are considered with two different Reynolds numbers that are 40,000 and 60,000. The error at 30° is the least when compared to the other incident angle which are 0.86% (Re = 40,000) and 0.98% (Re = 60,000). Error at 45° becomes larger than ones of less incident angle.

Figure 2-8 depicts schematic relationship of incident angle and the length of measurement line. From **Fig. 2-8**, it is clear that measurement with a larger incident angle (θ_{wl}) has a longer measurement line when compared with a smaller incident angle (θ_{ws}) and a shorter measurement line. The longer measurement line may be a reason of larger error at 45°. Another problem of larger incident angle is position of the measuring line. Measurement line with larger incident angle will cover larger area, as shown in **Fig. 2-8**. When a vortex exists at apposition a little far from measuring point, measurement with larger incident angle of (θ_{wl}) may be affected by the vortex though measurement with smaller incident angle of (θ_{ws}) may not. If the flow is simple and similar profile continually appears among long term, the problem of the distance from measuring point is negligible and large incident angle can be applied. However, complicated flow is the target of this study, and a small incident of 10° is applied for the experiments. The percentage of error at 10° is enough less as -0.97% and -1.2% for Reynolds number 40,000 and 60,000 respectively. In addition, a longer measurement line demands a longer maximum depth for UVP measurement, which decreases spatial and temporal resolution of UVP method. This is another reason of the application of the small incident angle 10°.

Table 2-2 shows the experimental conditions for instance, the measurement distance from the flow conditioner which used for clear the swirl to measurement position was set approximately 50 D (D is the inner diameter of the pipe) where fully developed flow was acquired. Reynolds number was setup at 40,000 and 60,000. Temperature of the fluid was kept with cooling system at 25°C. The distance between the measurement volumes is 0.74 mm which can calculate from the half of waves per pulse multiply by wave length. The measurement volumes along the measurement line are 74 points. The inner radius (R) of the pipe is 25 mm and wall thickness is 5 mm. Basic frequency of ultrasound which emitted from transducer is 8 MHz. The repetition of pulse wave is 128 times per velocity profile measurement.

Figure 2-11 is the velocity profile from the measurement. The ultrasound pulse was emitted from the transducer along the measurement line in UVP method. Using **Eq. (2-12)** N_R is calculated as

33.8.The position of maximum velocity in the profile is defined as N_{Vmax} =35. Therefore, the position of N_{PW1} is calculated as 1.2, that is round off as 2, and N_{PW2} is 68.8, that is round off as 68. Those points are also shown in **Fig. 2-11**. Measurement volumes which exist out of the flow, i.e., the volume number 1 and from 70 to 74, can be neglected to plot the velocity profile of the flow.

2.8 CONCLUSIONS

To design the conditions which appreciate for the experiment, we consider the incident angle and the accurate velocity profile from the effect of beam spread property. The results of sound transmission show the suitable setup angle which has a good transmission ratio at 30° with 0.7 % of error. However, the condition for the large pipe diameter the small angle is good for good transmission. When a sound wave is incident on a interface between two interface, part of it is reflected back into the original medium as the reflection wave. Its' amplitude will decrease when pass thought the interface of different medium. The amount of energy reflected back depends on impedance. When a sound wave is incident on an interface between two interfaces, part of it is reflected back into the original medium as the reflection wave. Its' amplitude will decrease when pass thought the interface of different medium. The amount of energy reflected back depends on impedance. For complicated flow which is the target of this study a small incident angle of 10° is applied for the experiments. The percentage of error at 10° is enough less as -0.97% and -1.2% for Reynolds number 40,000 and 60,000 respectively. In addition, a longer measurement line demands a longer maximum depth for UVP measurement, which decreases spatial and temporal resolution of UVP method. This is another reason of the application of the small incident angle 10°.

REFERENCE

[2-1] J. Sander, K. Hutter, On the development of the theory of the solitary wave. A historical essay, Springer, Volume 86, Issue 1-4, pp. 111-152, 1991

[2-2] L. E., Hargrove, E. A., Hiedemann and R., Robert, Diffraction of Light by Two Spatially Separated Parallel Ultrasonic Waves of Different Frequency, Zeitschrift fiir Physik 167, pp. 326-336, 1962

[2-3] S. Kalbfeld, D. Kucera, and J.B. Ketterson, Acoustic impedance measurements of transverse and longitudinal sound in superfluid ^{3}he, Journal of Low Temperature Physics, VoL 89, Nos. 3/4, 1992

[2-4] C. H., Kim · S. H., Lee · G. S. Gong and J. H., Lee, A basic study on the dynamic water level limit sensor utilizing acoustic impedance matching, J Electroceram 17, pp. 531–535, 2006

[2-5] J. Braz., The use of artificial neural network in the classification of pulse-echo and TOFD Ultra-Sonic signals Soc. Mech. Sci. & Eng. vol.27 no.4, 2005

[2-6] C.H., Liu, C.C., Liu, W.C., Huang, Application of astigmatic method and Snell's law on the thickness and refractive index measurement of a transparent plate. Microsyst Technol 19, pp. 1761–1766, 2013

Table 2-1 Comparison of basic properties between ultrasound and light

Ultrasound	Light
Transducers are phase sensitive	Transducer are phase insensitive
Wavelength between cm and μm	Wavelength between 0.5 and 1 μm
Frequency between 0.1 and 10^{13}Hz	Frequency between 3×10^{16} and 6×10^{16}
Coherence between pulses	No coherence between pulses
Responds to elastic, thermophysical, and density properties	Responds to dielectric and permeability properties
Particle motion parallel to the direction of propagation; no polarization	Field displacement perpendicular to direction of propagation; polarization is therefore possible
Propagates through optically opaque materials	Sample dilution is normally required

Table 2-2 Level frequency of sound and the classification

Frequency (Hz)	Classification
20–20,000	Audible sound
20,000–1,000,000	Ultrasound
1,000,000–30,000,000	Diagnostic medical ultrasound

Table 2-3 Experimental Conditions to set incident angle.

Testing conditions	Units	Values
Water temperature	°C	25
Reynolds Number	-	40,000 60,000
Test section		
Inner pipe diameter	mm	50
Incident angle	degree	10
Measurement setups		
Basic frequency of Ultrasound	MHz	8
Repetition of UVP	Times	128
Number of wave per pulse	Waves	8

Table 2-4 Experimental conditions to verify the pipe wall.

Testing conditions	Units	Values
Reynolds Number	-	60,000
Distance of measurement position	mm	2,500 (50 D)
Number of measurement volume	-	74
Channel width	mm	0.74

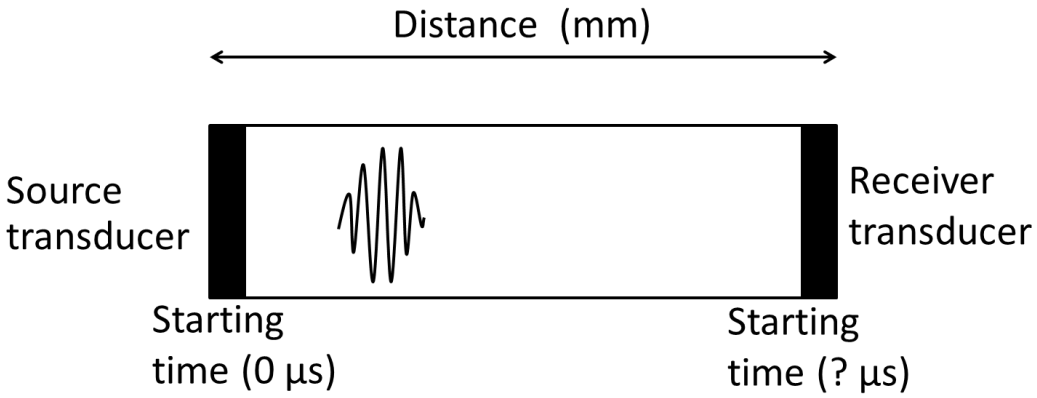

From the basic principle that v=s/t where v is velocity, s is distance and t is time for example, s = 150 mm and t = 100 µs then the velocity of sound is 1,500 m/s.

Fig. 2-1 Block diagram of an acoustic pulse-echo (Atom) apparatus. A representation of the pulse, based on an oscilloscope trace, is shown in the picture and explained

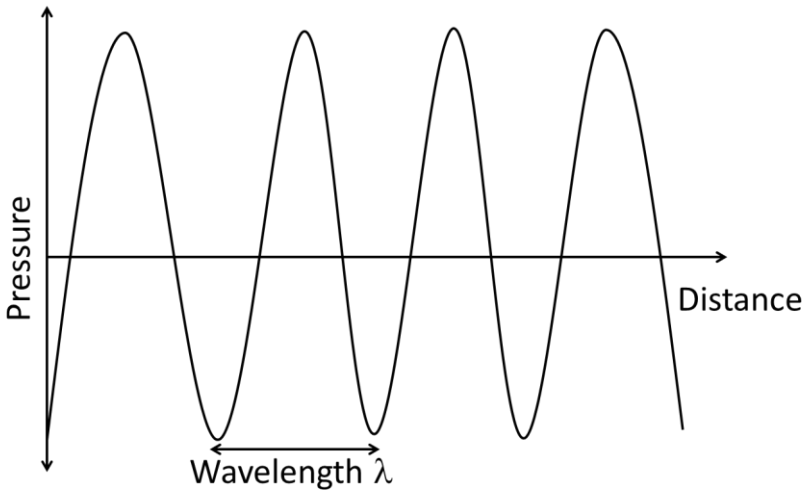

Fig. 2-2 Distance of wavelength in the waveform in function of pressure and distance.

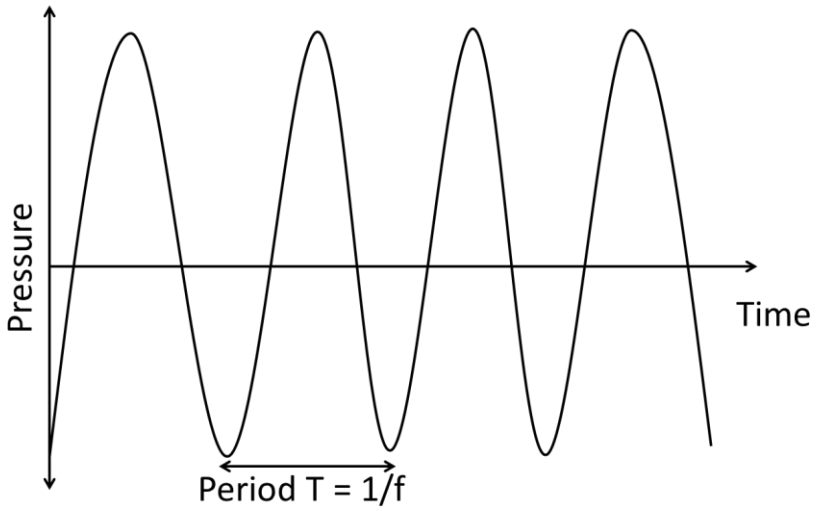

Fig. 2-3 Duration of one period in the waveform in function of pressure and time.

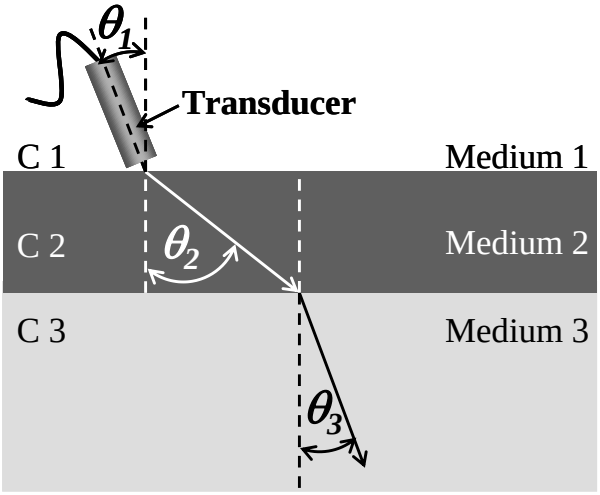

Fig.2-4 Schematic diagram of Snell's law principle.

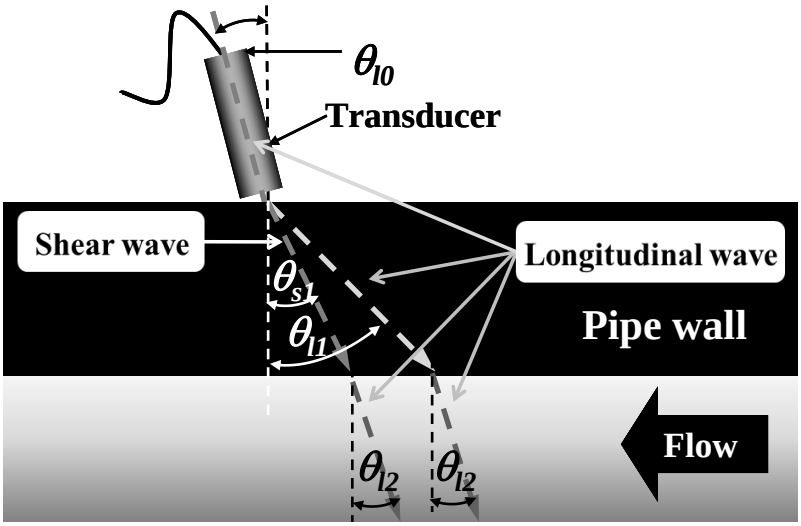

Fig. 2-5 Schematic diagram of the refractions of ultrasonic wave.

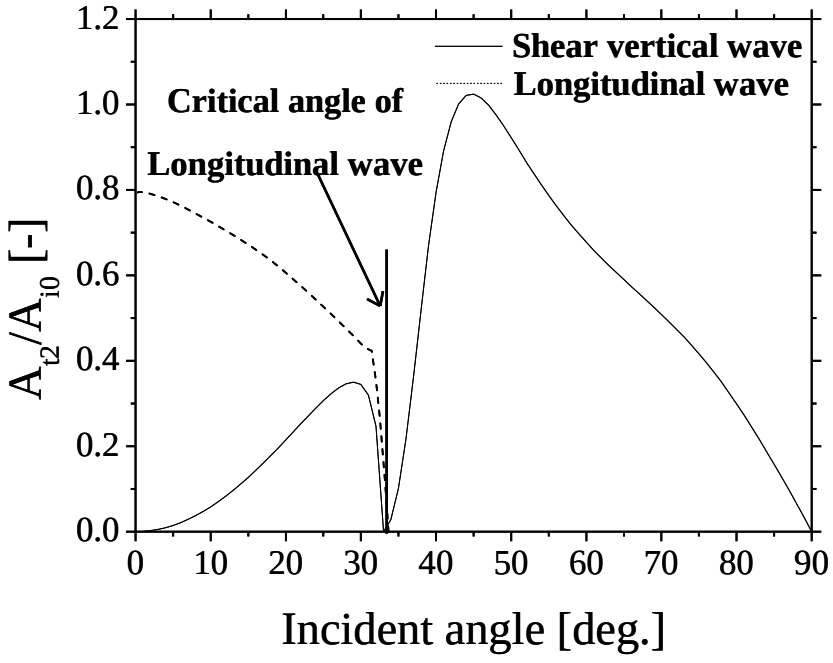

Fig. 2-6 Ultrasound transmission ratio from acryl to water versus the incident angle of ultrasound wave into acryl.

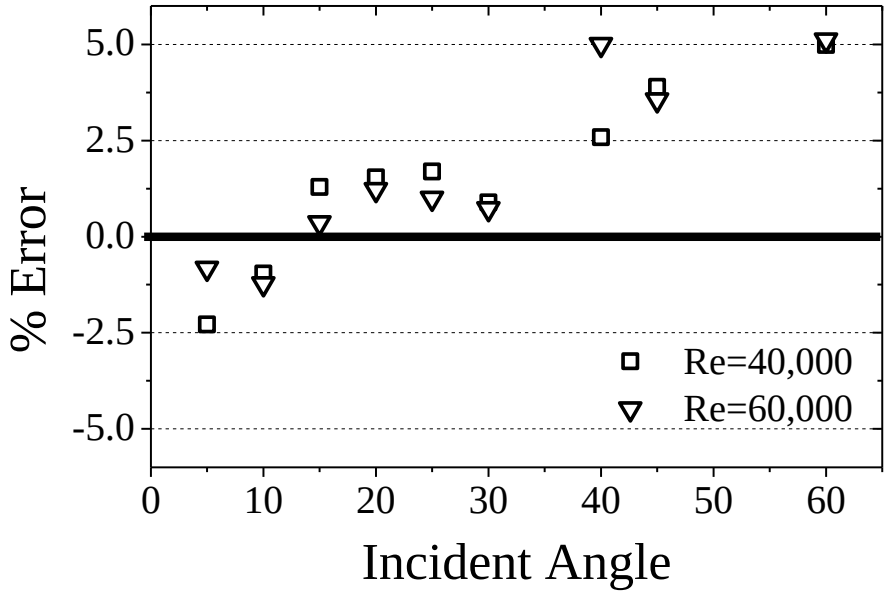

Fig. 2-7 Errors of flowrate calculations for different incident angles.

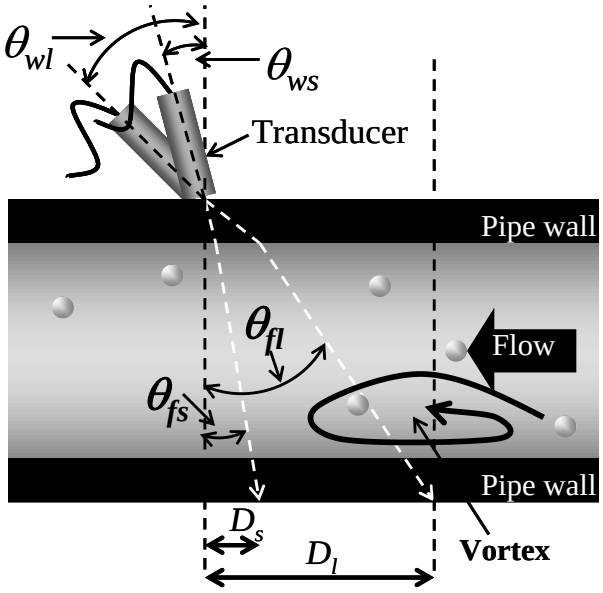

Fig. 2-8 Incident angle and measurement line.

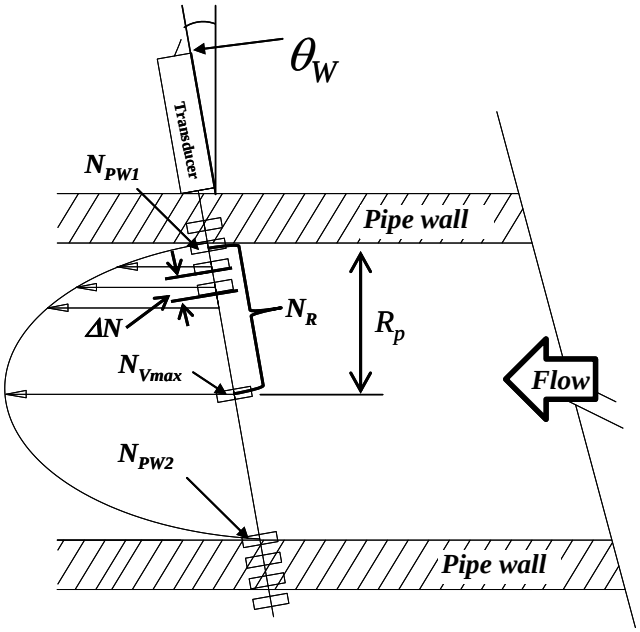

Fig. 2-9 Measurement volumes of UVP and the position of pipe wall.

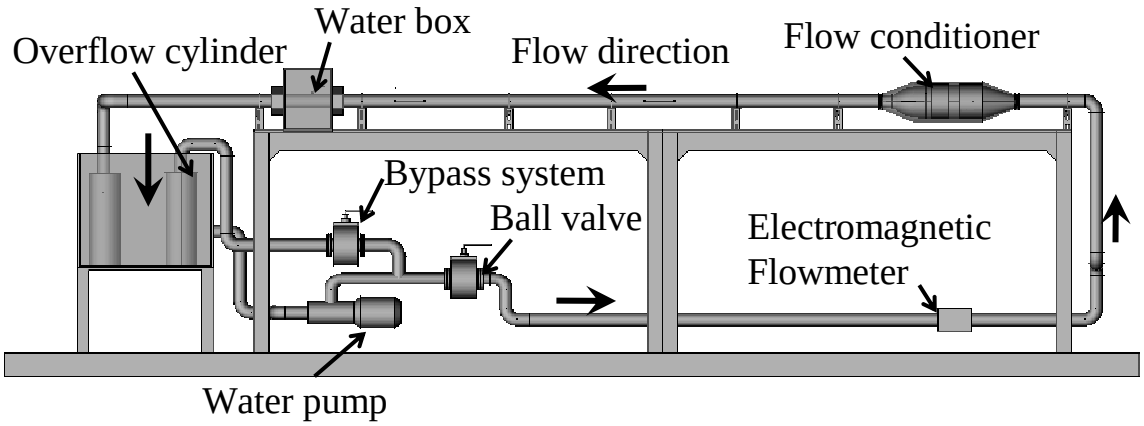

Fig. 2-10 Experimental apparatus of long straight pipe flow.

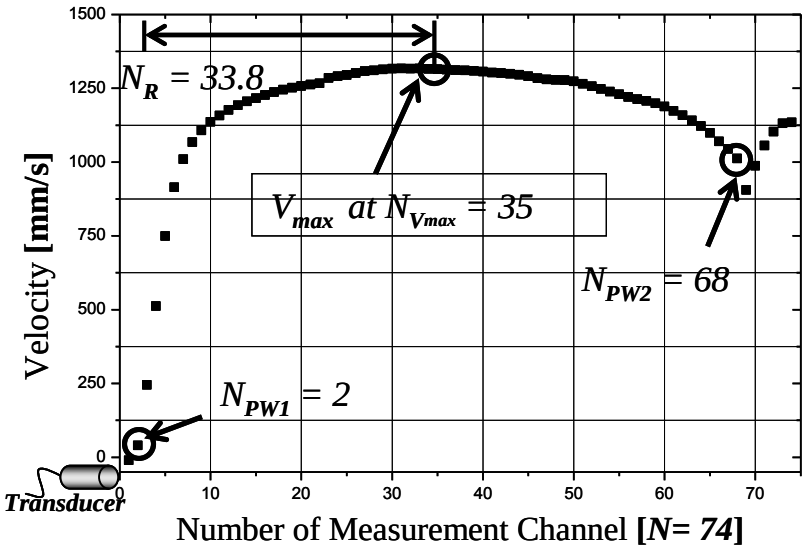

Fig.2-11 Raw profile of UVP for fully developed flow and indicated position of pipe wall on the profile.

CHAPTER 3

FLOWRATE MEASUREMENT DOWNSTREAM OF THE DOUBLE BENT PIPE USING UVP METHOD

3.1 INTRODUCTION

UVP is a method to obtain velocity profiles using ultrasonic wave. UVP method can measure detail and instantaneous velocity profiles without any installation of sensors into the pipe, and it doesn't need any calibration due to aging **[3-1]**. On the other hand, UVP method can measure only velocity profiles on the measuring line. One profile is enough to calculate flowrate if the flow is axially symmetric. However, real flow is not perfectly symmetric, and accumulation of velocity profiles is necessary for calculation of the flowrate. When the flow becomes complicated, optimization of the number of profiles, i.e. the number of ultrasonic sensors (transducers), becomes more important. Complicated flow can be realized easily after several flow bents, and the complexity is affected by distance from the bents. Here, basic characteristics of the UVP measurement is verified, and experiments using multiple transducers are executed against the flow after double bent. Accuracy of flowrate calculation using UVP method for the flow system is confirmed by comparison with flowrate of an electro-magnetic flowmeter, and optimization of the number of transducers and distance from the double bent is examined.

3.2 THEORY OF UVP METHOD

UVP method can measure instantaneous velocity profiles using ultrasound reflector. In nuclear plants, damage from Solid Particle has been found mostly in Steam generator blowdown lines transported from the steam generators, and Cooling water systems caused by ingested silt or sand. Kosel stated that: the size is above about 100 micro meter. UVP system includes at least one ultrasonic transducer, and the transducer can emit ultrasonic pulses. The ultrasound passes along the measuring line, going through the pipe wall and liquid **[3-2]**.

Pulse ultrasound waves are emitted from the transducer with basic frequency f_0 go into the flow with incident angle θ_w (see **Fig. 3-1**) and go along the measurement line. The ultrasonic pulses bounce back from the surface of particles flowing in the fluid with shifted frequency (shifted) f_d based on the Doppler principle, which is proportional to the velocity component along the measuring line of the particle, V_{TX}. Thus, UVP method can obtain only velocity component along ultrasonic path. By assuming a one-directional flow parallel to the streamwise direction, the velocity in the axial direction V_{axial} can be calculated as **Eq. (3-1):**

$$V_{axial} = V_{TX} / \sin \theta_f \quad \textbf{(3-1)}$$

where θ_f is the angle of ultrasound emitted into the fluid. V_{TX} is velocity in the direction of ultrasound beam path. V_{axial} is velocity in the direction of fluid flow.

The distance from transducer to the particle (L_f) on the measurement line can be also calculated from the ultrasonic echo signal. c_f is the sound velocity in the fluid. f_d is Doppler shift frequency at the instant gives us velocity information following relationship as **Eq. (3-2)**. f_0 is the basic frequency of ultrasonic which measuring instantaneous frequency as a function of time after the pulse emission. The traveling time (t_f) of the ultrasonic pulse is taken for the travel between the transducer and the reflecting particle. Thus, L_f can be calculated using t_f as following **Eqs. (3-2)-(3-3) [3-3]-[3.4].**

$$V_{TX} = \frac{c_f}{2 f_0} f_d \quad \textbf{(3-2)}$$

$$L_f = \frac{c_f t_f}{2} \quad \textbf{(3-3)}$$

3.3 MULTIPLE ULTRASONIC TRANSDUCERS MEASUREMENT ON DOUBLE BENT PIPE (USING UVP)

The flowmeter property of ultrasonic Doppler method in pipes depends on the alignment of measuring lines. The most accurate way is to make two-or three-dimensional flow mapping at a cross-section of the pipe. Accurate flow rate can be calculated by integrating the two- or three-dimensional and time-dependent velocity distributions. However, it requires a large number of measuring lines. Thus, optimization for the number of measuring lines is examined for complicated flow realized by double flow bent.

Figure 3-2 shows the multiple ultrasonic transducers measurement which all measuring lines were located along the diameter (passing the center of the pipe) with the fixed incident angle 10° as describe above to the main flow direction. The arrangement of the transducers and measuring lines is

shown in **Fig. 3-2 b).** Flow rate (*Q*) was calculated by the integration of velocity distributions in the directions of y-direction (vertical direction across center of the pipe) and z-direction (horizontal direction), two perpendicular directions to x-direction or fluid flow direction as shown in **Eq. (3-4).**

$$Q = \int \int \mathrm{V_x}\, \mathrm{dz}\, \mathrm{dy} \qquad \textbf{(3-4)}$$

Ultrasonic Doppler method for flowrate measurement requires only a single transducer whereby the measuring line goes through the center of the pipe as the simplest configuration, as shown in **Fig. 3-2 a).** If the flow is axially symmetric, the accurate flow rate *Q(t)* can be obtained accurately by integrating only the half of the velocity profile using **Eq. (3-5)**, which is obtained from the measuring line going through the center of the pipe:

$$Q(t) = \frac{\pi}{3}\left\{ \frac{R_0^3 - R_1^3}{R_0 - R_1} v_0 + \sum_{i=0}^{n-2} \frac{R_{i+1}^3 - R_{i+2}^3}{R_{i+1} - R_{i+2}} (v_{i+1} - v_i) + R_n^2 v_n \right\} \qquad (3\text{-}5)$$

where R_i is the distance from the pipe center to the calculating point, and v_i is the velocity of the point as shown in **Fig. 3-3**. Many ultrasonic transducers can be used when more accurate flowrate is desired or the flow is asymmetric flow. Flowrate using multiple flow profiles can be calculated by using the interpolation of each velocity profile. When flowrate near the bent pipe is measured by UVP method, many measurement lines are necessary to make two- or three-dimensional velocity profile mapping due to its asymmetric flow. The measuring lines shown in **Fig.3-2 b)** using equal angle is applied for interpolation **[3-5]**. At each measurement position, three transducer lines (line No.1, No.3 and No.4) were set on the outer surface of the measurement position with an interval angle of 120º for the measurement of three transducers, for example. Flow rate in the transient conditions downstream of double 90º bent was measured to investigate the accuracy of the flow rate measurement using this multi-lines method.

3.4 EXPERIMENTAL APPARATUS

Figure 3-4 shows the experimental apparatus that used in this study consists of a water circulation system piping system. It is designed to emphasize the formation of fully developed turbulent pipe flow. The flowrate can be changed and controlled by the bypass line and the valve. Water is circulated by a centrifugal pump. The pipeline system of almost all part is made of Polyvinyl

Chloride (PVC) except the test section. Before the test section, a flow conditioner designed to include the tube bundle, mesh plates and a turbulence promoter ring was installed to realize uniform velocity profiles[5]. Uniform velocity profile requires long pipe length. Therefore, the tube bundle flow conditioner is used at 30 D upstream of the double bent in order to reduce the flow rate measurement errors of the meter **[3-6]** (about ultrasonic reflector and two-phase flow).

Figure 3-5 illustrates the details of test section. The flow rate was monitored by an electromagnetic flow meter located upstream of the test section. The double bent pipe has an angle of curvature of 90º, average curvature of R = 30 mm. The test section at downstream of the double bent is made of acrylic pipe and the total length of the pipe is approximately 1.5 m, the inner diameter (D) and wall thickness are also 50 mm and 5 mm, respectively. Acrylic resin has a high transparency to both visible light and ultrasound.

Water box is used at the test section to apply water as couplant between the transducer and the pipe. The same material for couplant and working fluid makes angles the same for emission of ultrasound and the refraction into the working fluid. The couplant displaces the air and makes it possible to get more sound energy into the test specimen so that a usable ultrasonic. Signal can be obtained. In contact ultrasonic testing a thin film of oil, glycerin or water is generally used between the transducer and the test surface.

The flow measurement system is composed of the UVP-DUO model (Met Flow AG) and a PC, which records the flowrate obtained by an electromagnetic flow meter which error from the calculation in manual that is 0.54% and the error from volumetric flowrate measurement method is -0.35% as shown in **Table 3-1**. In addition, the temperature data by a thermometer. The summary of experimental conditions is shown in **Table 3-2**.

Table 3-2 shows the experimental conditions such as the basic frequency of the transducer is 8 MHz, Reynolds number was set at 40,000 and measuring points along the measurement line are 74. Nylon particles are dispersed in water as ultrasonic reflectors. Each particle has a diameter of approximately 80 μm, and a specific gravity of 1.02. The particles of this size can interweave with water, and can reflect ultrasonic wave of 8 MHz. As to size of the particle, experiment suggests approximately one fourth to one half of the wavelength is adequate. If the particle is smaller, then, this the reflection efficiency becomes lower and the energy of echo is too small to maintain a high

signal per noise ratio, reading to defection error. If the particle is larger, the probability of multiple reflections between particles becomes higher which would results in a distortion of the profile. The density of the particle is also important. A large different in densities between the fluid and particle might lead to an erroneous result because the particle does not follow the flow faithfully. Further, the concentration of the particles in the fluid is important. It should have only one particle per measuring volume, but this also depends on the velocity level of the flow field to be measured.

3.5 RESULTS AND DISCUSSIONS

Vortices and intensive turbulence flow will be occurred at downstream of the pipe bents, as mentioned above. Thus, complicated flow profile will be observed for this experimental apparatus.

Figure 3-6 a)-c) show velocity profiles at *L/D* = 4 D, 12 D and 20 D (D = Diameter of pipe). It is obvious that all velocity profile at 4 D **(Fig. 3-6 a))** are much different each other. The velocity profiles which locate at lower part of the pipe, i.e. far field (right side in the figure) of line No.1 and near field (left side) of line No.3 and 4, become lower than other parts. Horizontal velocity profile, line No.2, which measures velocity horizontally doesn't show such vertical position effect. The detail of the test section and the arrangement of measurement positions are also shown in **Fig. 3-5.** On the other hand, velocity profiles at 20 D, those are shown in **Fig. 3-6 c),** shows almost symmetric profiles similar to those of the fully developed flow because of the distance from the double bent enough to develop almost fully.

Table 3-3 summarizes the error of the calculated flowrates by UVP measurement to flowrate of the electro-magnetic flowmeter for each result. Flowrate calculations from obtained velocity profiles at each position were examined using the data of only the near field or the full data with **Eq. (16).** Interpolation results are also listed, one is using two profiles of No. 1 and No. 2, the other is using three profiles of No. 1, No. 3 and No. 4.

Figure 3-7 shows the error of the calculated flowrate against the distance after the double bent (*L/D*). They become lower as the distance from the bent becomes long. The result of interpolation shows good agreement with the flowrate of electro-magnetic flowmeter. Especially, the error of interpolation using 3 line measurements (line No.1, 3, 4) was not beyond 4 percent. Therefore, multiline ultrasonic velocity measurements are confirmed as very effective for flowrate measurement

even when the flow is complicated. Errors at 5 D are become less than those of nearer positions, i.e. 2 D, 3 D or 4 D. For example, the error of line no.1 is decreasing from 29.01% at 2 D to 6.22% at 5 D. At 20 D, as mentioned above around, the profiles are almost fully developed and symmetry. After all, the flowrate errors of interpolation calculations using three profiles are less than 1% at the distance over 5 D.

3.6 CONCLUSIONS

Flowrate measurement on the double bent pipe. Flow rate in the transient conditions downstream of double 90º bent was measured to investigate the accuracy of the flow rate measurement using this multi-lines method. Many ultrasonic transducers can be used when more accurate flowrate is desired or the flow is asymmetric flow. Flowrate using multiple flow profiles can be calculated by using the interpolation of each velocity profile. When flowrate near the bent pipe is measured by UVP method, many measurement lines are necessary to make two- or three-dimensional velocity profile mapping due to its asymmetric flow. Experimental flowrate measurements on the system were executed for Re ~ 40,000. The velocity profiles were obtained at the distance 2 D, 3 D and 5 D from the bent where the flow is complicated due to existence of vortices. From experimental results using 1-3 transducers, flowrate for each distance is calculated using integration and interpolation. The accuracy of this method is evaluated by comparison with the flowrate value of electro-magnetic flowmeter installed in the experimental loop. It is concluded that accurate flowrate will be calculated in the condition of using three transducers and the distance is over 3 D within 4% error.

REFERENCES

[3-1] Y. Inoue, H. Kikura, H. Murakawa, M. Aritomi, M. Mori: A study of ultrasonic propagation for ultrasonic flow rate measurement, Flow Measurement and Instrument, Vol. 19, pp. 223-232, 2008

[3-2] Y. Takeda, Development of an ultrasound velocity profile monitor, Nuclear engineering and design, Vol. 126, pp. 277-284, 1991

[3-3] W., Treenuson, N., Tsuzuki, H., Kikura, M., Aritomi, S., Wada and K., Tezuka, Accurate Flowrate Measurement on the Double Bent Pipe using Ultrasonic Velocity Profile Method, Japanese Society for Experimental Mechanics, Vol. 13, No.2, pp. 200-211, 2013

[3-4] S. Wada, K. Tezuka, W. Treenuson, N. Tsuzuki and H. Kikura, Study on the optimal number of

transducers or pipe flow rate measurement downstream of a single elbow using the ultrasonic velocity profile method, Science and Technology of Nuclear Installations, pp. 1-12, 2012.

[3-5] R. Rans, Flow conditioning and effects on accuracy for fluid flow measurement, Proc.7th South East Asia Hydrocarbon Flow Measurement Workshop, 2008.

[3-6] L. Johan and J. Driesen: Wavelet-Based Power Quantification Approaches, IEEE Transactions on Instrumentation and Measurement, vol. 52, No.4, 2003.

Accuracy

● Pulse output : For velocity ≥1.0m/s; ±0.5% of reading
For velocity <1.0m/s;
$\pm(0.3\%\text{ of reading} + 0.2\% \times \frac{1}{\text{Velocity (m/s)}})$

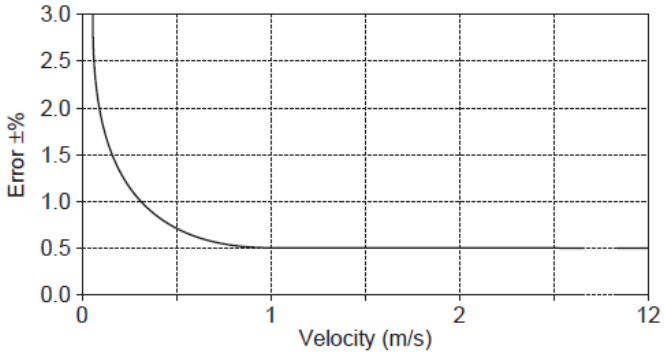

● Current output : The following additional error is to be added onto pulse output accuracy;
±0.05% of full scale

Table 3-1 Error of volumetric measuring method

no. test	Electromagnetic flow meter (l/min)		volumetric method (l/min)		%error	
1	124.5		124.88		-0.30429212	
2	124.9		125.9776		-0.85539016	
3	124.7		125.20421		-0.4027101	
4	125.1		124.95		0.120048019	
5	125.1		125.84727		-0.59379119	
6	125		125.17647		-0.14097697	
7	125.4		125.19111		0.166856896	
8	125.3		125.84727		-0.43486839	
9	124.4		126.23059		-1.45019523	
10	125.7		125.24522		0.363111662	
average	125.01	l/min	125.454974	l/min	-0.35468821	%

Table 3-2 Experimental conditions

Testing conditions	Units	Values
Reynolds Number	-	40,000
Number of measuring point	-	74
Channel width	mm	0.74
Basic frequency	MHz	8
Incident angle	Degree	10

Table 3-3 Flow rate and percentage of error using UVP.

	Line No.1		Line No.2		Line No.3		Line No.4		1- 2		1- 3 - 4	
	L/min	% error	L/min	% error	L/min	% error	L/min	% error	L/min	% error	L/min	% error
2*D*	144	35.21	101.8	-4.41	95.27	-10.54	95.75	-10.09	122.9	15.40	111.673	4.86
3*D*	136.5	28.17	104.5	-1.88	96.29	-9.59	96.54	-9.35	120.5	13.15	109.777	3.08
4*D*	121.01	13.62	98.82	-7.21	101.01	-5.15	102.6	-3.66	109.915	3.21	108.207	1.60
5*D*	113.12	6.22	102.6	-3.66	103.1	-3.19	106.02	-0.45	107.86	1.28	107.413	0.86
6*D*	112.4	5.54	105.27	-1.15	103.94	-2.40	107.14	0.60	108.835	2.19	107.827	1.25
12*D*	105.05	-1.36	107.02	0.49	106.61	0.10	105.83	-0.63	106.035	-0.44	105.83	-0.63
14*D*	107.04	0.51	106.68	0.17	106.68	0.17	106.92	0.39	106.86	0.34	106.88	0.36
16*D*	106.82	0.30	102.54	-3.72	105.77	-0.69	107.12	0.58	104.68	-1.71	106.57	0.07
18*D*	106.16	-0.32	108.64	2.01	107.37	0.82	106.19	-0.29	107.4	0.85	106.573	0.07
20*D*	105.85	-0.61	108.11	1.51	106.24	-0.24	107.37	0.82	106.98	0.45	106.487	-0.01

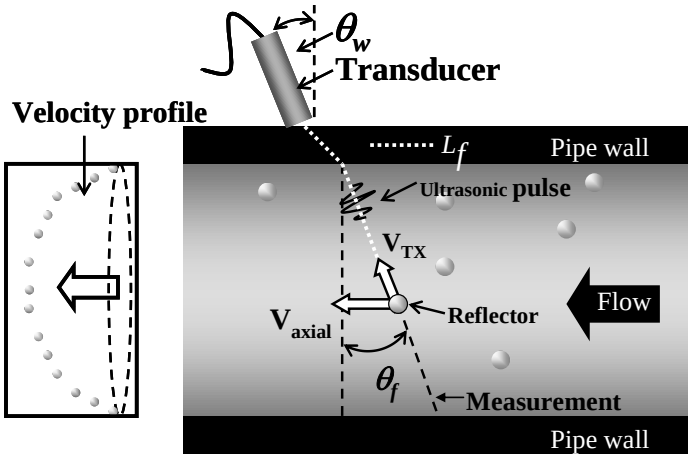

Fig. 3-1 Measurement scheme of the UVP measurement.

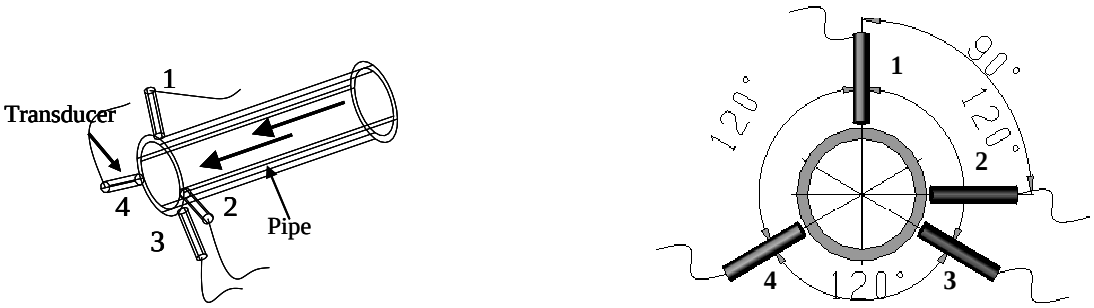

a) b)

Fig. 3-2 Transducers Arrangement.

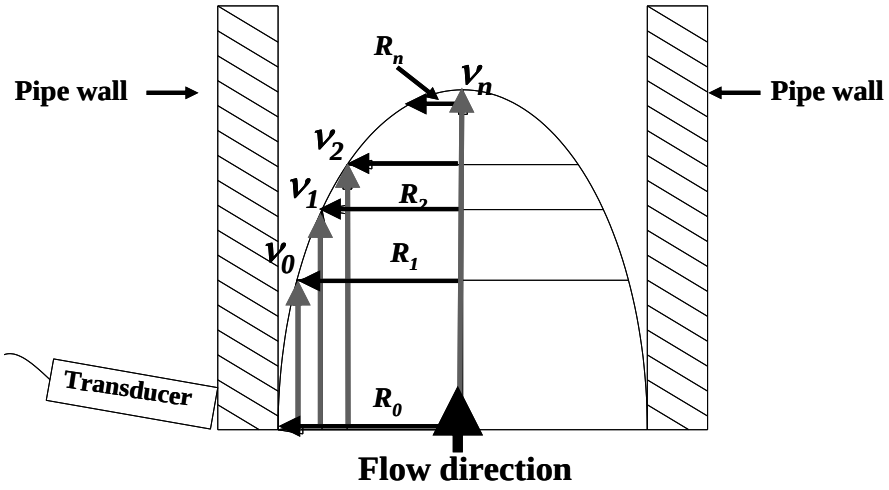

Fig. 3-3 Variable in the equation of flowrate calculation.

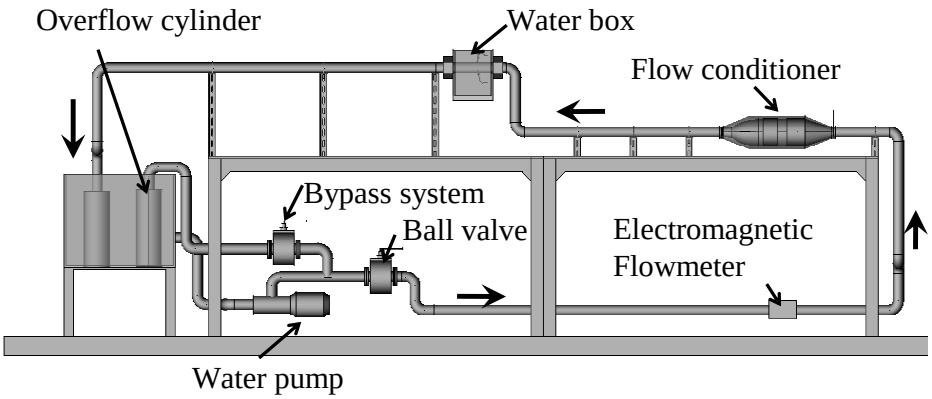

Fig. 3-4 Experimental apparatus of double bent pipe flow.

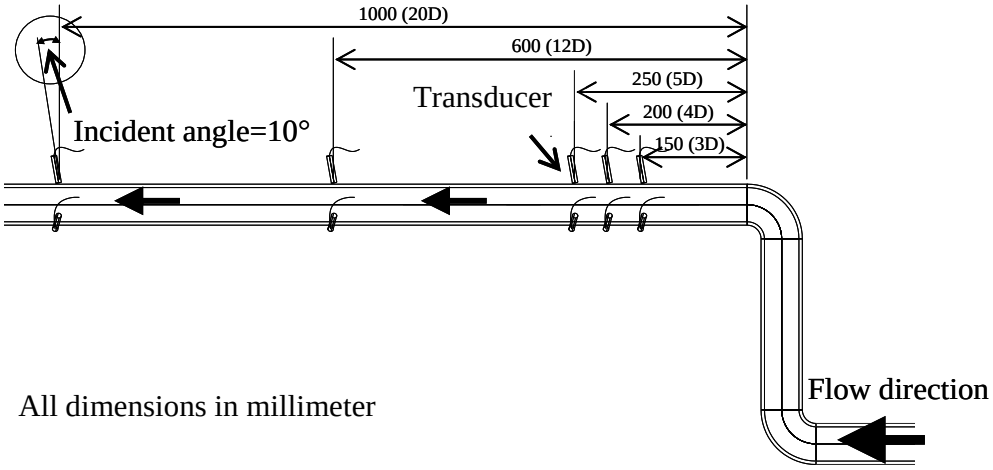

Fig. 3-5 Detail configurations at the test section (2 D – 20 D).

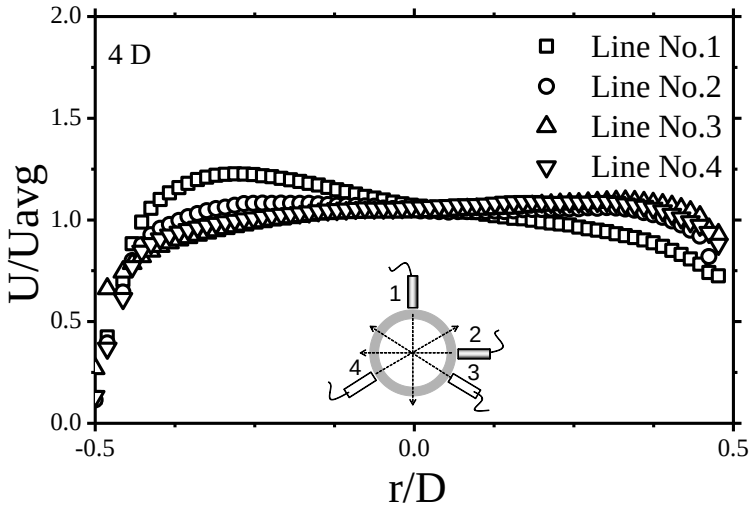

a) Velocity profiles at 4 D

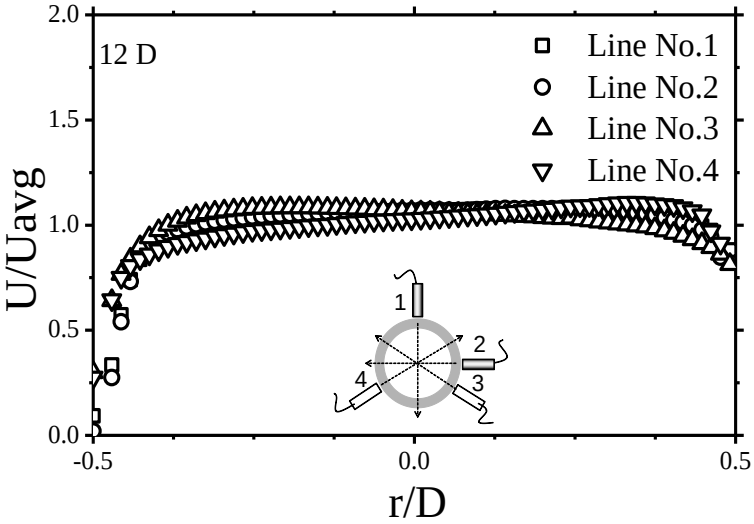

b) Velocity profiles at 12 D

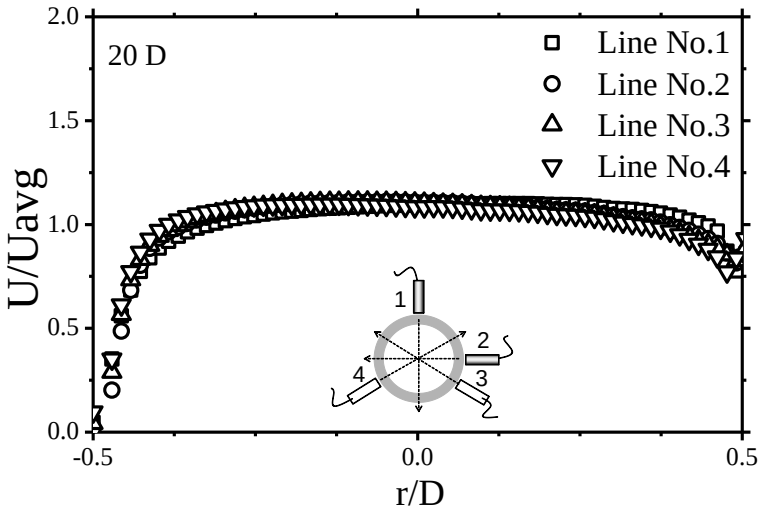

c) Velocity profiles at 20 D

Fig.3-6 Four velocity profiles at each of downstream position of the double bent.

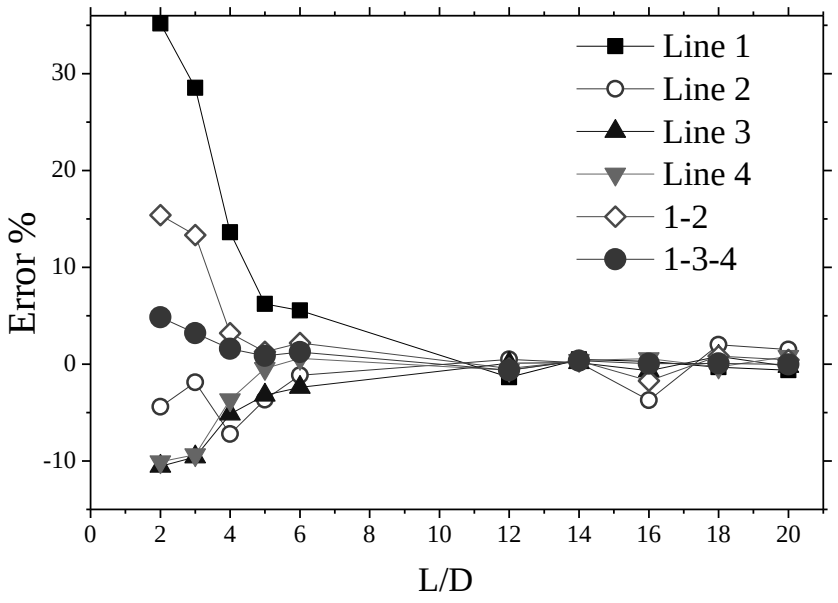

Fig. 3-7 Error of flow rate calculation from UVP.

CHAPTER 4

NUMERICAL CALCULATION DOWNSTREAM OF THE DOUBLE BENT PIPE

4.1 INTRODUCTION

UVP measurement can obtain only velocity profiles in line. Usual Particle Image Velocimetry (PIV) gives two-dimensional velocity mapping; however, PIV cannot obtain the flow distribution instantaneously. Hence, it is difficult to obtain fully three-dimensional velocity profile experimentally. To evaluate this limitation of experimental method, the numerical simulations using Computational Fluid Dynamics (CFD) were conducted.

Numerical simulation calculation can give fully three-dimensional velocity profiles as shown in **Fig.4-1**. In these days, computers are well developed, and numerical simulation becomes very popular and useful method to obtain velocity profiles because of its costs compare to the real experimental. Thus, simulation calculation was performed for the experimental condition, and the numerical result was compared with the experimental one as velocity profiles along the measuring lines. It can confirm both experimental and numerical results.

4.2 THEORY

4.2.1 Turbulent Model

Because of the condition in nuclear power plant is the turbulence flow especially at circulation water system, we need to model the simulation model as the fully turbulence flow. In addition, the turbulence model has many kinds of calculations. The outstanding feature of a turbulent flow, in the opposite of a laminar flow, is that the molecules move in a chaotic fashion along complex irregular paths. The strong chaotic motion causes the various layers of the fluid to mix together intensely. Because of the increased momentum and energy exchange between the molecules and solid walls, turbulent flows lead at the same conditions to higher skin friction and heat transfer as compared to laminar flows. Although the chaotic fluctuations of the flow variables are of deterministic nature, the simulation of turbulent flows still continues to present a significant problem. Basic Equations of turbulence can be rewritten the governing equations **(4-1)** in differential form, since this is used very often in literature on turbulence modelling. Furthermore, it allows for a compact and clear notation. However, we will also provide examples of turbulence equations in integral form. In the case of a compressible Newtonian fluid, the Navier-Stokes equations read in absence of source terms in

coordinate invariant formulation. Despite the performance of modern supercomputers, a direct simulation of turbulence by the time-dependent Navier-Stokes equations **(4-1).**

$$\frac{\partial}{\partial t}(\rho v_i)+\frac{\partial}{\partial x_j}(\rho v_j v_i)=-\frac{\partial p}{\partial x_i}+\frac{\partial \tau_{ij}}{\partial x_j} \qquad \textbf{(4-1)}$$

Direct Numerical Simulation (DNS) **[4-1]** - is applicable only to relatively simple flow problems at low Reynolds numbers *(Re).* A more widespread utilization of the DNS is prevented by the fact that the number of grid points needed for sufficient spatial resolution scales as $Re^{9/4}$ and the CPU-time as Re^3. Therefore, we are forced to account for the effects of turbulence in an approximate manner. For this purpose, a large variety of turbulence models was developed and the research still goes on. There are five principal classes of turbulence models:

- algebraic,
- one-equation,
- multiple-equation,
- second-order closures (Reynolds-stress models),
- Large-Eddy Simulation (LES).

The first tree models belong to the so-called first-order closures. They are based mostly on the *eddy-viscosity* hypothesis of Boussinesq **[4-2]-[4-3].** But for certain applications also on *non-linear eddy-viscosity* formulations. An overview of the classes of turbulence models, which are sorted according to their decreasing level of complexity, is displayed in Fig. **4-1.** One should be aware of the fact that there is no single turbulence model, which can predict reliably all kinds of turbulent flows. Each of the models has its strengths and weaknesses. For example, if a particular model works perfectly in the case of attached boundary layers, it may fail completely for separated flows. Thus, it is important always to ask whether the model includes all the significant features of the flow being investigated. Another point which should be taken into consideration is the computational effort versus the accuracy required by the particular application. It means that in many cases a numerically inexpensive turbulence model can predict some global measures with the same accuracy as a more complex model.

Many turbulence models are based upon the Boussinesq hypothesis. It was experimentally observed that turbulence decays unless there is shear in isothermal incompressible flows. Turbulence was found to increase as the mean rate of deformation increases. Boussinesq proposed in 1877 that the Reynolds stresses could be linked to the mean rate of deformation. Using the suffix notation where i, j, and k denote the x-, y-, and z-directions respectively, viscous stresses are given by:

$$\tau_{ij} = \mu\, e_{ij} = \mu\left(\frac{\partial u_i}{\partial x_j} + \frac{\partial u_j}{\partial x_i}\right) \qquad \textbf{(4-2)}$$

- Classical models. Based on Reynolds Averaged Navier-Stokes (RANS) equations (time averaged):

    1. Zero equation model: mixing length model.
    2. One equation model: Spalart-Almaras.
    3. Two equation models: k-ε style models (standard, RNG, realizable), k-ω model, and ASM.
    4. Seven equation model: Reynolds stress model.

- The number of equations denotes the number of additional PDEs that are being solved.
- Large eddy simulation. Based on space-filtered equations. Time dependent calculations are performed. Large eddies are explicitly calculated. For small eddies, their effect on the flow pattern is taken into account with a "subgrid model" of which many styles are available.

The numerical solution of the Navier–Stokes equations for turbulent flow is extremely difficult, and due to the significantly different mixing-length scales that are involved in turbulent flow, the stable solution of this requires such a fine mesh resolution that the computational time becomes significantly infeasible for calculation (see Direct numerical simulation). Attempts to solve turbulent flow using a laminar solver typically result in a time-unsteady solution, which fails to converge appropriately. To counter this, time-averaged equations such as the Reynolds-averaged Navier–Stokes equations (RANS), supplemented with turbulence models, are used in practical computational fluid dynamics (CFD) applications when modeling turbulent flows. Some models

include the Spalart-Allmaras, k-ω (k-omega), k-ε (k-epsilon), and SST models which add a variety of additional equations to bring closure to the RANS equations. Another technique for solving numerically the Navier–Stokes equation is the Large eddy simulation (LES). This approach is computationally more expensive than the RANS method (in time and computer memory). From RANS method, at high Reynolds numbers the rate of dissipation of kinetic energy epsilon $\in$ is equal to the viscosity multiplied by the fluctuating vorticity. An exact transport equation for the fluctuating vorticity, and thus the dissipation rate, can be derived from the Navier Stokes equation. The k - epsilon model consists of the turbulent kinetic energy equation:

$$\underset{\text{I}}{\frac{\partial(\rho k)}{\partial t}} + \underset{\text{II}}{div(\rho k U)} = \underset{\text{III}}{div\left[\frac{\mu_t}{\sigma_k} grad\ k\right]} + \underset{\text{IV}}{2\mu_t E_{ij} E_{ij} G} - \underset{\text{V}}{\rho \in} \qquad \textbf{(4-3)}$$

where E_{ij} is fluctuating component of rate of deformation tensor.

This equation can be read as:

I - the rate of change of k, plus

II - transport of k by convection, equals

III - transport of k by pressure, plus

IV - transport of k by viscous stresses, plus

V - transport of k by Reynolds stresses, minus.

and the dissipation rate equation:

$$\underset{(\text{I})}{\frac{\partial \in}{\partial t}} + \underset{(\text{II})}{div(\rho \underline{u} \in)} = \underset{(\text{III})}{div\left(\left[\mu_{lam} + \frac{\rho \upsilon_t}{\sigma_k}\right] grad \in\right)} + \underset{(\text{IV})}{C_{1\in} \rho \upsilon_t G \frac{\in}{k}} - \underset{(\text{V})}{C_{2\in} \rho \frac{\in^2}{k}} \qquad \textbf{(4-4)}$$

(I) Rate of increase

(II) Convective transport

(III) Diffusive transport

(IV) Rate of production

(V) Rate of destruction

where G represents the turbulent generation rate which is equal to

$$G = 2\left(\left[\frac{\partial u}{\partial x}\right]^2 + \left[\frac{\partial v}{\partial y}\right]^2 + \left[\frac{\partial w}{\partial z}\right]^2\right) + \left(\frac{\partial u}{\partial y} + \frac{\partial v}{\partial x}\right)^2 + \left(\frac{\partial u}{\partial z} + \frac{\partial w}{\partial x}\right)^2 + \left(\frac{\partial w}{\partial y} + \frac{\partial v}{\partial z}\right)^2 \quad \textbf{(4-5)}$$

In the implementation of this model the Kolmogorov - Prandtl expression for the turbulent viscosity is used

The eddy viscosity is obtained as:

$$G = C_\mu \frac{k^2}{\varepsilon} \quad \textbf{(4-6)}$$

The K-epsilon model is one of the most common turbulence models, although it just doesn't perform well in cases of large adverse pressure gradients **[4-4]**. It is a two equation model, that means, it includes two extra transport equations to represent the turbulent properties of the flow. This allows a two equation model to account for history effects like convection and diffusion of turbulent energy. The first transported variable is turbulent kinetic energy, *k*. The second transported variable in this case is the turbulent dissipation: ε. It is the variable that determines the scale of the turbulence, whereas the first variable, k, determines the energy in the turbulence.

There are two major formulations of K-epsilon models **[4-5, 4-6]**. That of Launder and Sharma is typically called the "Standard" K-epsilon Model. The original impetus for the K-epsilon model was to improve the mixing-length model, as well as to find an alternative to algebraically prescribing turbulent length scales in moderate to high complexity flows.

The k-epsilon model has been shown to be useful for free-shear layer flows with relatively small pressure gradients. Similarly, for wall-bounded and internal flows, the model gives good results only in cases where mean pressure gradients are small; accuracy has been shown experimentally to be

reduced for flows containing large adverse pressure gradients. One might infer then, that the k-epsilon model would be an inappropriate choice for problems such as inlets and compressors.

The description equations of the turbulent model illustrate as:
Turbulent Kinetic Energy Equation:

$$\frac{\partial}{\partial x_j}\left(\rho v_j k\right) = \frac{\partial}{\partial x_j}\left(\left(\mu + \frac{\mu_t}{\sigma_k}\right)\frac{\partial k}{\partial x_j}\right) + P - \rho\varepsilon - \rho\varepsilon_p \qquad \textbf{(4-7)}$$

RNG k - ε Model **[4-7]**

$$\frac{\partial}{\partial x_j}\left(\rho v_j \varepsilon\right) = \frac{\partial}{\partial x_j}\left(\left(\mu + \frac{\mu_t}{\sigma_\varepsilon}\right)\frac{\partial \varepsilon}{\partial x_j}\right) + \left(C_{\varepsilon 1} P - C_{\varepsilon 2}\rho\varepsilon\right)\frac{\varepsilon}{k} - S_\varepsilon \qquad \textbf{(4-8)}$$

$$P = \mu_t \frac{\partial v_i}{\partial x_j}\left(\frac{\partial v_i}{\partial x_j} + \frac{\partial v_j}{\partial x_i}\right) \qquad , \quad \mu_t = C_\mu \rho \frac{k^2}{\varepsilon}$$

$$C_\mu = 0.09 \quad , C_{\varepsilon 1} = 1.44 \quad , C_{\varepsilon 2} = 1.92 \quad , \sigma_k = 1.0 \quad , \sigma_\varepsilon = 1.3$$

4.2.1 Wall treatments and wall functions

A wall treatment is the set of near-wall modelling assumptions for each turbulence model. Three types of wall treatment are provided in FLUENT, although all three might not always be available, depending on the turbulence model: The high y+ wall treatment implies the wall function type approach in which it is assumed that the near-wall cell lies within the logarithmic region of the boundary layer. The low y+ wall treatment is suitable only for low Reynolds number turbulence models in which it is assumed that the viscous sub-layer is properly resolved. The all y+ wall treatment is a hybrid treatment that attempts to emulate the high wall treatment for coarse meshes

and the low y+ wall treatment for fine meshes. It is also formulated with the desirable characteristic of producing reasonable answers for meshes of intermediate resolution (that is, when the wall-cell centroid falls within the buffer region of the boundary layer).

The wall functions are a set of semi empirical functions used to satisfy the physics of the flow in the near wall region. Turbulence is affected in many ways by the presence of the wall through the non-slip condition that must be satisfied at the wall. Four areas in the near wall region are defined, the laminar sub-layer, the blending region, the log law region and the outer region. Each region has a different effect on turbulence and a particular care must be taken to the y+ position of the first cell in the boundary layer. A different set of equations will be used depending on the size of this cell but however this one must not be comprised between y+=5 and y+=30 because no turbulent model is available in this area. Instead of not resolving the entire boundary layer for a y+ comprised in the viscous sub-layer and buffer layer, wall functions are used to bridge the viscosity-affected region between the wall and the fully-turbulent region.

The standard wall functions described so far are provided as a default option in FLUENT. The standard wall functions work reasonably well for a broad range of wall-bounded flows. However, they tend to become less reliable when the flow situations depart too much from the ideal conditions that are assumed in their derivation. Among others, the constant-shear and local equilibrium hypotheses are the ones that most restrict the universality of the standard wall functions. Accordingly, when the near-wall flows are subjected to severe pressure gradients, and when the flows are in strong non-equilibrium, the quality of the predictions is likely to be compromised.

Non-Equilibrium Wall Functions In addition to the standard wall function described above (which is the default near-wall treatment) a two-layer-based, non-equilibrium wall function is also available. The key elements in the non-equilibrium wall functions are as follows Launder and Spalding's log-law for mean velocity is sensitized to pressure-gradient effects. The two-layer-based concept is adopted to compute the budget of turbulence kinetic energy in the wall-neighboring cells. The law-of-the-wall for mean temperature or species mass fraction remains the same as in the standard wall function described above.

Enhanced wall treatment is a near-wall modeling method that combines a two-layer model with enhanced wall functions. If the near-wall mesh is fine enough to be able to resolve the laminar

sublayer (typically), then the enhanced wall treatment will be identical to the traditional two-layer zonal model (see below for details). However, the restriction that the near-wall mesh must be sufficiently fine everywhere might impose too large a computational requirement. Ideally, then, one would like to have a near-wall formulation that can be used with coarse meshes (usually referred to as wall-function meshes) as well as fine meshes (low-Reynolds-number meshes). In addition, excessive error should not be incurred for intermediate meshes that are too fine for the near-wall cell centroid to lie in the fully turbulent region, but also too coarse to properly resolve the sublayer. To achieve the goal of having a near-wall modeling approach that will possess the accuracy of the standard two-layer approach for fine near-wall meshes and that, at the same time, will not significantly reduce accuracy for wall-function meshes, **FLUENT** can combine the two-layer model with enhanced wall functions, as described in the following sections.

4.3 CALCULATION MODEL

CFD analysis was performed with the same configuration as around the test section of the experimental apparatus. A CFD code, ANSYS FLUENT, was used to simulate a pipe flow downstream of double elbows. To collect as the real case, the modelling every dimension of experimental apparatus such as pipe diameter, bent pipe inner radius and outer pipe radius of the bent etc. are designed as shown in **Fig. 4-2**. The evaluating regions of velocity profiles were located at 3 times of a pipe diameter (3 D), 4 times of a pipe diameter (4 D) and 5 times of a pipe diameter (5 D) downstream of the second bent pipe same as the experimental condition. Reynolds numbers is 4×10^4.

Figure 4-3 shows the mesh layout around the elbows. The average size of meshes is 0.8 mm and boundary layers of 5 meshes are placed near the pipe wall. The thickness of the boundary layer at the vicinity of the wall is 0.02 mm, and the thickness becomes gradually larger with the distance from the wall. The number of meshes is 5,134,179.

As mentioned above, FLUENT 12.0 was used as simulation code. Turbulent model is K-epsilon, and second order discretization is used for flow, pressure, turbulent energy and turbulence dissipation rate. SIMPLE method is applied as coupling scheme of velocity and pressure. Intel R Xeon (TM) processor of 3.2 GHz and Windows 7 Professional edition (TM) of 64 bit version as operating

system are used for the simulation calculation, and 6.39 hours are taken for the calculation.

4.4 RESULTS AND DISCUSSIONS

4.4.1 STRAIGHT DOUBLE BENT PIPE FLOW

Figure 4-5 shows the velocity vector in the plane which includes the center line of the pipe. A vortex exists close to the elbow, between 1 D and 2 D. Thus, velocity profiles in this area become complicated because of this vortex which results to the asymmetric velocity profile.

Table 4-2 shows the value of calculated flowrate from each velocity profiles on line and interpolation results of the profiles using **Eq. (16)** for 2 D to 20 D, each profiles are obtained from the simulation result. The Reynolds number is 40,000, as same as experimental condition. Flowrate of line no.1 is significant higher than line no. 3 and 4 at left side of **Fig. 4-6** because the directions of profiles are different which the upper side of pipe are higher than the lower half area of the pipe, as shown experimentally in **Table 4-1**.

Figure 4-6 illustrates velocity profiles on 4 measurement lines of the simulation result at the distance L/D is 5 D from the second elbow. Measurement line no. 1 the velocity at near field that is the area near the transducer were higher than the far field according the velocity vector as shown in **Fig. 4-7**. On the other hand, the velocity near field from measurement line no. 3 and 4 were lower than the far field area. These profiles were similar to the experimental results using UVP, as already shown in **Fig. 4-7**.

Figure 4-7 shows the error of the flowrate for measurement lines and interpolation results at 2D, 3D, 4 D, 5 D, 12 D and 20 D. The difference between No.3 and No.4 may be caused by asymmetrical mesh distribution to the vertical plane. The percentage of errors from these results shows that is decreasing when the distance far from the double bent pipe. Between 2 D to 6 D, the errors are quite high. Then after 12 D, the errors become lower because the transient area from asymmetrical velocity to symmetrical velocity profile.

In order to investigate the CFD model and corrected the experimental data, we try to test for the according model to the experiment. Therefore, many turbulent models such as K-epsilon RNG

model with enhance wall treatment function **Fig.4-8-4-9**. The results show the difference of the velocity profile on measurement line number 2 at 2D as shown in **Fig 4-10**. The velocity profile at 2D from K-epsilon RNG model with enhance wall treatment function are quite different from the real experiment results. So, this is not match in the theoretical with the pipe flow of our condition.

The results from K-epsilon RNG model with standard wall treatment function **Fig.4-11-4-12**. The results show a acceptance of the velocity profiles on measurement line number 2 at 2D as shown in **Fig 4-13**. The velocity profile at 2D from K-epsilon RNG model with enhance wall treatment function are quite different from the real experiment results. So, this is not match in the theoretical with the pipe flow of our condition. The results from K-epsilon RNG model with standard wall treatment function **Fig.4-14-4-15** at 3D. The results from K-epsilon RNG model with standard wall treatment function **Fig.4-16-4-17** at 4D. The results from K-epsilon RNG model with standard wall treatment function **Fig.4-18-4-19** at 5D.

4.4.2 INCLINATION DOUBLE BENT PIPE FLOW (OUT OF PLANE) K-EPSILON RNG MODEL STANDARD WALL CONDITION.

In order to investigate the CFD model and corrected the experimental data in the case of out-of-plane double bent pipe, we try to test for the according model to the experiment. Therefore, there are main 4 turbulent models such as K-epsilon model RNG with standard wall K-epsilon model with enhance wall treatment function, K-omega model shear stress transport (SST), LES (large eddy simulation) had been determined. The velocity profiles from the measurement lines same as the experiment are shown in every turbulence model.

Figure 4-20-28 show the velocity contour and vector contour at 2D, 3D, 4D and 5D respectively from K-epsilon RNG model with standard wall treatment function. These velocity profiles are good agreement with experimental data. The standard wall treatment function is good for the logarithmic law for mean velocity is known to be valid and it works reasonably well for a broad range of wall-bounded flows. **Figure 4-29-37** show velocity profile at 2D, 3D, 4D and 5D from K-epsilon RNG model with enhance wall treatment function are quite different from the real experiment results. This is because enhance wall treatment function is good for wall thermal formulation, laminar sub-layer, buffer region, and fully turbulent outer region and the function of wall is variable wall condition.

Figure 4-38-42 show velocity profile at 2D, 3D, 4D and 5D from K-epsilon Standard model with standard wall treatment function are quite different from the real experiment results. Because this turbulent model is poor predictions for swirling and rotating flows, flows with strong separation, fully developed flows.

Figure 4-43-56 show velocity profile at 2D, 3D, 4D and 5D from K-omega Shear Stress Transport (SST) model with standard wall treatment function are quite different from the real experiment results. Because this model is useful for the flow as physically most complete model and strong depend on the turbulent stress. However, the weak point of this model is requirement of more CPU of calculation time and it is strongly depend on momentum and turbulence equations.

Figure 4-57-68 show velocity profile at 2D, 3D, 4D and 5D from Realizable K-epsilon with standard wall treatment function are quite different from the real experiment results. This is because of the application of this model is good for the round-jet anomaly. This model is poor predictions for swirling and rotating flows, flows with strong separation, fully developed flows

Figure 4-69-82 show velocity profile at 2D, 3D, 4D and 5D from Large eddy simulation (LES). The results of this model are quite different from the real experiment results. The comparison with this turbulent model to the experimental results are not agree, because it will make a very large error. The advantage to this turbulent model is for not complicated flow and without swirling flow and secondary flow.

4.5 CONCLUSSIONS

Numerical calculation for the same condition is executed using CFD code, FLUENT. Those results of experimental and numerical are almost coincident; accordingly, the results are validated each other. The CFD result is almost coincident as experimental one. Accordingly, the numerical result can confirm the experimental results. The confirmation of the simulation model was tested in many kinds of the model as illustrated below. In the case of in-plane double bent pipe, the results of K-epsilon RNG model with standard wall function is the best agreement with the experimental results. In addition, for the out-of-plane double bent pipe, the K-epsilon RNG model with standard wall function is also the best agreement compare with the experimental results. In numerical

calculation, measurement lines were setup in simulation model like the demonstration of experiment in theoretical method. The number of data should sufficient to plot the velocity profile precisely. For this reason, the number of mesh should be considered. It can confirm both experimental and numerical results.

REFERENCES

[4-1] J., Blazek, Computational Fluid Dynamics: Principles and Applications, Elsevier, Great Britain, 2005.

[4-2] J., Boussinesq, Essai sur la the'orie des eaux courantes. Mem. Pres. Acad. Sci., XXIII, 46, Paris, 1877.

[4-3] J., Boussinesq, Theorie de I' 6coulement tourbillonant et tumubteur des liquides dans les lits rectiligues. Comptes Rendus de 1' Acad. des Sciences, CXXII, p. 1293, 1896.

[4-4] C.W., David, "Turbulence Modeling for CFD". Second edition. Anaheim: DCW Industries, 1998. pp. 174. 1998.

[4-5] P.W., Jones and Launder, B. E., The Prediction of Laminarization with a Two-Equation Model of Turbulence, International Journal of Heat and Mass Transfer, vol. 15, 1972, pp. 301-314. 1972.

[4-6] B. E., Launder and B. I., Sharma, Application of the Energy Dissipation Model of Turbulence to the Calculation of Flow Near a Spinning Disc, Letters in Heat and Mass Transfer, vol. 1, no. 2, pp. 131-138. 1974.

[4-7] D., Choudhury, Introduction to the Renormalization Group Method and Turbulence Modeling, Fluent Inc. Technical Memorandum TM-107, 1993

Table 4-1 Flow rate calculation and percentage of error from CFD

Model	Strengths	Weaknesses
STD k-ε	Robust, economical, reasonably accurate; long accumulated performance data.	Mediocre results for complex flows with severe pressure gradients, strong streamline curvature, swirl and rotation. Predicts that round jets spread 15% faster than planar jets whereas in actuality they spread 15% slower.
RNG k-ε	Good for moderately complex behavior like jet impingement, separating flows, swirling flows, and secondary flows.	Subjected to limitations due to isotropic eddy viscosity assumption. Same problem with round jets as standard k-ε.
Realizable k-ε	Offers largely the same benefits as RNG but also resolves the round-jet anomaly.	Subjected to limitations due to isotropic eddy viscosity assumption.
Shear Stress Transport	Physically most complete model (history, transport, and anisotropy of turbulent stresses are all accounted for).	Requires more cpu effort (2-3x); tightly coupled momentum and turbulence equations.

Table 4-2 Flow rate calculation and percentage of error from CFD

L/D	Line No.1		Line No.2		Line No.3		Line No.4		1- 2		1- 3 - 4	
	l/min	% error	*l*/min	% error	*l*/min	% error	*l*/min	% error	*l*/min	% error	*l*/min	% error
2D	140.8	32.21	104.1	-2.25	95.8	-10.05	96.22	-9.65	122.45	14.98	110.94	4.17
3*D*	137.465	29.08	105.3	-1.13	96.08	-9.78	96.51	-9.38	121.383	13.97	110.018	3.30
4*D*	127	19.25	104.35	-2.02	97.95	-8.03	98.96	-7.08	115.675	8.62	107.97	1.38
5*D*	123.54	16.00	103.01	-3.28	98.9	-7.14	99.79	-6.30	113.275	6.36	107.41	0.85
6*D*	120.04	12.71	103.01	-3.28	98.9	-7.14	99.79	-6.30	111.525	4.72	106.243	-0.24
12*D*	106.25	-0.23	100.63	-5.51	106.18	-0.30	106.13	-0.35	103.44	-2.87	106.187	-0.29
14*D*	105.77	-0.69	100.61	-5.53	106.11	-0.37	106.11	-0.37	103.19	-3.11	105.997	-0.47
16*D*	105.5	-0.94	100.72	-5.43	105.6	-0.85	105.65	-0.80	103.11	-3.18	105.583	-0.86
18*D*	105.19	-1.23	100.74	-5.41	106.13	-0.35	106.15	-0.33	102.965	-3.32	105.823	-0.64
20*D*	105.51	-0.93	100.73	-5.42	106.12	-0.36	106.12	-0.36	103.12	-3.17	105.917	-0.55

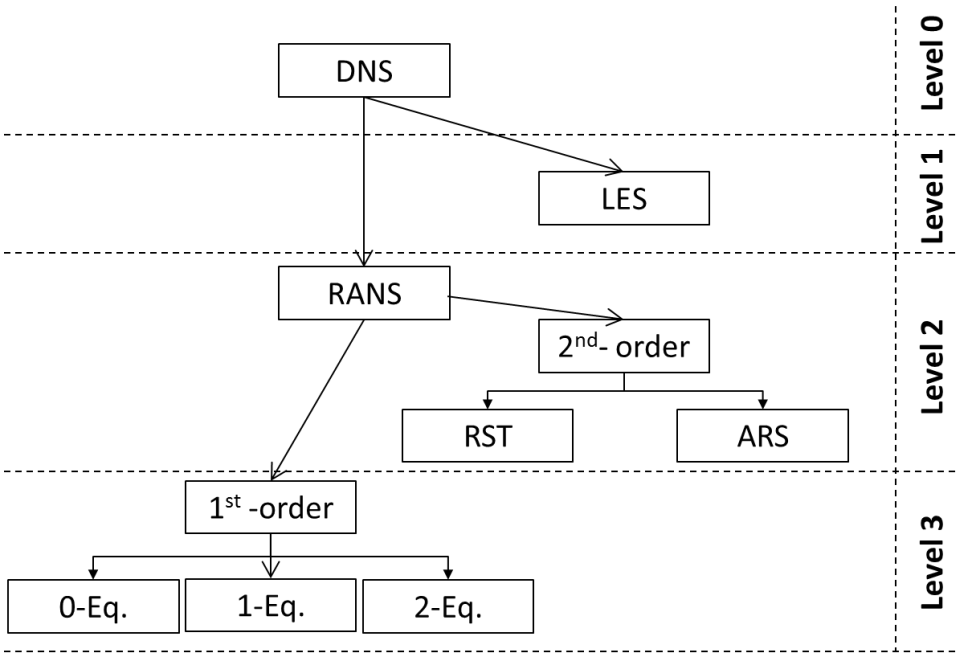

Figure 4-1: Hierarchy of turbulence models. Abbreviations:
DNS = Direct Numerical Simulation
LES = Large-Eddy Simulation
RANS = Reynolds-Averaged Navier-Stokes equations
1st-order = first-order closures
2nd-order = second-order closures
RST = Reynolds-Stress Transport models
ARS = Algebraic Reynolds-Stress models
0-, 1-, 2-Eq. = zero- (algebraic), one-, two-equations models.

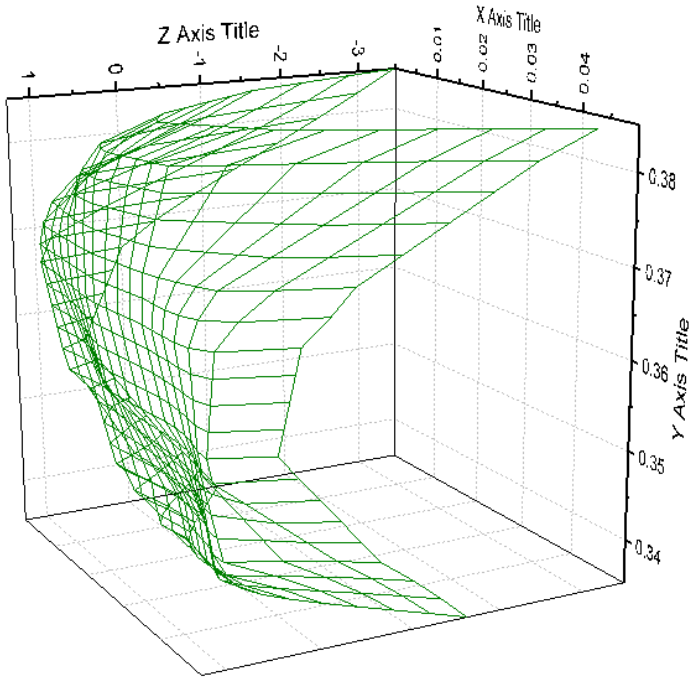

Fig.4-2 Three-dimension velocity profile from ANSYS 12.0 data at 3 D out of plane double bent pipe

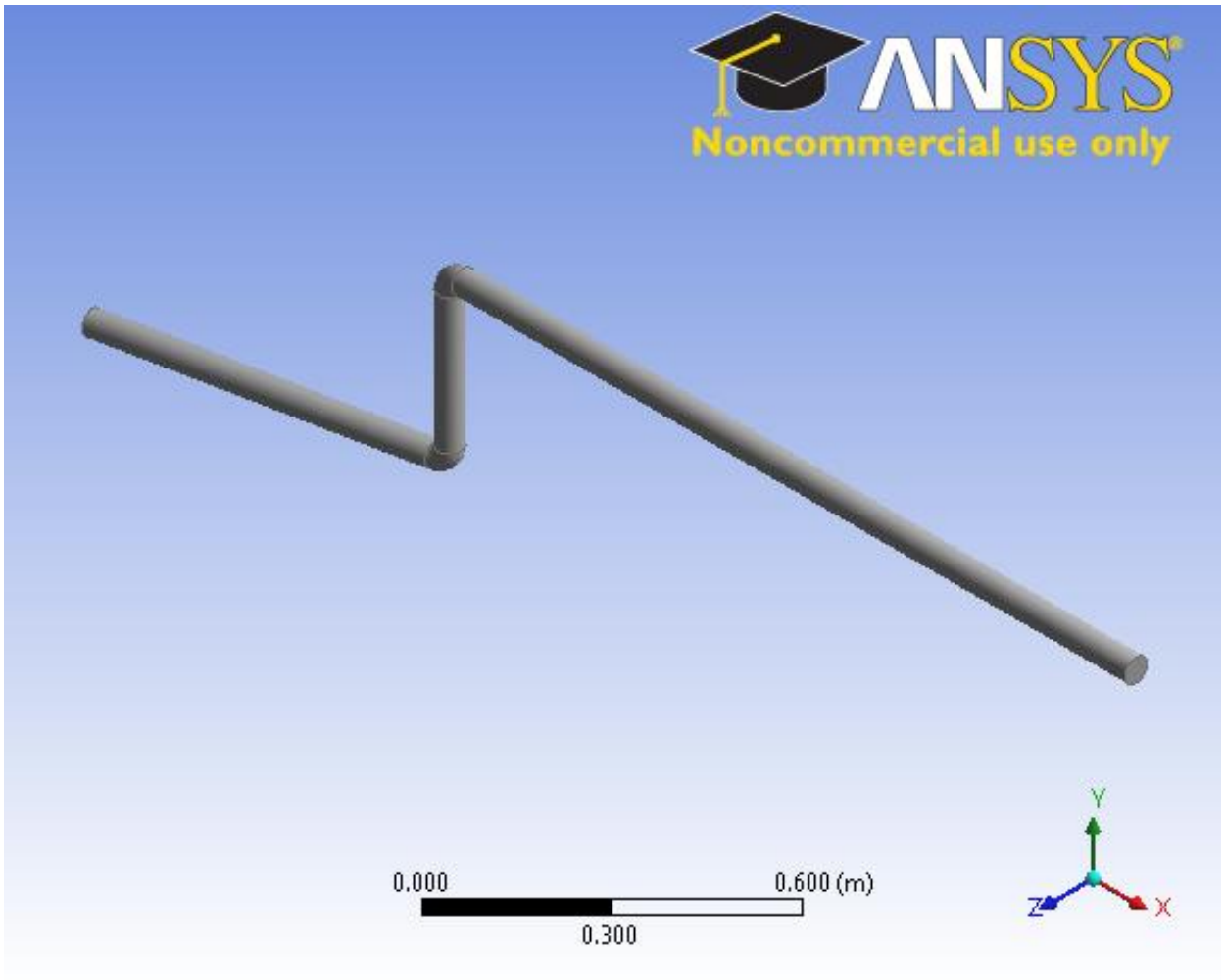

Fig.4-3 Geometry of the simulation model using ANSYS 12.0

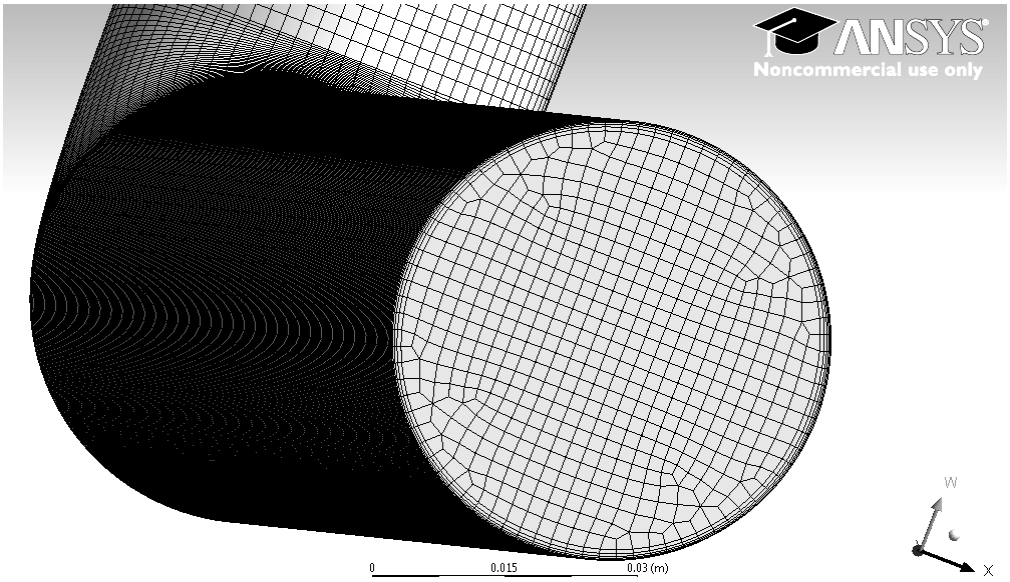

Fig.4-4 Mesh layout.

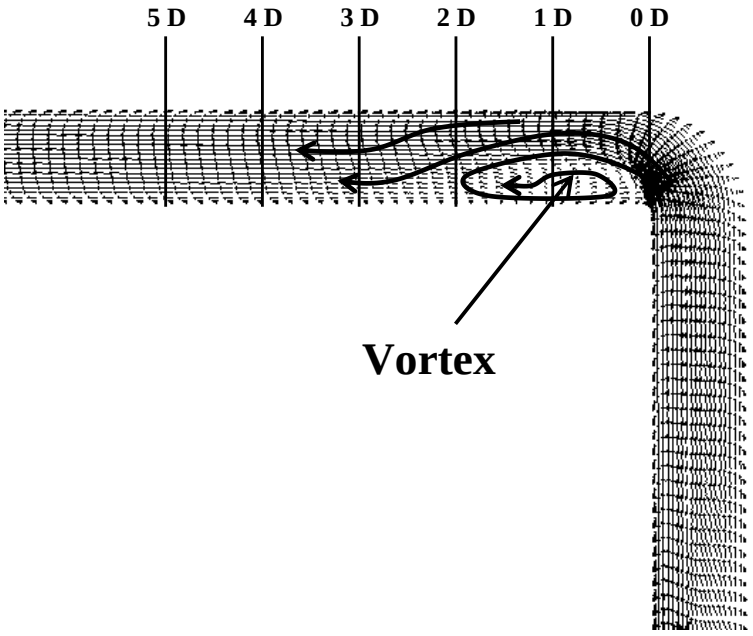

Fig.4-5 Vector of velocity after the second elbow (Re = 40,000).

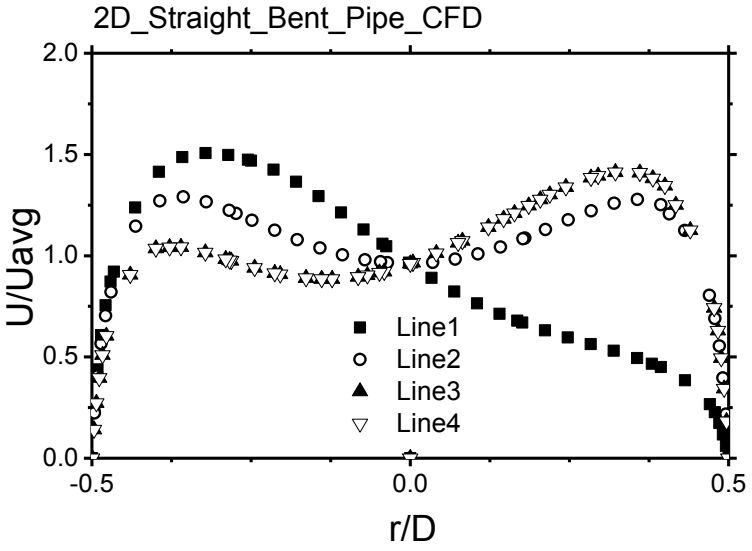
2D_Straight_Bent_Pipe_CFD
U/Uavg
r/D
Line1
Line2
Line3
Line4
2.0
1.5
1.0
0.5
0.0
-0.5
0.0
0.5

a) At 2 D

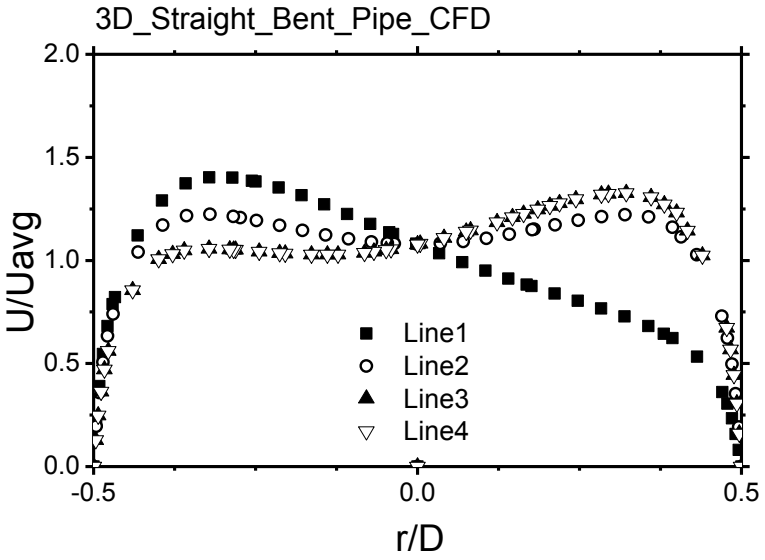
3D_Straight_Bent_Pipe_CFD
U/Uavg
r/D
Line1
Line2
Line3
Line4
2.0
1.5
1.0
0.5
0.0
-0.5
0.0
0.5

b) At 3 D

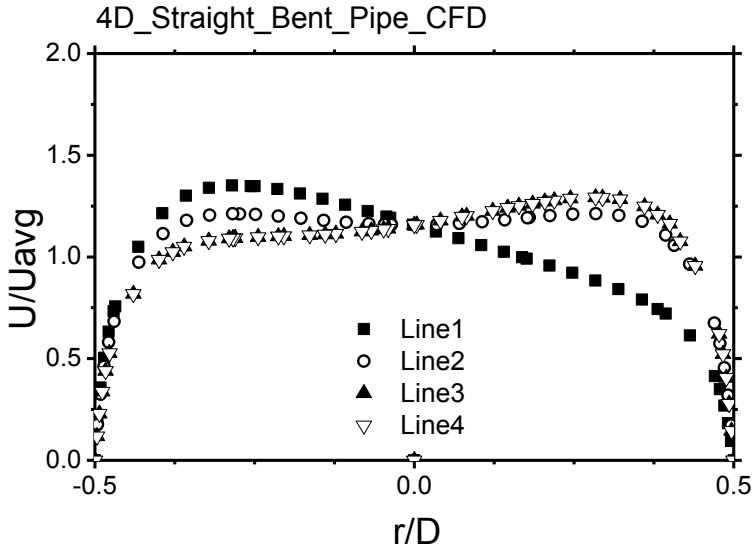
4D_Straight_Bent_Pipe_CFD
U/Uavg
r/D
Line1
Line2
Line3
Line4
2.0
1.5
1.0
0.5
0.0
-0.5
0.0
0.5

c) At 4 D

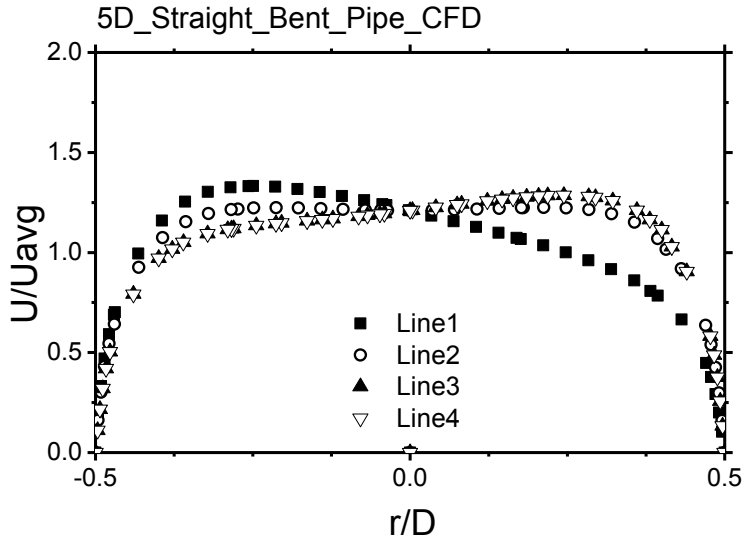
5D_Straight_Bent_Pipe_CFD
U/Uavg
r/D
Line1
Line2
Line3
Line4
2.0
1.5
1.0
0.5
0.0
-0.5
0.0
0.5

d) At 5 D

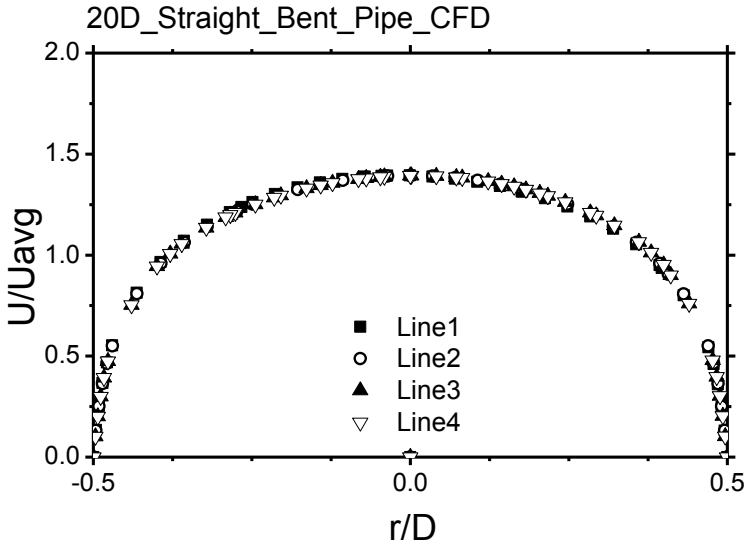

e) At 20 D

Fig.4-6 Velocity profile of 4 lines downstream double bent pipe from CFD

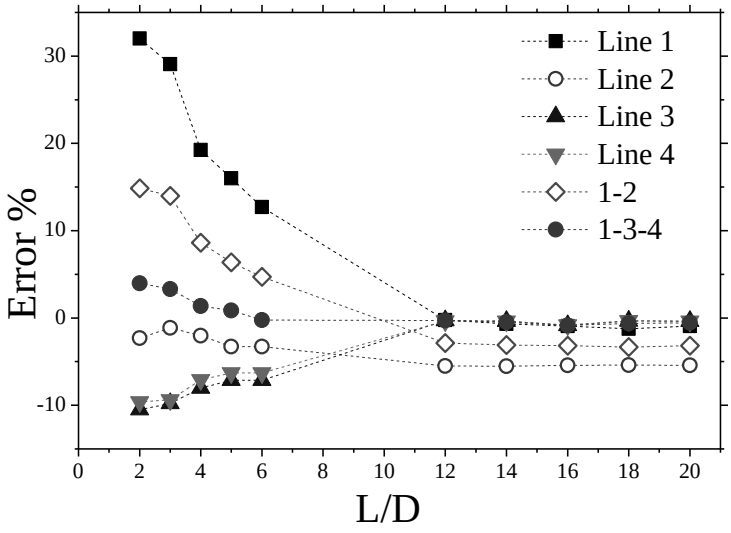

Fig.4-7 Percent error of flow rate calculation from CFD.

4.5.1 K-epsilon RNG (re-normalizable group) enhanced wall treatment gravity in Z-axis is +9.81 m/s

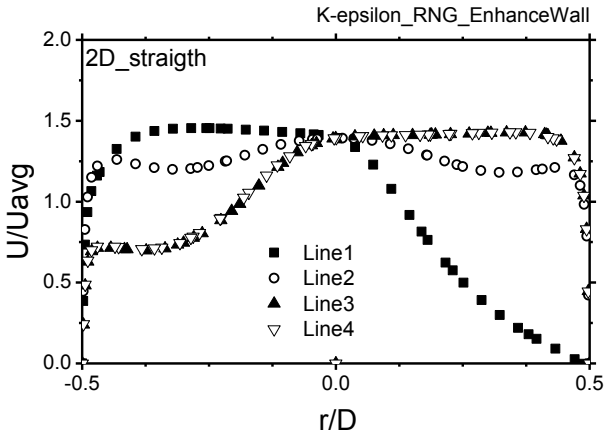

Fig. 4-8 Velocity profiles at 2 D from CFD using K-epsilon RNG model and enhance wall treatment function

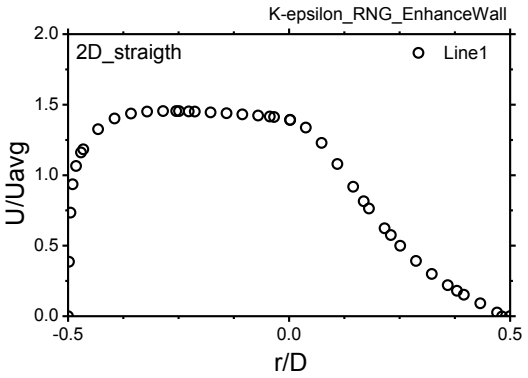

Fig.4-9 a) Velocity profile at 2D straight pipe flow line no. 1.

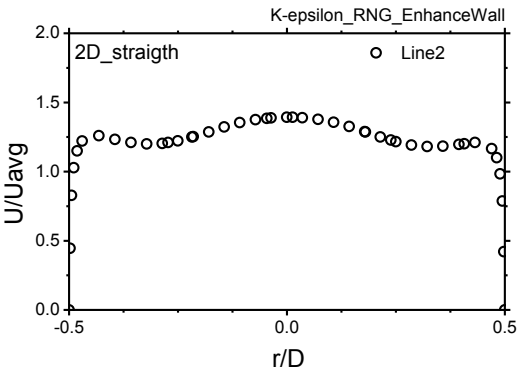

Fig. 4-9 b) Velocity profile at 2D straight pipe flow line no. 2.

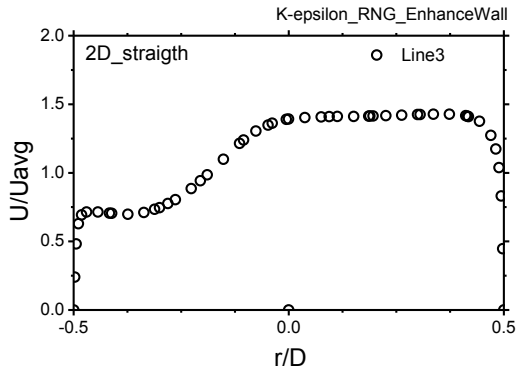

Fig. 4-9 c) Velocity profile at 2D straight pipe flow line no. 3.

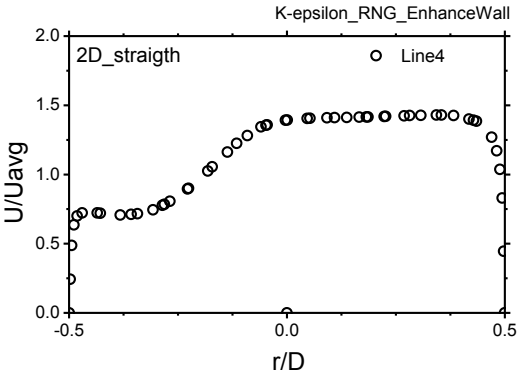

Fig. 4-9 d) Velocity profile at 2D straight pipe flow line no. 4.

Fig. 4-9 Velocity profiles at 2 D from CFD using K-epsilon RNG model and **enhance wall function**

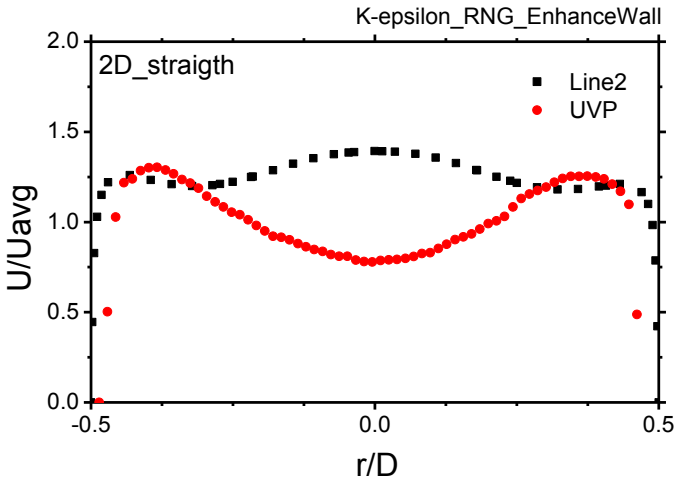

Fig. 4-10 Velocity profiles at 2 D from CFD using K-epsilon RNG model and enhance wall treatment function compare to experimental data at 2 D

4.5.2 K-epsilon RNG (Re-Normalizable Group) Standard wall treatment

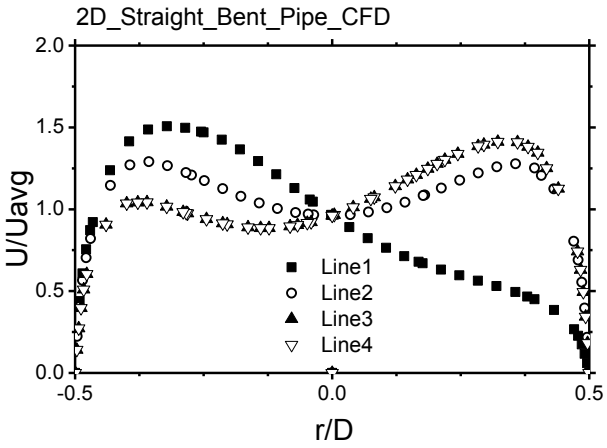

Fig. 4-11 Velocity profiles at 2 D from CFD using K-epsilon RNG model and enhance wall treatment function

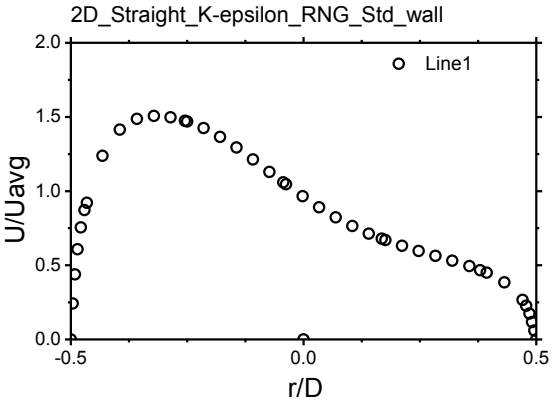

Fig.4-12 a) Velocity profile at 2D straight pipe flow line no. 1.

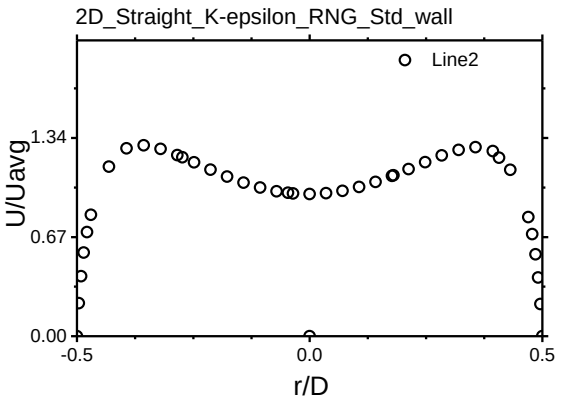

Fig. 4-12 b) Velocity profile at 2D straight pipe flow line no. 2.

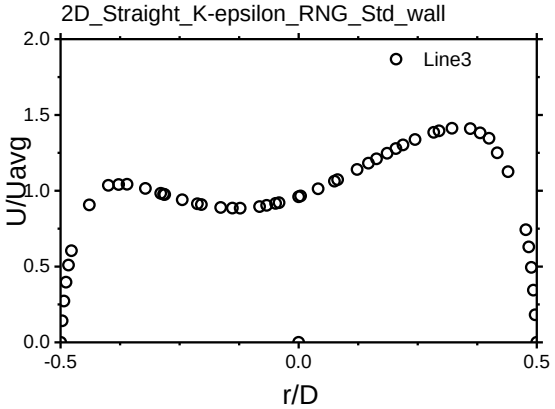

Fig. 4-12 c) Velocity profile at 2D straight pipe flow line no. 3.

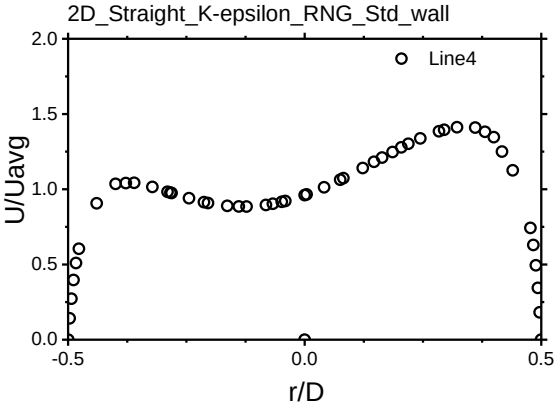

Fig. 4-12 d) Velocity profile at 2D straight pipe flow line no. 4.

Fig. 4-12 Velocity profiles at 2 D from K-epsilon RNG model and **Standard wall function**

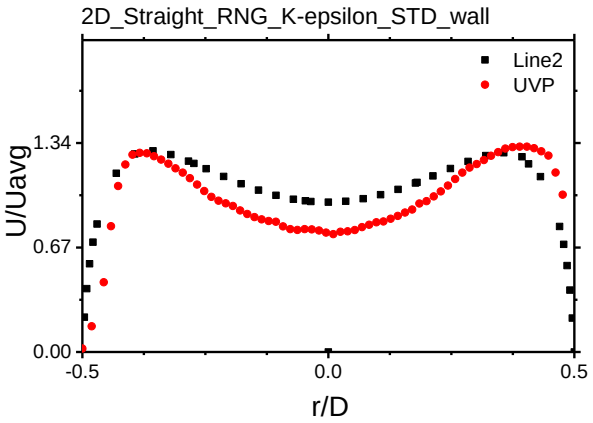

Fig. 4-13 Velocity profiles at 2 D from CFD using K-epsilon RNG model and Standard wall function

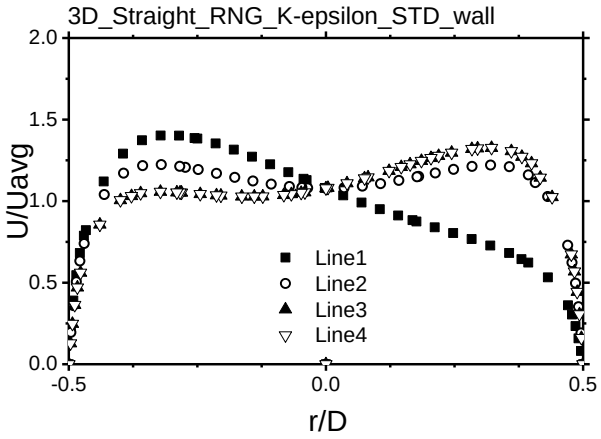

Fig. 4-14 Velocity profiles at 3 D from CFD using K-epsilon RNG model and enhance wall treatment function

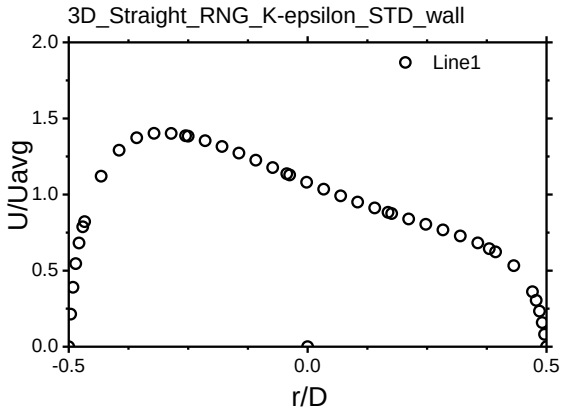

Fig.4-15 a) Velocity profile at 3D straight pipe flow line no. 1.

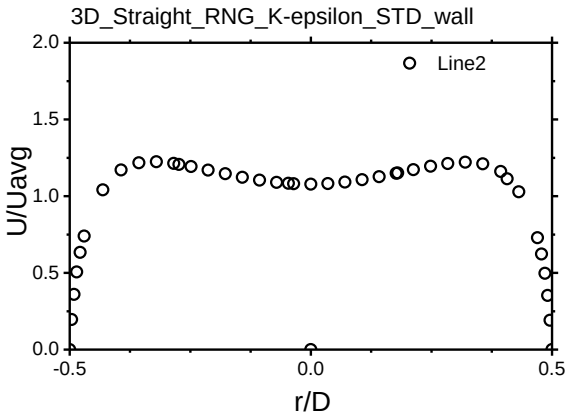

Fig. 4-15 b) Velocity profile at 3D straight pipe flow line no. 2.

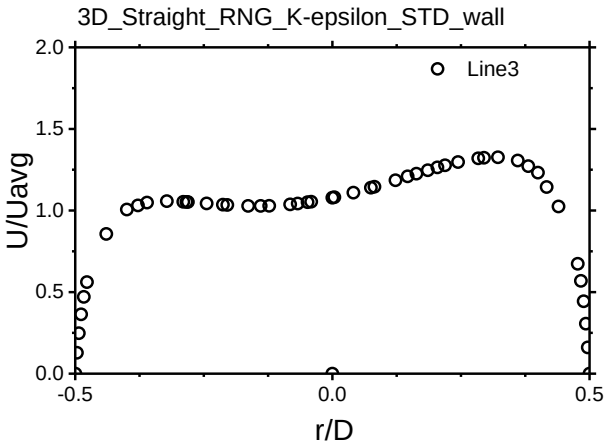

Fig. 4-15 c) Velocity profile at 3D straight pipe flow line no. 3.

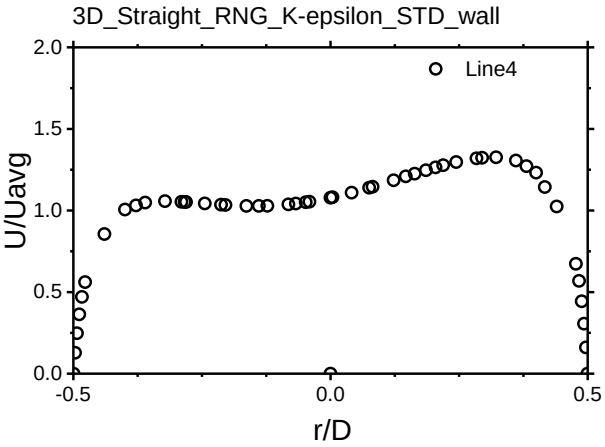

Fig. 4-15 d) Velocity profile at 3D straight pipe flow line no. 4.

Fig. 4-15 Velocity profiles at 3 D from K-epsilon RNG model and **Standard wall function**

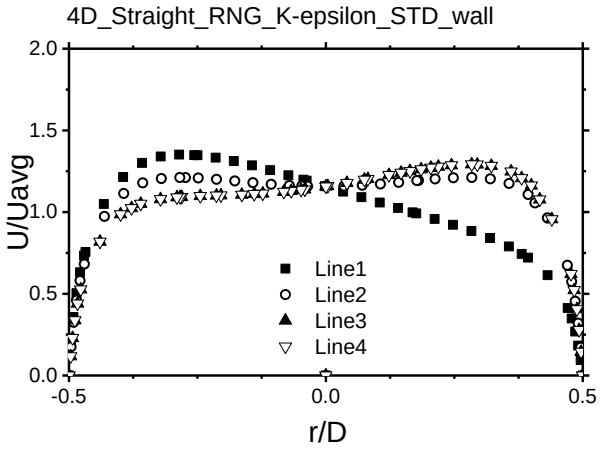

Fig. 4-16 Velocity profiles at 4 D from CFD using K-epsilon RNG model and enhance wall treatment function

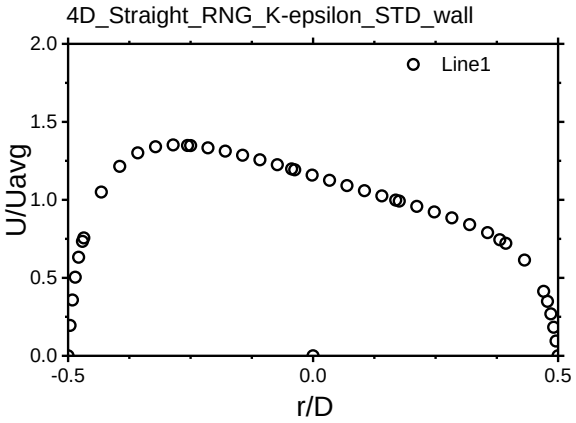

Fig.4-17 a) Velocity profile at 4D straight pipe flow line no. 1.

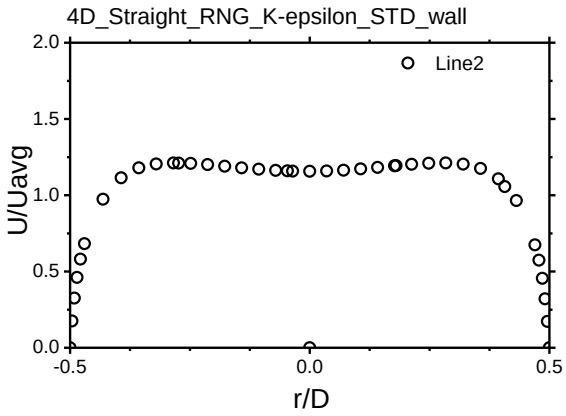

Fig. 4-17 b) Velocity profile at 4D straight pipe flow line no. 2.

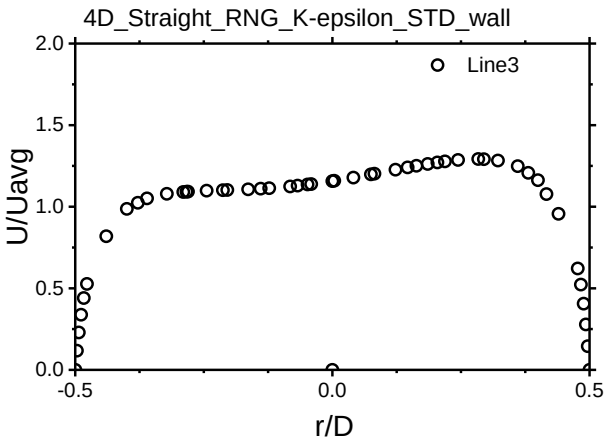

Fig. 4-17 c) Velocity profile at 4D straight pipe flow line no. 3.

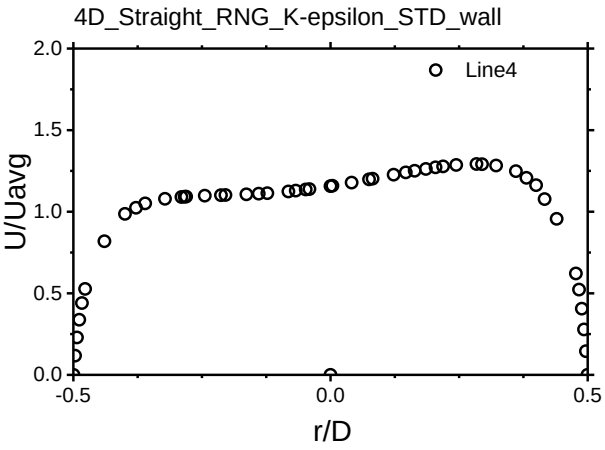

Fig. 4-17 d) Velocity profile at 4D straight pipe flow line no. 4.

Fig. 4-17 Velocity profiles at 4 D from K-epsilon RNG model and **Standard wall function**

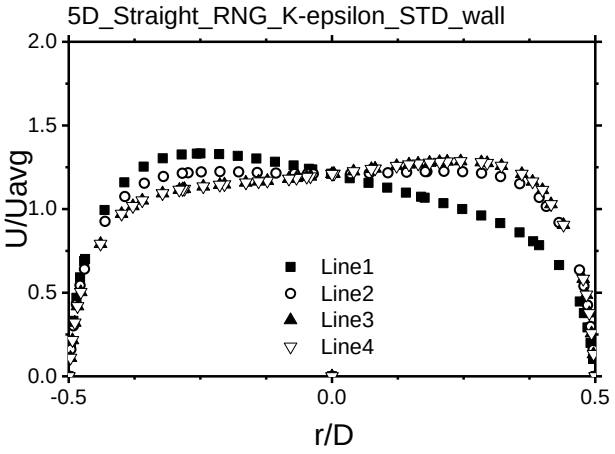

Fig. 4-18 Velocity profiles at 5 D from CFD using K-epsilon RNG model and enhance wall treatment function

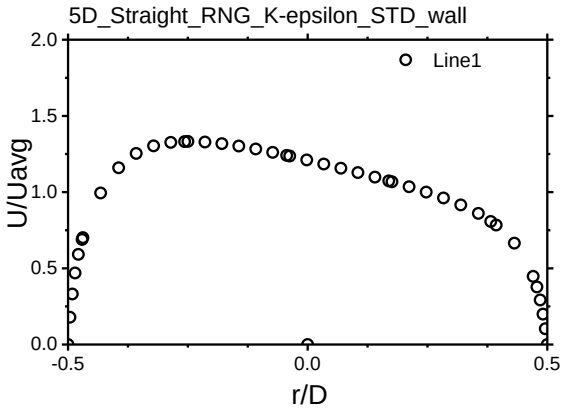

Fig.4-19 a) Velocity profile at 5D straight pipe flow line no. 1.

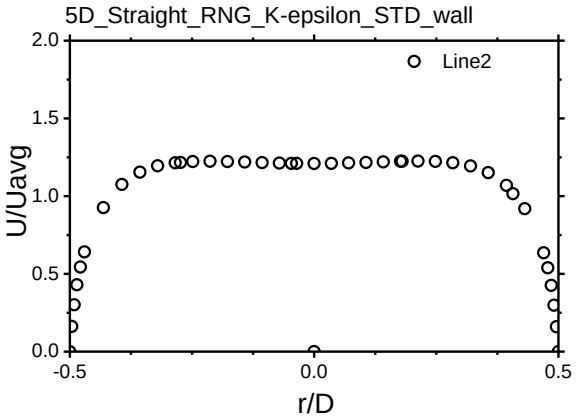

Fig. 4-19 b) Velocity profile at 5D straight pipe flow line no. 2.

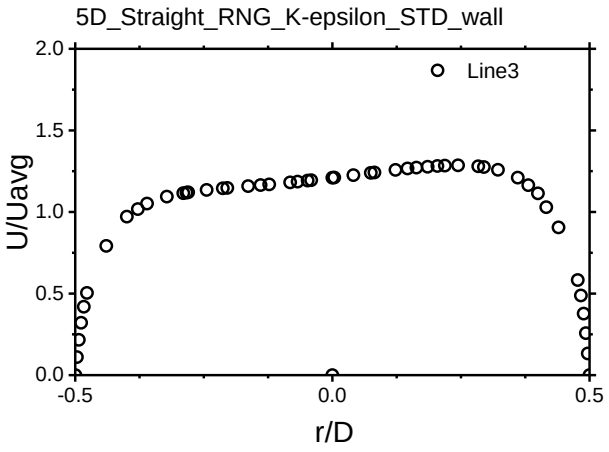

Fig. 4-19 c) Velocity profile at 5D straight pipe flow line no. 3.

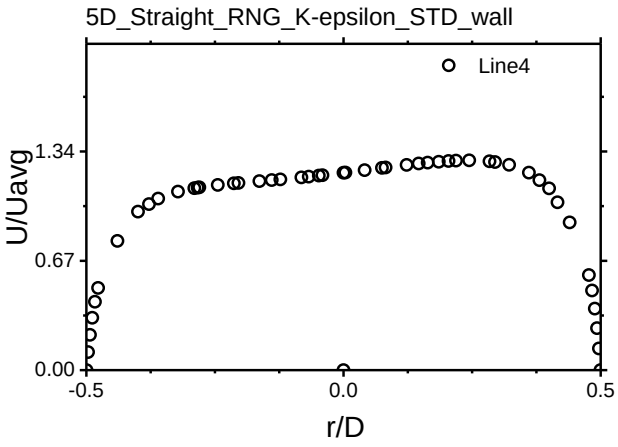

Fig. 4-19 d) Velocity profile at 5D straight pipe flow line no. 4.

Fig. 4-19 Velocity profiles at 5 D from K-epsilon RNG model and **Standard wall function**

4.6.1 K-epsilon RNG (re-normalizable group) enhanced wall treatment

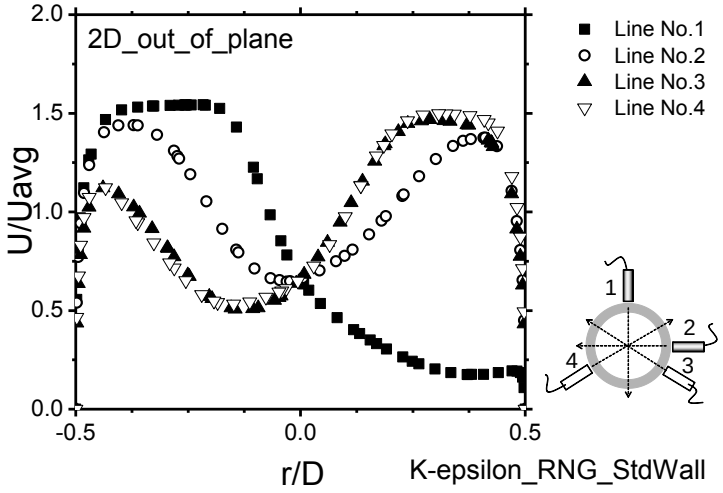

Fig. 4-20 Velocity profiles at 2 D from K-epsilon RNG model and **standard wall function with out of plane angle 8°**

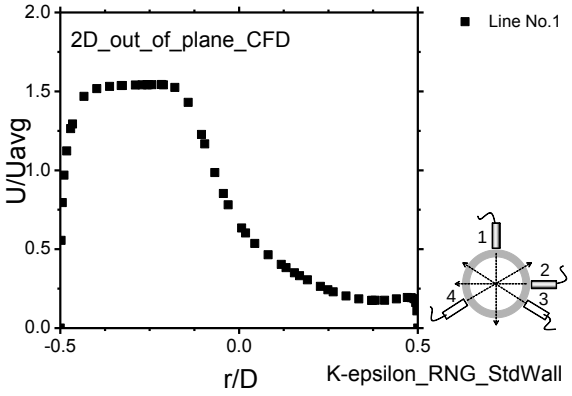

Fig.4-21 (a) Velocity profile at 2D line no. 1.

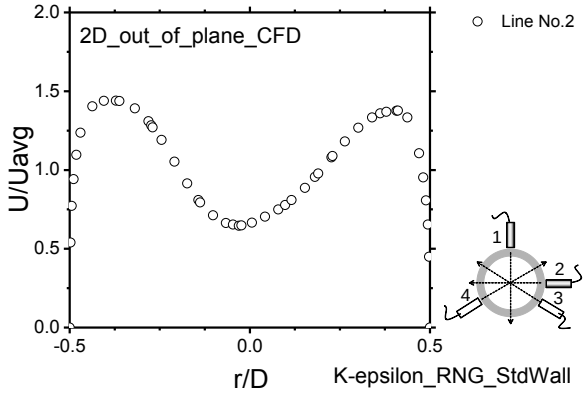

Fig.4-21 (b) Velocity profile at 2D line no. 2.

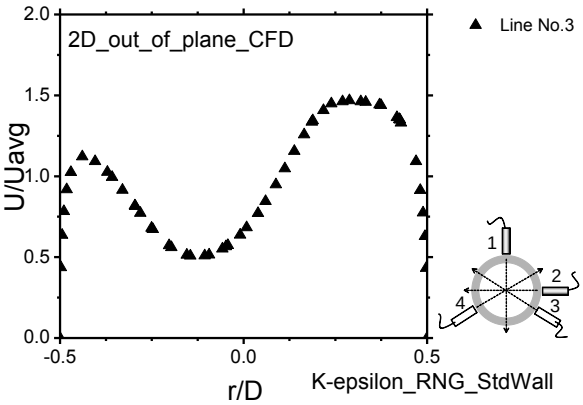

Fig.4-21 (c) Velocity profile at 2D line no. 3.

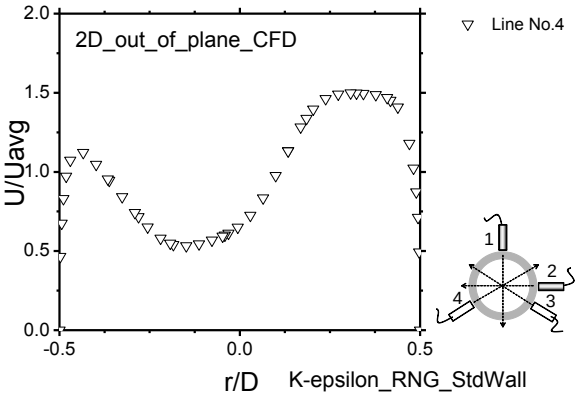

Fig.4-21 (d) Velocity profile at 2D line no. 4.

Fig. 4-21 Velocity profiles at 2 D from K-epsilon RNG model and **standard wall function**

4.6.2 Inclination double bent pipe flow (out of plane) K-epsilon RNG model standard wall condition.

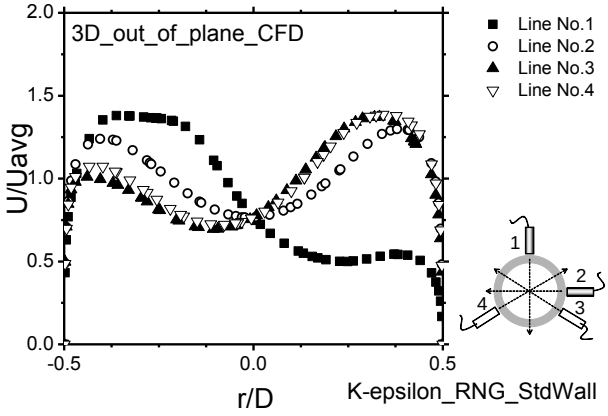

Fig. 4-22 Velocity profiles at 3 D from CFD using K-epsilon RNG model and **standard wall function**

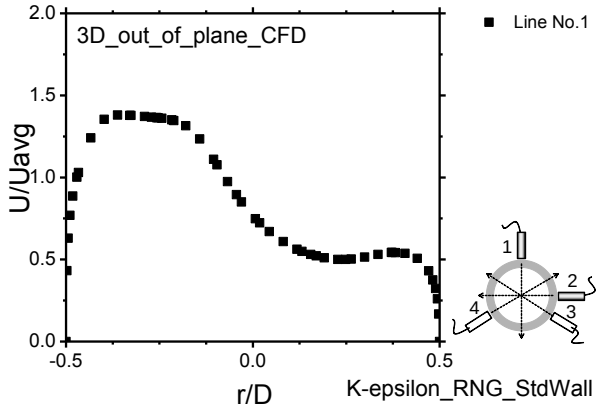

Fig.4-23 (a) Velocity profile at 3D line no. 1.

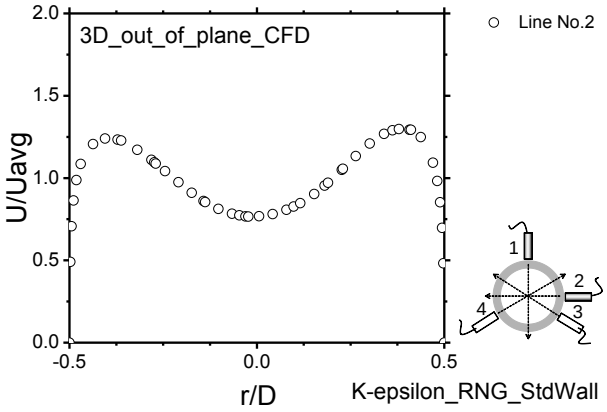

Fig.4-23 (b) Velocity profile at 3D line no. 2.

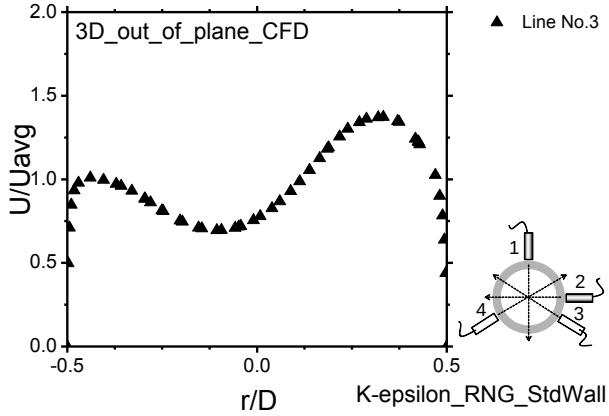

Fig.4-23 (c) Velocity profile at 3D line no. 3.

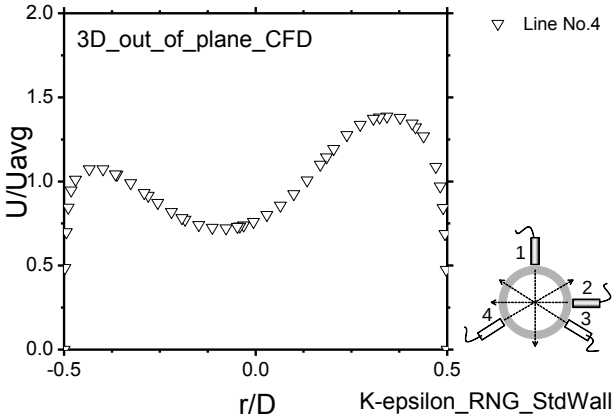

Fig.4-23 (d) Velocity profile at 3D line no. 4.

Fig. 4-23 Velocity profiles at 3 D from K-epsilon RNG model and **standard wall function**

4.6.3 Inclination double bent pipe flow (out of plane) k-epsilon RNG model standard wall condition.

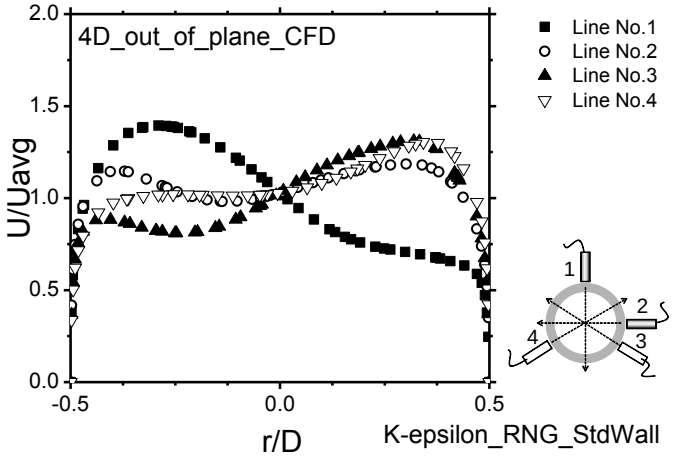

Fig. 4-24 Velocity profiles at 4 D from K-epsilon RNG model and **standard wall function**

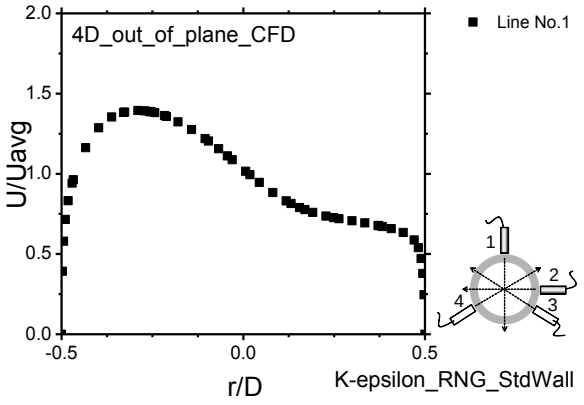

Fig.4-25 (a) Velocity profile at 4D line no. 1.

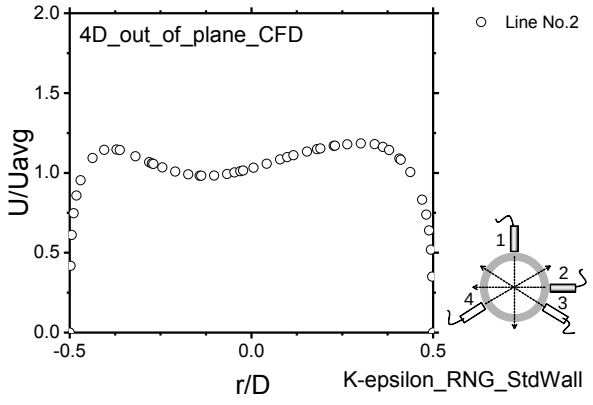

Fig.4-25 (b) Velocity profile at 4D line no. 2.

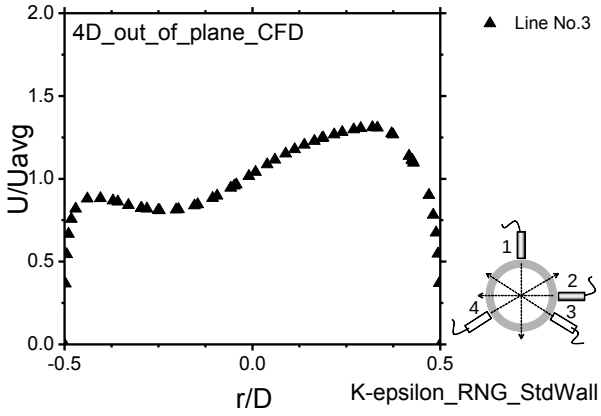

Fig.4-25 (c) Velocity profile at 4D line no. 3.

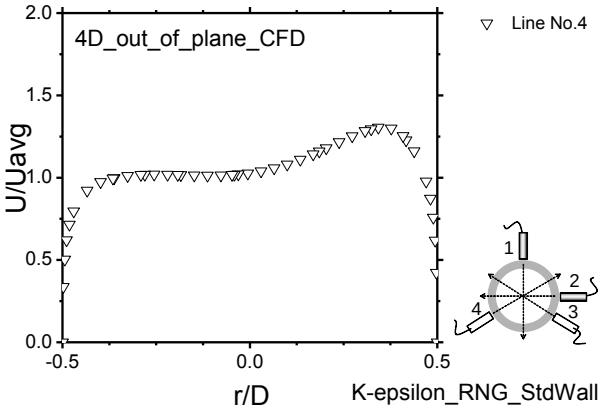

Fig.4-25 (d) Velocity profile at 4D line no. 4.

Fig. 4-25 Velocity profiles at 4 D from K-epsilon RNG model and **standard wall function**

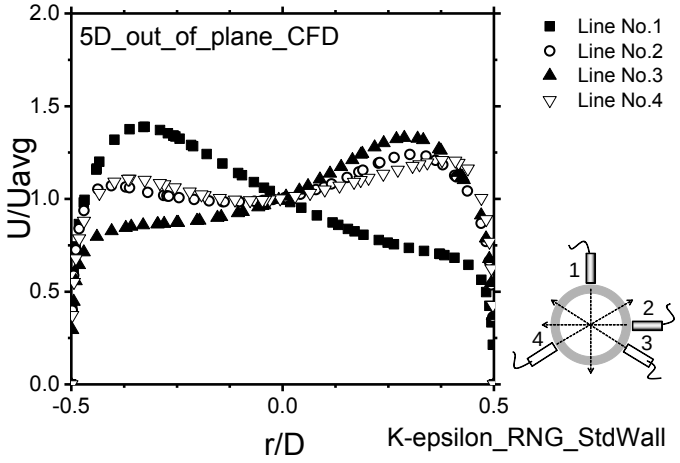

Fig. 4-26 Velocity profiles at 5 D from K-epsilon RNG model and **standard wall function**

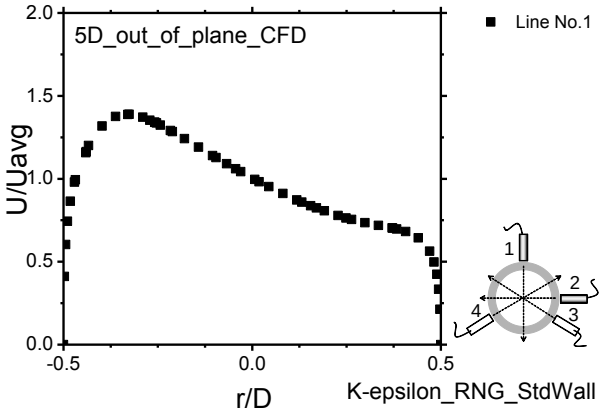

Fig.4-27 (a) Velocity profile at 5D line no. 1.

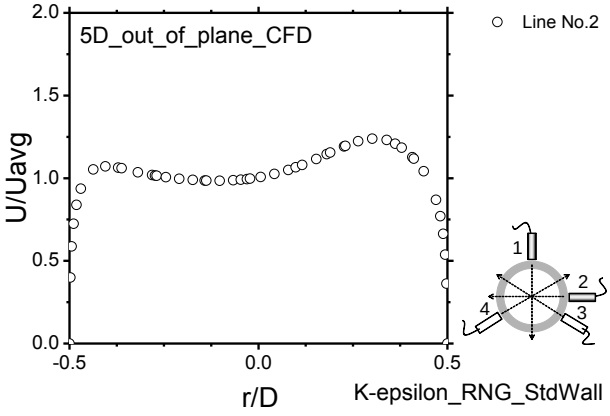

Fig.4-27 (b) Velocity profile at 5D line no. 2.

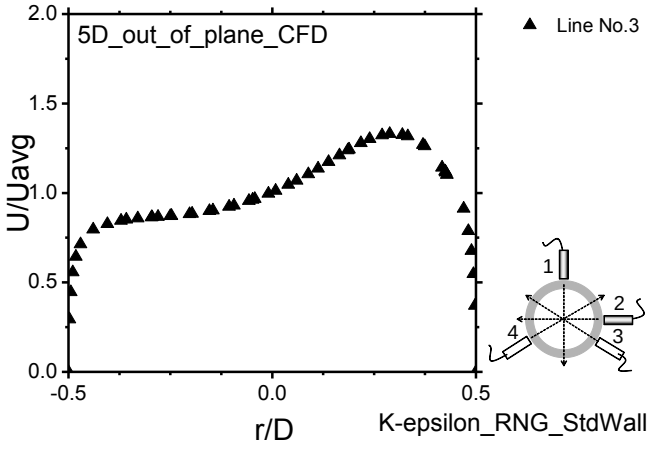

Fig.4-27 (c) Velocity profile at 5D line no. 3.

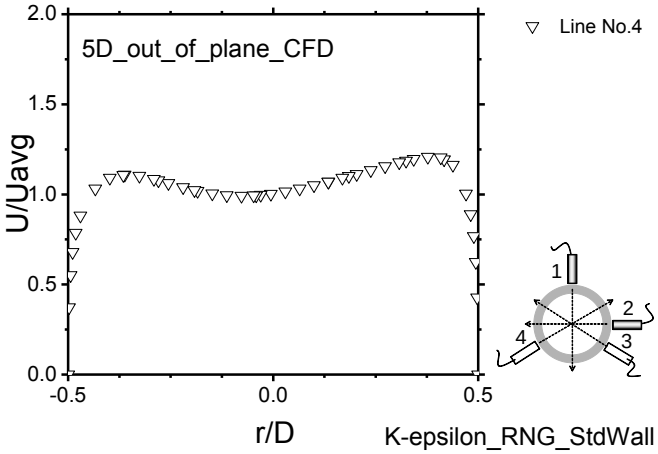

Fig.4-27 (d) Velocity profile at 5D line no. 4.

Fig. 4-27 Velocity profiles at 5 D from K-epsilon RNG model and **standard wall function**

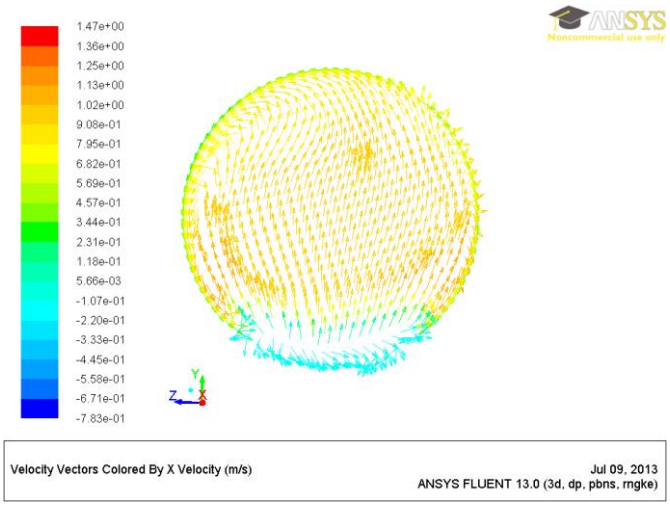

Fig. 4-28 (a) Velocity vectors colored at 0D.

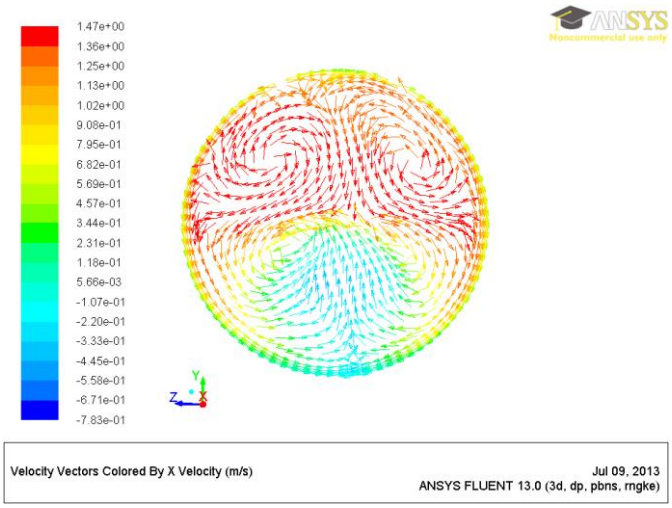

Fig. 4-28 (b) Velocity vectors colored at 1D.

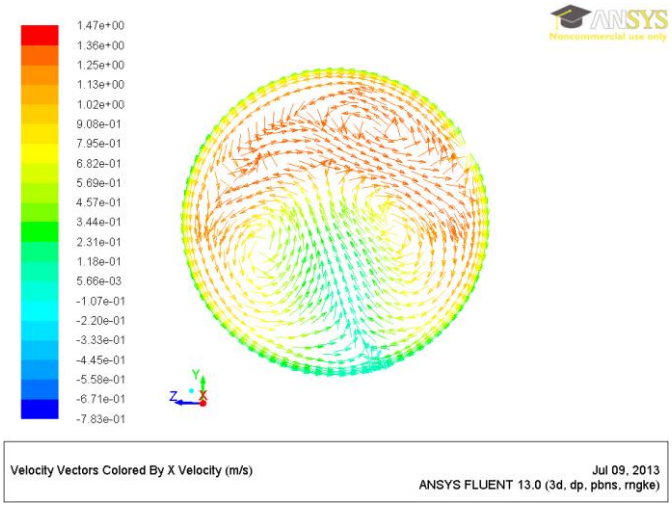

Fig. 4-28 (c) Velocity vectors colored at 2D.

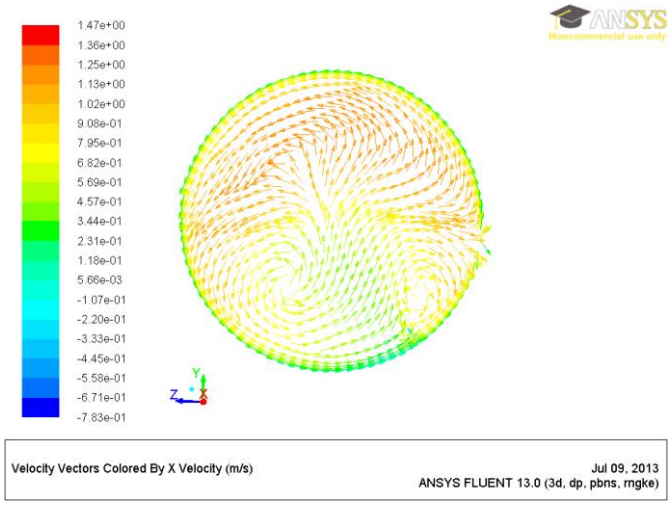

Fig. 4-28 (d) Velocity vectors colored at 3D.

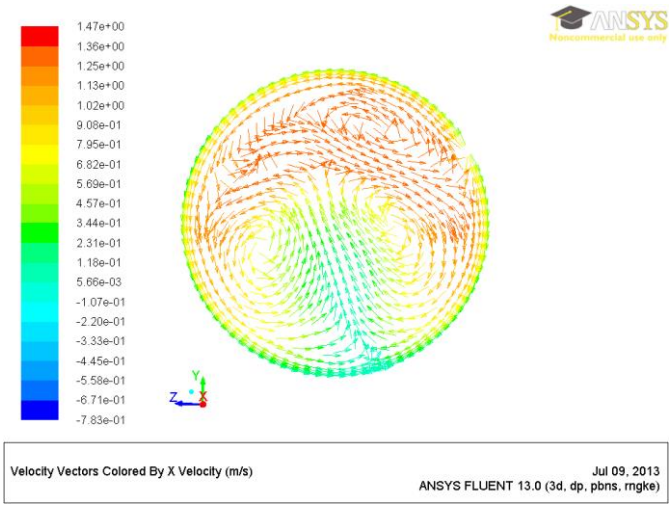

Fig. 4-28 (e) Velocity vectors colored at 4D.

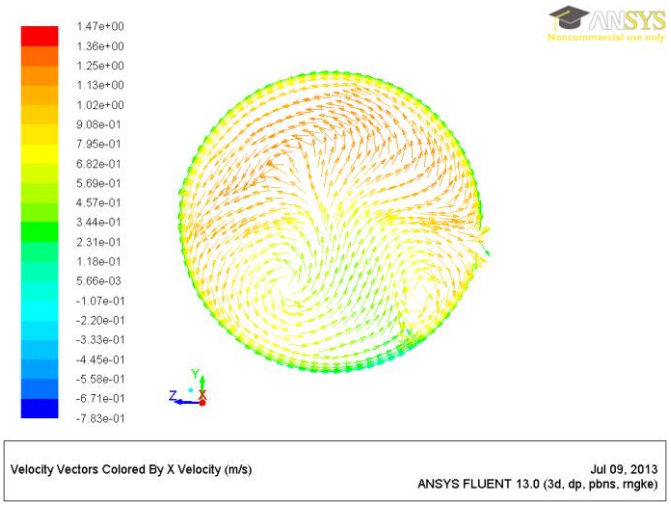

Fig. 4-28 (f) Velocity vectors colored at 5D.

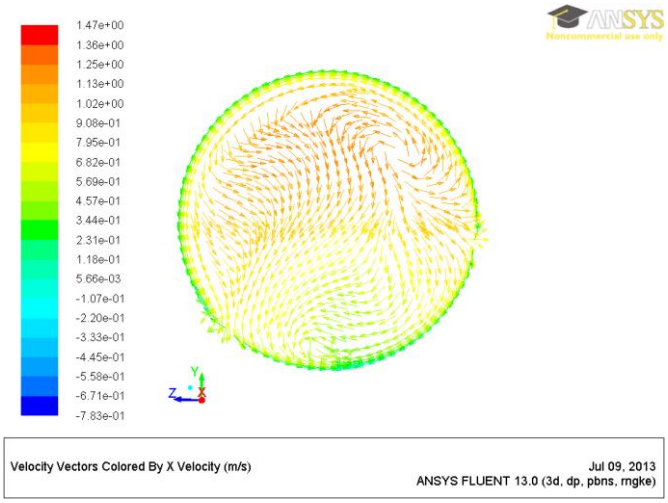

Fig. 4-28 (g) Velocity vectors colored at 6D.

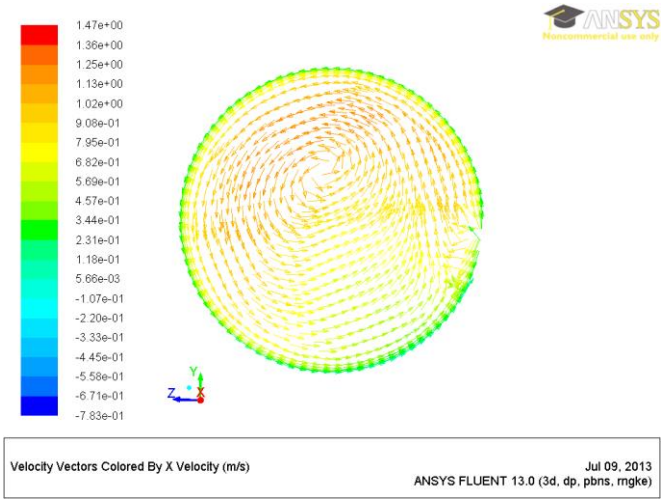

Fig. 4-28 (h) Velocity vectors colored at 20D.

Fig. 4-28 Velocity profiles at 5 D from CFD using K-epsilon RNG model and **standard wall function**

K-epsilon Standard model Standard wall

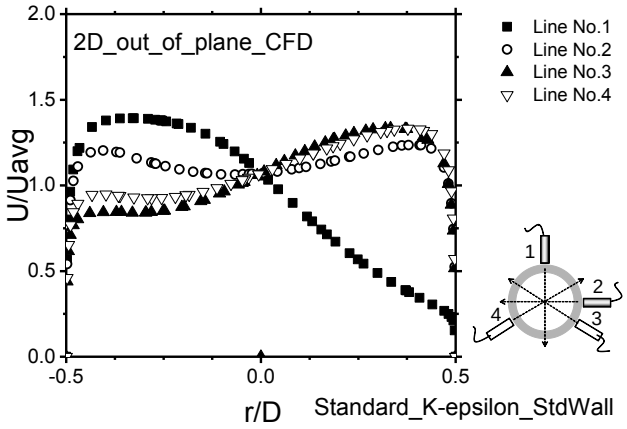

Fig. 4-29 Velocity profiles at 2 D from CFD using K-epsilon Standard model and **standard wall function**

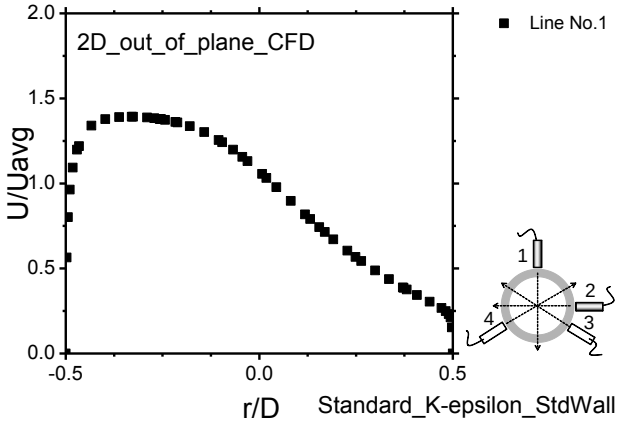

Fig. 4-30 a) Velocity profile at 2D line no. 1.

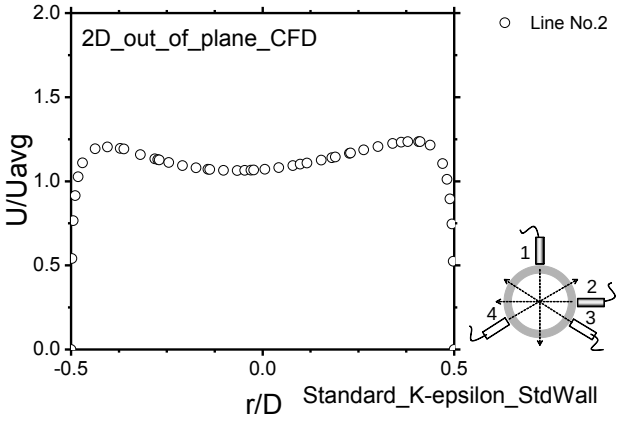

Fig. 4-30 b) Velocity profile at 2D line no. 2.

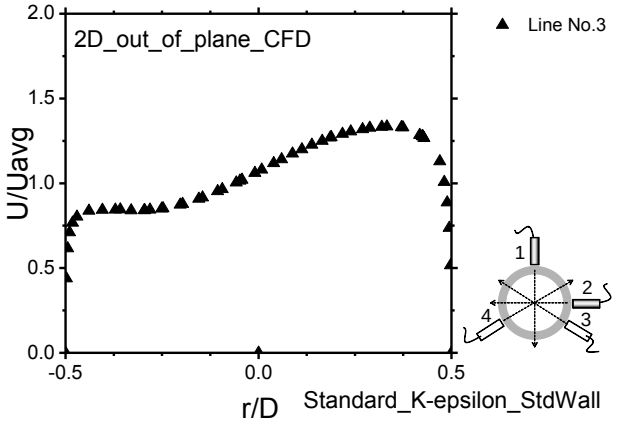

Fig. 4-30 c) Velocity profile at 2D line no. 3.

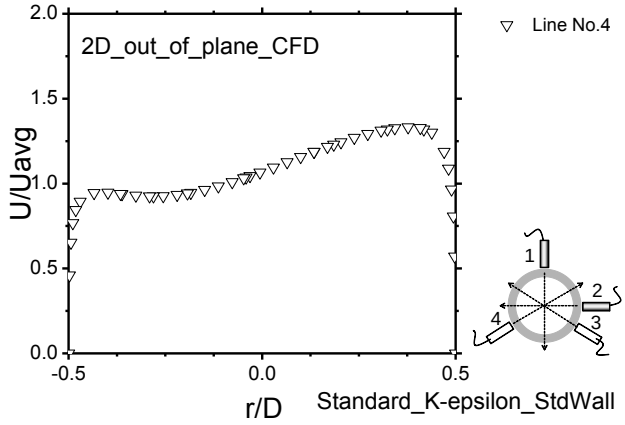

Fig. 4-30 d) Velocity profile at 2D line no. 4.

Fig. 4-30 Velocity profiles at 2 D from K-epsilon Standard model and **standard wall function**

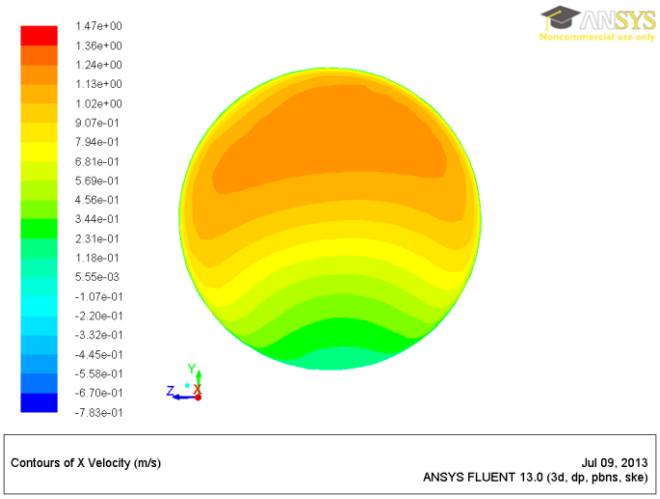

Fig. 4-31 a) Contours of x velocity at 2D

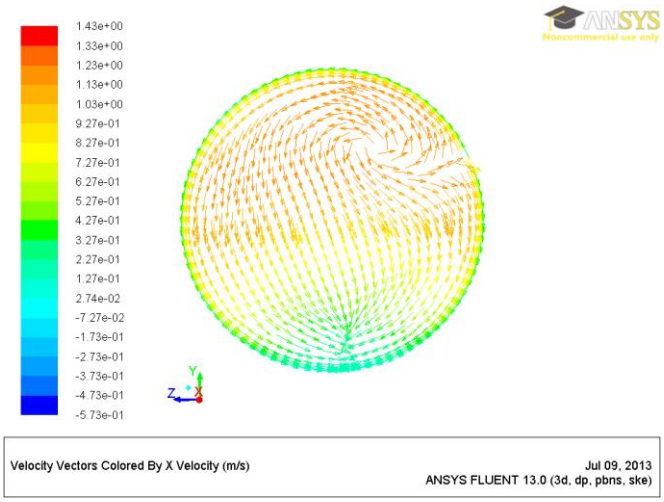

Fig. 4-31 b) Velocity Vectors by x velocity at 2D

Fig. 4-31 Velocity profiles at 2 D from CFD using K-epsilon Standard model and **standard wall function**

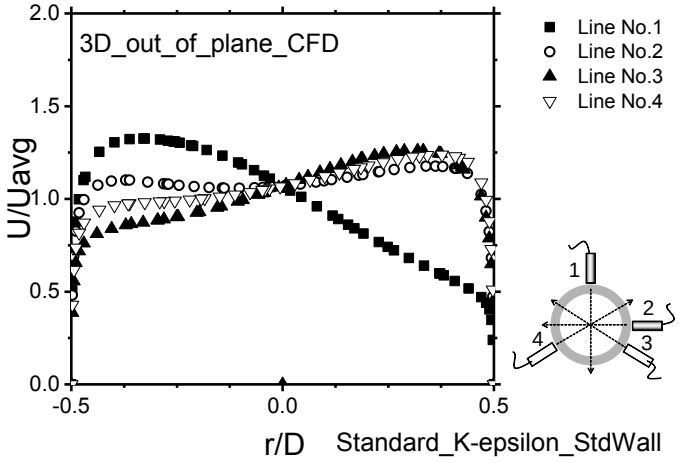

Fig. 4-32 Velocity profiles at 3 D from CFD using K-epsilon Standard model and **standard wall function**

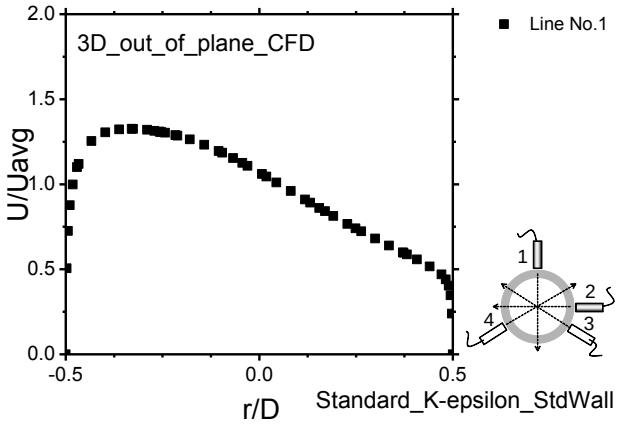

Fig. 4-33 a) Velocity profile at 3D line no. 1.

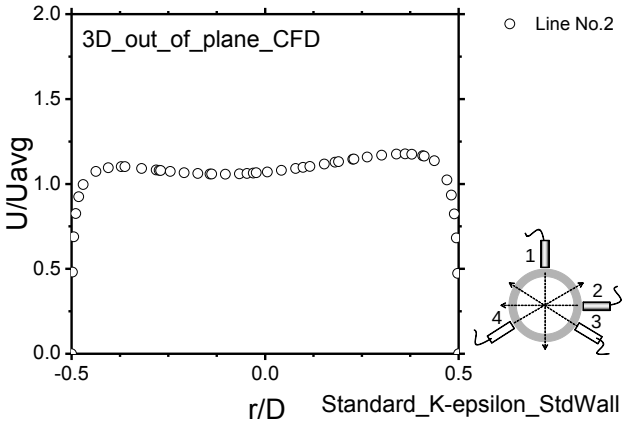

Fig. 4-33 b) Velocity profile at 3D line no. 2.

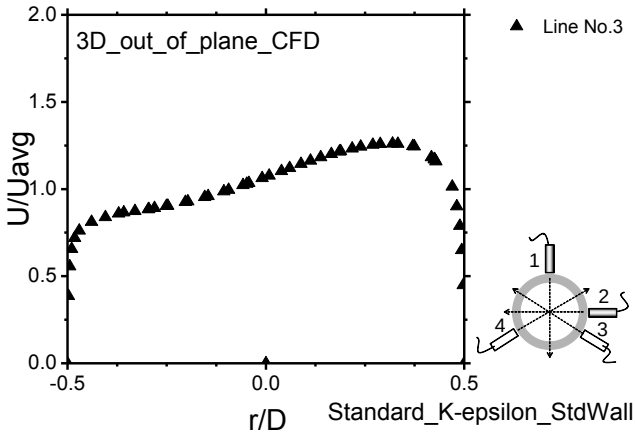

Fig. 4-33 c) Velocity profile at 3D line no. 3.

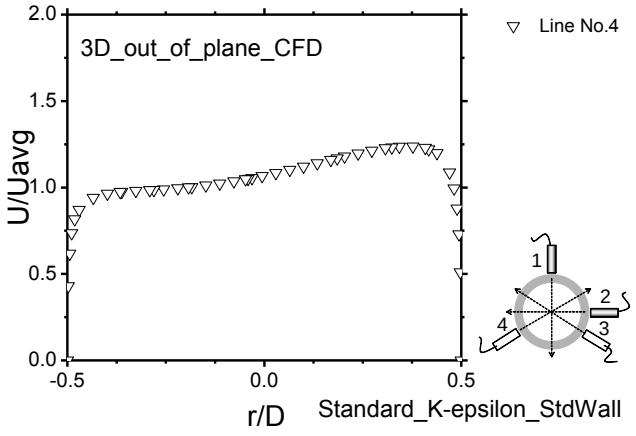

Fig. 4-33 d) Velocity profile at 3D line no. 4.

Fig. 4-33 Velocity profiles at 3 D from K-epsilon Standard model and **standard wall function**

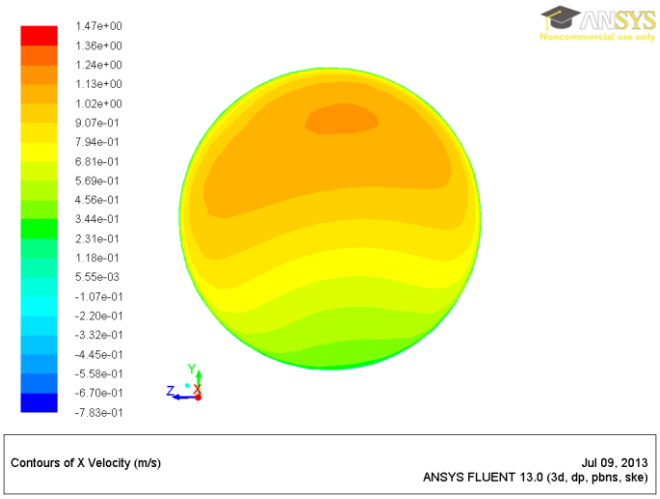

Fig. 4-34 a) Contours of x velocity at 3D

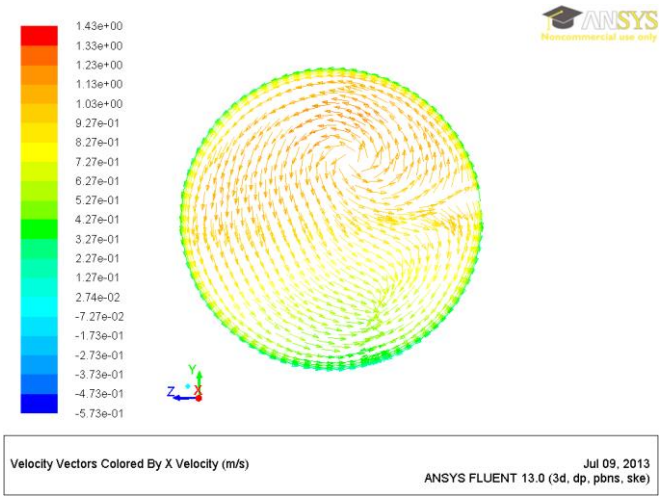

Fig. 4-34 b) Velocity Vectors by x velocity at 3D

Fig. 4-34 Contours of x velocity at 3 D from CFD using K-epsilon Standard model and **standard wall function**

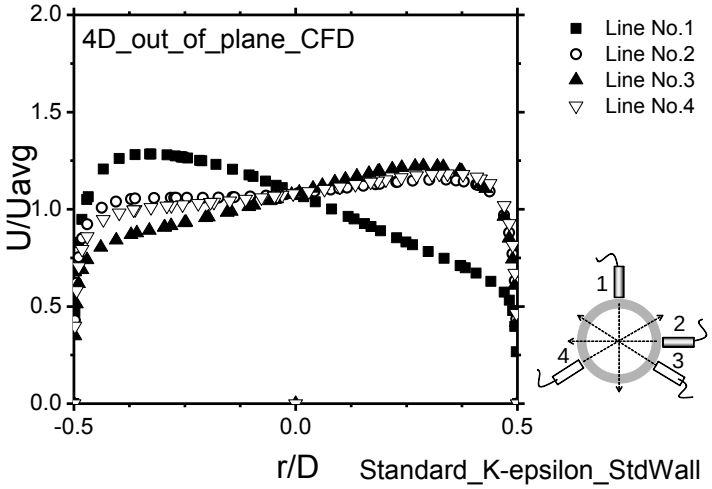

Fig. 4-35 Velocity profiles at 3 D from CFD using K-epsilon Standard model and **standard wall function**

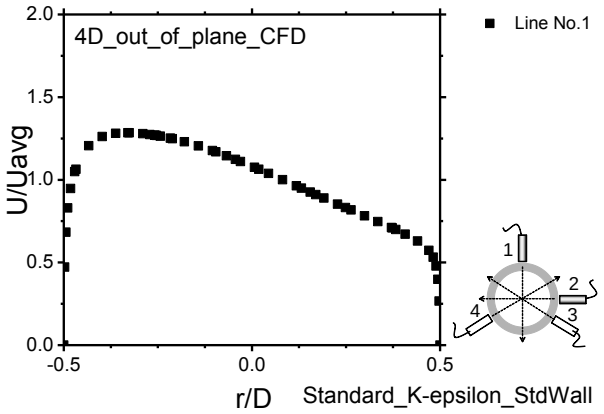

Fig. 4-36 a) Velocity profile at 4D line no. 1.

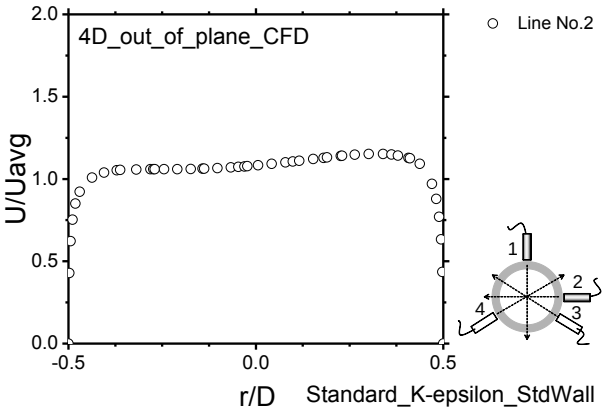

Fig. 4-36 b) Velocity profile at 4D line no. 2.

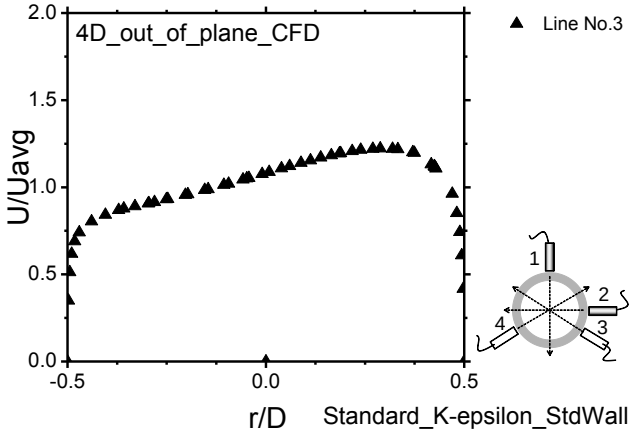

Fig. 4-36 c) Velocity profile at 4D line no. 3.

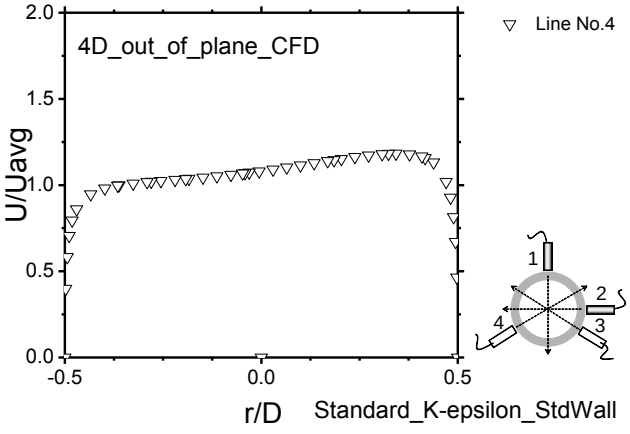

Fig. 4-36 d) Velocity profile at 4D line no. 4.

Fig. 4-36 Velocity profiles at 4 D from K-epsilon Standard model and **standard wall function**

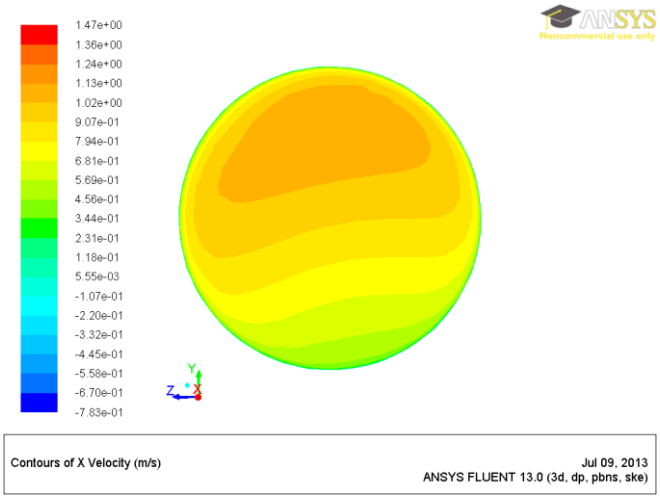

Fig. 4-37 a) Contours of x velocity at 4D

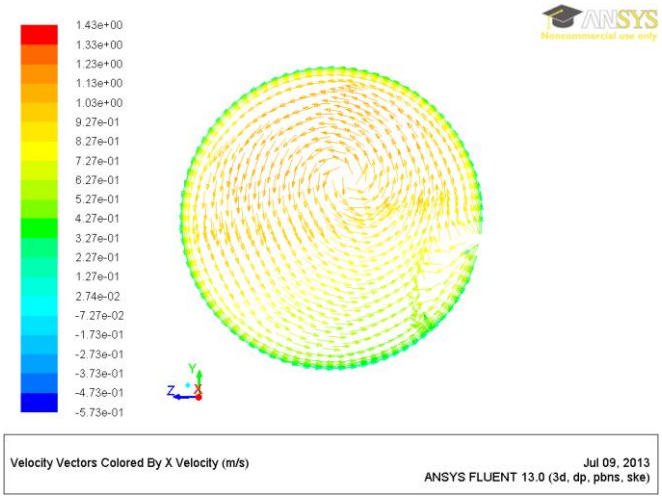

Fig. 4-37 b) Velocity Vectors by x velocity at 4D

Fig. 4-37 Contours of x velocity at 4 D from CFD using K-epsilon Standard model and **standard wall function**

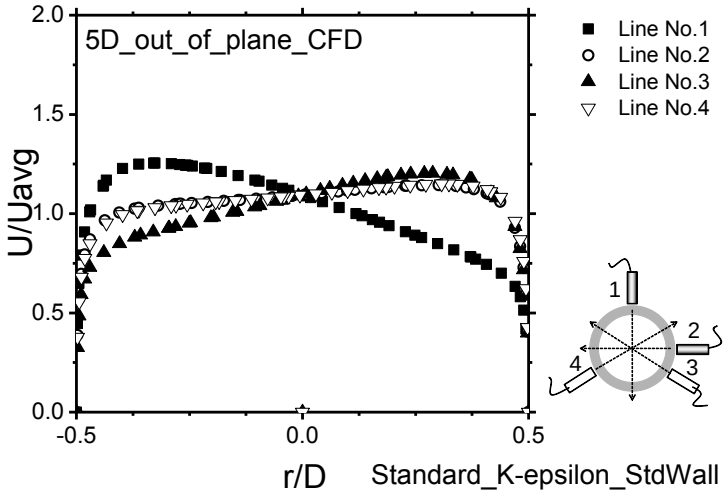

Fig. 4-37 Velocity profiles at 5 D from CFD using K-epsilon Standard model and **standard wall function**

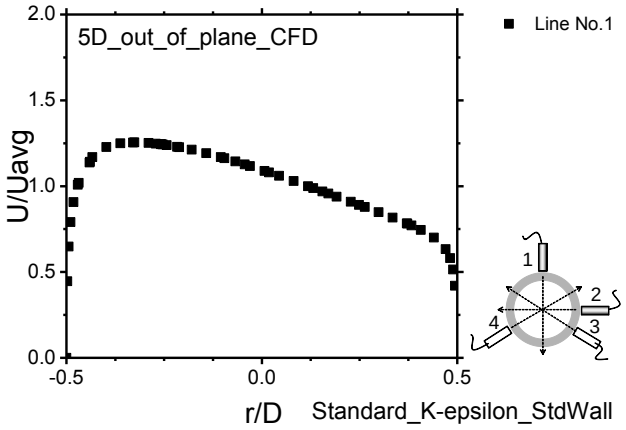

Fig. 4-38 a) Velocity profile at 5D line no. 1.

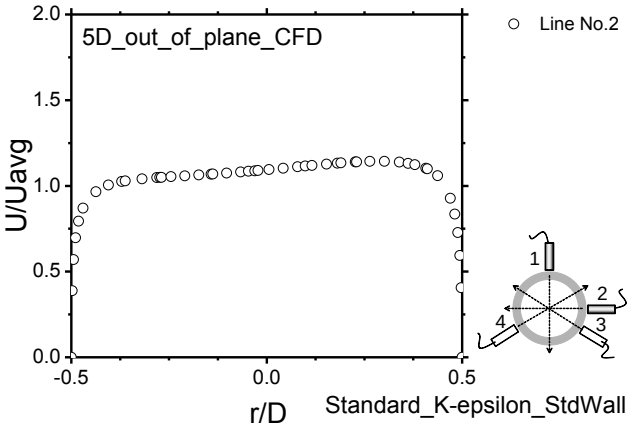

Fig. 4-38 b) Velocity profile at 5D line no. 2.

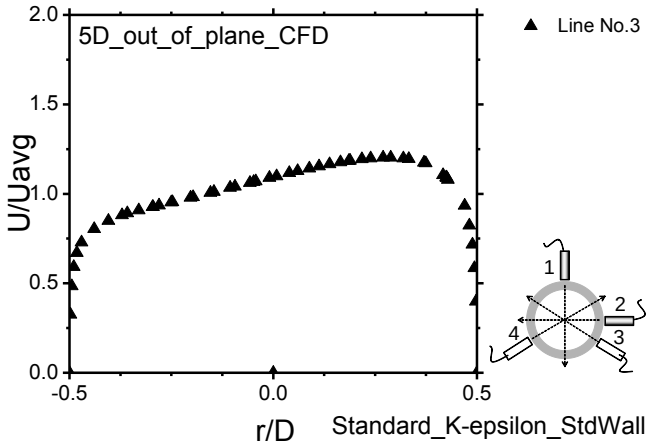

Fig. 4-38 c) Velocity profile at 5D line no. 3.

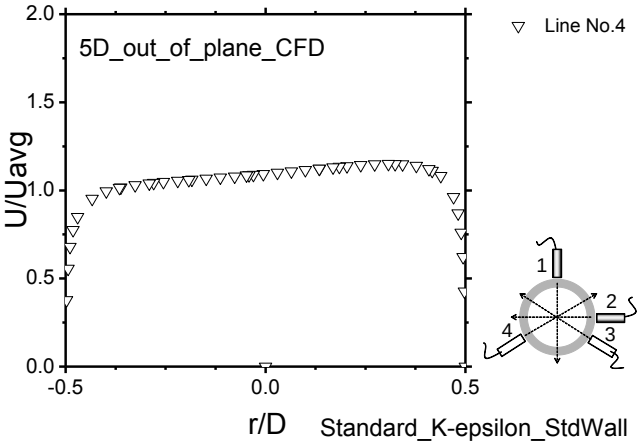

Fig. 4-38 d) Velocity profile at 5D line no. 4.

Fig. 4-38 Velocity profiles at 5 D from K-epsilon Standard model and **standard wall function**

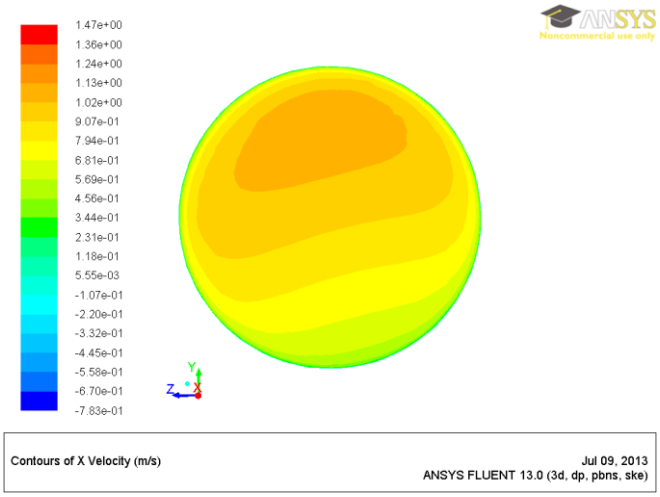

Fig. 4-39 a) Contours of x velocity at 5D

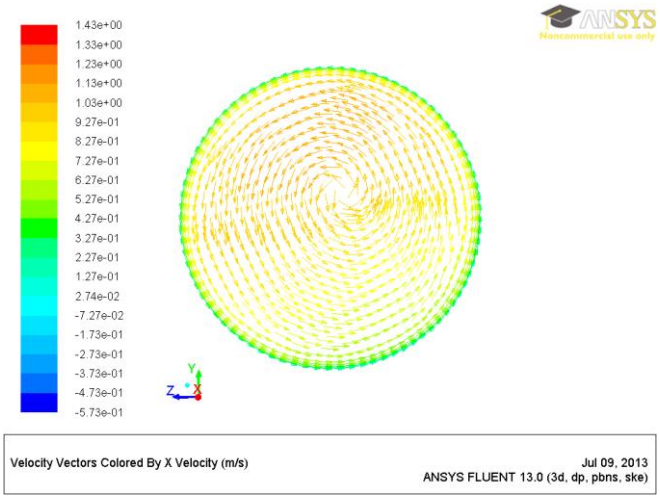

Fig. 4-39 b) Velocity Vectors by x velocity at 5D

Fig. 4-39 Velocity profiles at 5 D from CFD using K-epsilon Standard model and **standard wall function**

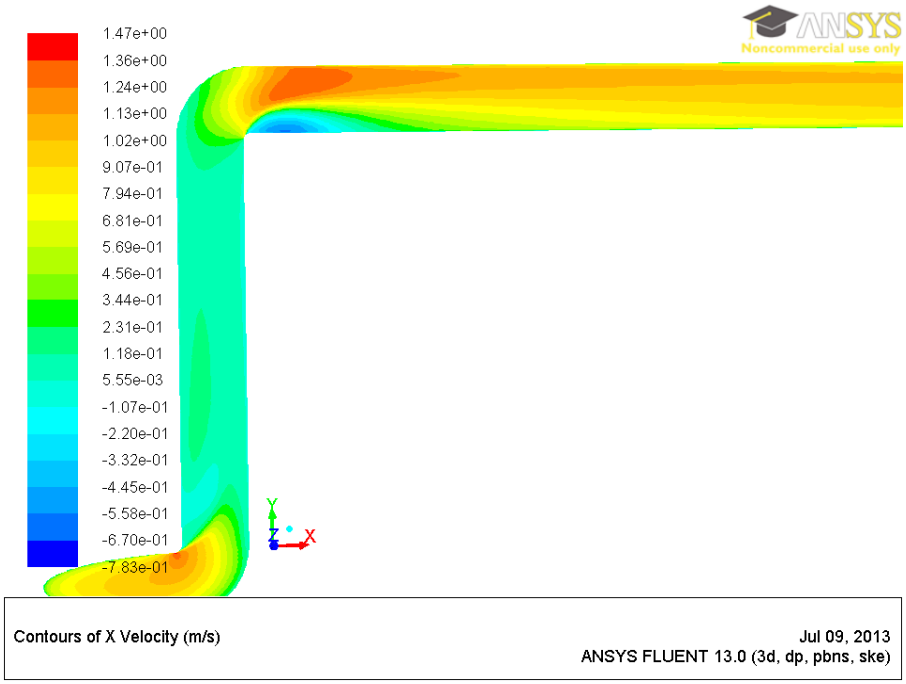

Fig. 4-40 Contours of X velocity K-epsilon Standard model and **standard wall function**

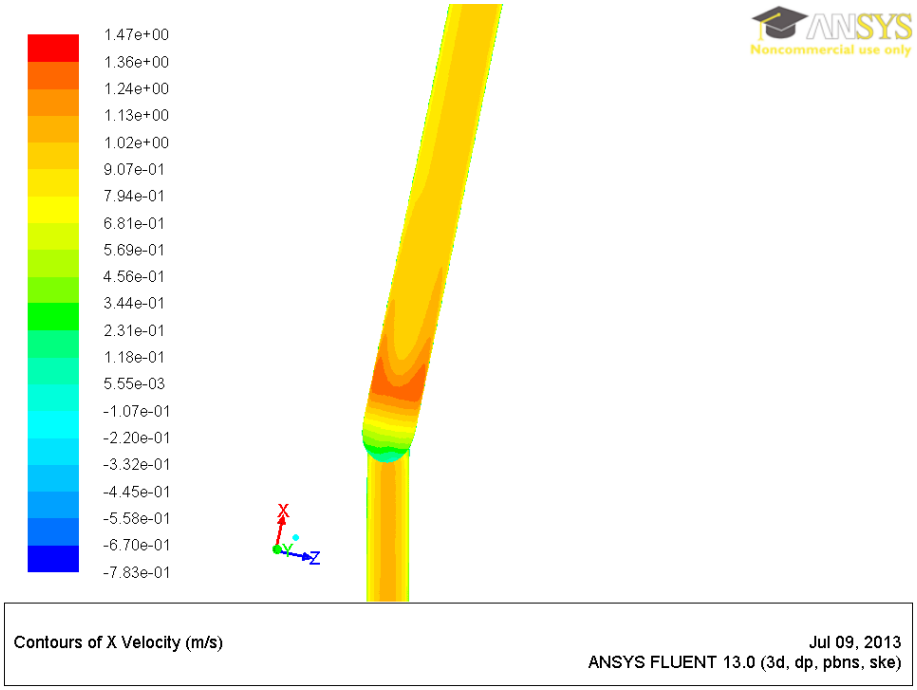

Fig. 4-41 Contours of X velocity K-epsilon Standard model and **standard wall function**

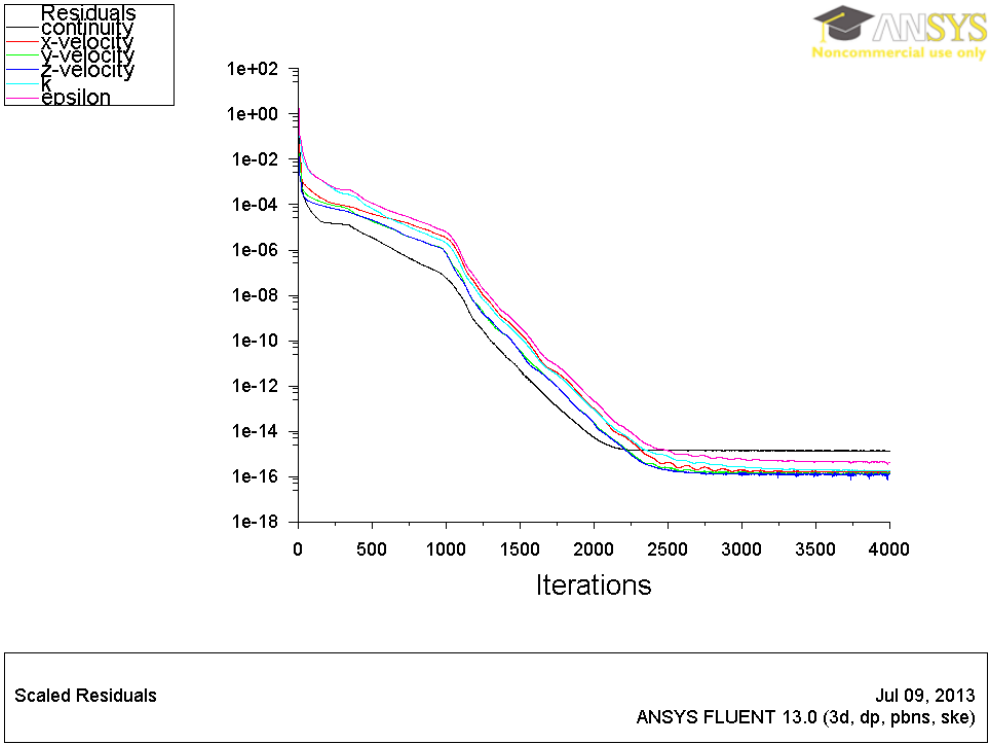

Fig. 4-42 Number of iterations of K-epsilon Standard model and **standard wall function**

K-omega SST model Standard wall treatment

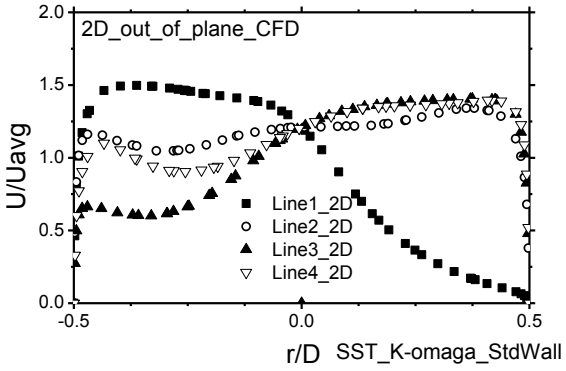

Fig. 4-43 Velocity profiles at 2 D from CFD using K-omega SST model and **standard wall function**

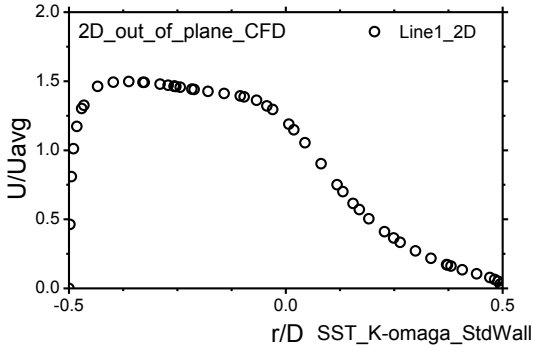

Fig. 4-44 a) Velocity profile at 2D line no. 1.

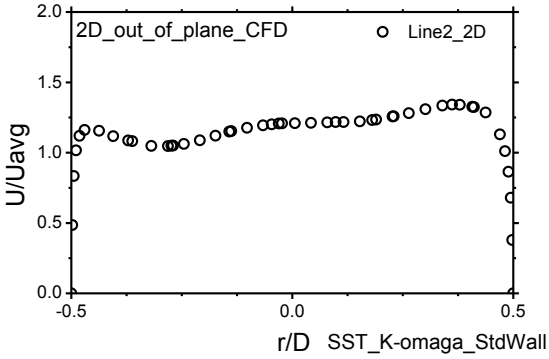

Fig. 4-44 b) Velocity profile at 2D line no. 2.

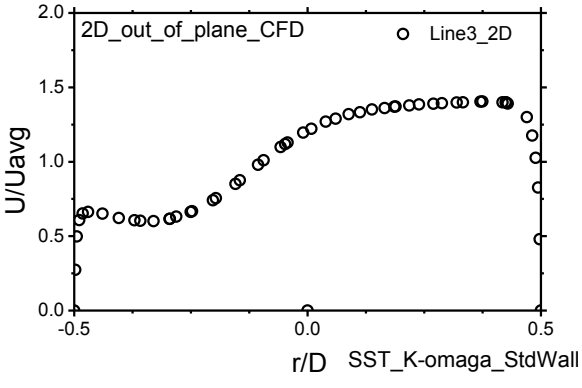

Fig. 4-44 c) Velocity profile at 2D line no. 3.

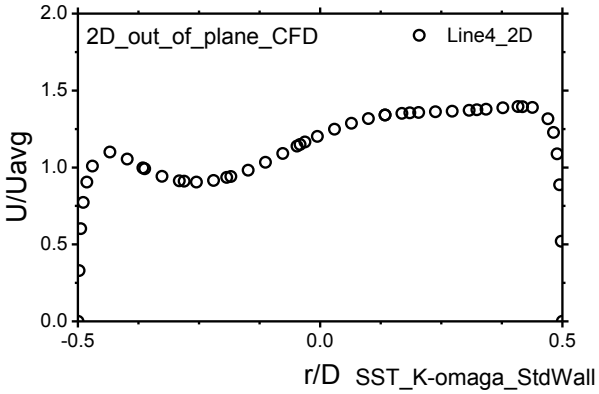

Fig. 4-44 d) Velocity profile at 2D line no. 4.

Fig. 4-44 Velocity profiles at 2 D from K-omega SST model and **standard wall function**

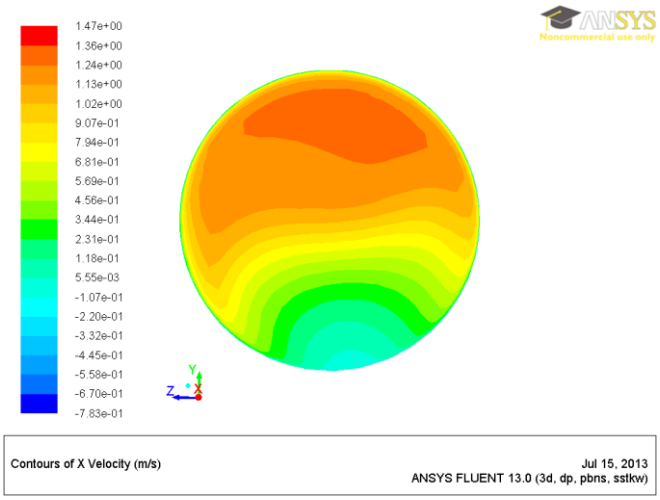

Fig. 4-45 a) Contours of x velocity at 2D

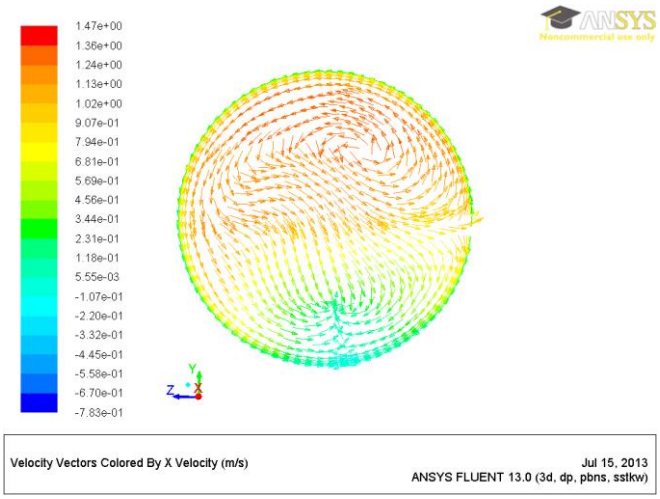

Fig. 4-45 a) Velocity Vectors by x velocity at 2D

Fig. 4-45 At 2 D from CFD using K-omega SST model and **standard wall function**

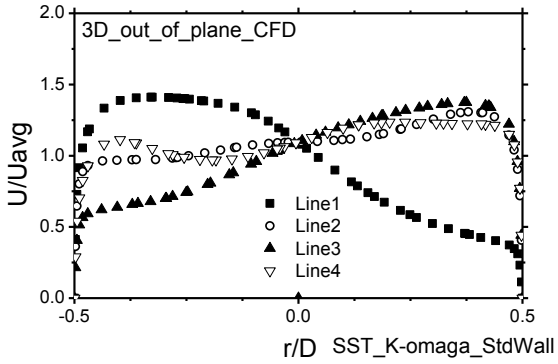

Fig. 4-43 Velocity profiles at 3 D from K-omega SST model and **standard wall function**

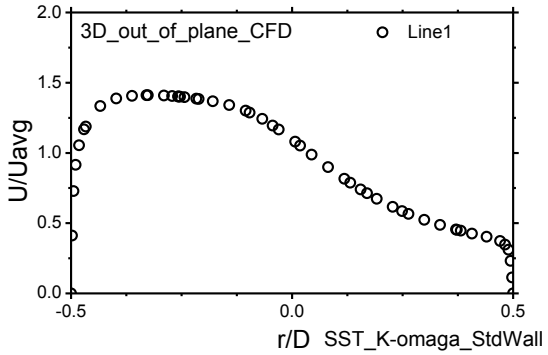

Fig. 4-47 a) Velocity profile at 3D line no. 1.

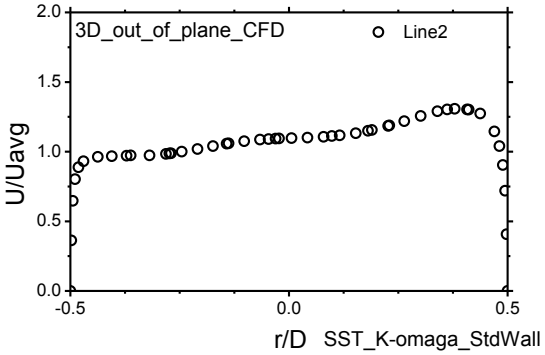

Fig. 4-47 b) Velocity profile at 3D line no. 2.

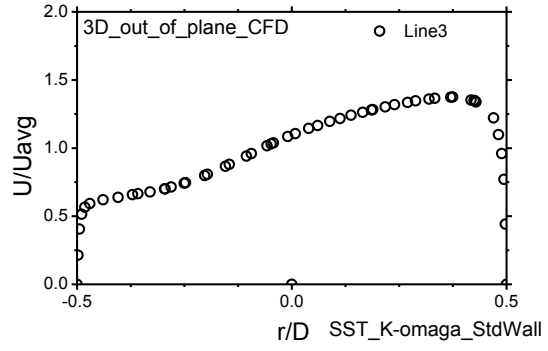

Fig. 4-47 c) Velocity profile at 3D line no. 1.

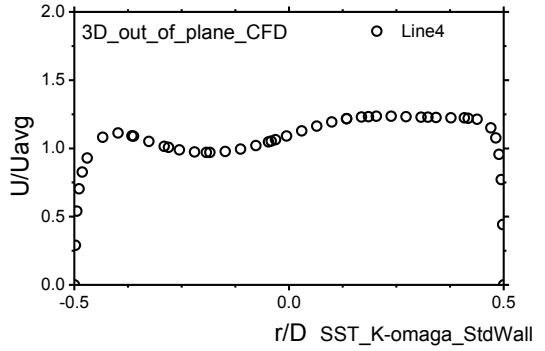

Fig. 4-47 d) Velocity profile at 3D line no. 2.

Fig. 4-47 Velocity profile at 3 D from CFD using K-omega SST model and **standard wall function**

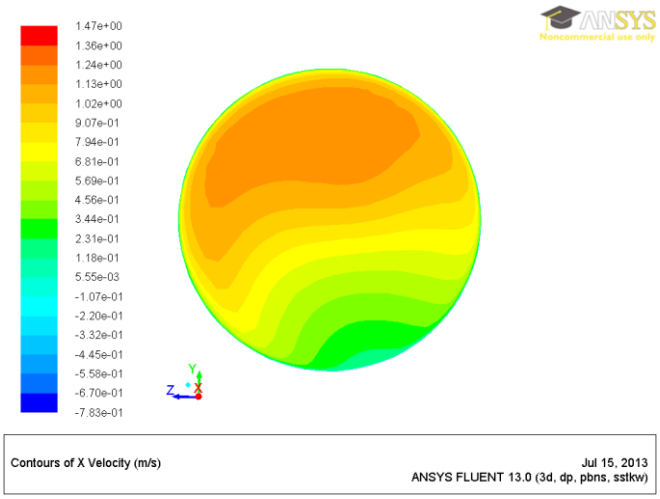

Fig. 4-48 a) Contours of x velocity at 3D

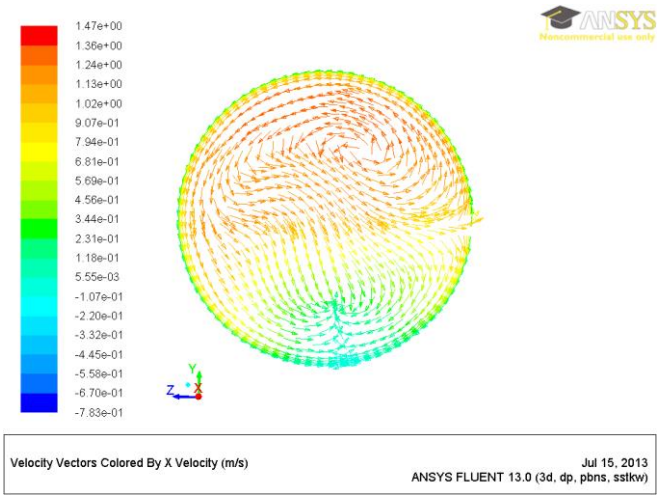

Fig. 4-48 b) Velocity Vectors by x velocity at 3D

Fig. 4-48 Contours of x velocity at 3 D from CFD using K-omega SST model and **standard wall function**

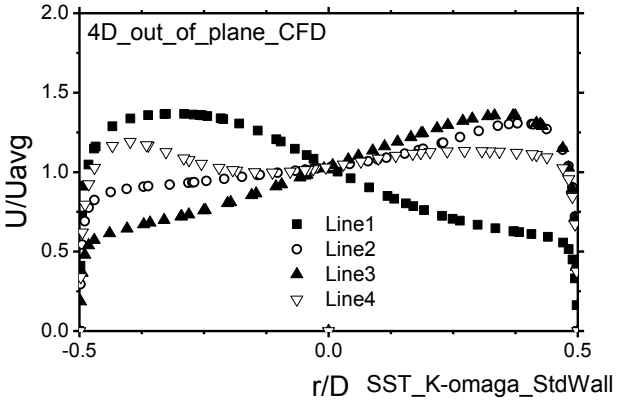

Fig. 4-49 Velocity profiles at 4 D from CFD using K-omega SST model and **standard wall function**

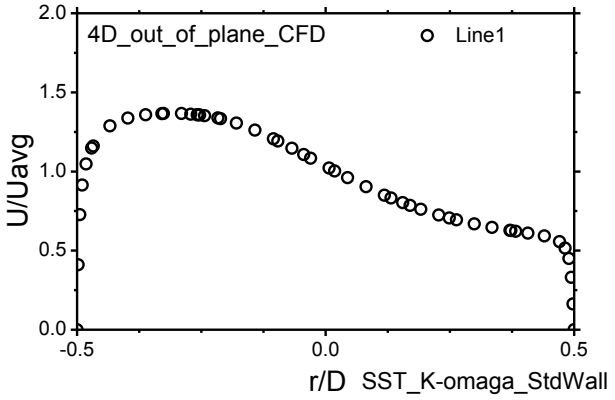

Fig. 4-50 a) Velocity profile at 4D line no. 1.

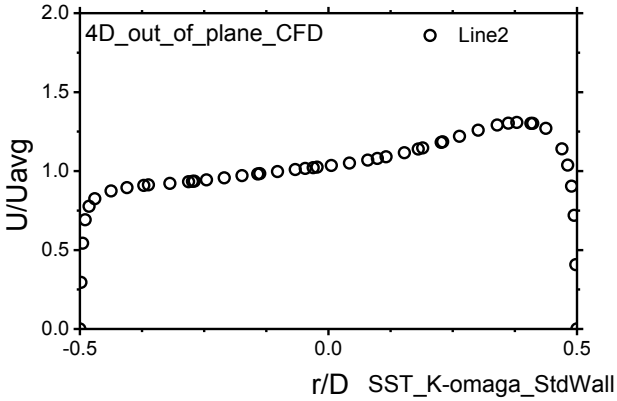

Fig. 4-50 b) Velocity profile at 4D line no. 2.

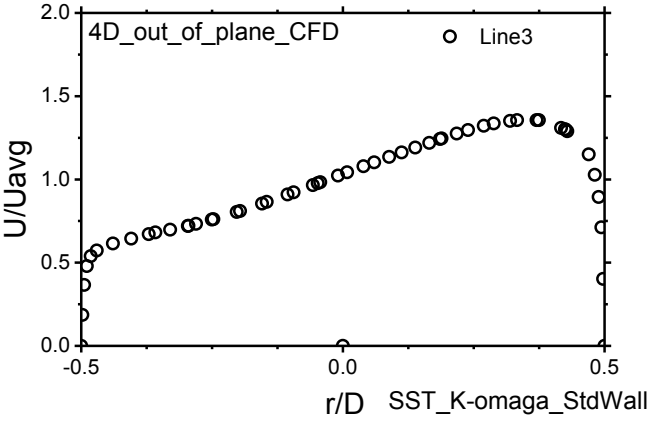

Fig. 4-50 c) Velocity profile at 4D line no. 3.

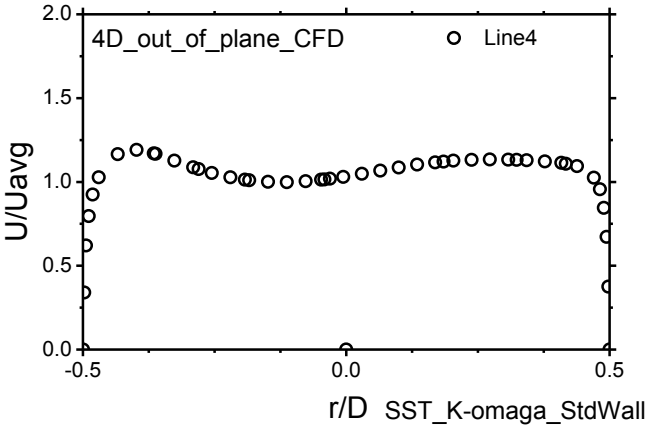

Fig. 4-50 d) Velocity profile at 4D line no. 4.

Fig. 4-50 Velocity profiles at 4 D from K-omega SST model and **standard wall function**

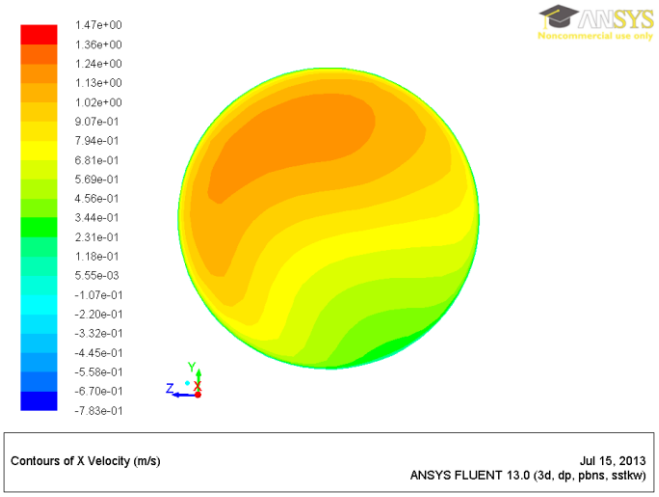

Fig. 4-51 a) Contours of x velocity at 4D

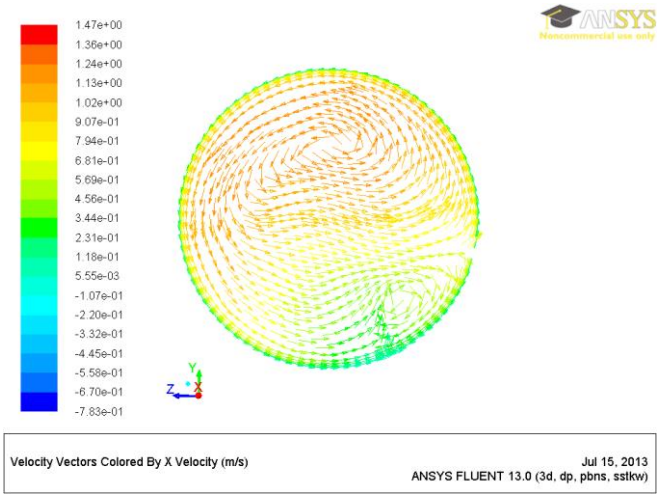

Fig. 4-51 b) Velocity Vectors by x velocity at 4D

Fig. 4-51 Contours of x velocity at 4 D from CFD using K-omega SST model and **standard wall function**

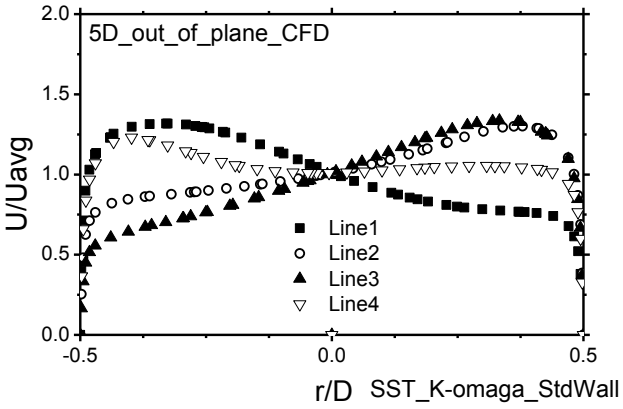

Fig. 4-52 Velocity profiles at 4 D from CFD using K-omega SST model and **standard wall function**

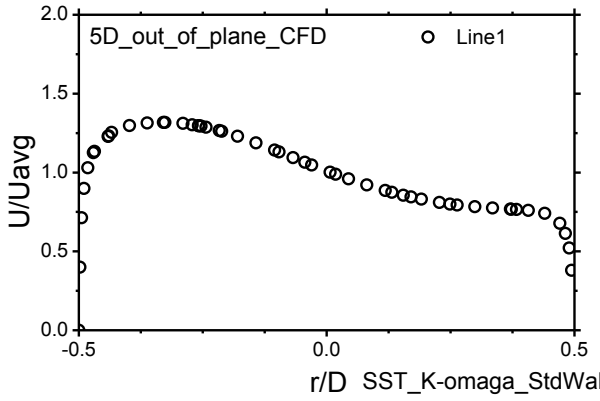

Fig. 4-53 a) Velocity profile at 5D line no. 1.

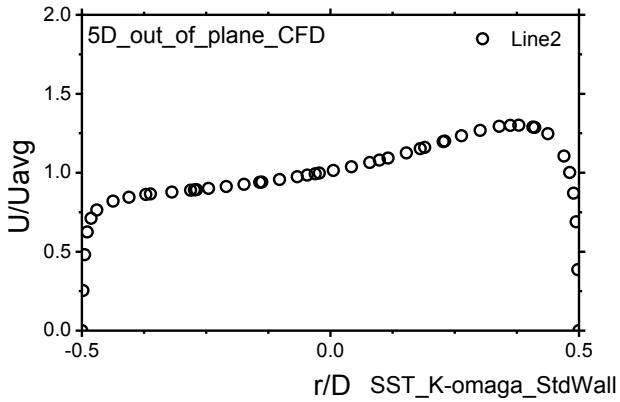

Fig. 4-53 b) Velocity profile at 5D line no. 2.

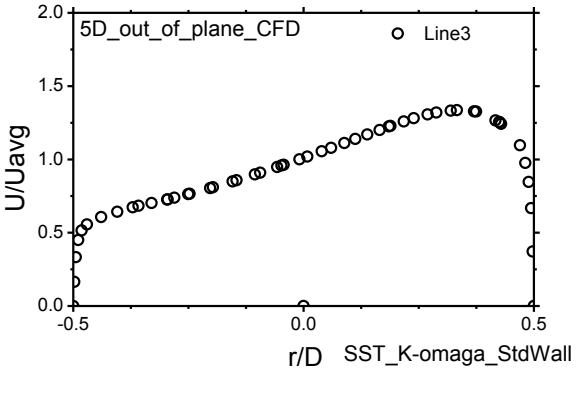

Fig. 4-53 c) Velocity profile at 5D line no. 3.

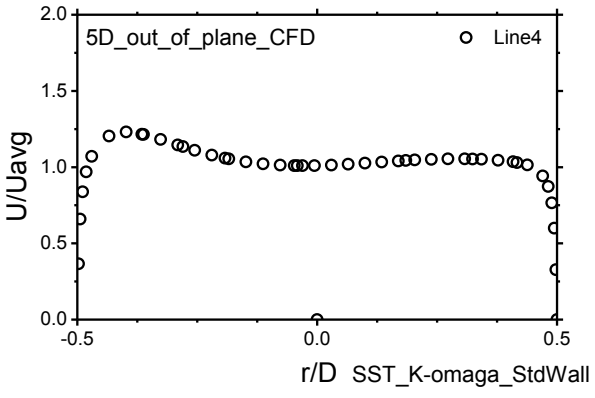

Fig. 4-53 d) Velocity profile at 5D line no. 4.

Fig. 4-53 Velocity profiles at 4 D from K-omega SST model and **standard wall function**

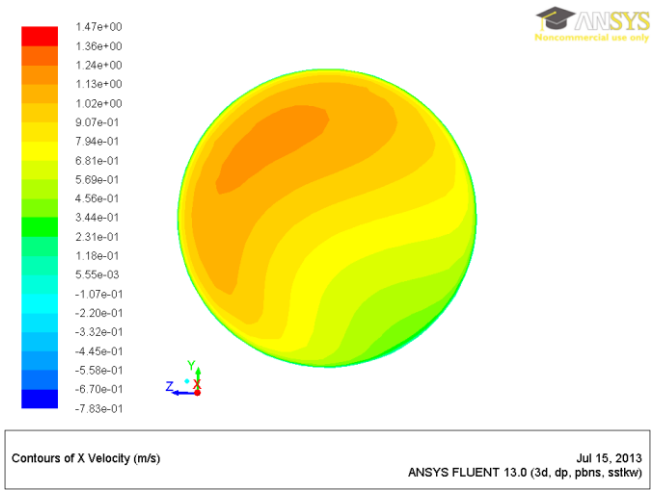

Fig. 4-54 a) Contours of x velocity at 5D

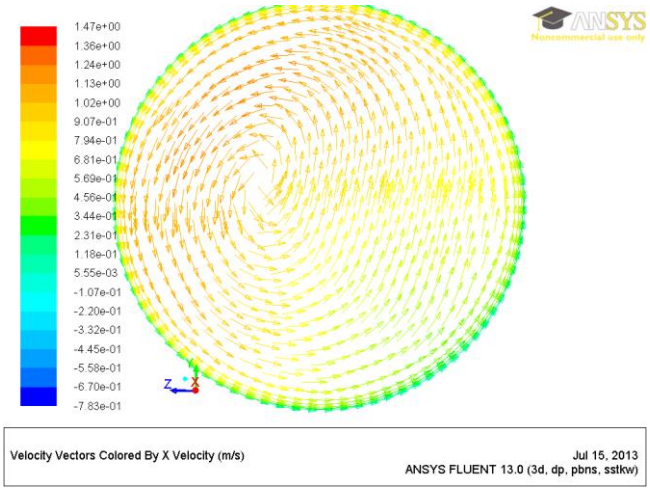

Fig. 4-54 b) Velocity Vectors by x velocity at 5D

Fig. 4-54 Velocity profiles at 4 D from CFD using K-omega SST model and **standard wall function**

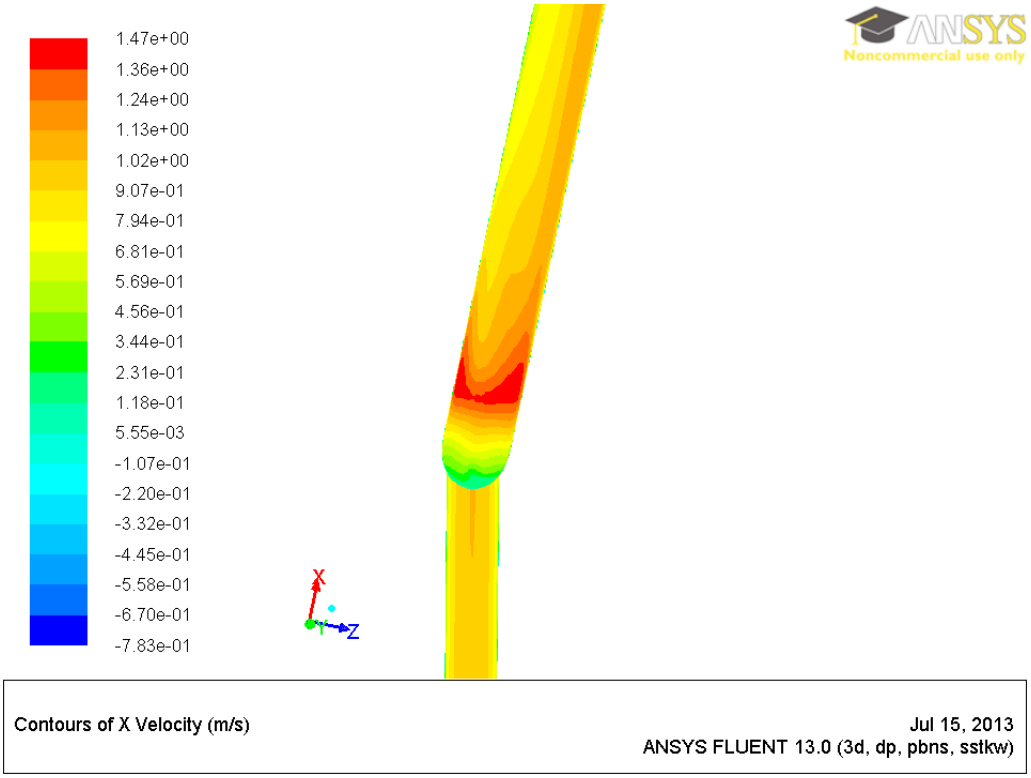

Fig. 4-55 Contours of X velocity on top view K-omega SST model and **standard wall function**

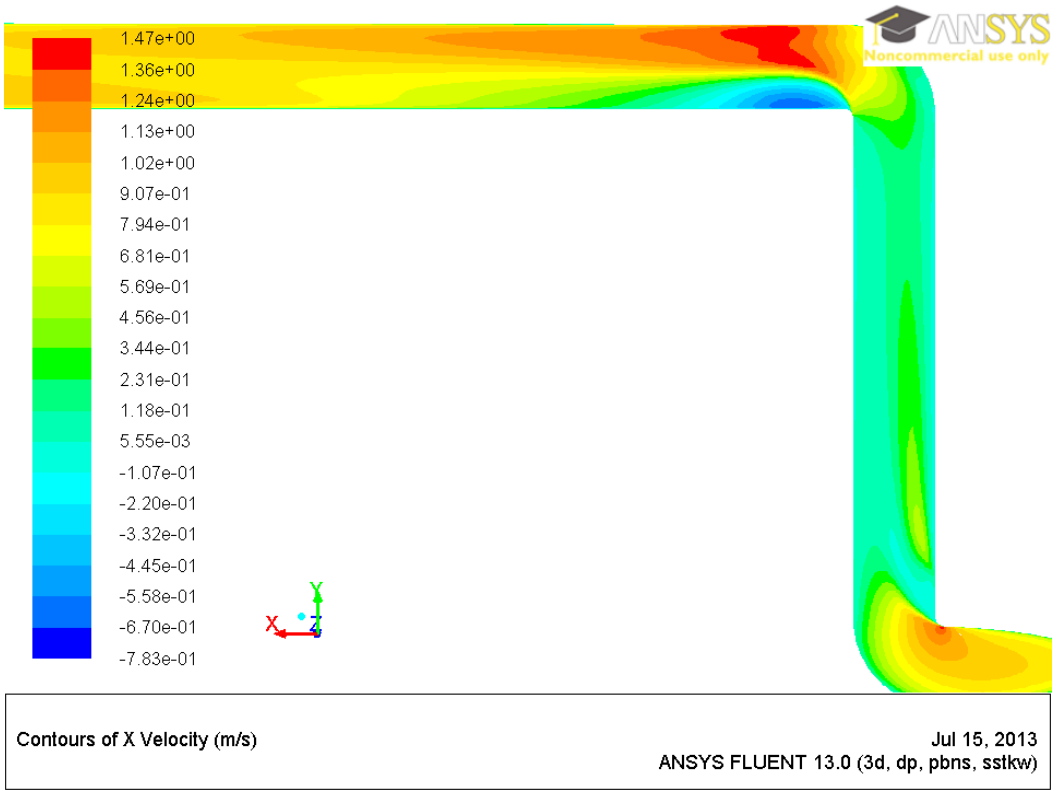

Fig. 4-56 Contours of X velocity side view of K-omega SST model and **standard wall function**

Realizable K-epsilon standard wall treatment

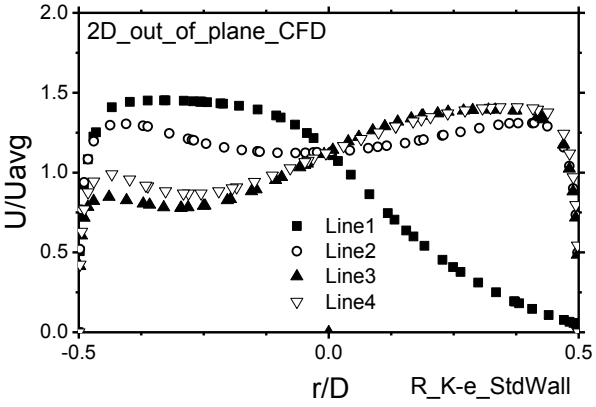

Fig. 4-57 Velocity profiles at 2 D from CFD using K-epsilon Standard model and **standard wall function**

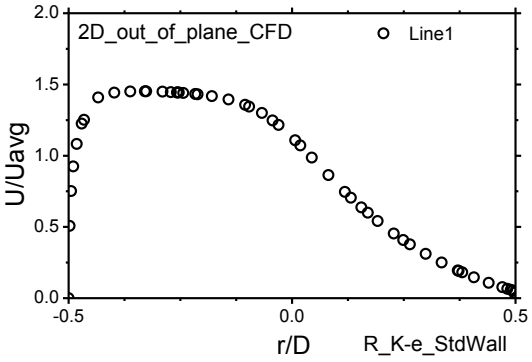

Fig. 4-58 a) Velocity profile at 2D line no. 1.

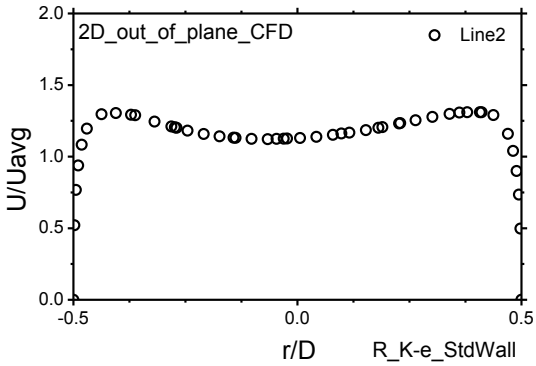

Fig. 4-58 b) Velocity profile at 2D line no. 2.

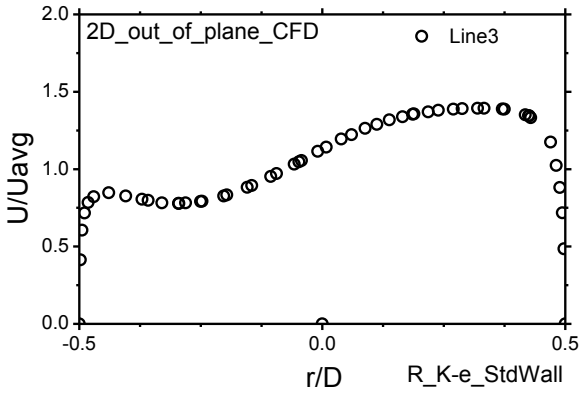

Fig. 4-58 c) Velocity profile at 2D line no. 3.

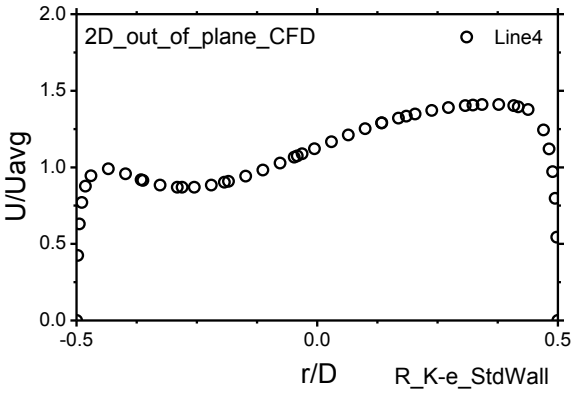

Fig. 4-58 d) Velocity profile at 2D line no. 4.

Fig. 4-58 Velocity profiles at 2 D from K-epsilon Standard model and **standard wall function**

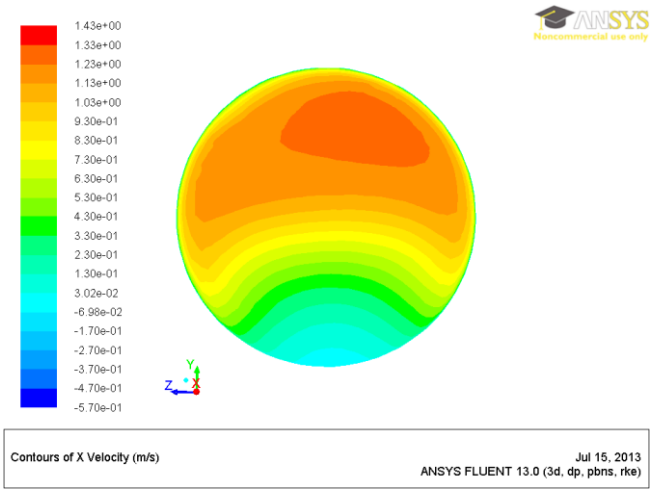

Fig. 4-59 c) Contours of x velocity at 2D

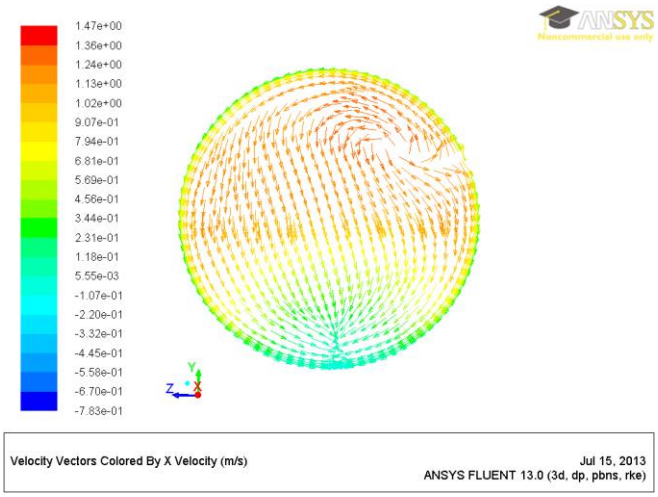

Fig. 4-59 d) Velocity Vectors by x velocity at 2D

Fig. 4-59 Contours of x at 2 D from CFD using K-epsilon Standard model and **standard wall function**

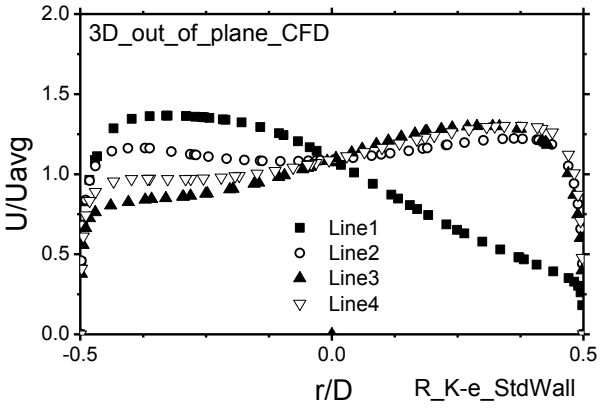

Fig. 4-60 Velocity profiles at 3 D from CFD using K-epsilon Standard model and **standard wall function**

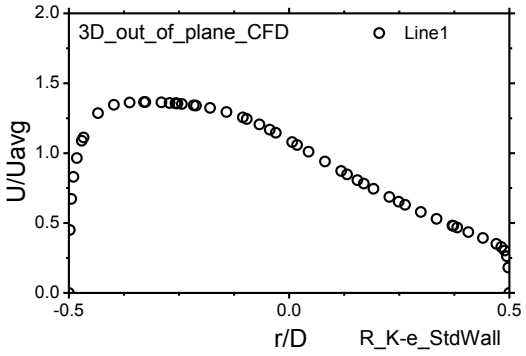

Fig. 4-61 a) Velocity profile at 3D line no. 1.

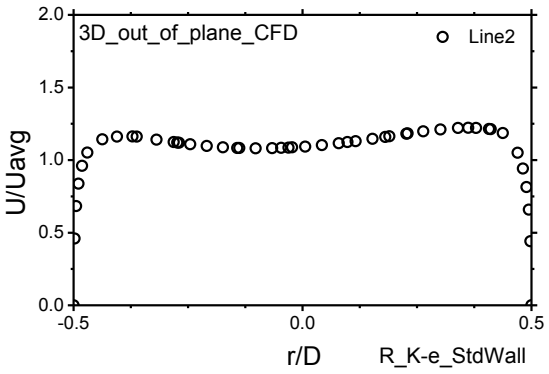

Fig. 4-61 b) Velocity profile at 3D line no. 2.

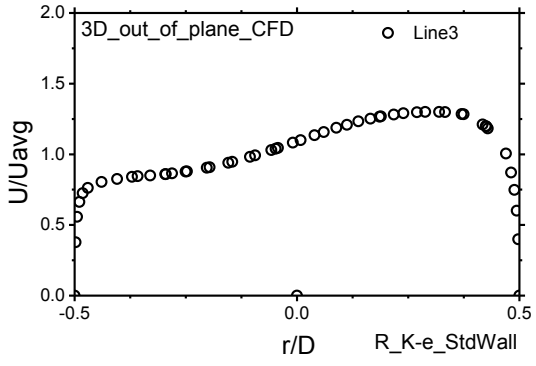

Fig. 4-61 c) Velocity profile at 3D line no. 3.

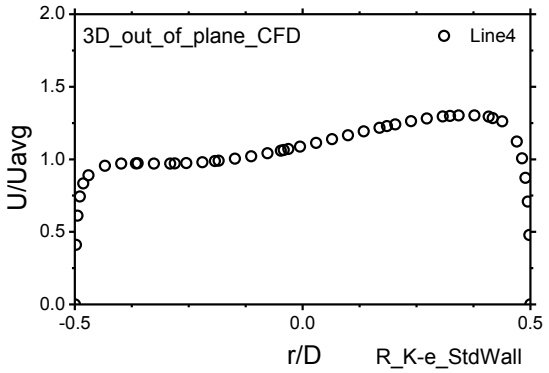

Fig. 4-61 d) Velocity profile at 3D line no. 4.

Fig. 4-61 Velocity profile at 3 D from CFD using K-epsilon Standard model and **standard wall function**

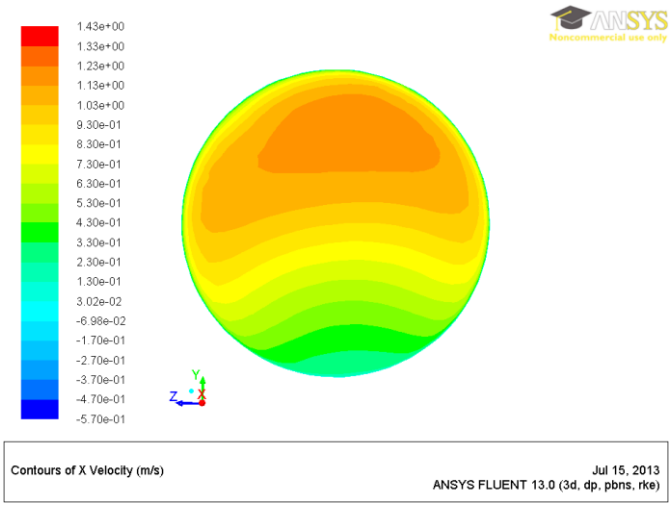

Fig. 4-62 a) Contours of x velocity at 3D

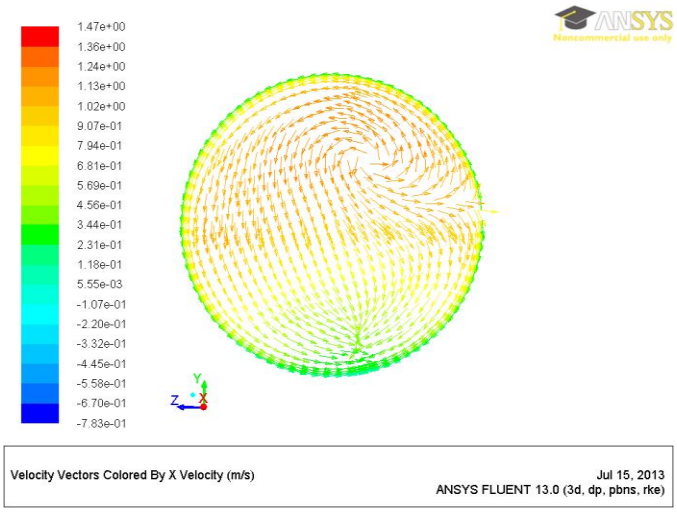

Fig. 4-62 b) Velocity Vectors by x velocity at 3D

Fig. 4-62 Contours of x velocity at 3 D from CFD using K-epsilon Standard model and **standard wall function**

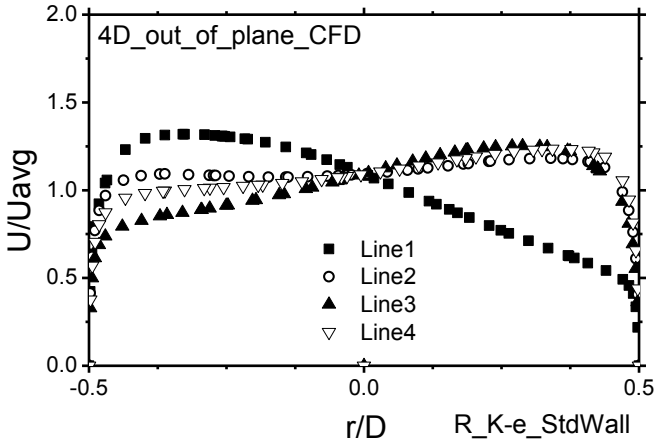

Fig. 4-63 Velocity profiles at 4 D from CFD using K-epsilon Standard model and **standard wall function**

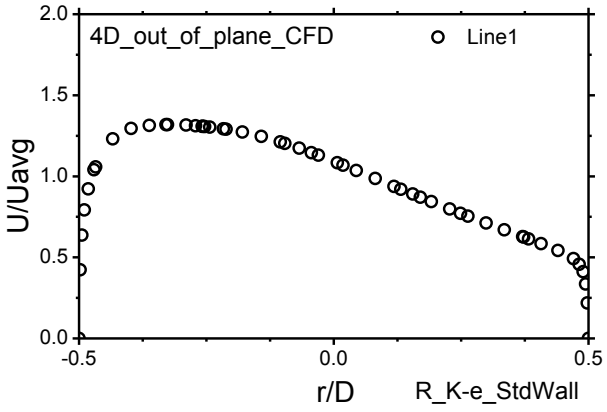

Fig. 4-64 a) Velocity profile at 4D line no. 1.

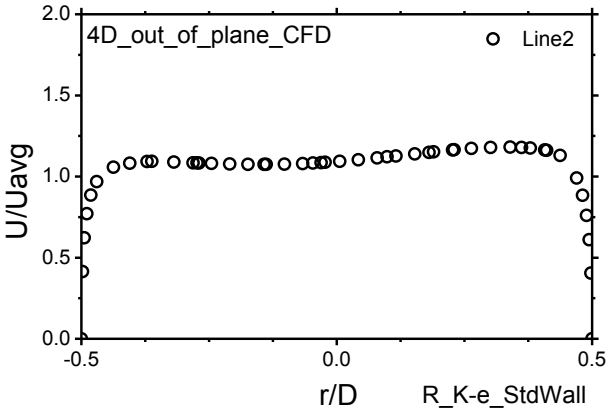

Fig. 4-64 b) Velocity profile at 4D line no. 2.

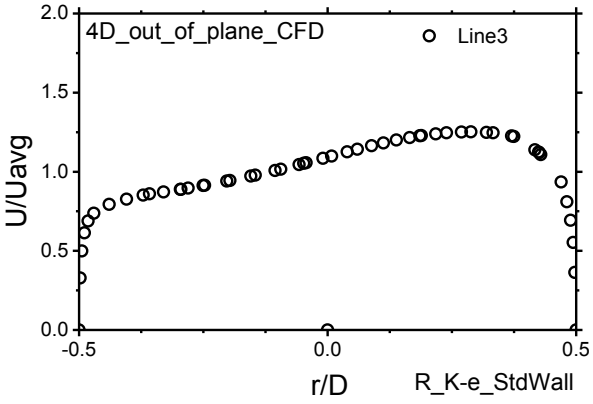

Fig. 4-64 c) Velocity profile at 4D line no. 3.

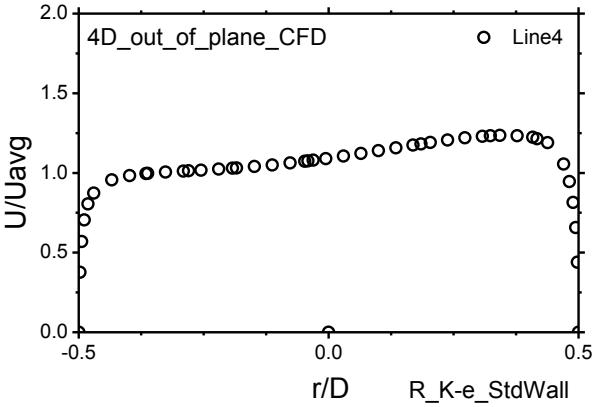

Fig. 4-64 d) Velocity profile at 4D line no. 4.

Fig. 4-64 Velocity profiles at 4 D from K-epsilon Standard model and **standard wall function**

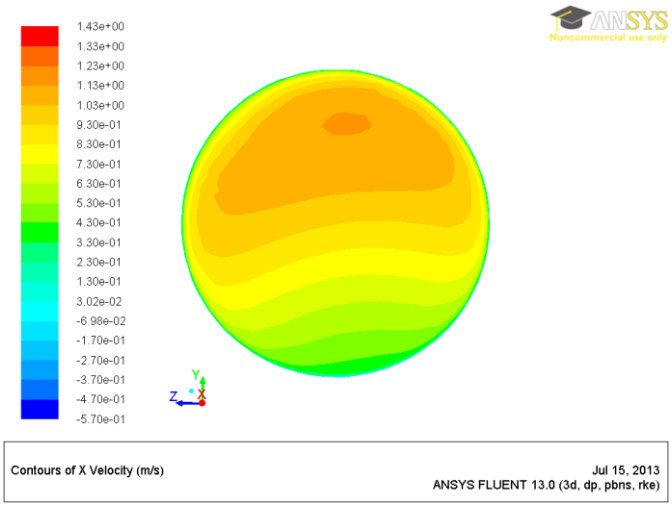

Fig. 4-65 a) Contours of x velocity at 4D

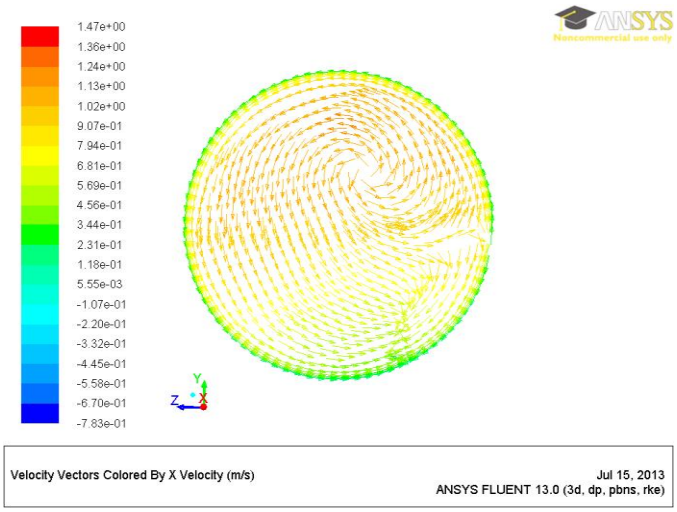

Fig. 4-65 b) Velocity Vectors by x velocity at 4D

Fig. 4-65 Contours of x velocity at 4 D from CFD using K-epsilon Standard model and **standard wall function**

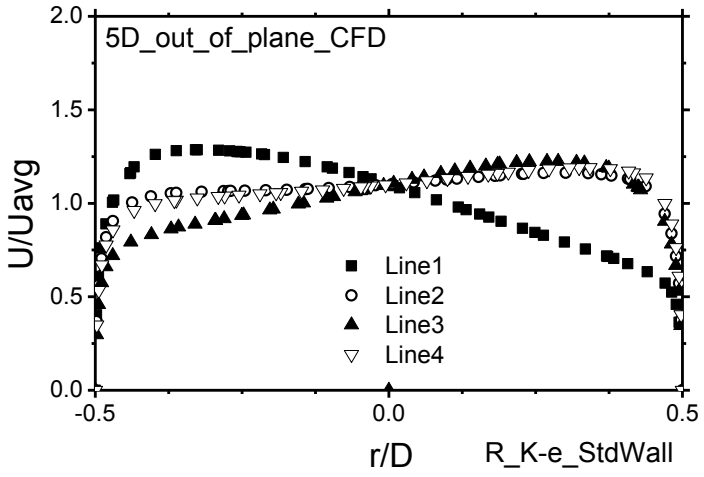

Fig. 4-66 Velocity profiles at 5 D from CFD using K-epsilon Standard model and **standard wall function**

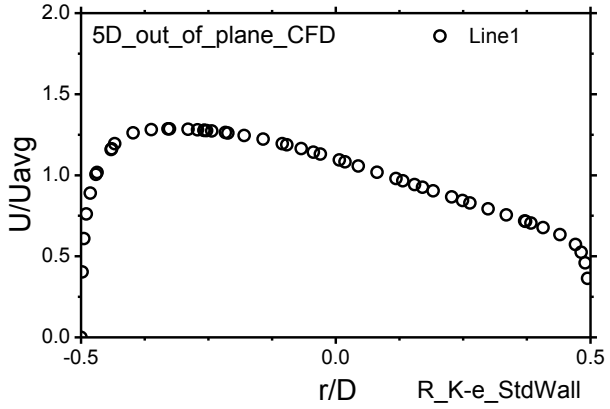

Fig.…Velocity profile at 5D line no. 1.

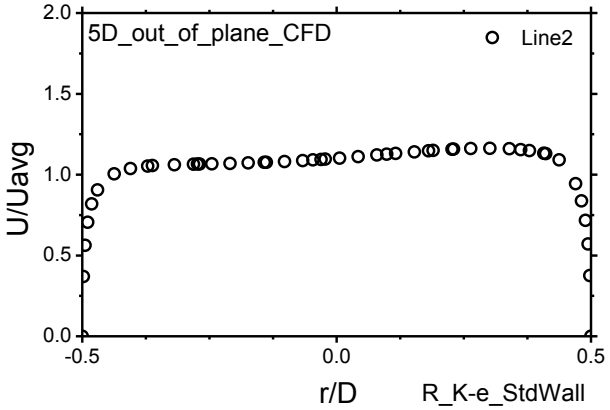

Fig.…Velocity profile at 5D line no. 2.

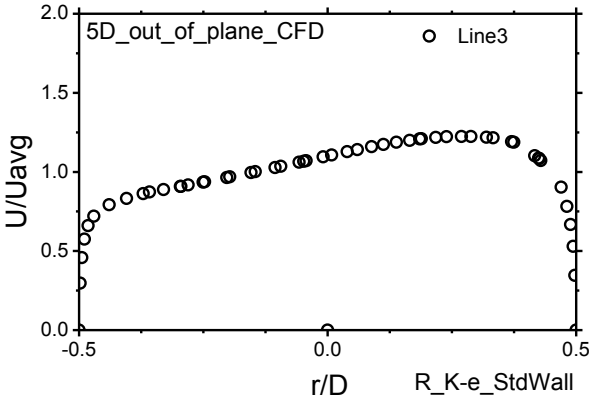

Fig. 4-67 a) Velocity profile at 5D line no. 3.

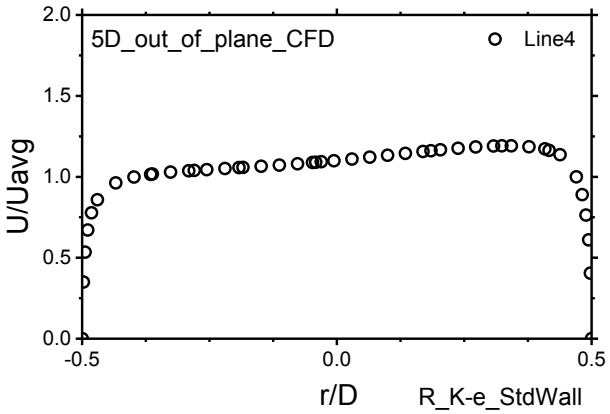

Fig. 4-67 b) Velocity profile at 5D line no. 4.

Fig. 4-67 Velocity profiles at 5 D from K-epsilon Standard model and **standard wall function**

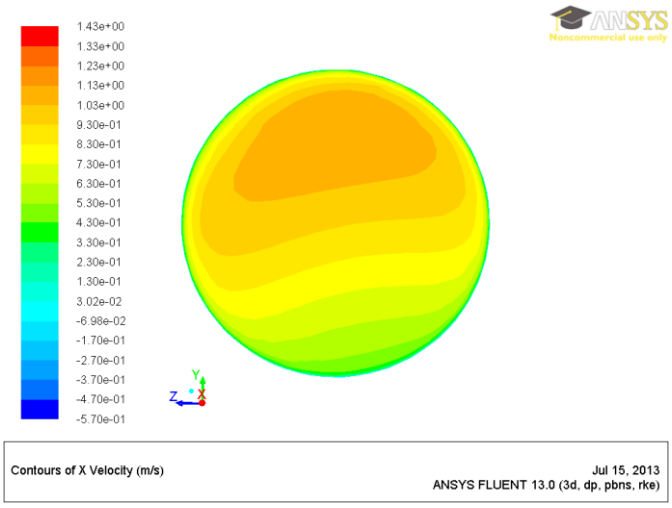

Fig. 4-68 a) Contours of x velocity at 5D

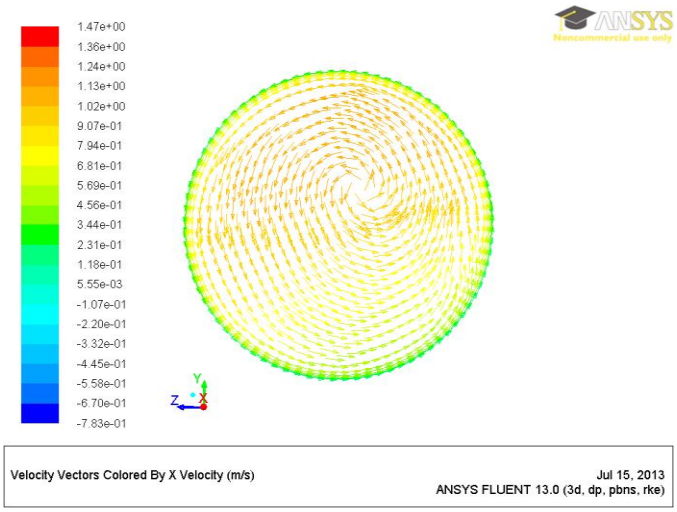

Fig. 4-68 b) Velocity Vectors by x velocity at 5D

Fig. 4-68 Contours of x velocity at 5 D from K-epsilon Standard model and **standard wall function**

Large eddy simulation (LES)

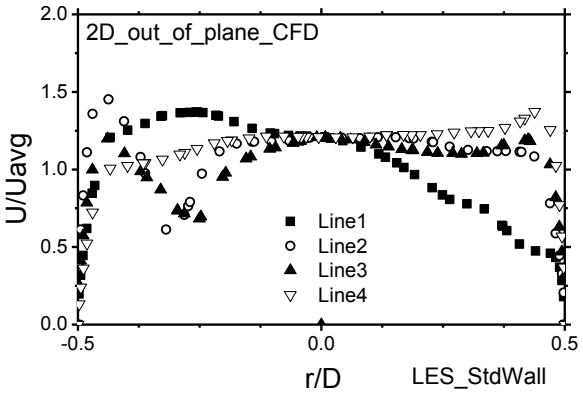

Fig. 4-69 Velocity profiles at 2 D from LES model and **standard wall function**

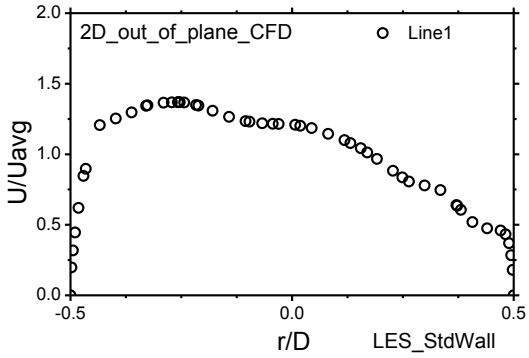

Fig. 4-70 a) Velocity profile at 2D line no. 1.

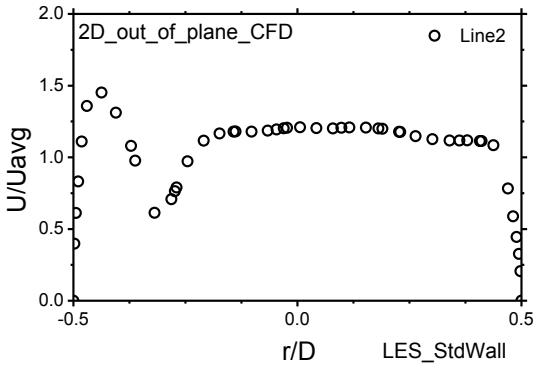

Fig. 4-70 b) Velocity profile at 2D line no. 2.

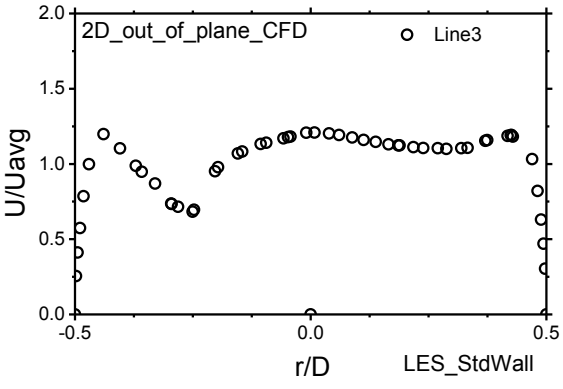

Fig. 4-70 c) Velocity profile at 2D line no. 3.

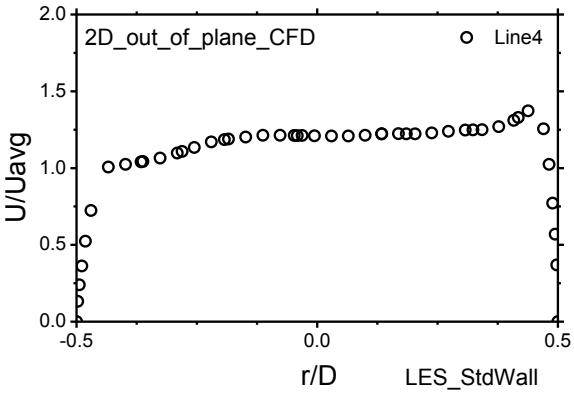

Fig. 4-70 d) Velocity profile at 2D line no. 4.

Fig. 4-70 Velocity profiles at 5 D from CFD using LES model and **standard wall function**

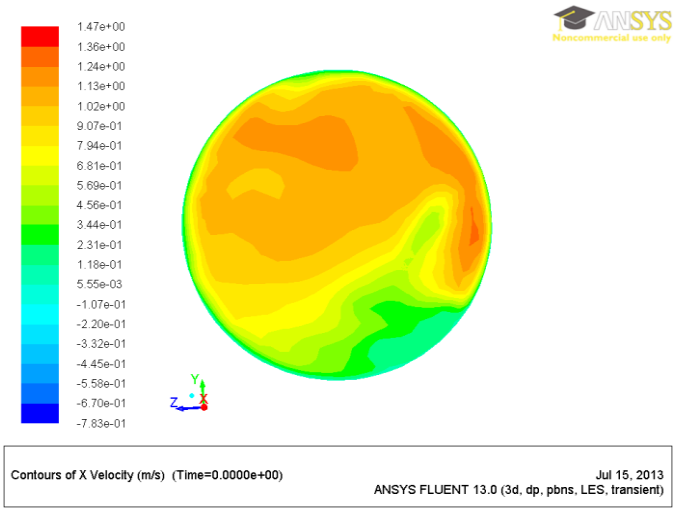

Fig. 4-70 c) Contours of x velocity at 2D

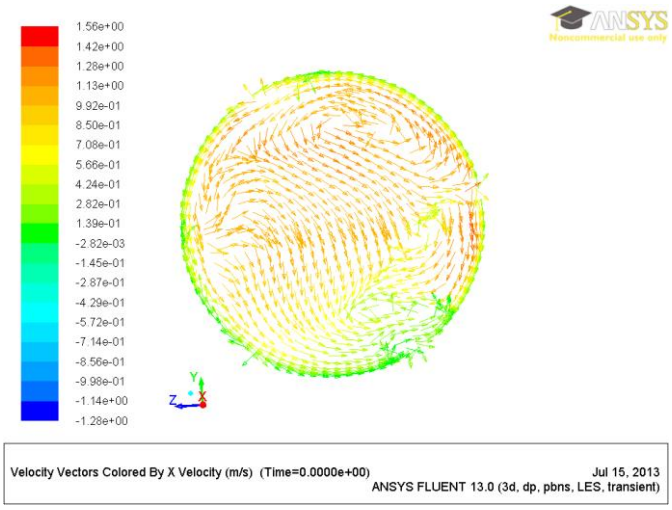

Fig. 4-70 d) Velocity Vectors by x velocity at 2D

Fig. 4-71 Contours of x velocity at 2 D from LES model and **standard wall function**

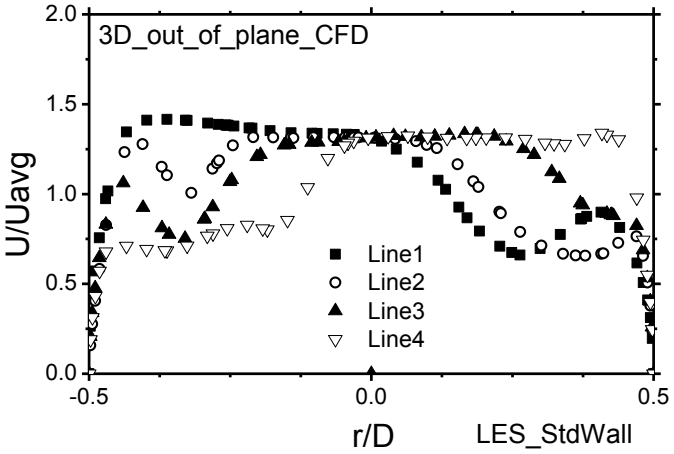

Fig. 4-72 Velocity profiles at 2 D from LES model and **standard wall function**

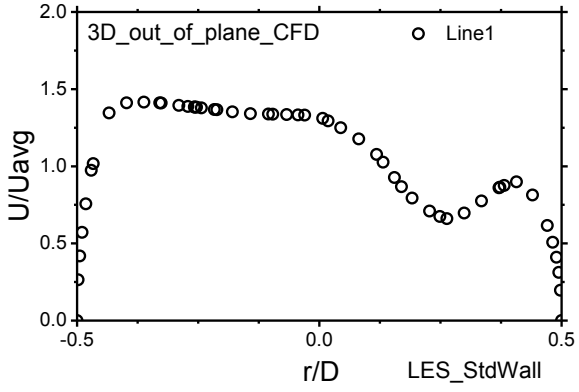

Fig. 4-73 a).Velocity profile at 3D line no. 1.

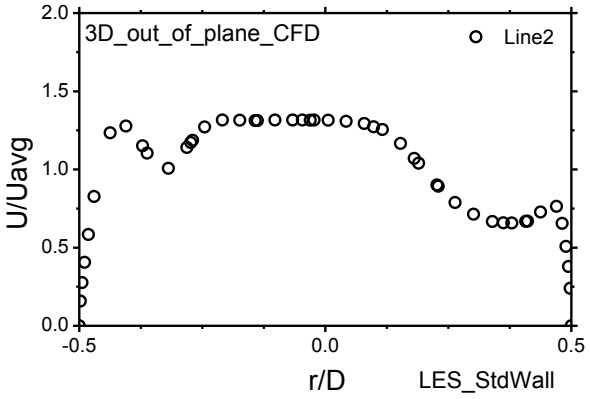

Fig. 4-73 b) Velocity profile at 3D line no. 2.

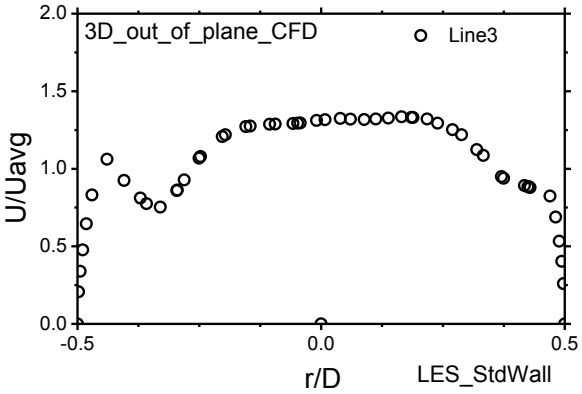

Fig. 4-73 c) Velocity profile at 3D line no. 3.

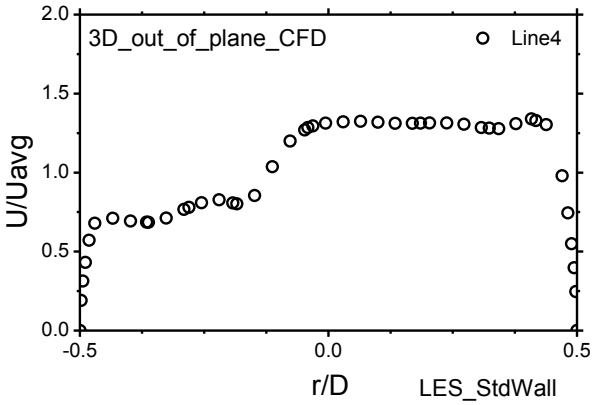

Fig. 4-73 d) Velocity profile at 3D line no. 4.

Fig. 4-73 Velocity profiles at 3 D from LES model and **standard wall function**

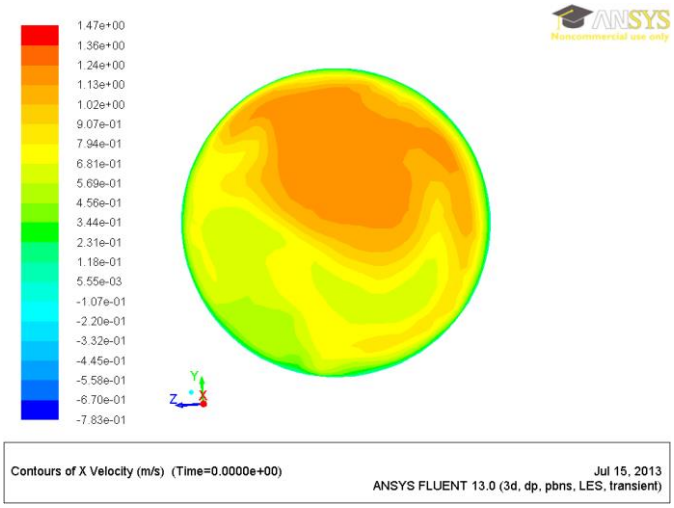

Fig. 4-74 a) Contours of x velocity at 3D

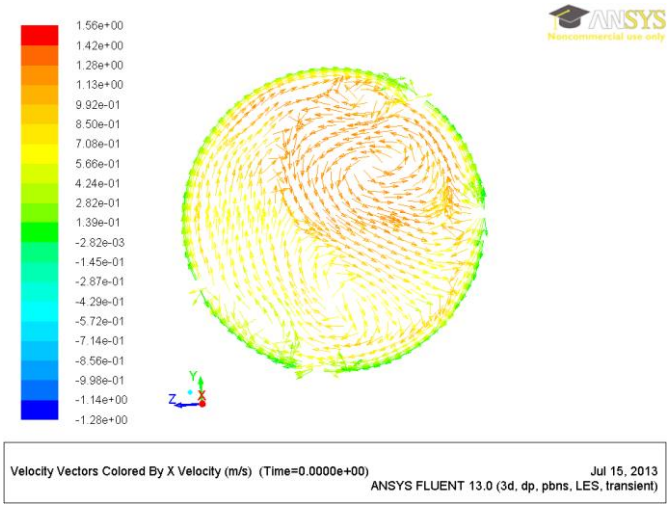

Fig. 4-72 b) Velocity Vectors by x velocity at 3D

Fig. 4-74 Contours of x velocity at 3 D from LES model and **standard wall function**

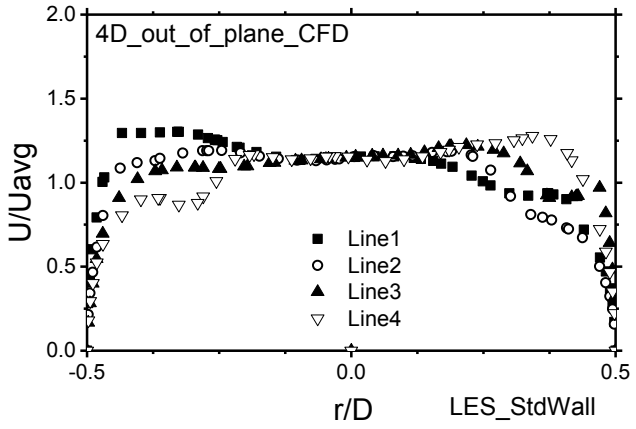

Fig. 4-75 Velocity profiles at 4 D from LES model and **standard wall function**

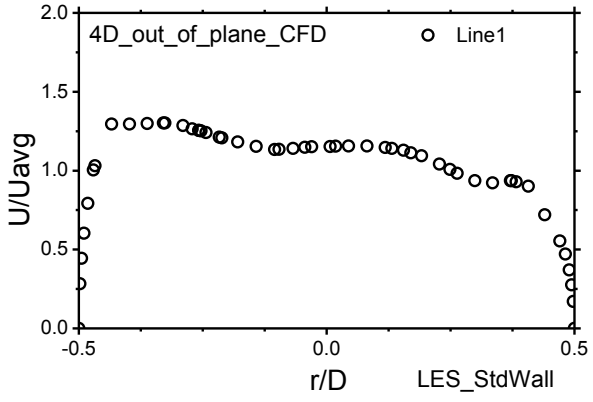

Fig. 4-76 a) Velocity profile at 4D line no. 1.

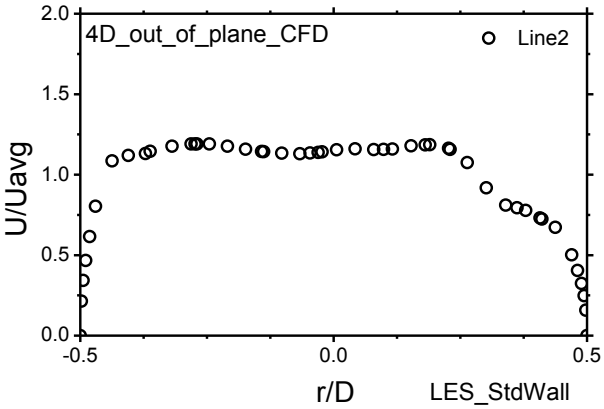

Fig. 4-76 b) Velocity profile at 4D line no. 2.

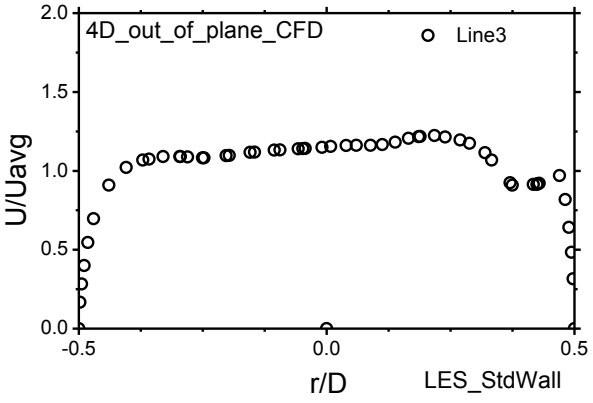

Fig. 4-76 c) Velocity profile at 4D line no. 3.

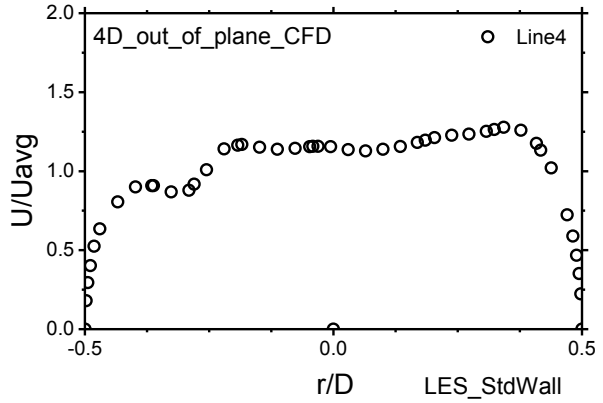

Fig. 4-76 d) Velocity profile at 4D line no. 4.

Fig. 4-76 Velocity profiles at 2 D from LES model and **standard wall function**

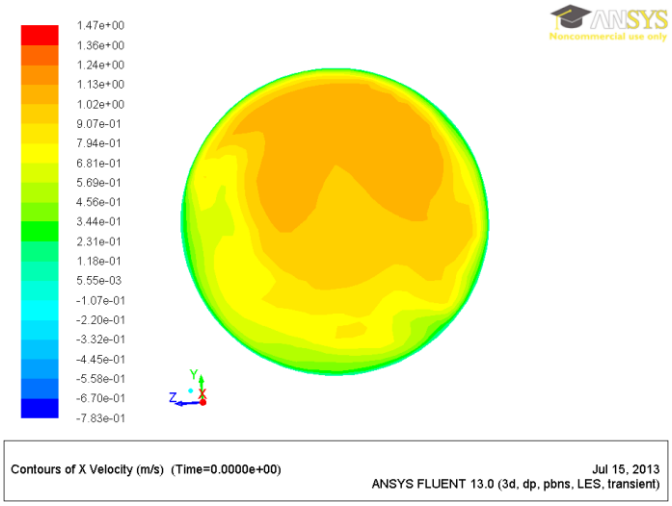

Fig. 4-77 a) Contours of x velocity at 4D

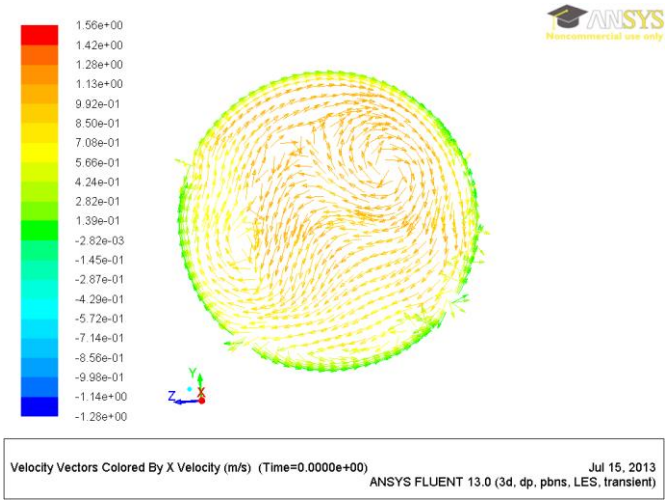

Fig. 4-77 a) Velocity Vectors by x velocity at 4D

Fig. 4-77 Contours of x velocity at 4 D from LES model and **standard wall function**

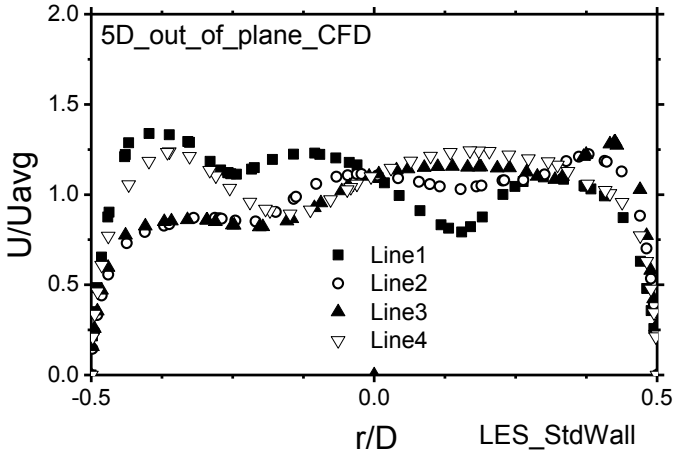

Fig. 4-78 Velocity profiles at 5 D from CFD using LES model and **standard wall function**

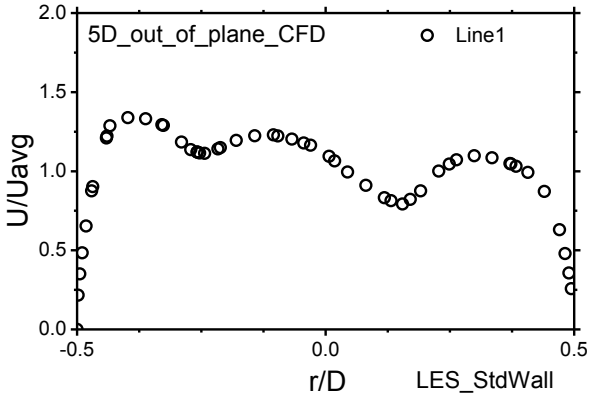

Fig. 4-79 a) Velocity profile at 5D line no. 1.

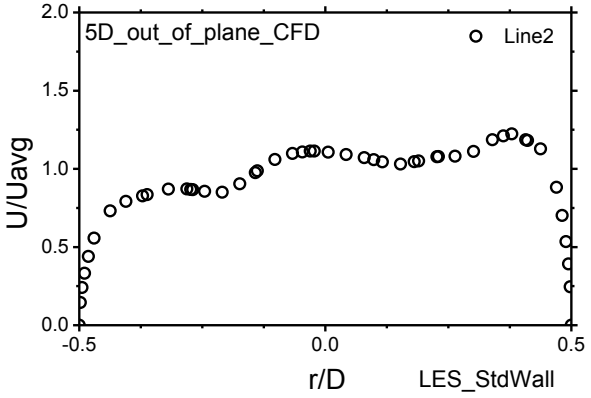

Fig. 4-79 b) Velocity profile at 5D line no. 2.

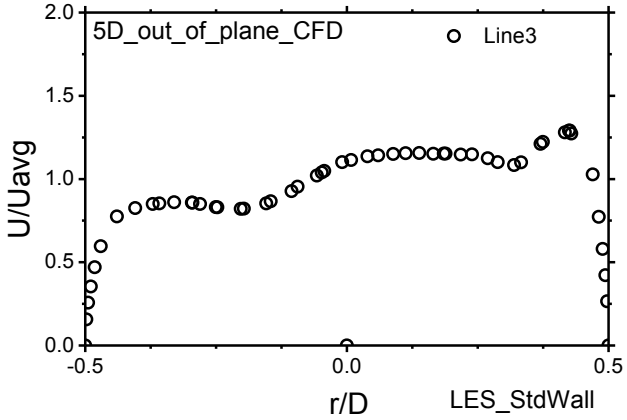

Fig. 4-79 c) Velocity profile at 5D line no. 3.

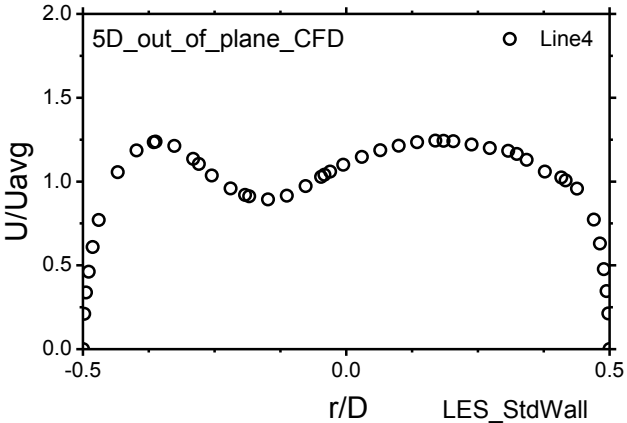

Fig. 4-79 d) Velocity profile at 5D line no. 4.

Fig. 4-79 Velocity profiles at 5 D from CFD using LES model and **standard wall function**

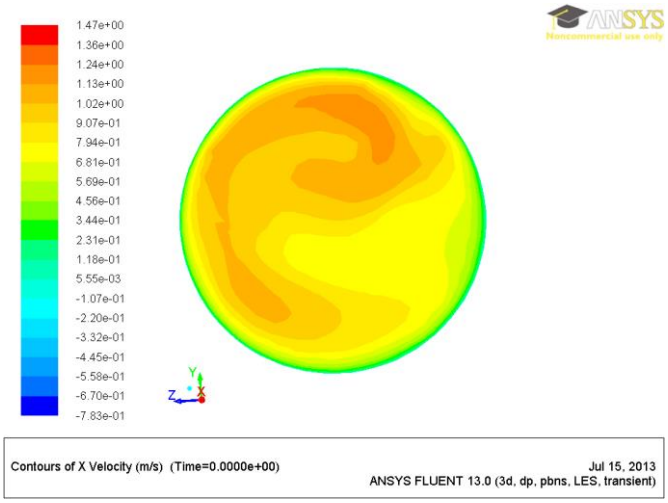

Fig. 4-80 a) Contours of x velocity at 5D

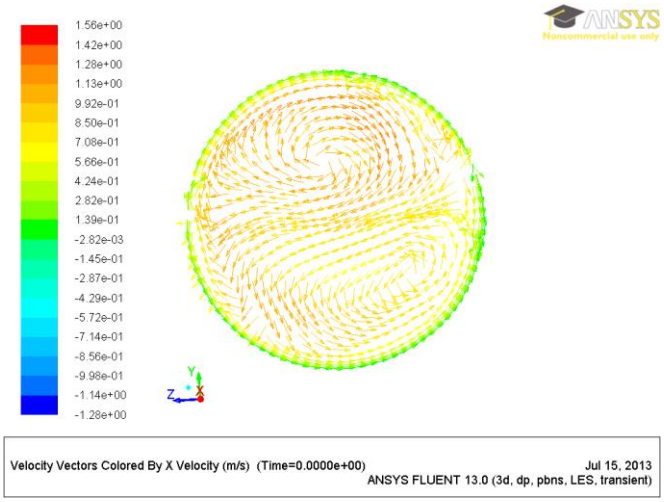

Fig. 4-80 b) Velocity Vectors by x velocity at 5D

Fig. 4-80 Contours velocity at 5 D from CFD using LES model and **standard wall function**

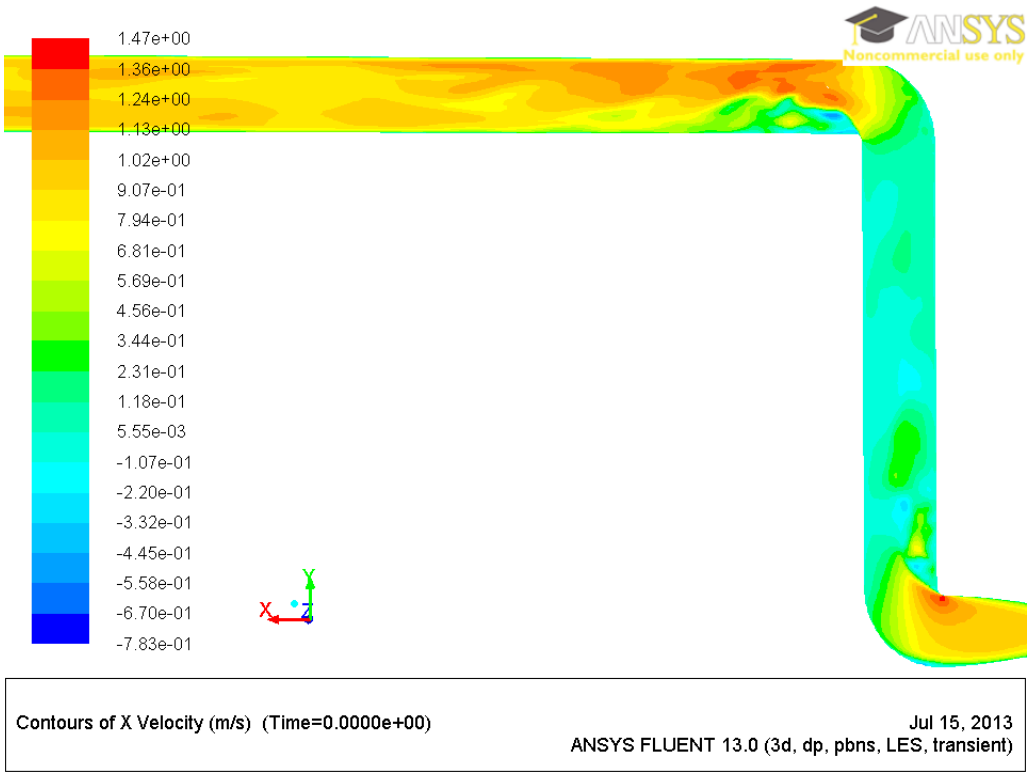

Fig. 4-81 Contours of X- Velocity at side view 5 D from CFD using LES model and **standard wall function**

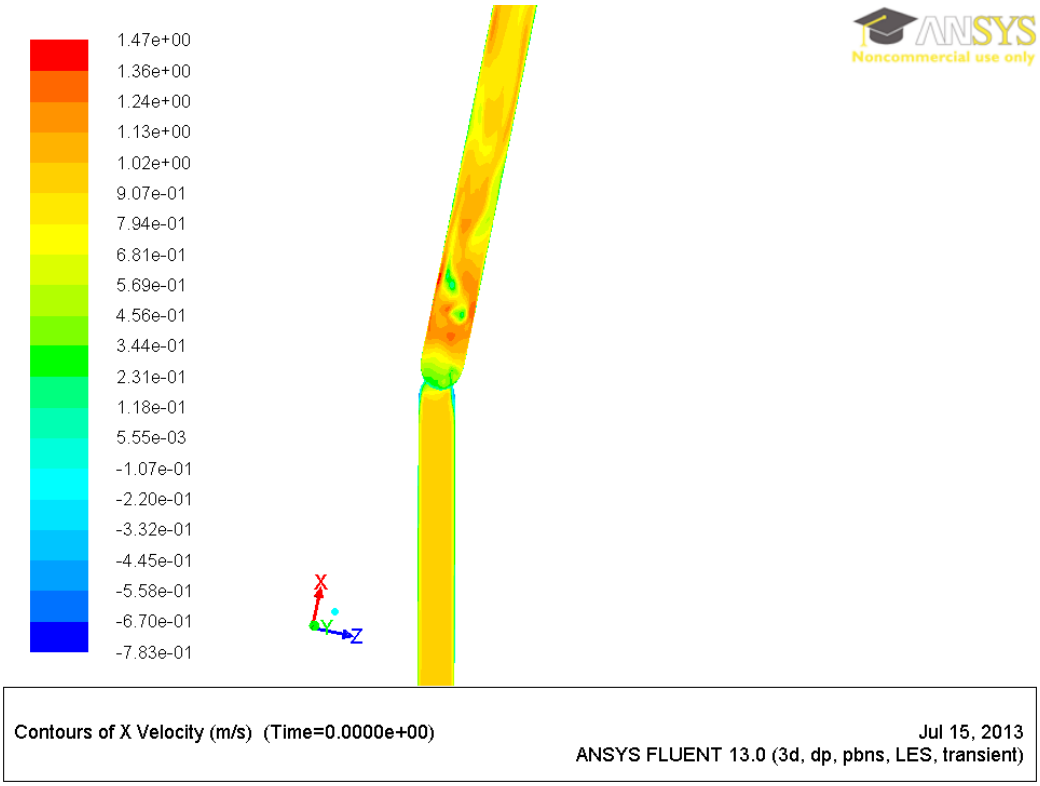

Fig. 4-82 Contours of X- Velocity on top view at 5 D from CFD using LES model and **standard wall function**

CHAPTER 5

ESTIMATING METHOD OF THE NUMBER OF MEASUREMENT LINES USING UVP METHOD

5.1 INTRODUCTION

The estimation of measurement lines is important to measure accurate flowrate effectively. From this aspect, the number of velocity profiles was optimized experimentally to calculate the flowrate in former chapter. However, necessary number of sensors can be calculated analytically by regarding velocity profiles as a kind of wave. Sampling rate theorem for waves can indicate the necessary number of the sensors. To apply the theorem to this kind of measurement by UVP method, the velocity profiles on the radial measurement lines must be converted into circumferential profile(s). Therefore, multiple measurements changing circumferential angle by 10° were examined and observed profiles on line were accumulated for conversion into circumferential velocity profiles on concentric circles. Every velocity profile shows harmonic wave[14)] that the horizontal axis means the transducer circumferential position of transducer, while the vertical axis means the time-averaged velocity normalized by the mean velocity. From each harmonic wave, we can verify the circumferential position where peaks of waves occur. Then, it is simply to set the position of measurement line.

Figure 5-1 a) shows the harmonic wave of velocity profile on circular measurement line of -0.4 r/D at 3D. The horizontal axis means the transducer circumferential position of transducer, while the vertical axis means the time-average velocity was normalized by mean velocity. After the transformation of raw data with Fast Fourier Transform technique, the frequency and amplitude data can obtain as shown in **Fig. 5-1 b).**

5.2 THEORY

5.2.1 Signal processing

The principles of signal processing can be found in the classical numerical analysis techniques of the 17th century. Oppenheim and Schafer further state that the "digitalization" or digital refinement of these techniques can be found in the digital control systems of the 1940s and 1950s **[5-1].** In general, the term signal processing refers to the science of analyzing time-varying physical processes. As such, signal processing is divided into two categories, analog signal processing and digital signal processing. The term analog is used to describe a waveform that’s continuous in time and can take

on a continuous range of amplitude values. An example of an analog signal is some voltage that can be applied to an oscilloscope resulting in a continuous display as a function of time. Analog signals can also be applied to a conventional spectrum analyzer to determine their frequency content **[5-2].**

In signal processing, sampling is the reduction of a continuous signal to a discrete signal. A common example is the conversion of a sound wave (a continuous signal) to a sequence of samples (a discrete-time signal). A sample refers to a value or set of values at a point in time and/or space. A sampler is a subsystem or operation that extracts samples from a continuous signal. A theoretical ideal sampler produces samples equivalent to the instantaneous value of the continuous signal at the desired points.

5.2.2 Analog signal processing

In the case of circumferential velocity profile which were measured inner of pipe flow around the center point of pipe as circle measuring lines, we assumed these circumferential velocity profiles as analog signal. The angular data started at 0° around the center point to 360°. It becomes to time-series data and the amplitude is the velocity at each measurement points. Analog signal processing is any signal processing conducted on analog signals by analog means. "Analog" indicates something that is mathematically represented as a set of continuous values. This differs from "digital" which uses a series of discrete quantities to represent signal. Analog values are typically represented as a voltage, electric current, or electric charge around components in the electronic devices. An error or noise affecting such physical quantities will result in a corresponding error in the signals represented by such physical quantities. Common analog processing elements include capacitors, resistors, inductors and transistors. Analog signal processing is mathematically represented as a set of continuous values. Analog values are typically represented as a voltage, electric current or electric charge around components in the electronic devices. An error or noise affecting such physical quantities will result in a corresponding error in the signals represented by such physical quantities **[5-3]**.

Tools used in analog signal processing can be mathematically modeled and is represented in the time domain as h(t) and in the frequency domain as H(s), where s is a complex number in the form of s=a+ib, or s=a+jb in electrical engineering terms (electrical engineers use j because current is represented by the variable i). Input signals are usually called x(t) or X(s) and output signals are

usually called y(t) or Y(s) **[5-4]**.

5.2.3 Fast Fourier Transform Analysis

Fourier analysis is a mathematical method used to break down and transform a periodic function i.e., a mathematical relationship between a quantity and a variable or variables whose relative values consistently repeat over some regular period of time into a set of simpler functions which can then be summed and transformed back into the original form. Today, it has been applied to a wider variety of problems in the physical and natural sciences. Improved, expanded upon, and the core of what has come to be known as the field of harmonic analysis, Fourier analysis has evolved and progressed to include the study of more abstract and general phenomena. Then, in this study, it was applied to estimate the largest number of waves, and necessary numbers of transducers for each position are indicated analytically by using sampling rate theorem **[5-5]**. The Fourier transform is a function that transforms a signal or system in the time domain into the frequency domain, but it only works for certain functions. The constraint on which systems or signals can be transformed by the Fourier Transform is that:

$$\hat{f}(\xi) = \int_{-\infty}^{\infty} f(x) e^{-2\pi i x \xi} dx \qquad \textbf{(5-1)}$$

Fourier transform of an integral function. When the independent variable x represents time (with SI unit of seconds), the transform variable ξ represents frequency (in hertz). Under suitable conditions

5.2.4 Sampling rate

The sampling rate, sample rate, or sampling frequency (f_s) defines the number of samples per unit of time (usually seconds) taken from a continuous signal to make a discrete signal. For time-domain signals, the unit for sampling rate is hertz (inverse seconds, 1/s, s^{-1}), sometimes noted as Sa/s or S/s (samples per second). The reciprocal of the sampling frequency is the sampling period or sampling interval, which is the time between samples **[5-6]**.

The Nyquist–Shannon sampling theorem states that perfect reconstruction of a signal is possible when the sampling frequency is greater than twice the maximum frequency of the signal being sampled, or equivalently, when the Nyquist frequency (half the sample rate) exceeds the highest

frequency of the signal being sampled. If lower sampling rates are used, the original signal's information may not be completely recoverable from the sampled signal **[5-7].** For example, if a signal has an upper band limit of 100 Hz, a sampling frequency greater than 200 Hz will avoid aliasing and would theoretically allow perfect reconstruction. The full range of human hearing is between 20 Hz and 20 kHz**.** The minimum sampling rate that satisfies the sampling theorem for this full bandwidth is 40 kHz. The 44.1 kHz sampling rate used for Compact Disc was chosen for this and other technical reasons.

The Nyquist sampling rule **[5-8]** provides a prescription for the nominal sampling interval required to avoid aliasing. Aliasing occurs when a signal is discretely sampled at a rate insufficient to capture the changes in the signal. Nyquist sampling theorem suggests that the sampling frequency should be higher than twice of the highest frequency contained in the signal. In theory, a Nyquist frequency just larger than the signal bandwidth is sufficient to allow perfect reconstruction of the signal from the samples. However, in practice, the perfect reconstruction is unattainable.

Figure 5-2 shows simple examples of the circumferential velocity profile with one sinuous wave. The number of waves is 1 in **Fig. 5-2 a)** and **Fig. 5-2 b),** and 1.5 in **Fig. 5 c)**. The necessary numbers of transducers for each is calculated as 2 for the case of a) and b), and 3 for the case of c), respectively, that is twice of the wave number. When two measurement lines are applied as shown in **Fig. 5-2 a)**, the transducers can capture both two peaks of the wave. However, two transducers cannot obtain any signal if the sensors are placed at the position of 0° and 180°. When the number of transducers (i.e. measurement lines) is 3 and 4 as shown in **Fig. 5-2 b)** and c), respectively, that is over twice of the wave number, the shape of the profile can be captured by the transducers. Accordingly, the suitable number of transducers is estimated by using sampling rate theorem, as just over twice of the wave number.

5.3 EXPERIMENTAL CONDITIONS

Figure 5-3 shows the experimental apparatus that used in this study consists of a water circulation system piping system. It is designed to emphasize the formation of fully developed turbulent pipe flow. The flowrate can be changed and controlled by the bypass line and the valve. Water is circulated by a centrifugal pump. The pipeline system of almost all part is made of Polyvinyl Chloride (PVC) except the test section. Before the test section, a flow conditioner designed to

include the tube bundle, mesh plates and a turbulence promoter ring was installed to realize uniform velocity profiles. Uniform velocity profile requires long pipe length. Therefore, the tube bundle flow conditioner is used at 30 D upstream of the double bent in order to reduce the flow rate measurement errors of the meter[13] (about ultrasonic reflector and two-phase flow). The double bent pipe can change the direction as out of plane angle as shown in **Fig. 5-4**. The out of plane angles are setup at 0°, 8° and 16°.

Figure 5-4 illustrates the details of test section. The flow rate was monitored by an electromagnetic flow meter located upstream of the test section. The double bent pipe has an angle of curvature of 90º, average curvature of R = 30 mm. The test section at downstream of the double bent is made of acrylic pipe and the total length of the pipe is approximately 1.5 m, the inner diameter (D) and wall thickness are also 50 mm and 5 mm, respectively. Acrylic resin has a high transparency to both visible light and ultrasound.

Water box is used at the test section to apply water as couplant between the transducer and the pipe. The same material for couplant and working fluid makes angles the same for emission of ultrasound and the refraction into the working fluid. The couplant displaces the air and makes it possible to get more sound energy into the test specimen so that a usable ultrasonic. Signal can be obtained. In contact ultrasonic testing a thin film of oil, glycerin or water is generally used between the transducer and the test surface.

The flow measurement system is composed of the UVP-DUO model (Met Flow AG) and a PC, which records the flowrate obtained by an electromagnetic flow meter and the temperature data by a thermometer. The summary of experimental conditions is shown in **Table 5-1**.

Table 5-1 shows the experimental conditions such as the basic frequency of the transducer is 8 MHz, Reynolds number was set at 40,000, and measuring points along the measurement line are 74. Nylon particles are dispersed in water as ultrasonic reflectors. Each particle has a diameter of approximately 80 μm, and a specific gravity of 1.02. The particles of this size can interweave with water, and can reflect ultrasonic wave of 8 MHz. As to size of the particle, experiment suggests approximately one fourth to one half of the wavelength is adequate. If the particle is smaller then this the reflection efficiency becomes lower and the energy of echo is too small to maintain a high signal per noise ratio, reading to defection error. If the particle is larger, the probability of multiple

reflections between particles become higher which would results in a distortion of the profile. The density of the particle is also important. A large different in densities between the fluid and particle might lead to an erroneous result because the particle does not follow the flow faithfully. Further, the concentration of the particles in the fluid is important. It should have only one particle per measuring volume, but this also depends on the velocity level of the flow field to be measured.

Experimental conditions of experimental apparatus, ultrasonic transducers, and method for determining the wall positions are the same as used in the experiments explained above.

Figure 9 illustrates the positions on the measuring line on the inner wall, the center of the pipe and on the farther pipe wall are indicated as the point of r/D = -0.5, 0 and +0.5, respectively. The area of r/D = -0.5 to 0 is named as 'near field', and the area of r/D = 0 to +0.5 as 'far field'. The circle passing through the points of the same r/D for different circumferential position is named as 'measuring circle'.

To evaluate the suitable number of transducers near the second bent where the accurate flowrate measurement is necessary, circumferential velocity profiles are necessary. Thus, multiple UVP measurements were applied. Measurement lines are changed circumferentially with angle of every 10° as shown in **Fig. 5-6**. Thus, 36 radial measurements of UVP method were repeated to obtain one circumferential velocity profile. **Figure 5-7** shows the schematic diagram around the measuring line.

Therefore, observed velocity magnitudes at the same r/D position among different circumferential positions are listed against the circumferential angle, and they converted into a circumferential velocity profile on the measurement circle. Velocity profile on the circle of r/D = -0.5 and 0.5 cannot be obtained because these points are on the wall surface, and also profile on the circle of r/D = 0 cannot be obtained because it indicates the same position, the center of the pipe. Thus, circumferential velocity profiles are obtained only for r/D = -0.4, -0.3, -0.2, -0.1, 0.1, 0.2, 0.3 and 0.4. The relationship of the locations of transducer, measurement lines, measurement circles, near field and far field are also summarized in **Fig. 5-5**, **Fig. 5-6** and **Fig.5-7**.

5.4 RESULTS AND DISCUSSIONS

Furthermore, the analytical technique can estimate the number of measurement lines which achieves to capture a peak of simple harmonic wave where the velocity in the profile shows highest fluctuation. The Number of wave which used for estimating the number of measurement lines can determine with the size of main lobe (peak lobe). However, it generally includes some sidelobes. These sidelobes affect the frequency of wave. From this reason, there are many types of window function can reduce the sidelobes amplitudes for example Hamming, Hanning, Rectangular or Triangular window function. **[5-9]** In this study, Hanning window function was used to estimate the largest number of wave as shown as the dot lines in **Fig. 5-10 a)-c)**.

Figure 5-10 a) presents the results of FFT which from all 8 circumferential velocity profiles. The results of -0.1R has the largest frequency as 2.7. Then, we can calculate the sampling rate using Nyquist theory by multiplied 2 that is 5.4 measurement lines. Actually, the number of measurement lines have to be designed in the integer number. Therefore, the number of measurement lines at 2 D is 6 measurement lines.

In addition, **Fig. 5-10 b)** and **Fig. 5-10 c)** present the results of FFT which from all 8 circumferential velocity profiles at 3 D and 5D, respectively. The results of +0.3R has the largest frequency at 3 D as 2.4. The detail of FFT results are shown in **Fig. 5-13** and **Fig. 5-14**. After that, we can calculate the sampling rate using Nyquist theory by multiply by 2 that is 4.8 measurement lines that means 5 measurement lines. At the same time, the number of measurement lines at 5 D is designed as 4 measurement lines from the largest frequency on +0.1R which is 2 as shown in **Table 5-2.**

Figure 5-11 a) – c) show the arrangements of measurement lines in the cases of 4, 5 and 6 transducers. At 2 D, the setup of measurement lines of 6 measurement lines can be located the ϕ angle between measurement line each other at 90° such as line no.1 at ϕ angle at 30°, line no.2 at ϕ angle at 90°, line no.3 at ϕ angle at 150°, line no.4 at ϕ angle at 210°, line no.5 at ϕ angle at 270° and line no.6 at ϕ angle at 330° as shown in **Fig 5-11 c).** At 3D, the setup of measurement lines of 5 measurement lines can be located the ϕ angle between measurement line each other at 72.5° such as line no.1 at ϕ angle at 17.5°, line no.2 at ϕ angle at 90°, line no.3 at ϕ angle at 162.5°, line no.4 at ϕ angle at 235° and line no.5 at ϕ angle at 307.5° as shown in **Fig 5-11 b).** In the last case, at 5 D, the

setup of measurement lines of 4 measurement lines can be located the ϕ angle between measurement line each other at 90° such as line no.1 at ϕ angle at 0°, line no.2 at ϕ angle at 90°, line no.3 at ϕ angle at 180° and line no.4 at ϕ angle at 270° as shown in **Fig 5-11 a).**

Figure 5-12 show the velocity profiles in every 10° of ϕ angle. The velocity profile measurement started at 0° as shown in **Fig. 5-6**. **Figure 5-12 1)** shows the first measurement line at 0° which cross the center of pipe in the horizontal direction. On the right haft of velocity profile (-0.5 to 0 r/D) is the near field of transducer and on the left side of velocity profile (0 to +0.5 r/D) is the far field of transducer. **Figure 5-12 1) - 10)** show the velocity at near field is increasing when the ϕ angle was also increasing from ϕ = 0° to ϕ = 90° because the direction of flow in this area is influenced of the centrifugal force in vertical directions from the center of bent pipe to the outer of bent pipe. From this reason, the maximum velocity theoretical highly on the outer area from the bent pipe. It makes non-symmetry flow as non-symmetrical twin vortices. **[5-10]** In the case of double bent pipe in vertical direction piping system, the outer area of the bent pipe is on the top of the outlet. On the other hand, the minimum velocity in the pipe flow always at the bottom of the outlet or inner of the center of bent curve.

Figure 5-12 11) - 28) show the velocity at near field is decreasing when the ϕ angle was increasing from ϕ = 100° to ϕ = 270° because the direction of flow in this area is influenced of the centrifugal force in vertical directions from the center of bent pipe to the outer of bent pipe. From this reason, the velocity at the inner area of bent pipe. On the other hand, the far field of transducer is increasing when the when the ϕ angle was increasing from ϕ = 100° to ϕ = 270° same the case of near field of transducer at ϕ = 0° to ϕ = 90°.

Figure 5-12 29) - 36) show the velocity at near field is increasing when the ϕ angle was increasing from ϕ = 280° to ϕ = 0° and from ϕ = 10° to ϕ = 90°. This is same as the case of ϕ = 0° to ϕ = 90° because the direction of flow in this area is influenced of the centrifugal force in vertical directions from the center of bent pipe to the outer of bent pipe. In the case of double bent pipe in vertical direction piping system, the outer area of the bent pipe is on the top of the outlet. On the other hand, the minimum velocity in the pipe flow always at the bottom of the outlet or inner of the center of bent curve.

Figure 5-13 show circumferential velocity profiles totally 8 profiles such as 4 profiles at near field of transducer (r/D = -0.4, -0.3, -0.2 and -0.1) at 2 D. These near field circumferential velocity profiles are increasing when the ϕ angle was increasing from ϕ = 0° to ϕ = 90°. In addition, the velocities are decreasing when ϕ = 100° to ϕ = 270°. As the mention above about the direction of flow in this area is influenced of the centrifugal force in vertical directions from the center of bent pipe to the outer of bent pipe. On the other hand, at the far field of transducer (r/D = +0.4, +0.3, +0.2 and +0.1). These far field circumferential velocity profiles are decreasing when the ϕ angle was increasing from ϕ = 0° to ϕ = 90°.

Figure 5-14 and fig. 5-15 show FFT results in detail from all circumferential velocity profiles totally 8 profiles such as 4 profiles at near field of transducer (r/D = -0.4, -0.3, -0.2 and -0.1) and 4 profiles at far field of transducer (r/D = +0.4, +0.3, +0.2 and +0.1) at 2 D. The results of -0.1R has the largest frequency as 2.7. Then, we can calculate the sampling rate using Nyquist theory by multiplied 2 that is 5.4 measurement lines. Actually, the number of measurement lines have to be designed in the integer number. Therefore, the number of measurement lines at 2 D is 6 measurement lines.

Figure 5-16 show the velocity profiles at 3D in every 10° of ϕ angle. The velocity profile measurement started at 0° as shown in **Fig. 5-6**. **Figure 5-12 1)** shows the first measurement line at 0° which cross the center of pipe in the horizontal direction. On the right haft of velocity profile (-0.5 to 0 r/D) is the near field of transducer and on the left side of velocity profile (0 to +0.5 r/D) is the far field of transducer. **Figure 5-16 1) - 10)** show the velocity at near field is increasing when the ϕ angle was also increasing from ϕ = 0° to ϕ = 90° same as the case of the velocity profile at 2 D as mention above.

Figure 5-16 11) - 28) show the velocity at near field is decreasing when the ϕ angle was increasing from ϕ = 100° to ϕ = 270° because the direction of flow in this area is influenced of the centrifugal force in vertical directions from the center of bent pipe to the outer of bent pipe. From this reason, the velocity at the inner area of bent pipe. On the other hand, the far field of transducer is increasing when the when the ϕ angle was increasing from ϕ = 100° to ϕ = 270° same the case of near field of transducer at ϕ = 0° to ϕ = 90°.

Figure 5-16 29) - 36) show the velocity at near field is increasing when the ϕ angle was increasing from $\phi = 280°$ to $\phi = 0°$ and from $\phi = 10°$ to $\phi = 90°$. This is same as the case of $\phi = 0°$ to $\phi = 90°$ because the direction of flow in this area is influenced of the centrifugal force in vertical directions from the center of bent pipe to the outer of bent pipe. In the case of double bent pipe in vertical direction piping system, the outer area of the bent pipe is on the top of the outlet. On the other hand, the minimum velocity in the pipe flow always at the bottom of the outlet or inner of the center of bent curve.

Figure 5-17 show circumferential velocity profiles totally 8 profiles such as 4 profiles at near field of transducer (r/D = -0.4, -0.3, -0.2 and -0.1) at 2 D. These near field circumferential velocity profiles are increasing when the ϕ angle was increasing from $\phi = 0°$ to $\phi = 90°$. In addition, the velocities are decreasing when $\phi = 100°$ to $\phi = 270°$. As the mention above about the direction of flow in this area is influenced of the centrifugal force in vertical directions from the center of bent pipe to the outer of bent pipe. On the other hand, at the far field of transducer (r/D = +0.4, +0.3, +0.2 and +0.1). These far field circumferential velocity profiles are decreasing when the ϕ angle was increasing from $\phi = 0°$ to $\phi = 90°$.

Figure 5-18 and fig. 5-19 show FFT results in detail from all circumferential velocity profiles totally 8 profiles such as 4 profiles at near field of transducer (r/D = -0.4, -0.3, -0.2 and -0.1) and 4 profiles at far field of transducer (r/D = +0.4, +0.3, +0.2 and +0.1) at 3 D. The results of r/D = +0.3 has the largest frequency as 2.4. Then, we can calculate the sampling rate using Nyquist theory by multiplied 2 that is 4.8 measurement lines. Actually, the number of measurement lines have to be designed in the integer number. Therefore, the number of measurement lines at 3 D is 5 measurement lines.

Figure 5-20 show the velocity profiles at 5D in every 10° of ϕ angle. The velocity profile measurement started at 0° as shown in **Fig. 5-6**. **Figure 5-20 1)** shows the first measurement line at 0° which cross the center of pipe in the horizontal direction. On the right haft of velocity profile (-0.5 to 0 r/D) is the near field of transducer and on the left side of velocity profile (0 to +0.5 r/D) is the far field of transducer. **Figure 5-20 1) - 10)** show the velocity at near field is increasing when the ϕ angle was also increasing from $\phi = 0°$ to $\phi = 90°$ same as the case of the velocity profile at 5 D as mention above.

Figure 5-20 11) - 28) show the velocity at near field is decreasing when the ϕ angle was increasing from $\phi = 100°$ to $\phi = 270°$ because the direction of flow in this area is influenced of the centrifugal force in vertical directions from the center of bent pipe to the outer of bent pipe. From this reason, the velocity at the inner area of bent pipe. On the other hand, the far field of transducer is increasing when the when the ϕ angle was increasing from $\phi = 100°$ to $\phi = 270°$ same the case of near field of transducer at $\phi = 0°$ to $\phi = 90°$.

Figure 5-20 29) - 36) show the velocity at near field is increasing when the ϕ angle was increasing from $\phi = 280°$ to $\phi = 0°$ and from $\phi = 10°$ to $\phi = 90°$. This is same as the case of $\phi = 0°$ to $\phi = 90°$ because the direction of flow in this area is influenced of the centrifugal force in vertical directions from the center of bent pipe to the outer of bent pipe. In the case of double bent pipe in vertical direction piping system, the outer area of the bent pipe is on the top of the outlet. On the other hand, the minimum velocity in the pipe flow always at the bottom of the outlet or inner of the center of bent curve.

Figure 5-21 show circumferential velocity profiles totally 8 profiles such as 4 profiles at near field of transducer (r/D = -0.4, -0.3, -0.2 and -0.1) at 2 D. These near field circumferential velocity profiles are increasing when the ϕ angle was increasing from $\phi = 0°$ to $\phi = 90°$. In addition, the velocities are decreasing when $\phi = 100°$ to $\phi = 270°$. As the mention above about the direction of flow in this area is influenced of the centrifugal force in vertical directions from the center of bent pipe to the outer of bent pipe. On the other hand, at the far field of transducer (r/D = +0.4, +0.3, +0.2 and +0.1). These far field circumferential velocity profiles are decreasing when the ϕ angle was increasing from $\phi = 0°$ to $\phi = 90°$.

Figure 5-22 and fig. 5-23 show FFT results in detail from all circumferential velocity profiles totally 8 profiles such as 4 profiles at near field of transducer (r/D = -0.4, -0.3, -0.2 and -0.1) and 4 profiles at far field of transducer (r/D = +0.4, +0.3, +0.2 and +0.1)at 5 D. The results of r/D = +0.1 has the largest frequency as 2. Then, we can calculate the sampling rate using Nyquist theory by multiplied 2 that is 4.0 measurement lines. Actually, the number of measurement lines have to be designed in the integer number. Therefore, the number of measurement lines at 5 D is 4 measurement lines.

Table 5-2 shows the number of measurement lines from the estimation analytical technique. The

number of measurement lines are decreasing when the inlet length is farther. This is because when the fluid enters any pipe or channel, boundary layers keep on growing to be a stable flow condition after some distance downstream from the entrance region. Velocity in the core of the flow outside the boundary layer increases with increasing distance from entrance. This is due to the fact that through any cross section same amount of fluid flows, and boundary layer is growing. That means the stability of flow behavior will increase when the distance downstream from the inlet is increasing. It affects the number of measurement line directly such as the number of measurement lines are decreasing from 2 D, 3 D and 5 D as 6, 5 and 4 measurement lines, respectively.

5.5. CONCLUSIONS

Development of accurate flowrate measurement for a complicated flow is executed using UVP measurement. Double bent pipe system is used to realize the complicated flow. Experimental flowrate measurements on the system were executed for Re ~ 40,000. The velocity profiles were obtained at the distance 2 D, 3 D and 5 D from the bent where the flow is complicated due to existence of vortices. From experimental results using 1-3 transducers, flowrate for each distance is calculated using integration and interpolation. The accuracy of this method is evaluated by comparison with the flowrate value of electro-magnetic flowmeter installed in the experimental loop. It is concluded that accurate flowrate will be calculated in the condition of using three transducers and the distance is over 3 D within 4% error.

To confirm the optimization, the velocity profiles are also obtained changing the circumferential measuring angle by 10°. Velocity profiles on the measurement lines through the center of the pipe are transferred to velocity profiles along the circles which concentric center is as same as the pipe center. FFT analysis is performed to obtain largest number of wave for circumferential direction, and optimized number of transducer for each position is calculated from the FFT results. The result indicates more transducers are necessary for very accurate flowrate measurement. However, enough accurate measurement can be realized with less transducer.

The accuracy of flowrate measurements for the complicated flow by double bent pipe system was confirmed experimentally and numerically. The experimental result is confirmed using the analytical method for circumferential velocity profile adopting the sampling theory and the signal analytical method. The method for accurate flow rate measurement at the region near the bent will be validated,

and it will make plants for power generation or engineering etc. more efficient and compact.

REFERENCES

[5-1] Oppenheim, Alan V.; Schafer, Ronald W., Digital Signal Processing. Prentice Hall. p. 5. ISBN 0-13-214635-5, 1975

[5-2] R.G., Lyons, Understanding Digital Signal Processing, Addison Wesley Longman, Self, Douglas, 2012.

[5-3] Martin H. Weik, Communications Standard Dictionary. Springer. ISBN 0412083914, 1996

[5-4] Audio Engineering Explained. Taylor & Francis US. pp. 200, 446. ISBN 0240812735, 1997

[5-5] Fourier, J. B. Joseph; Freeman, Alexander, translator, The Analytical Theory of Heat, The University Press, 1878

[5-6] M., Pharr and G., Humphreys, Physically Based Rendering: From Theory to Implementation, Morgan Kaufmann, 2004

[5-7] C. E. Shannon, Communication in the presence of noise, Proc. Institute of Radio Engineers, vol. 37, no.1, pp. 10–21, Jan. 1949. Reprint as classic paper in: Proc. IEEE, Vol. 86, No. 2, 1998

[5-8] H., Nyquist, Certain topics in Telegraph Transmission Theory, Trans. AIEE, 47, pp. 617 – 644, 1928

[5-9] R. G., Lyons, Understanding of Digital Signal Processing, 2nd ed. Bernard Goodwin, 2004

[5-10] Smith, F.T.: Fluid flow into the curved pipe, Proceedings of the Royal Society of London, vol. 351, no. 1664 (1976)

Table 5-1 Experimental conditions

Testing conditions	Units	Values
Reynolds Number	-	40,000
Number of measuring point	-	74
Channel width	mm	0.74
Basic frequency	MHz	8
Incident angle	Degree	10

Tabel 5-2 Number of measurement lines

Inlet length	Largest frequency	Measurement lines
2 D	2.7	6
3 D	2.4	5
5 D	2	4

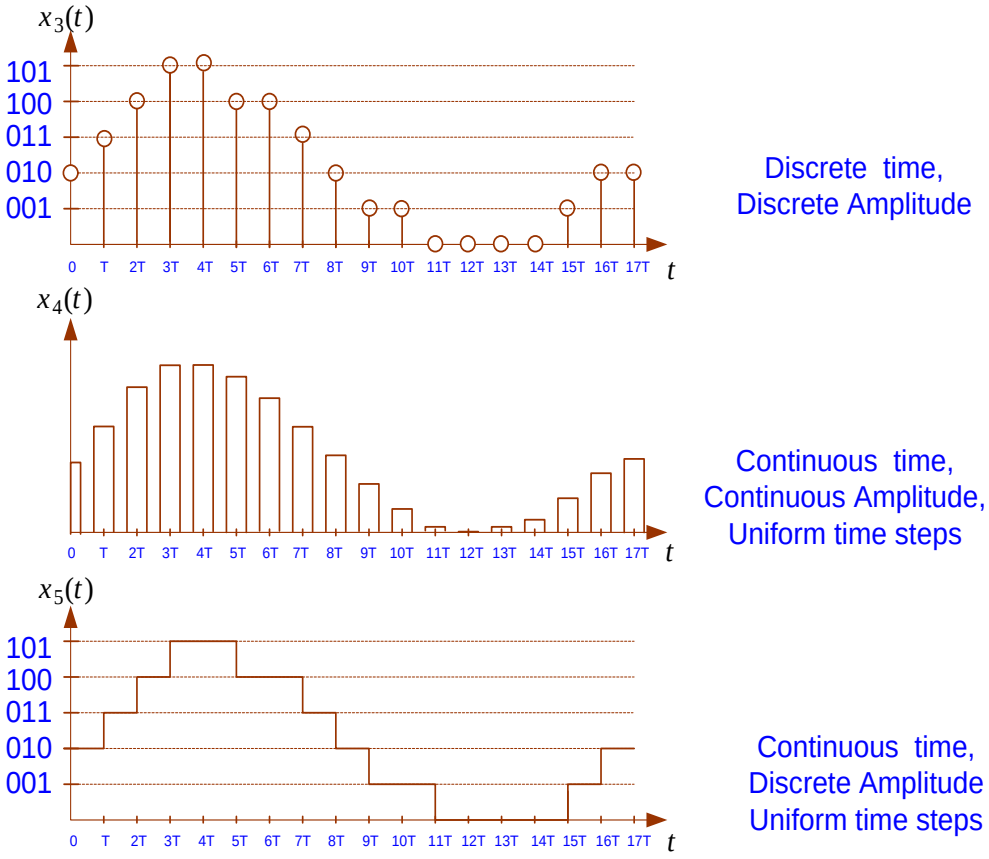

Fig. 5.1 Types of signal

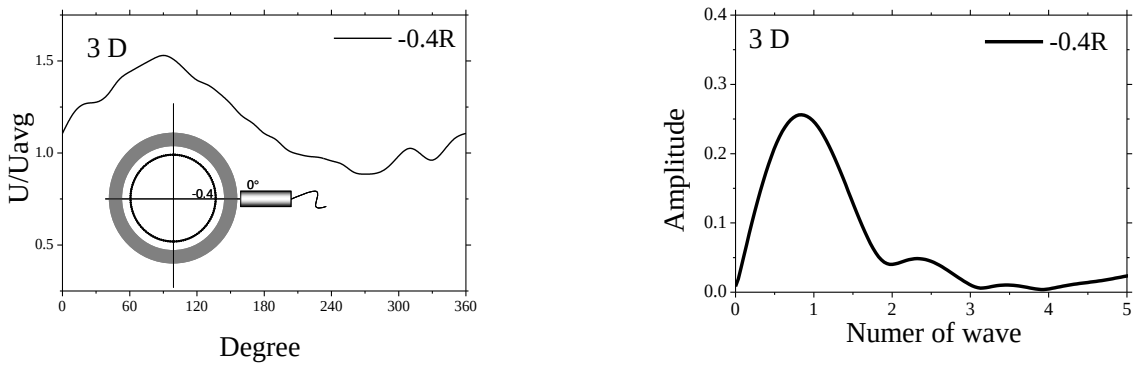

a) Velocity profile from circle measurement line **b)** Frequency from FFT

Fig.5.2 Velocity profile from circle measurement line -0.4R and the frequency data from Fast Fourier Transform

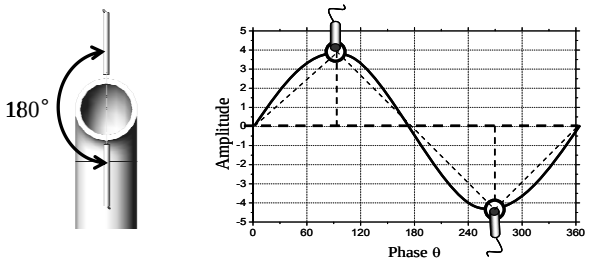

a) 2 Measurement lines

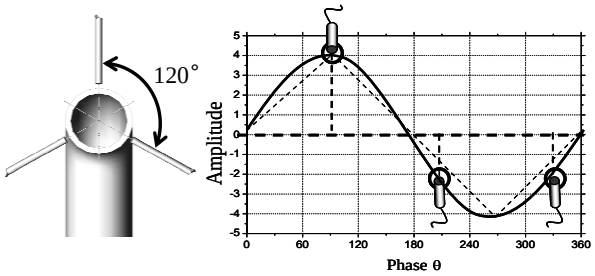

b) 3 Measurement lines

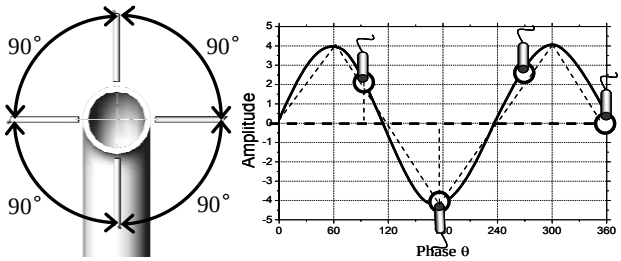

c) 4 Measurement lines

Fig.5-3 Measurement lines located and number of measurement lines related to phase of wave and sampling rate theorem to protect the error from aliasing

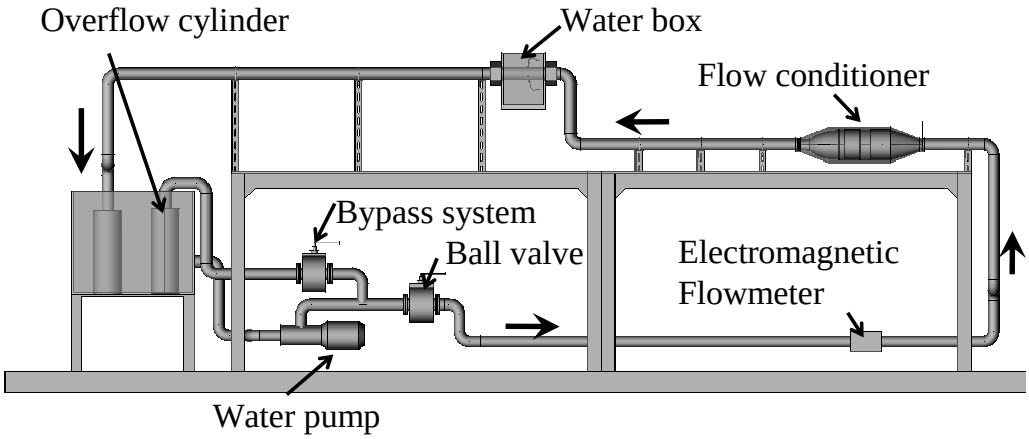

Fig. 5-4 Experimental apparatus of in plane double bent pipe flow

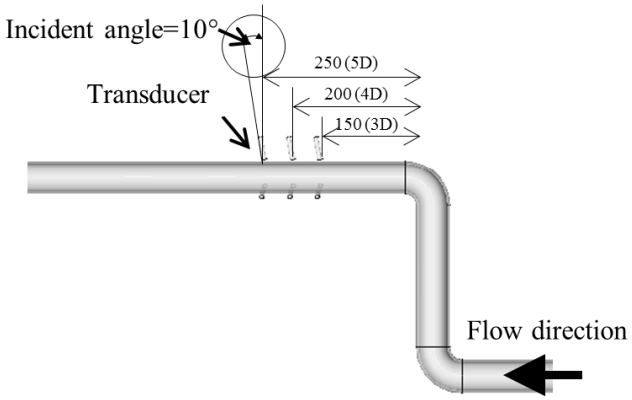

Fig. 5-5 Detail configuration at the test section (2 D – 20 D)

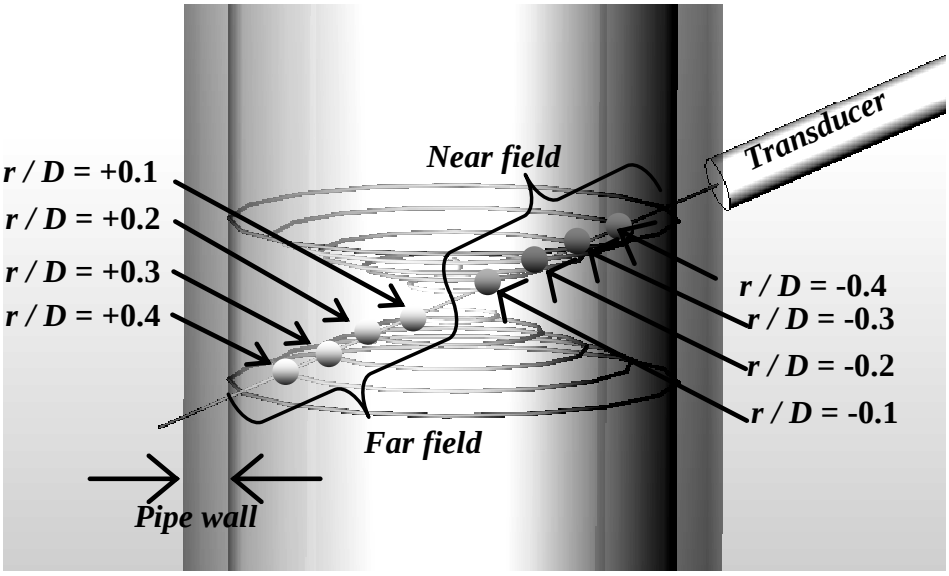

Fig.5-6 Measuring lines and circles of velocity profiles

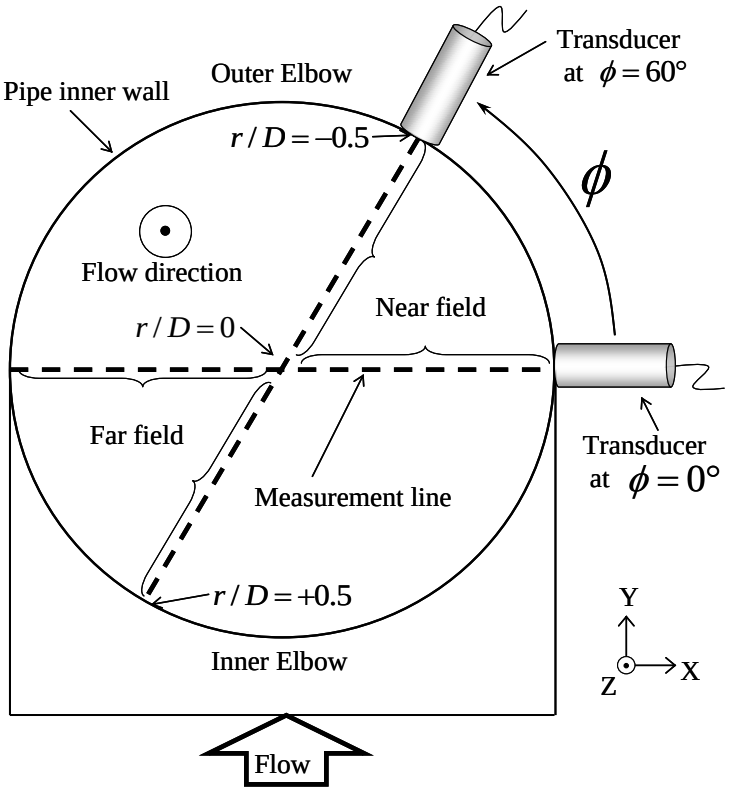

Fig.5-7 Circumferential transducer position ∅ around the pipe

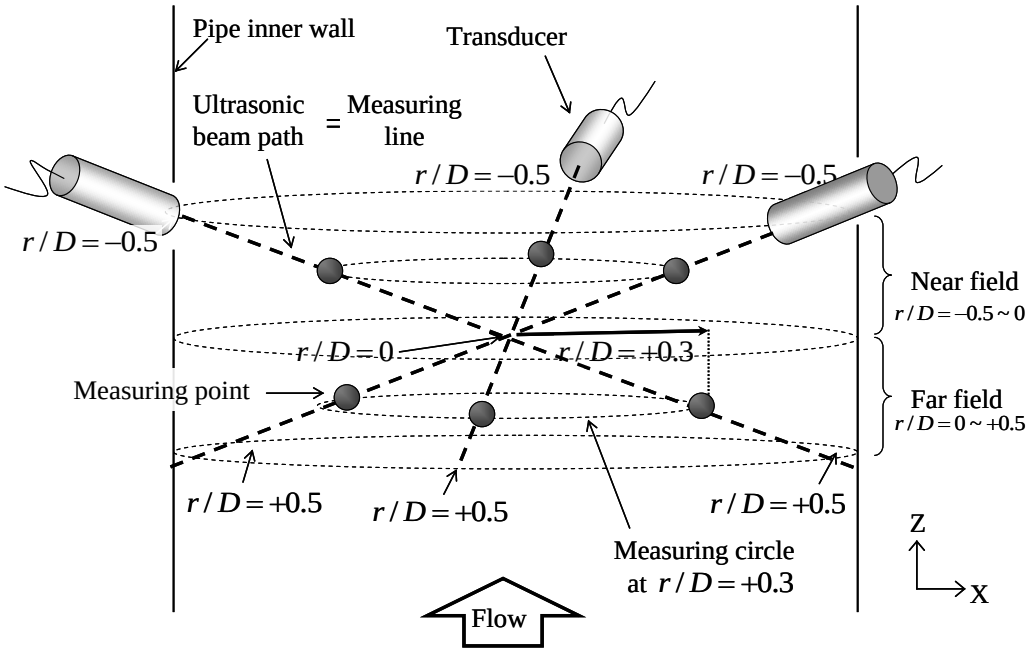

Fig.5-8 Measurement lines and circle of velocity profiles

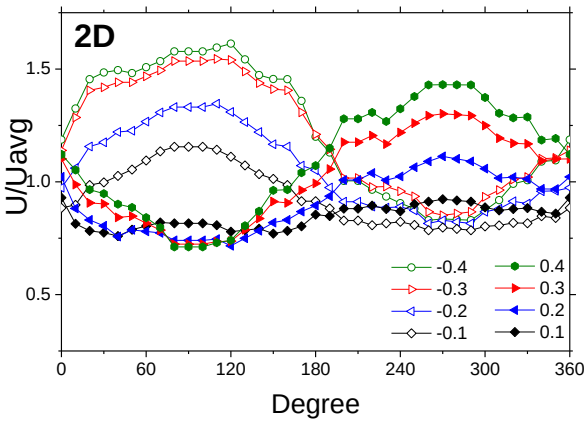

a) At 2 D

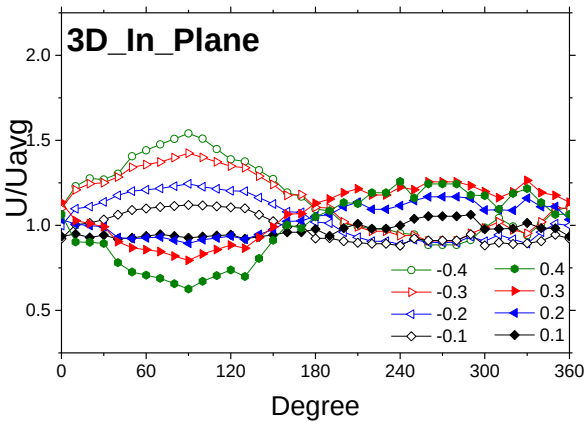

b) At 3 D

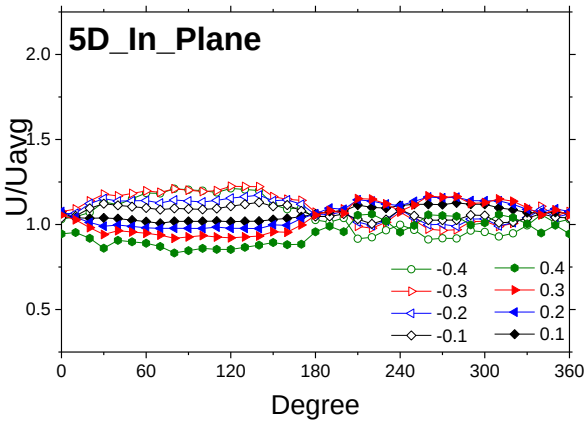

c) At 5 D

Fig. 5-9 Velocity profiles along the measuring circles (Re = 4×10^4) at a) 2 D, b) 3 D and c) 5 D

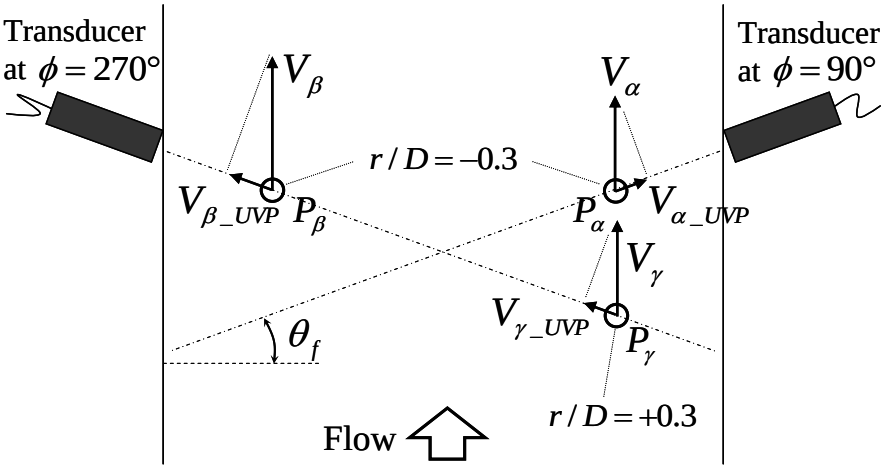

a) Straight flow

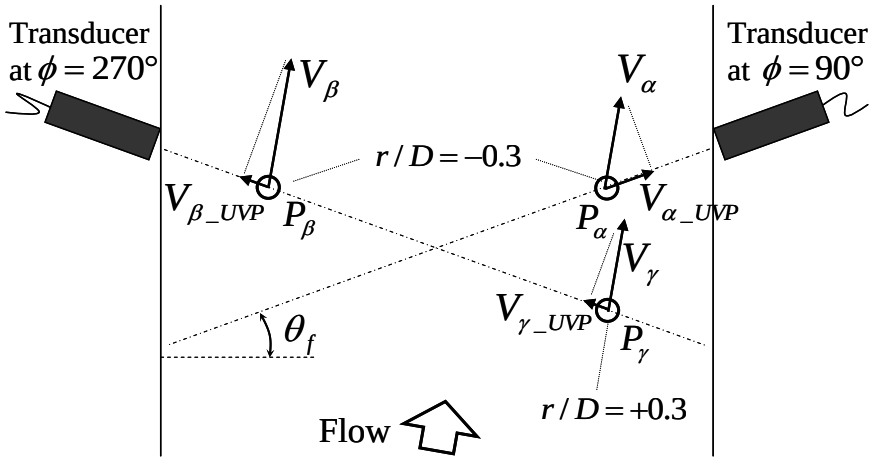

b) inclined flow

Fig.5-10 Schematic diagram of the velocity component measured by UVP method[12] flow straight and inclined flow

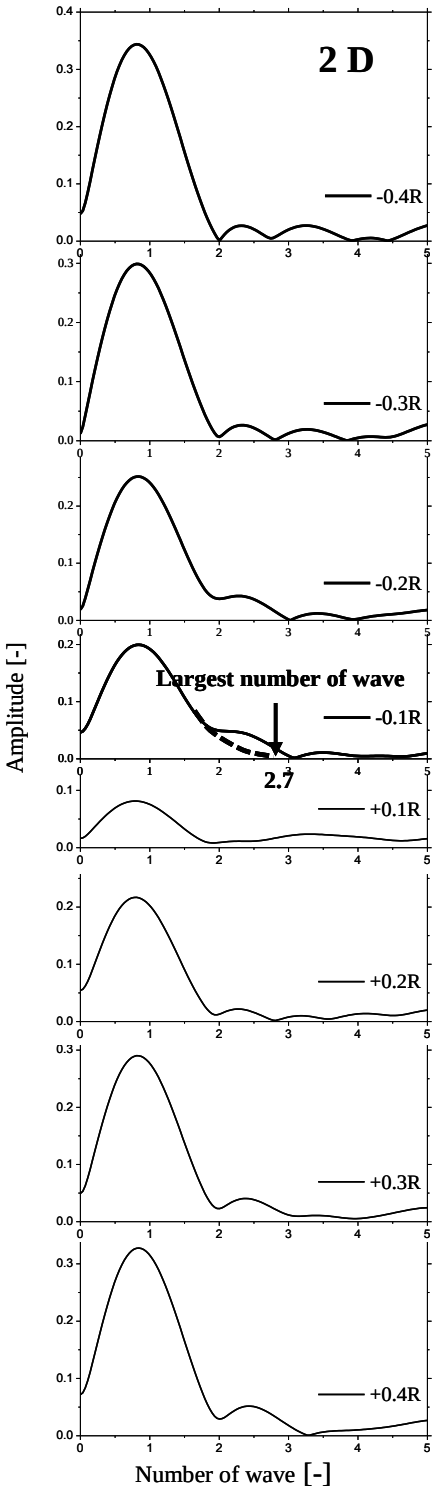

a) At 2 D

Fig. 5-11 Fourier amplitude of velocity profile along the measuring circle at a) 2 D, b) 3 D and c) 5 D

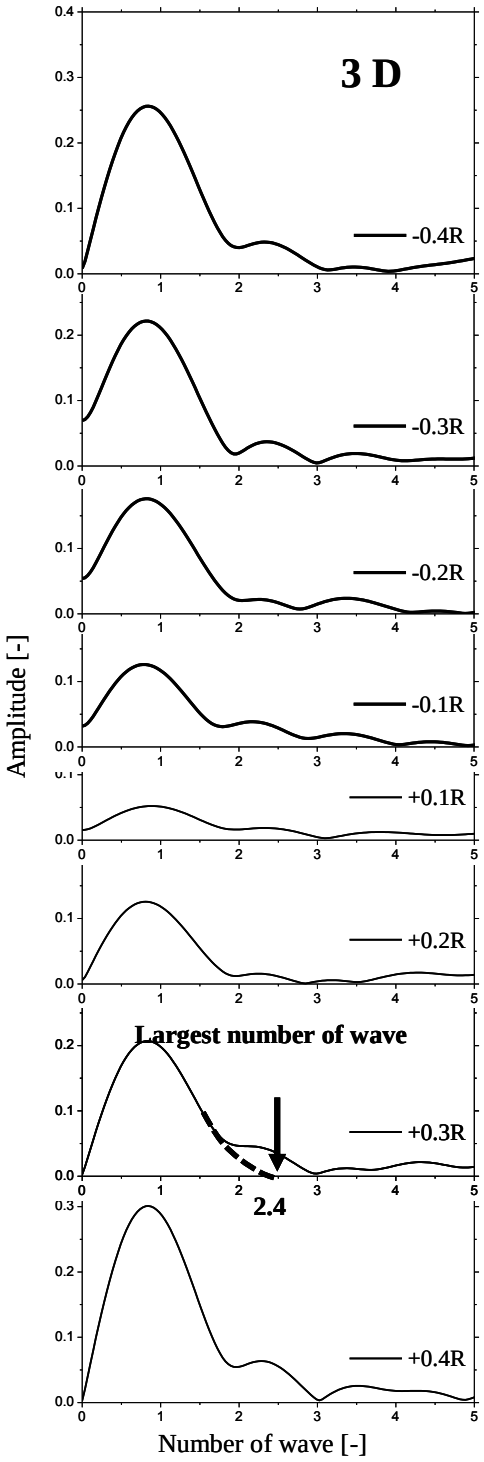

b) At 3 D

Fig. 5-11 (cont')

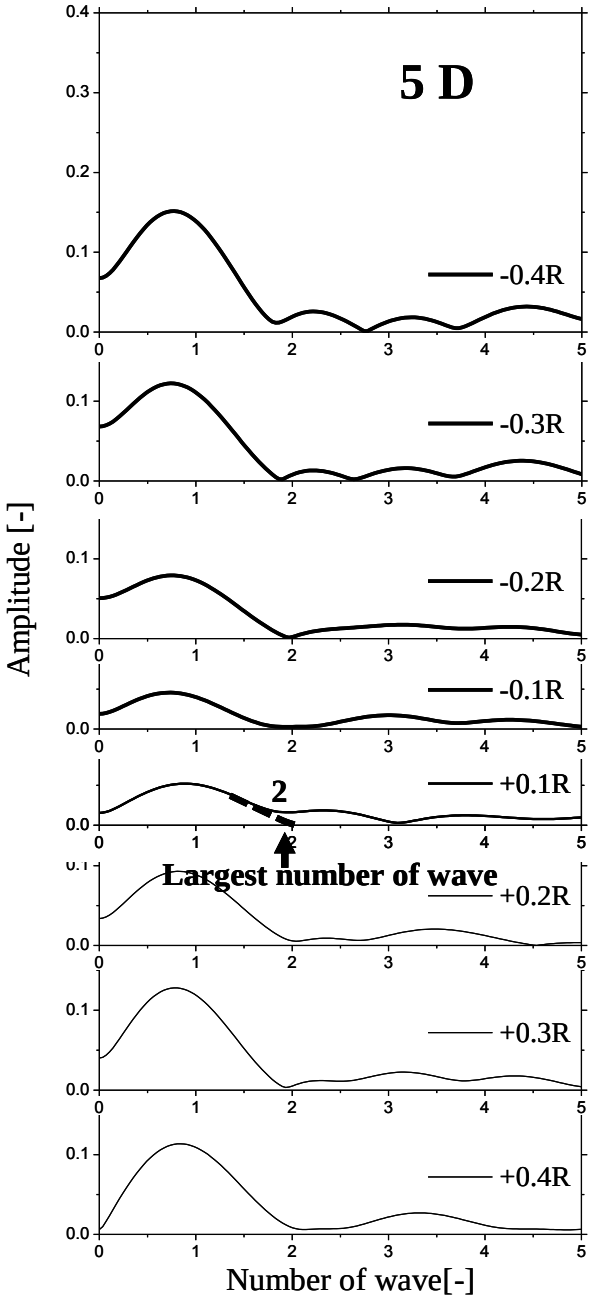

c) At 5 D

Fig. 5-11 (cont')

a) At 2 D

Fig. 5-11 Fourier amplitude of velocity profile along the measuring circle at a) 2 D, b) 3 D and c) 5 D

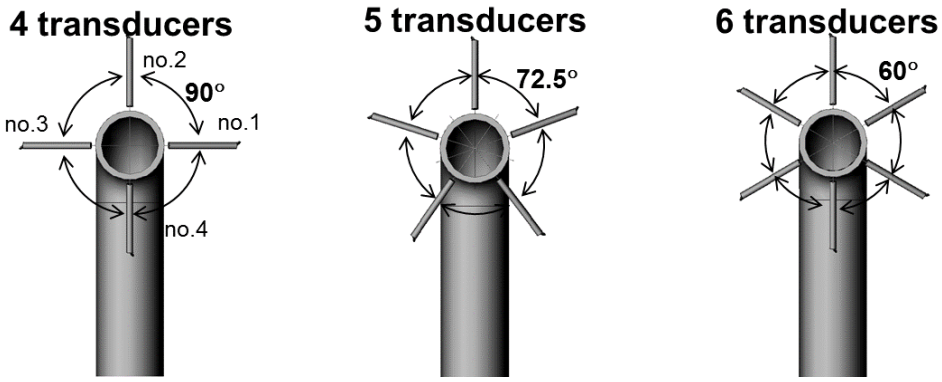

a) 4 measurement lines b) 5 measurement lines c) 6 measurement lines

Fig. 5-12 The arrangement of measurement lines

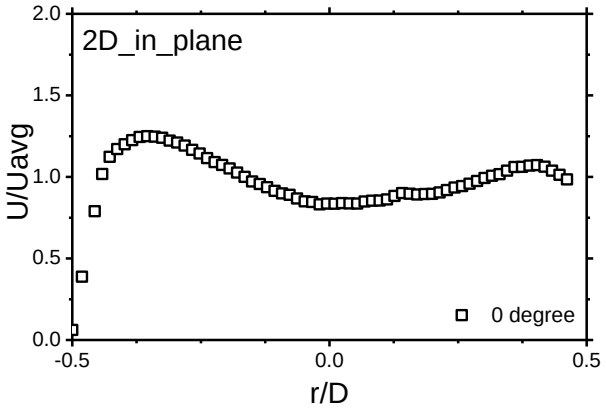

1) Velocity profile at 0 degree (2 D)

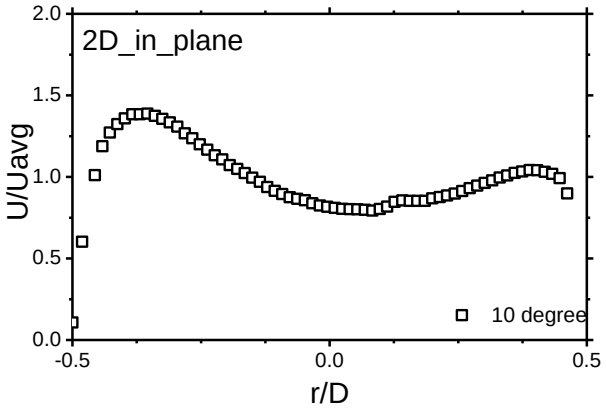

2) Velocity profile at 10 degree (2 D)

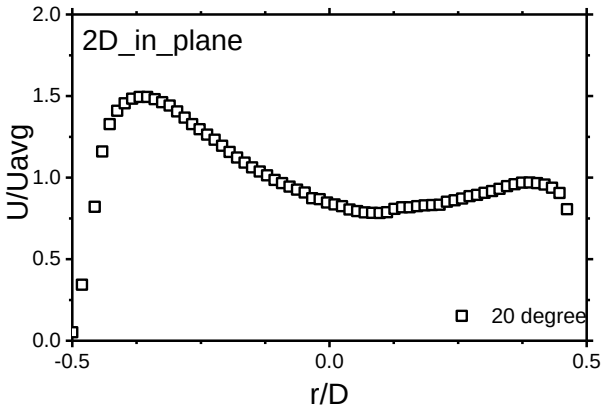

3) Velocity profile at 20 degree (2 D)

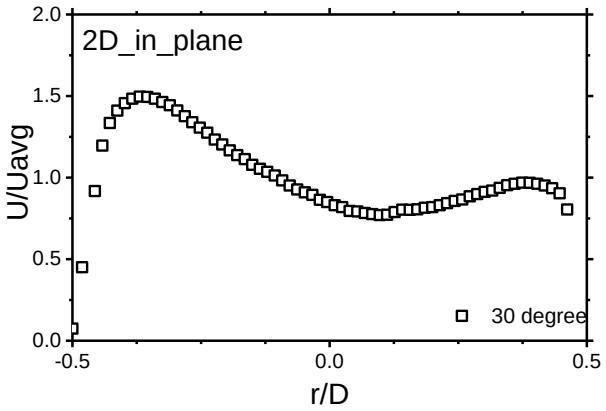

4) Velocity profile at 30 degree (2 D)

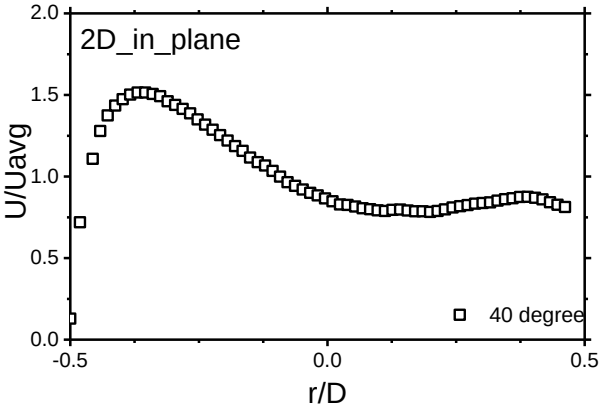

5) Velocity profile at 40 degree (2 D)

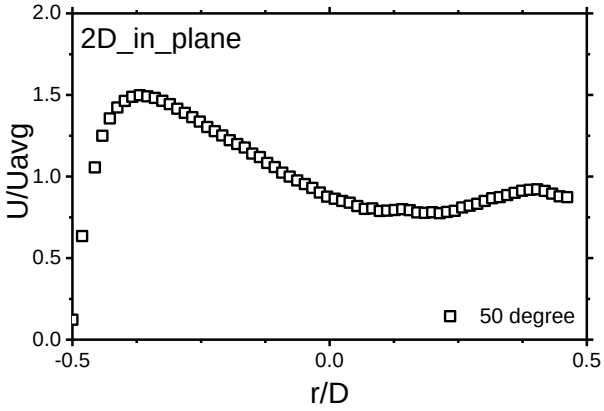

6) Velocity profile at 50 degree (2 D)

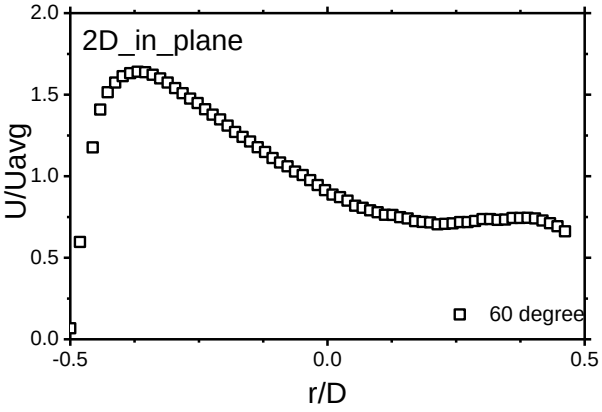

7) Velocity profile at 60 degree (2 D)

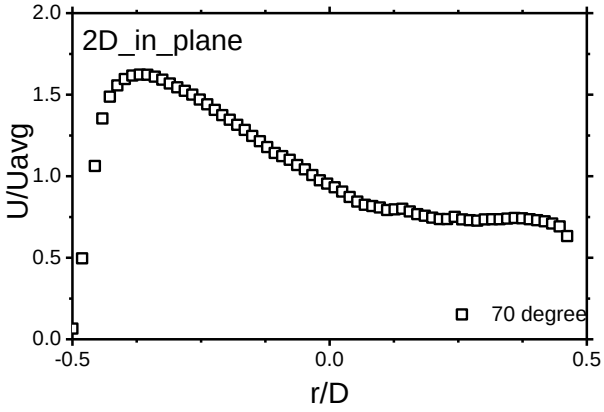

8) Velocity profile at 70 degree (2 D)

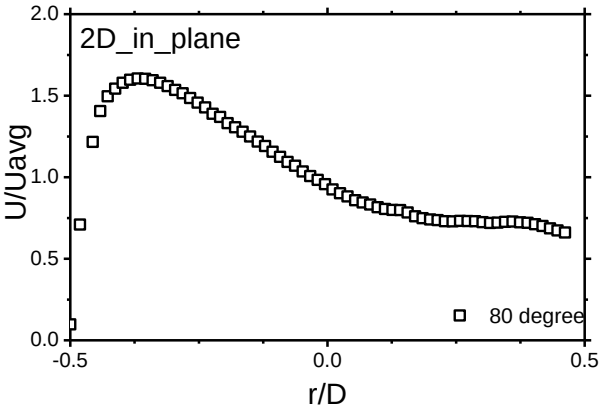

9) Velocity profile at 80 degree (2 D)

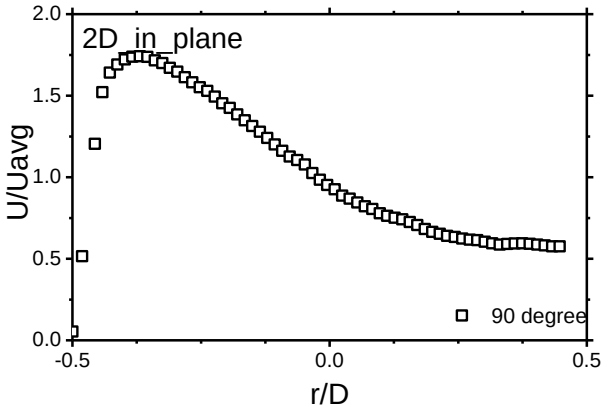

10) Velocity profile at 90 degree (2 D)

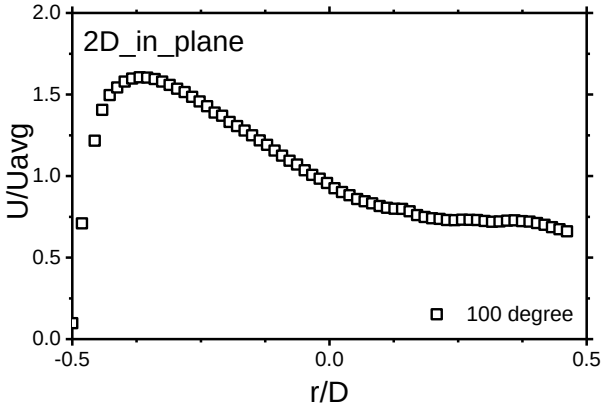

11) Velocity profile at 100 degree (2 D)

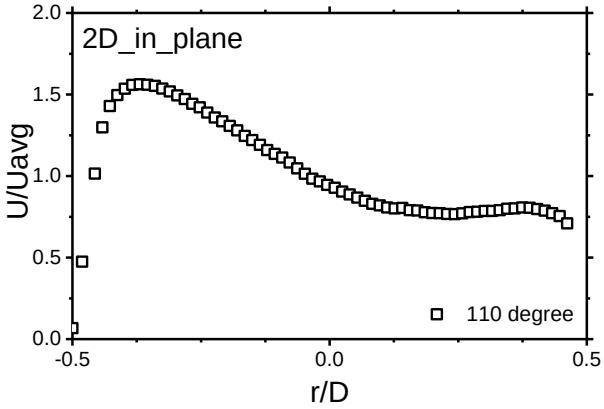

12) Velocity profile at 110 degree (2 D)

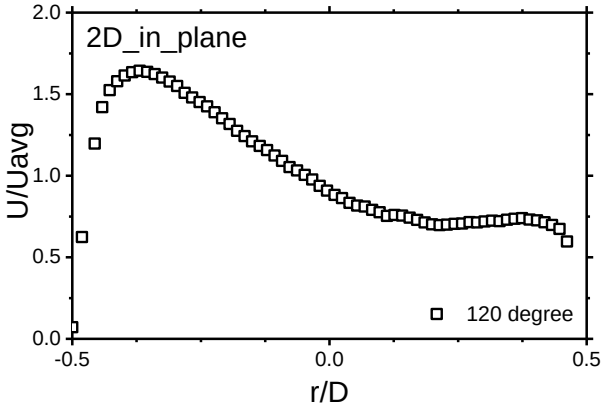

13) Velocity profile at 120 degree (2 D)

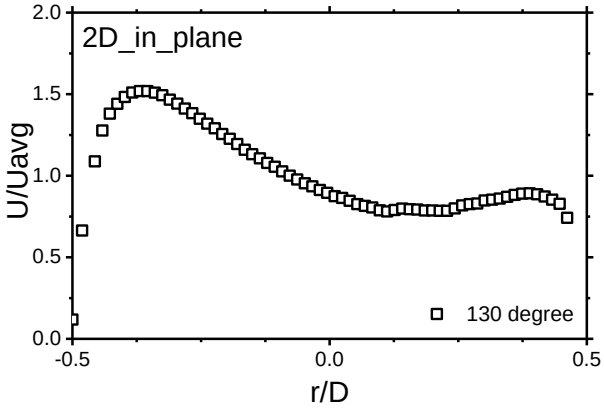

14) Velocity profile at 130 degree (2 D)

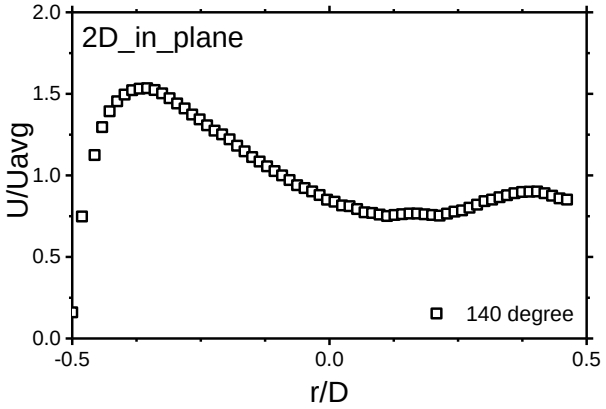

15). Velocity profile at 140 degree (2 D)

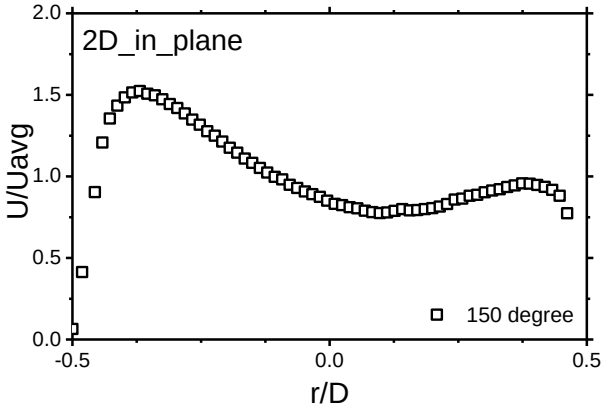

16) Velocity profile at 150 degree (2 D)

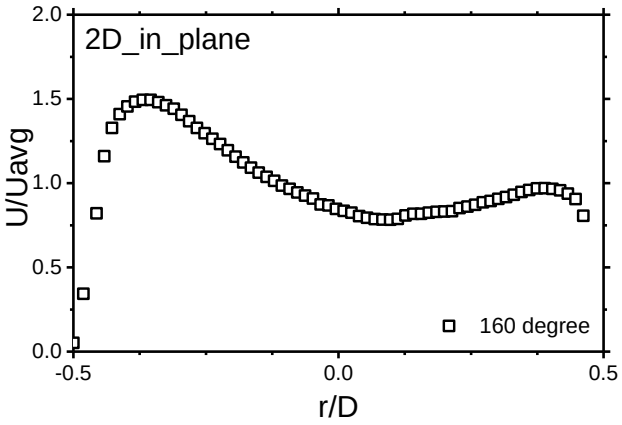

17) Velocity profile at 160 degree (2 D)

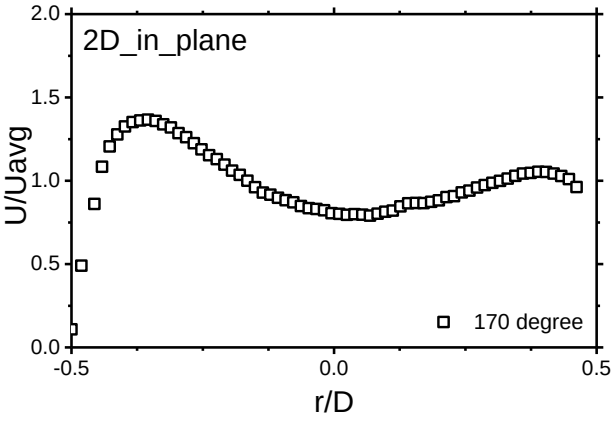

18) Velocity profile at 170 degree (2 D)

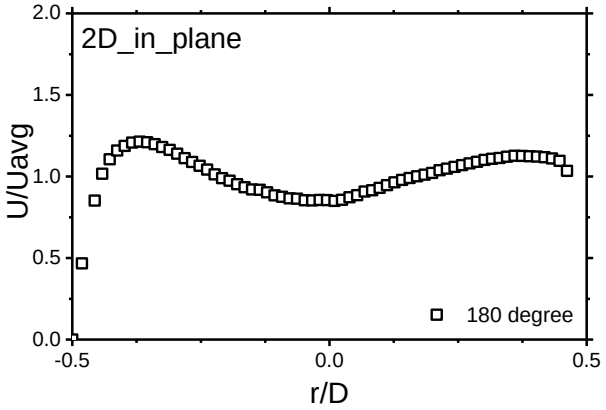

19) Velocity profile at 180 degree (2 D)

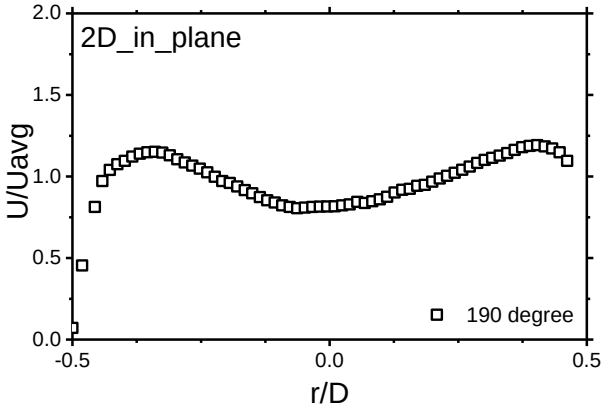

20) Velocity profile at 190 degree (2 D)

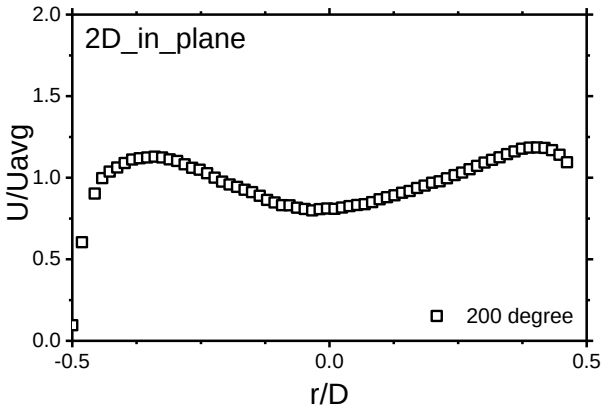

21) Velocity profile at 200 degree (2 D)

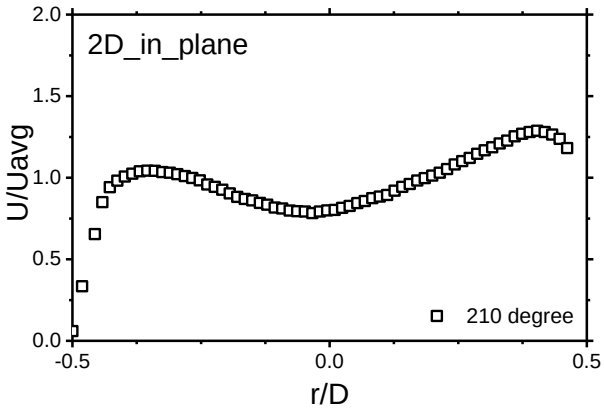

22) Velocity profile at 210 degree (2 D)

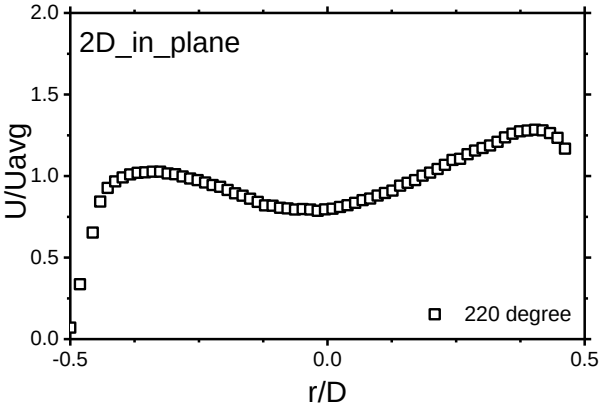

23) Velocity profile at 220 degree (2 D)

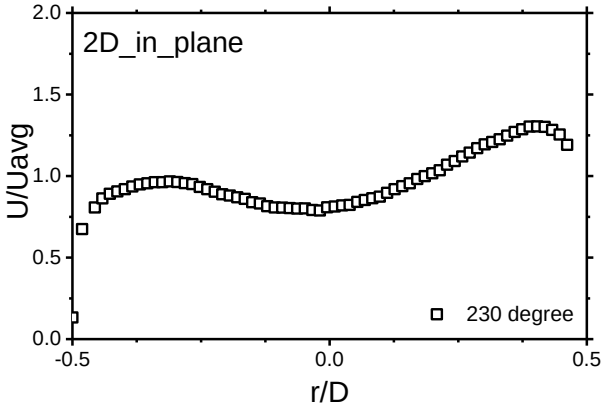

24) Velocity profile at 230 degree (2 D)

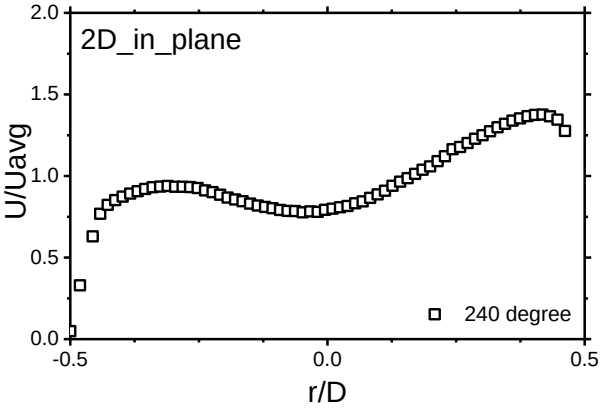

25) Velocity profile at 240 degree (2 D)

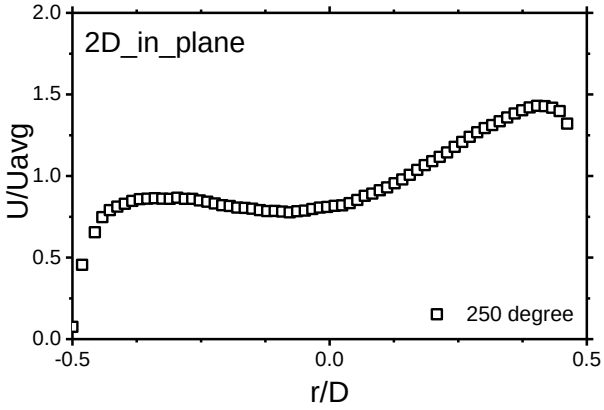

26) Velocity profile at 250 degree (2 D)

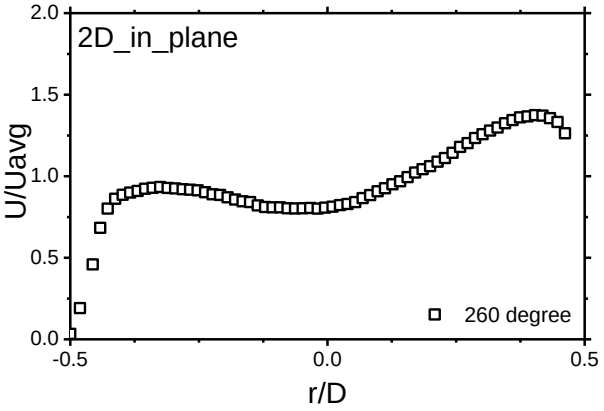

27) Velocity profile at 260 degree (2 D)

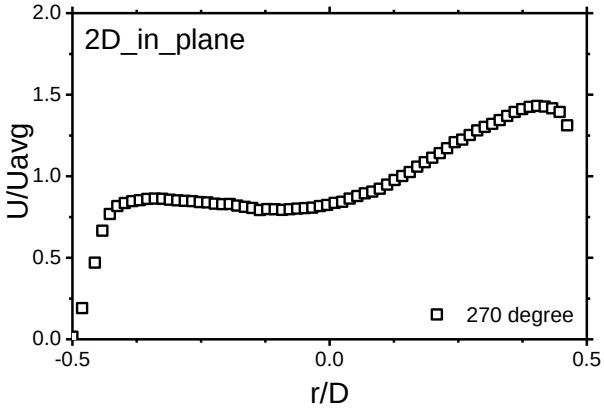

28) Velocity profile at 270 degree (2 D)

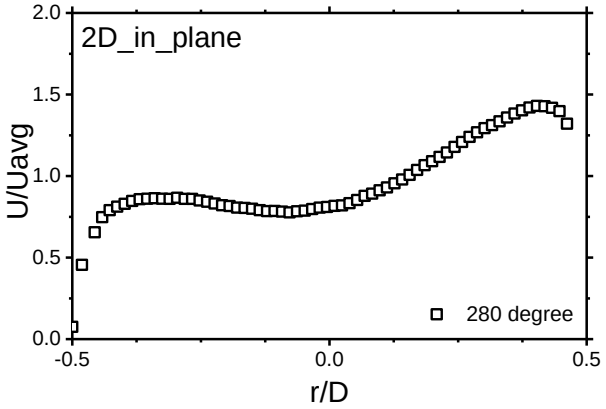

29) Velocity profile at 280 degree (2 D)

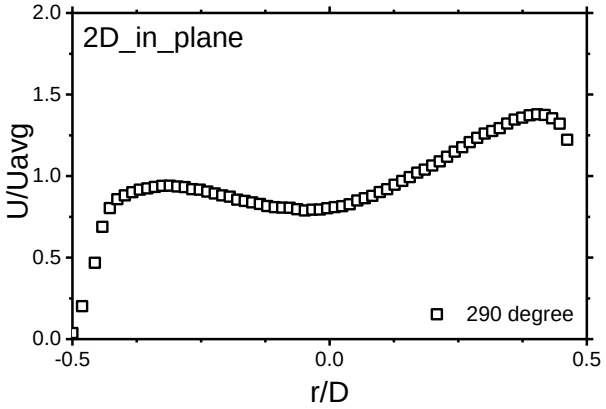

30) Velocity profile at 290 degree (2 D)

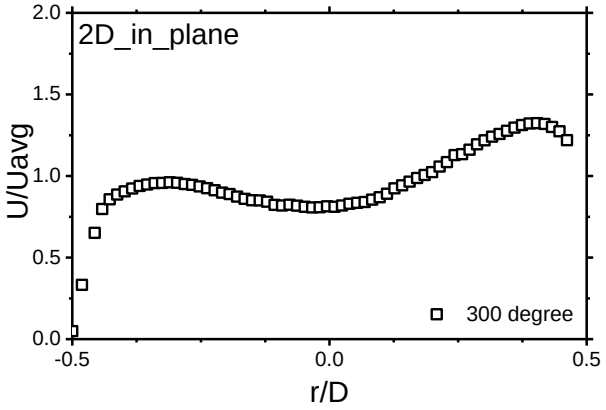

31) Velocity profile at 300 degree (2 D)

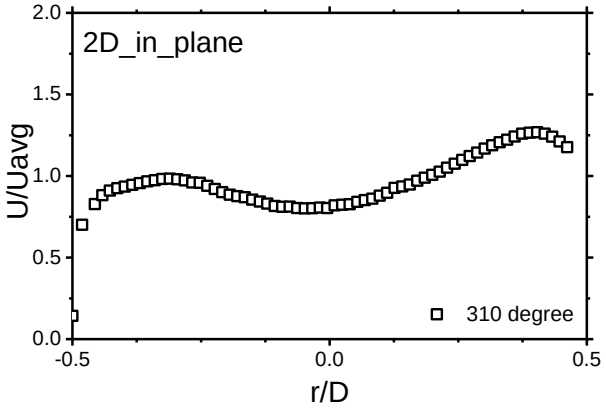

32) Velocity profile at 310 degree (2 D)

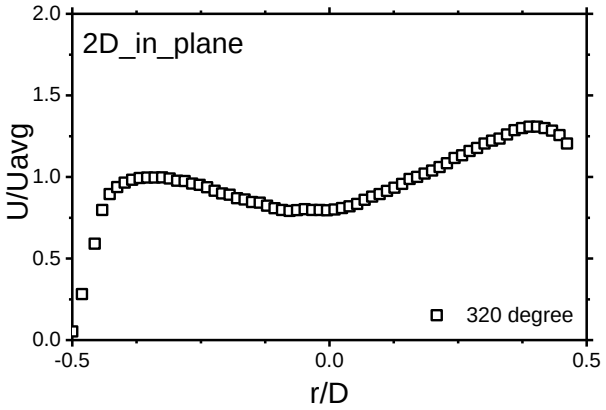

33) Velocity profile at 320 degree (2 D)

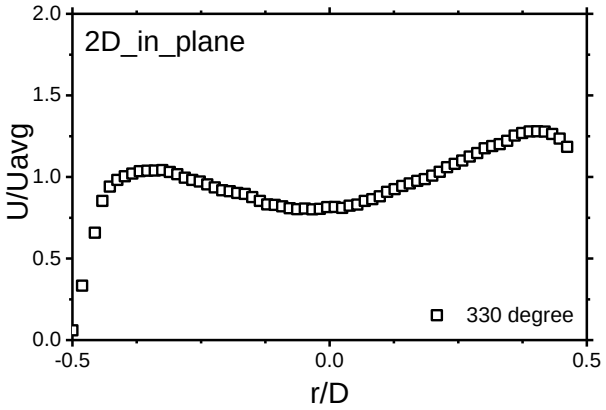

34) Velocity profile at 330 degree (2 D)

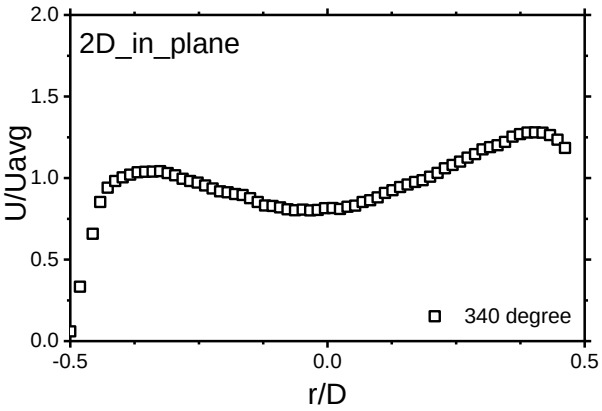

35) Velocity profile at 340 degree (2 D)

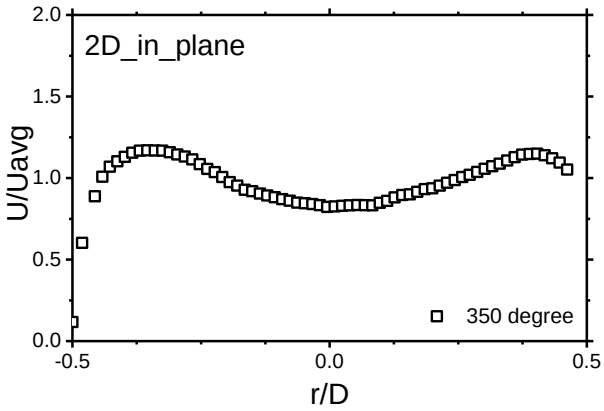

36) Velocity profile at 350 degree (2 D)

Fig. 5-13 Velocity profile at 2D

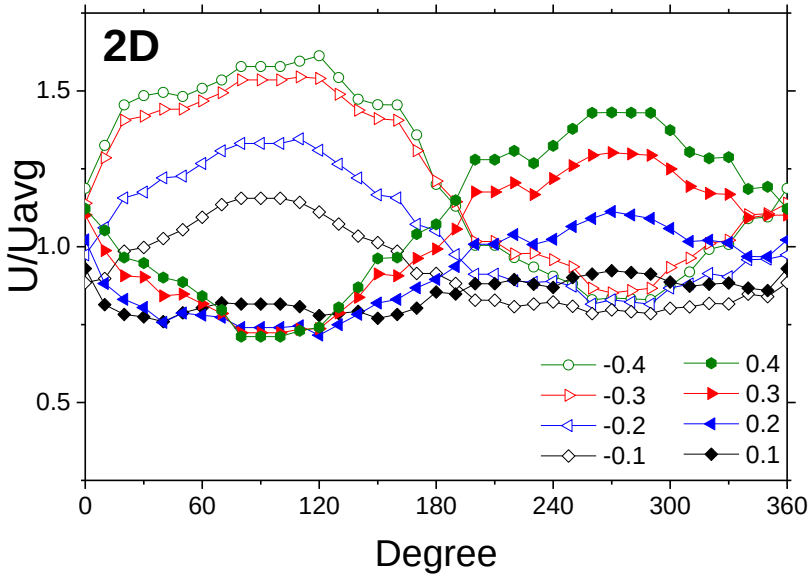

Fig.5-14 Circumferential velocity profiles at 2D

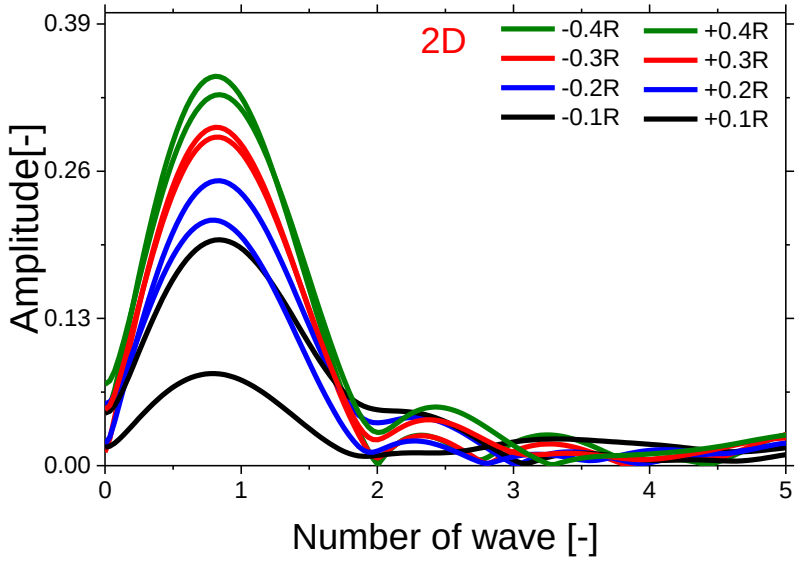

Fig. 5-15 Fast Fourier Transform (FFT) results at 2D

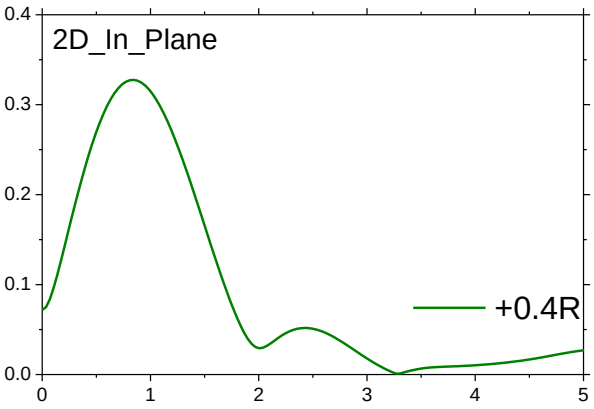

a) Number of waves from line -0.4 R (2 D)

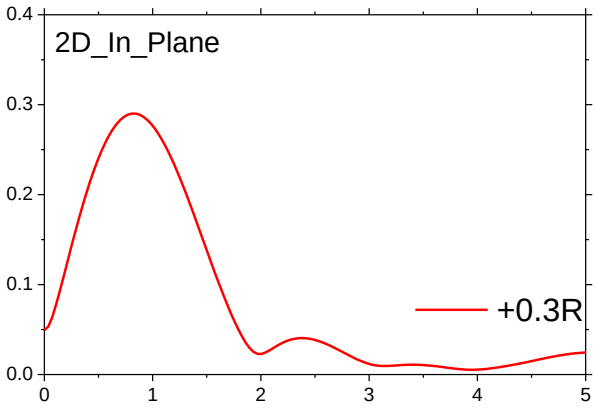

b) Number of waves from line -0.3 R (2 D)

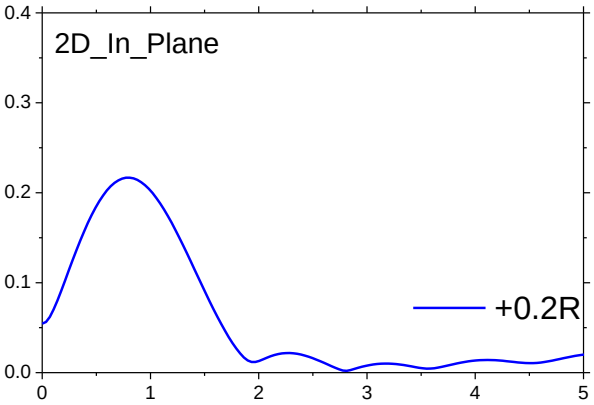

c) Number of waves from line -0.2 R (2 D)

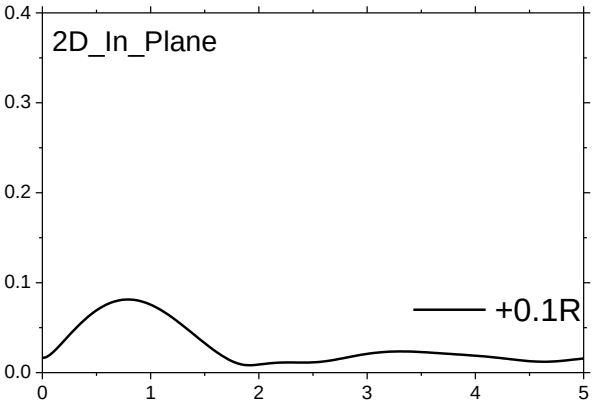

d) Number of waves from line -0.1 R (2 D)

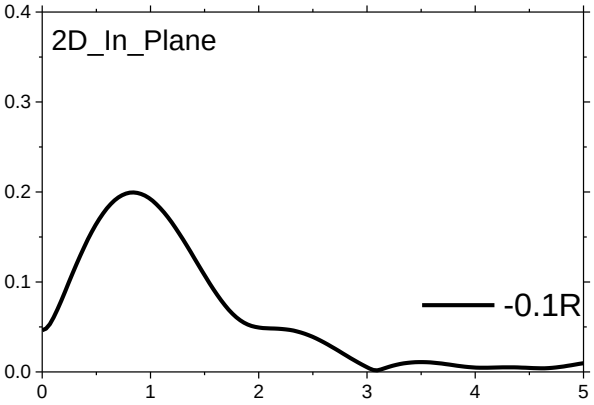

g) Number of waves from line +0.4 R (2 D)

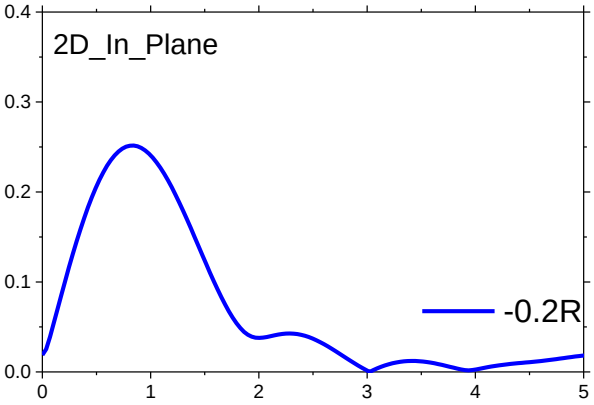

h) Number of waves from line +0.3 R (2 D)

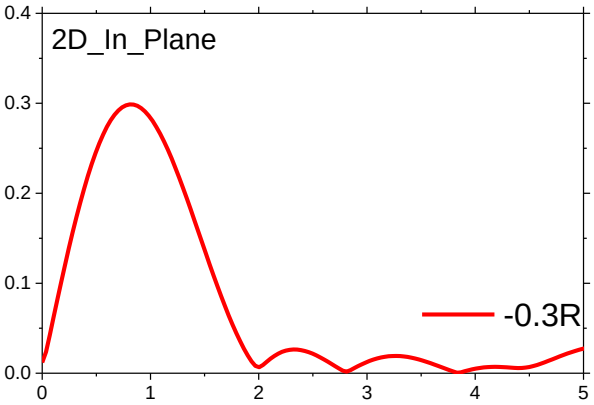

i) Number of waves from line +0.2 R (2 D)

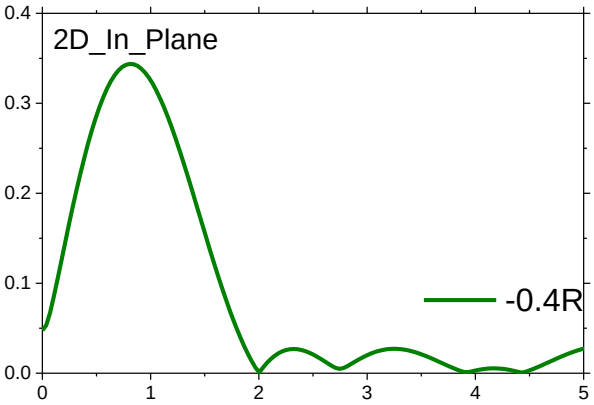

j) Number of waves from line +0.1 R (2 D)

Fig. 5-16 FFT results of circumferential velocity profiles at 2D

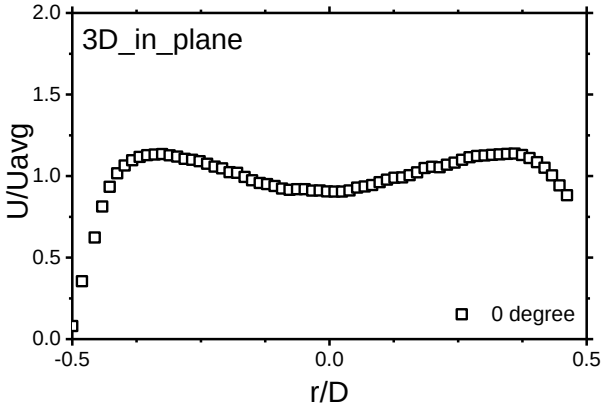

1) Velocity profile at 0 degree (3 D)

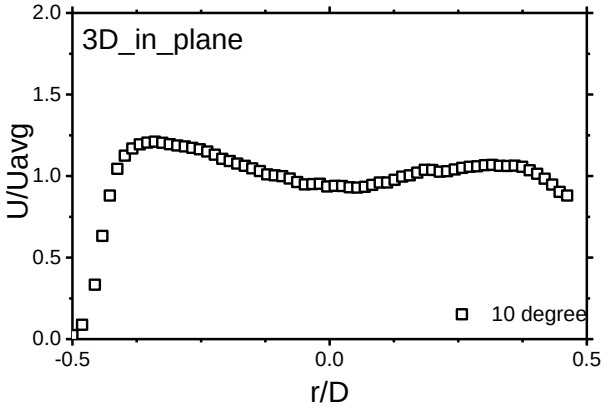

2) Velocity profile at 10 degree (3 D)

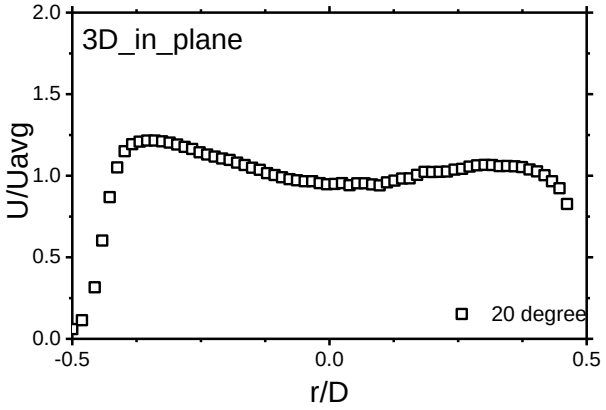

3) Velocity profile at 20 degree (3 D)

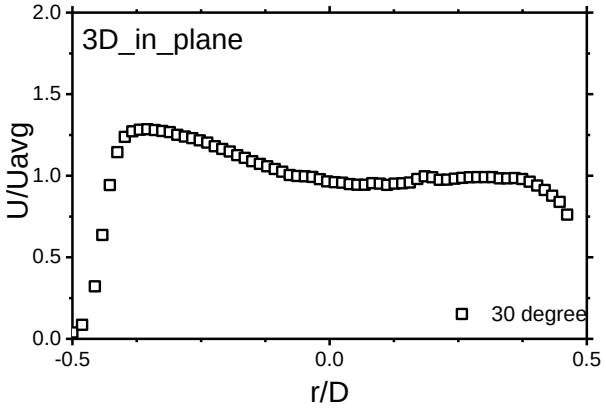

4) Velocity profile at 30 degree (3 D)

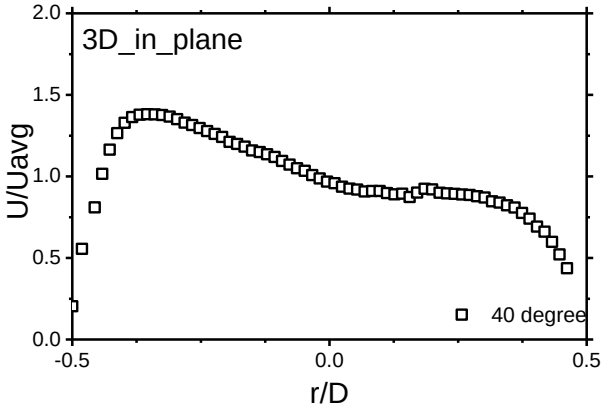

5) Velocity profile at 40 degree (3 D)

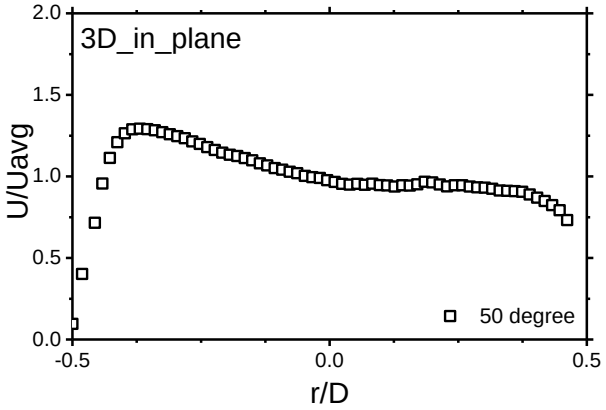

6) Velocity profile at 50 degree (3 D)

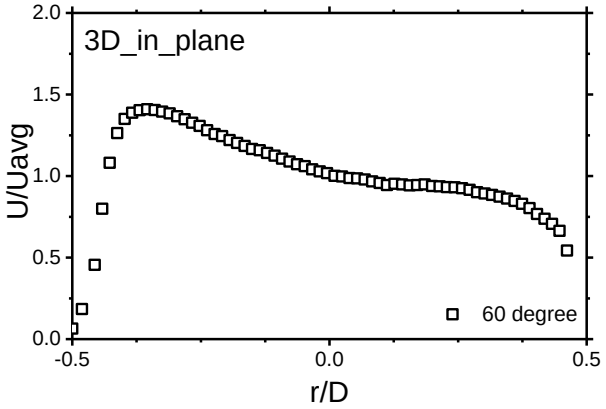

7) Velocity profile at 60 degree (3 D)

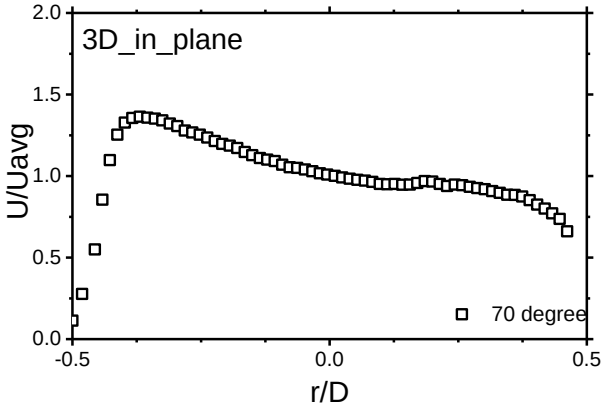

8) Velocity profile at 70 degree (3 D)

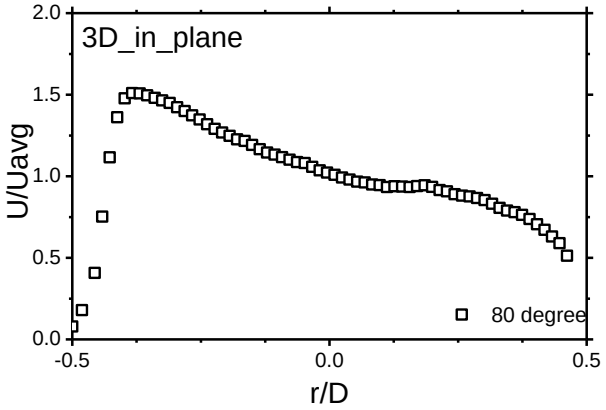

9) Velocity profile at 80 degree (3 D)

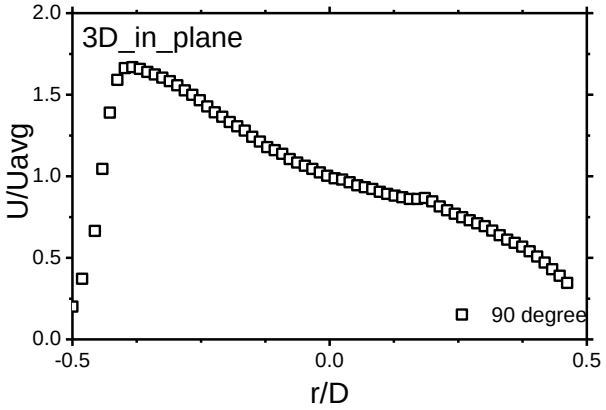

10) Velocity profile at 90 degree (3 D)

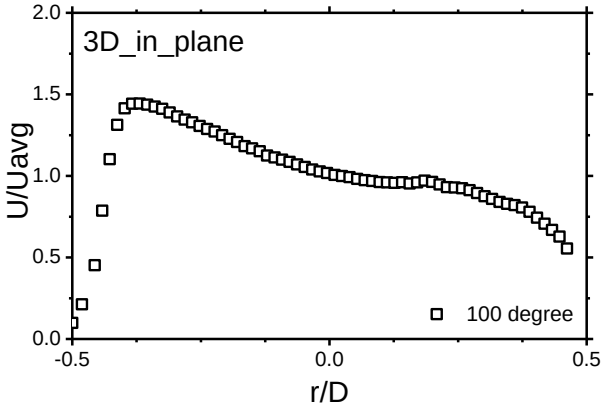

11) Velocity profile at 100 degree (3 D)

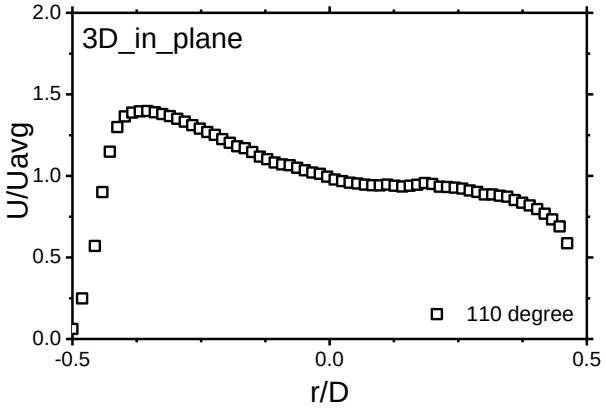

12) Velocity profile at 110 degree (3 D)

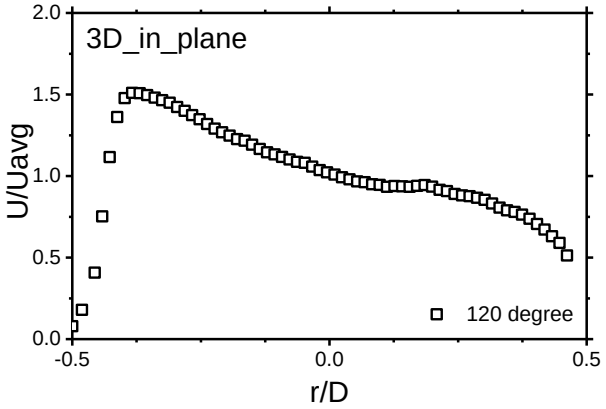

13) Velocity profile at 120 degree (3 D)

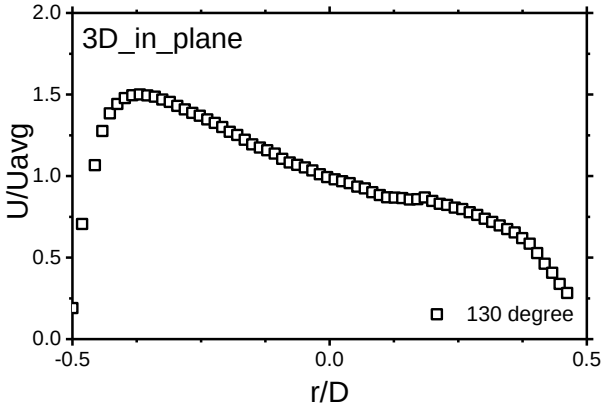

14) Velocity profile at 130 degree (3 D)

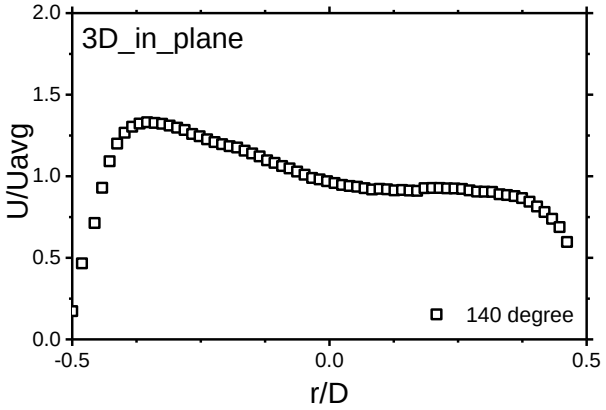

15) Velocity profile at 140 degree (3 D)

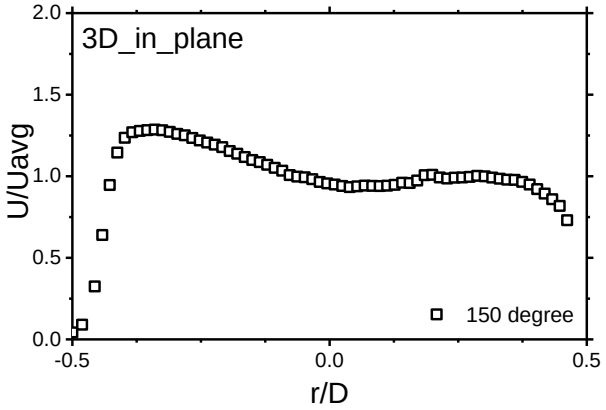

16) Velocity profile at 150 degree (3 D)

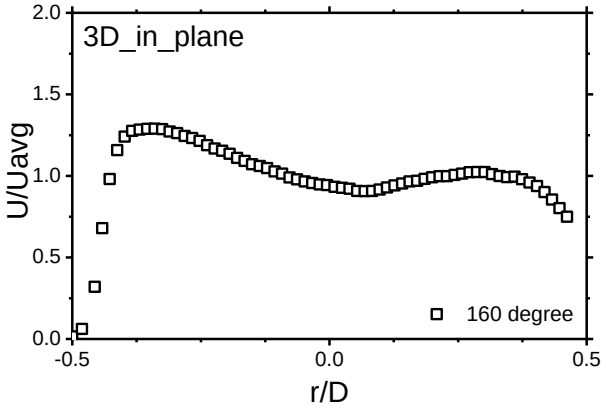

17). Velocity profile at 160 degree (3 D)

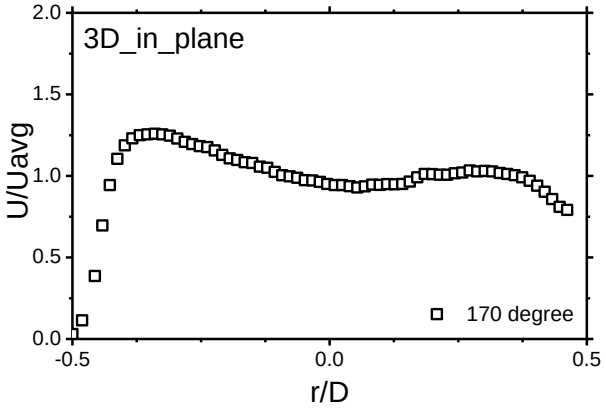

18) Velocity profile at 170 degree (3 D)

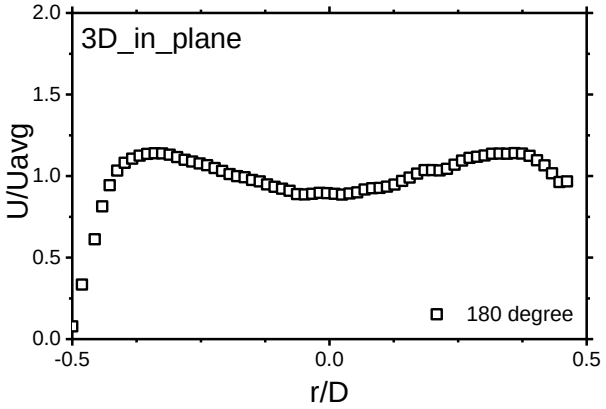

19) Velocity profile at 180 degree (3 D)

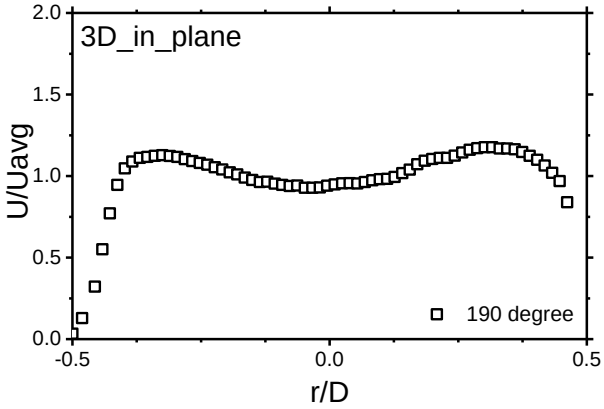

20) Velocity profile at 190 degree (3 D)

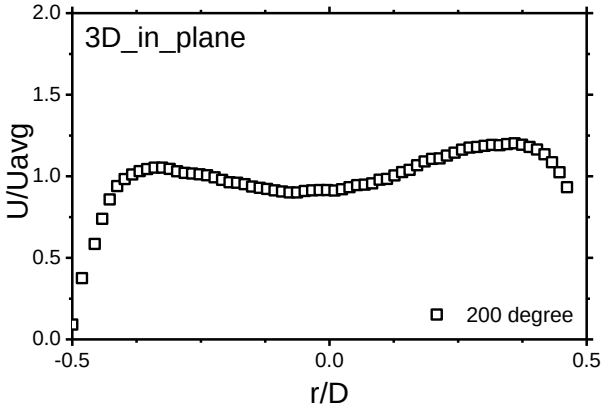

21) Velocity profile at 200 degree (3 D)

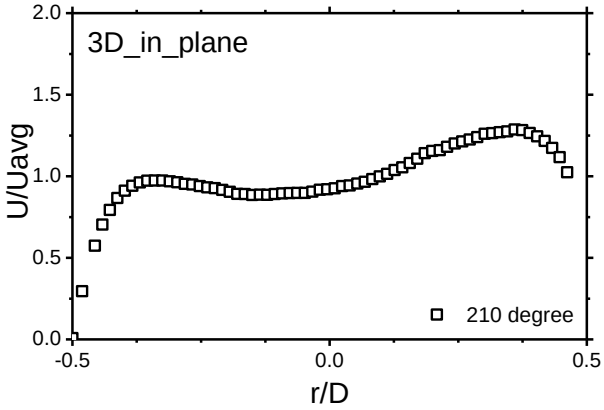

22) Velocity profile at 210 degree (3 D)

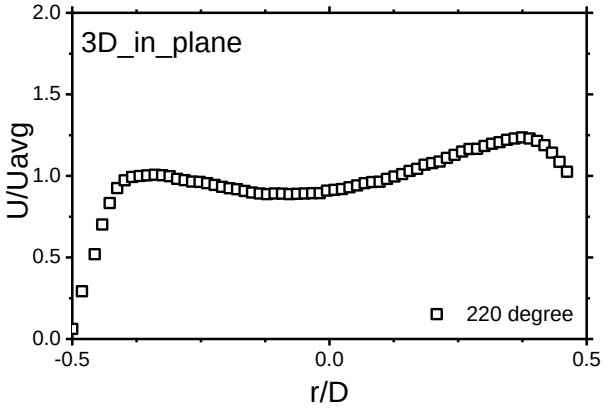

23) Velocity profile at 220 degree (3 D)

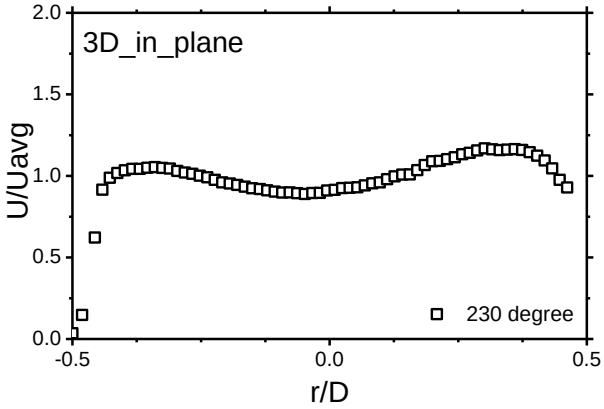

24) Velocity profile at 230 degree (3 D)

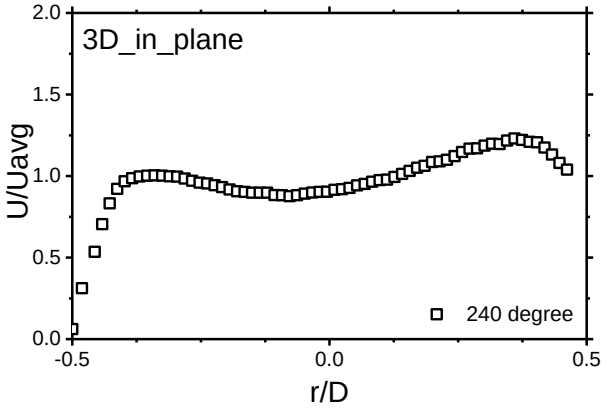

25) Velocity profile at 240 degree (3 D)

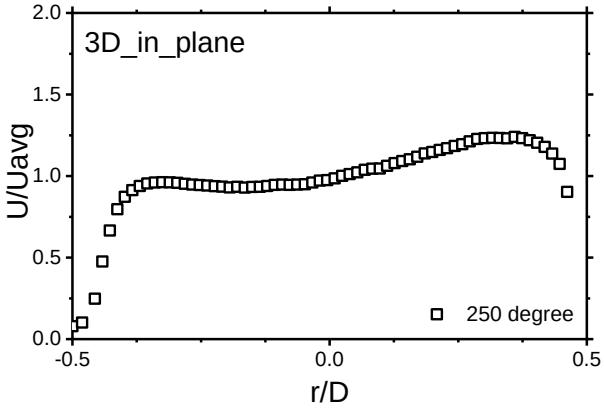

26) Velocity profile at 250 degree (3 D)

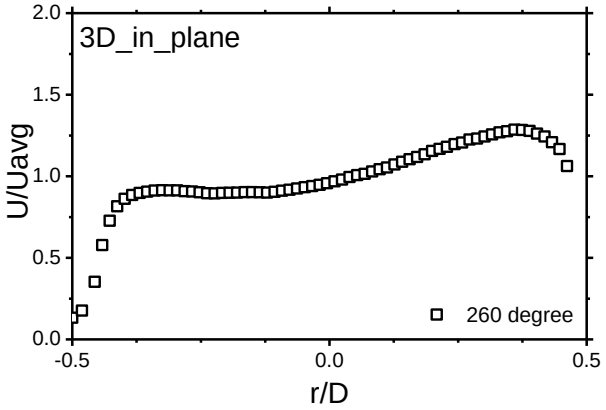

27) Velocity profile at 260 degree (3 D)

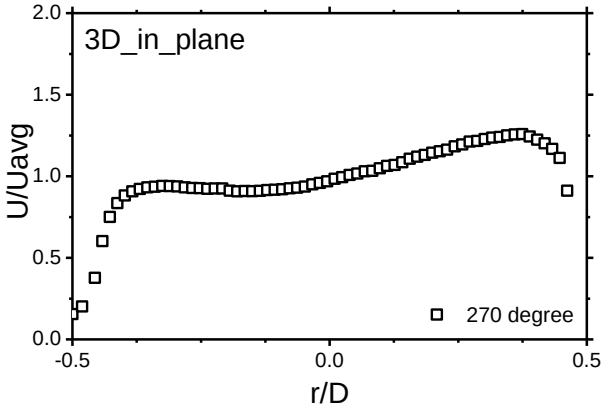

28) Velocity profile at 270 degree (3 D)

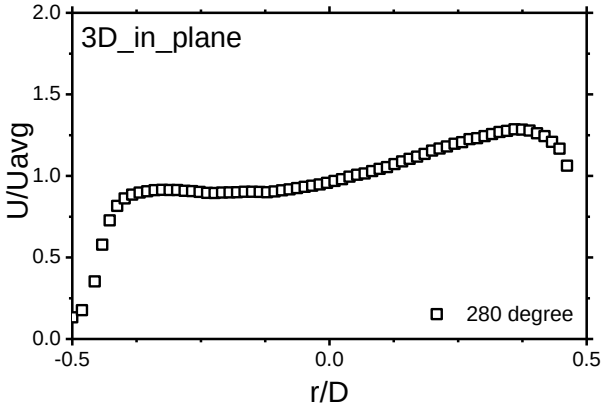

29) Velocity profile at 280 degree (3 D)

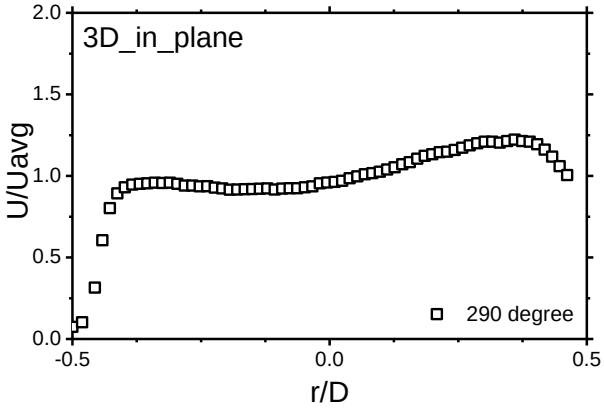

30) Velocity profile at 290 degree (3 D)

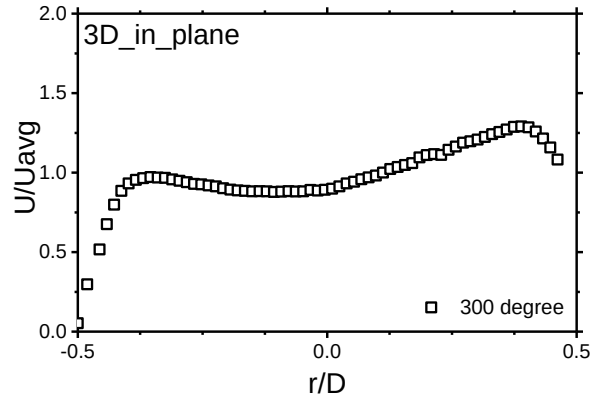

31) Velocity profile at 300 degree (3 D)

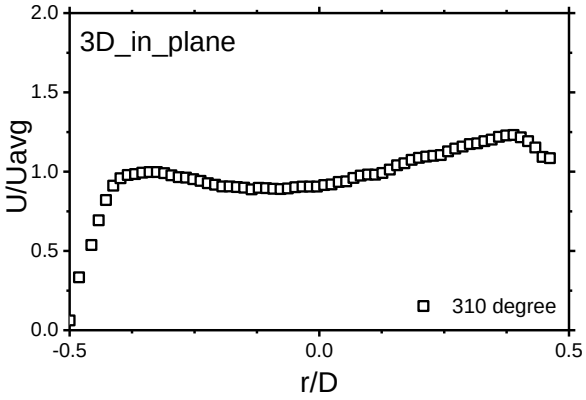

32) Velocity profile at 310 degree (3 D)

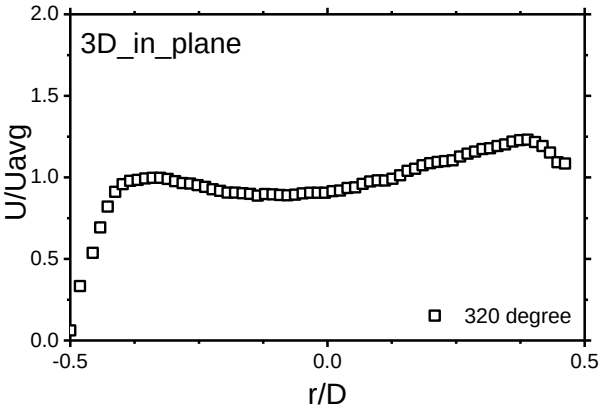

33) Velocity profile at 320 degree (3 D)

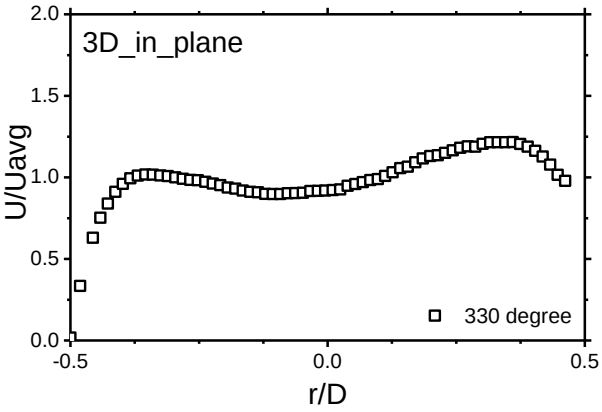

34) Velocity profile at 330 degree (3 D)

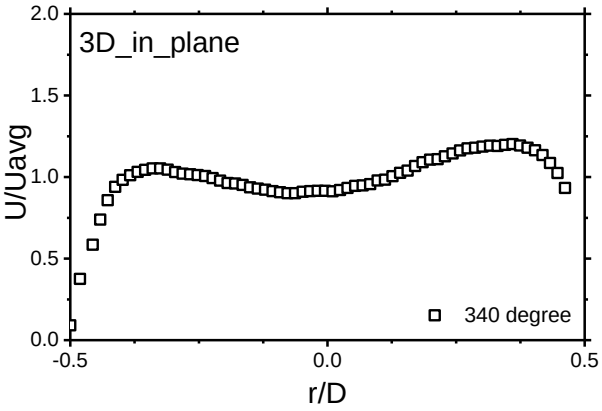

35) Velocity profile at 340 degree (3 D)

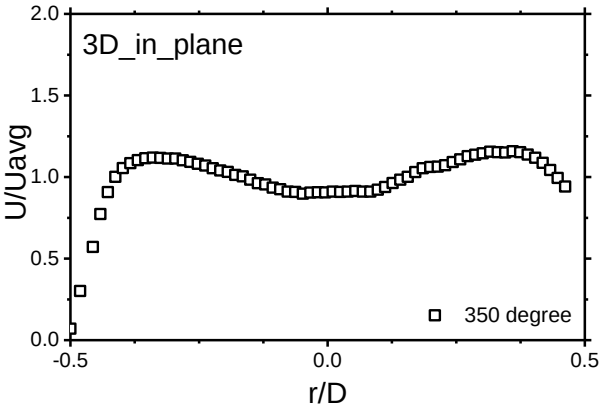

36) Velocity profile at 350 degree (3 D)

Fig. 5-17 Velocity profiles at 3D

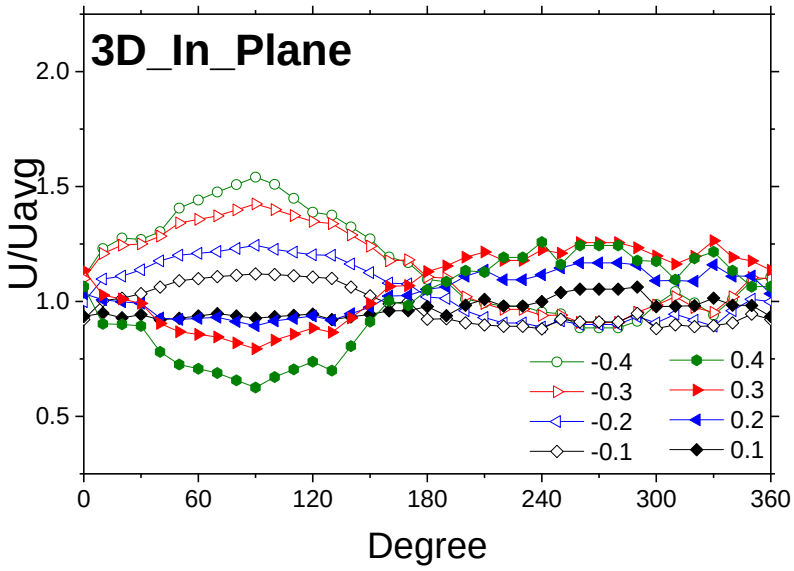

Fig. 5-18 Circumferential velocity profiles at 3D

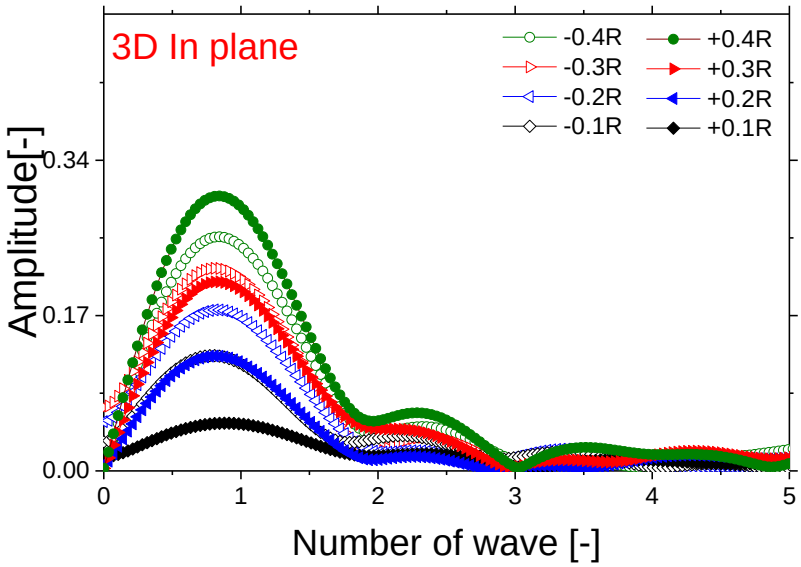

Fig. 5-19 Fast Fourier Transform (FFT) results at 3D

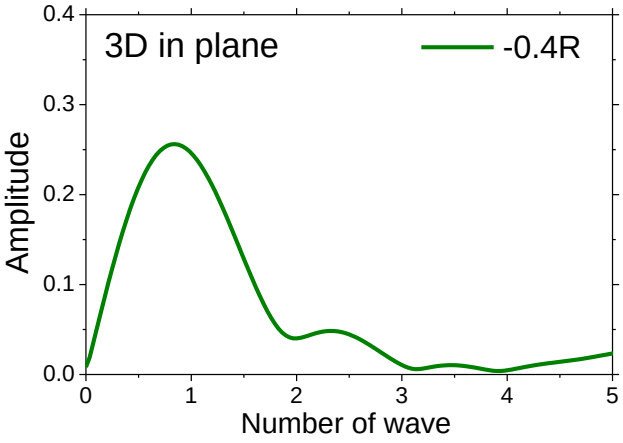

a) Number of waves from line -0.4 R (3 D)

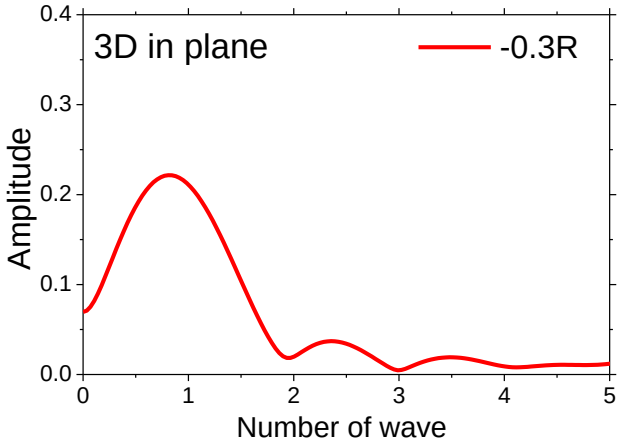

b) Number of waves from line -0.3 R (3 D)

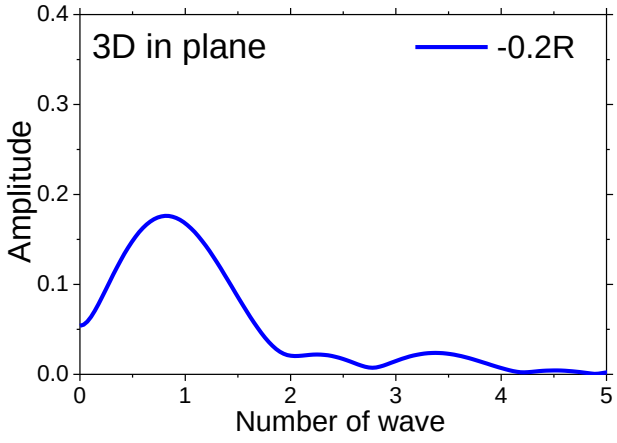

c) Number of waves from line -0.2 R (3 D)

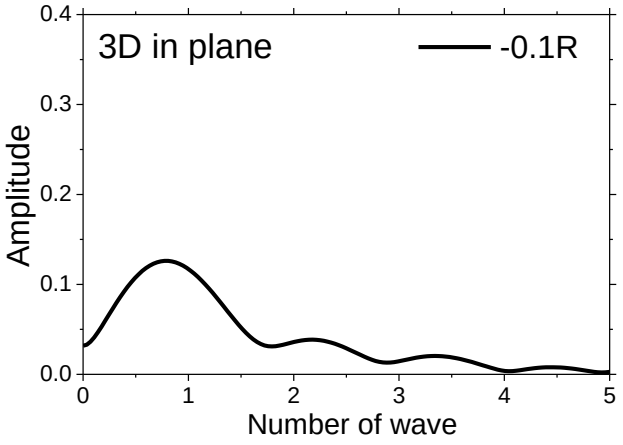

d) Number of waves from line -0.4 R (3 D)

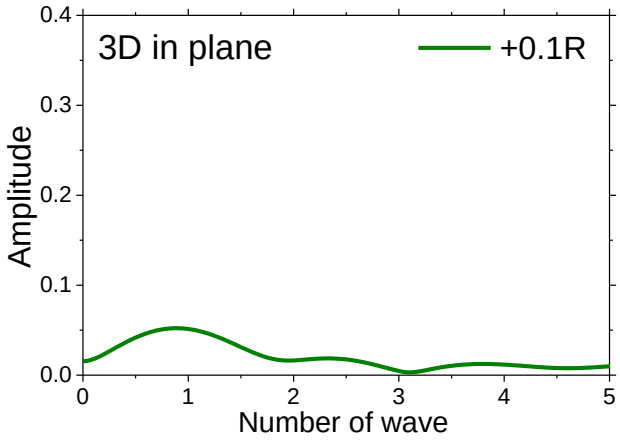

e) Number of waves from line +0.1 R (3 D)

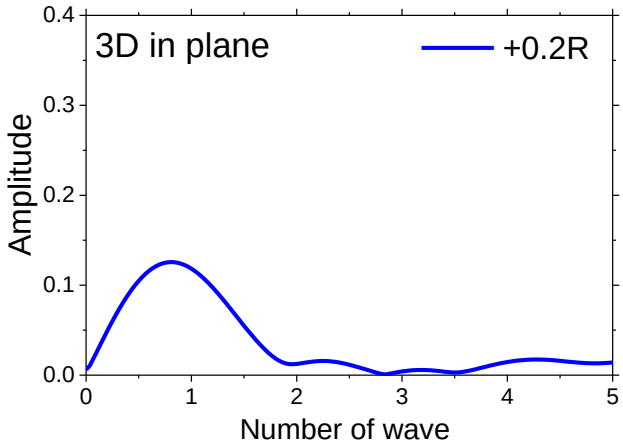

f) Number of waves from line +0.2 R (3 D)

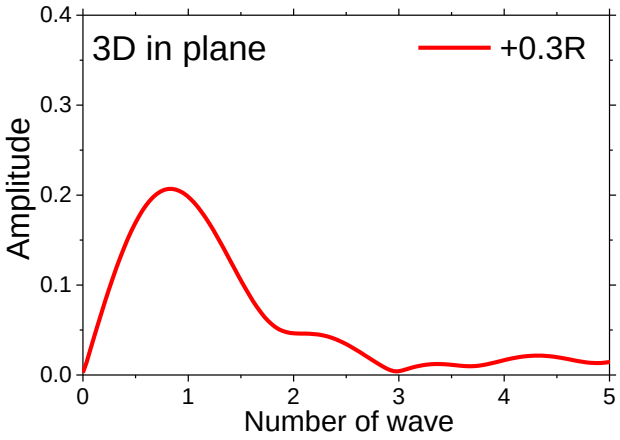

g) Number of waves from line +0.3 R (3 D)

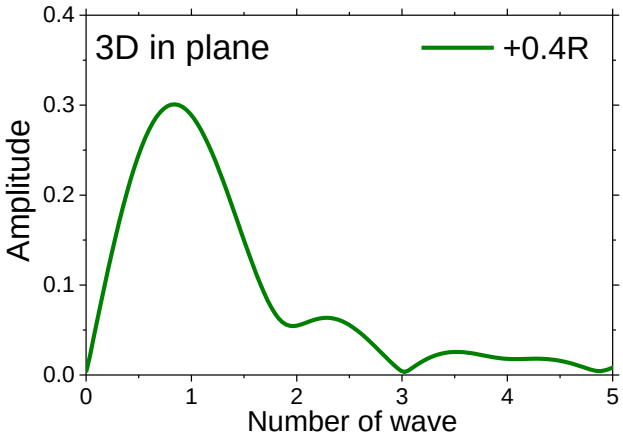

h) Number of waves from line +0.4 R (3 D)

Fig. 5-19 FFT results of circumferential velocity profiles at 3D

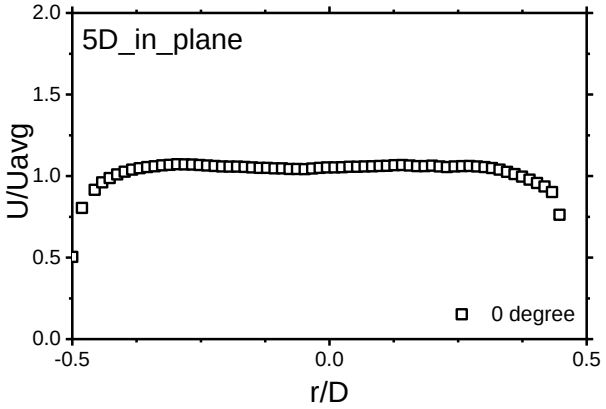

1) Velocity profile at 0 degree (5 D)

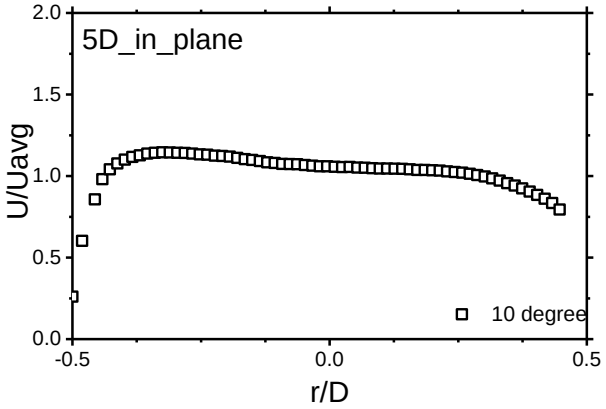

2) Velocity profile at 10 degree (5 D)

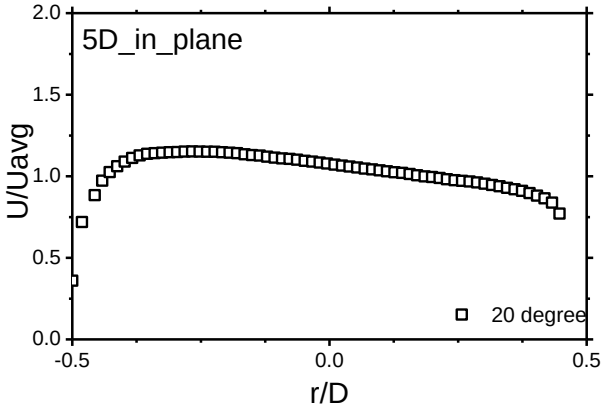

3) Velocity profile at 20 degree (5 D)

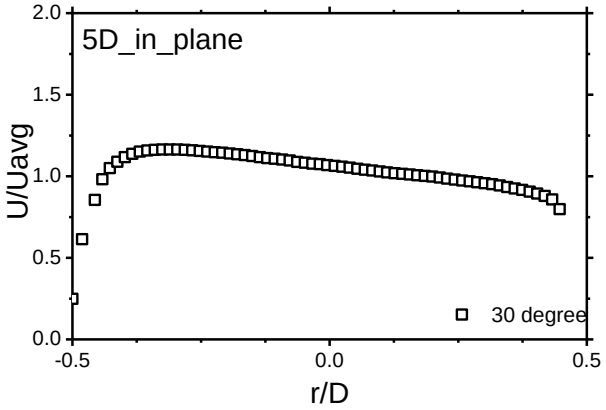

4) Velocity profile at 30 degree (5 D)

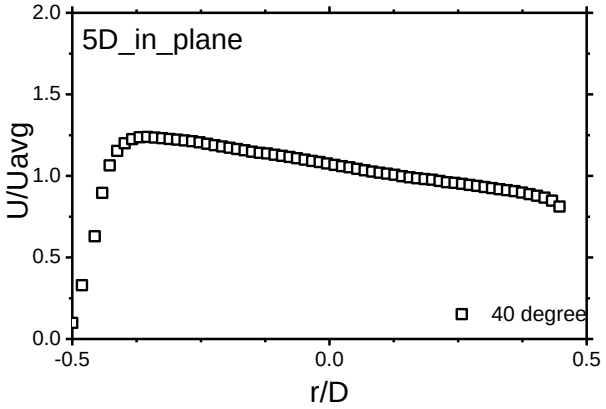

5) Velocity profile at 40 degree (5 D)

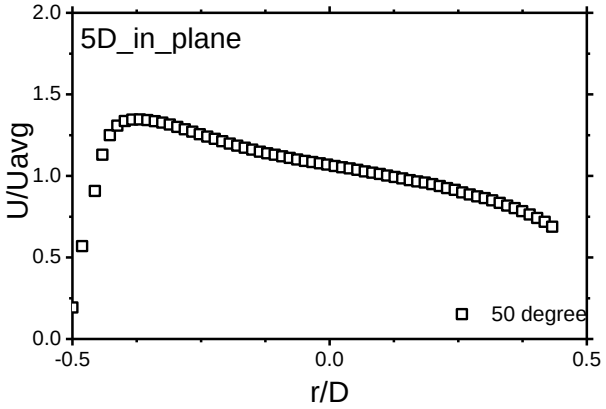

6) Velocity profile at 50 degree (5 D)

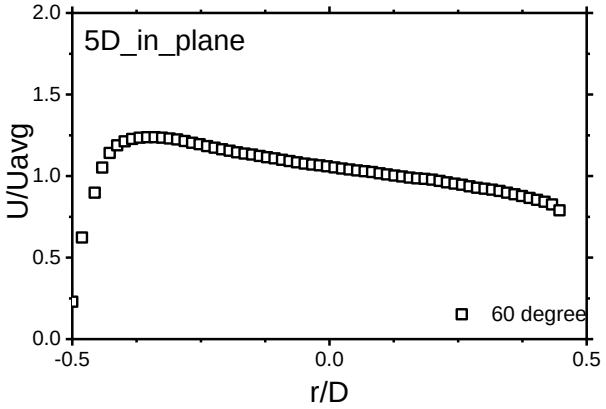

7) Velocity profile at 60 degree (5 D)

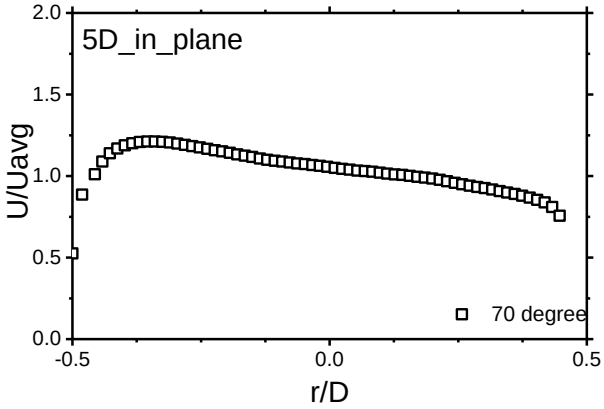

8) Velocity profile at 70 degree (5 D)

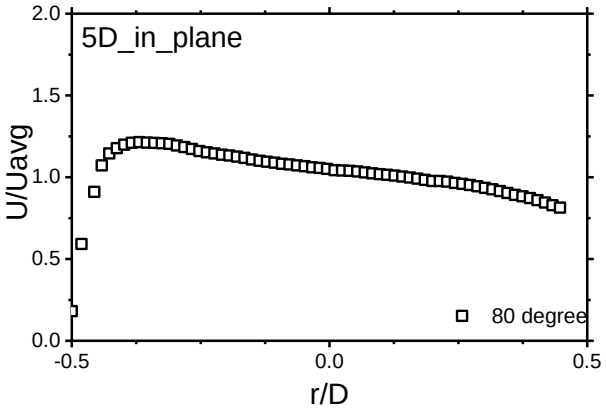

9) Velocity profile at 80 degree (5 D)

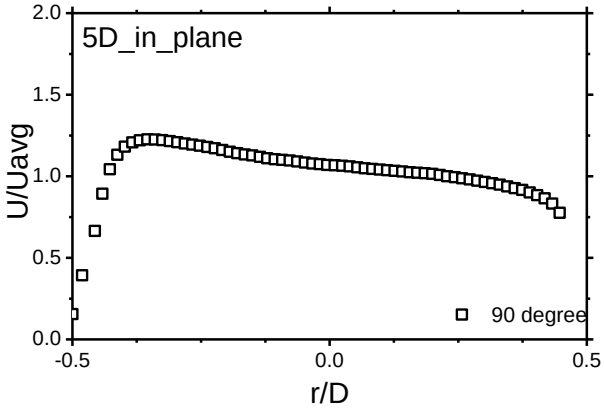

10) Velocity profile at 90 degree (5 D)

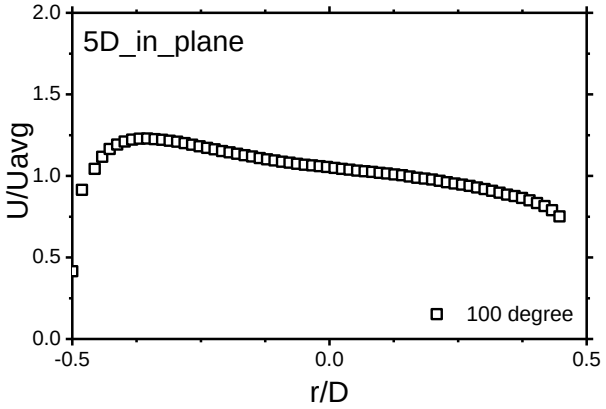

11) Velocity profile at 100 degree (5 D)

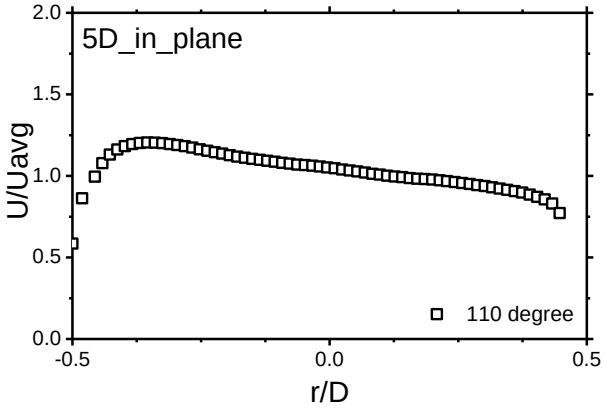

12) Velocity profile at 110 degree (5 D)

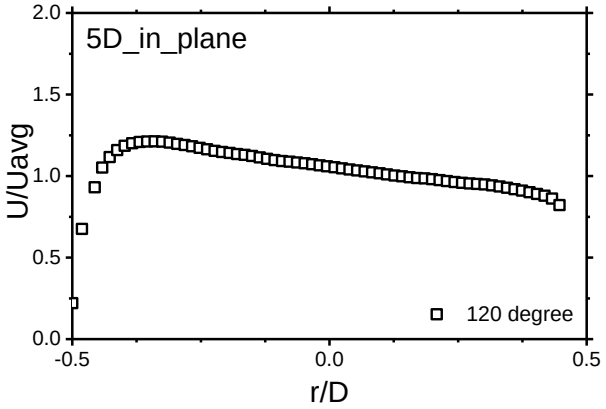

13) Velocity profile at 120 degree (5 D)

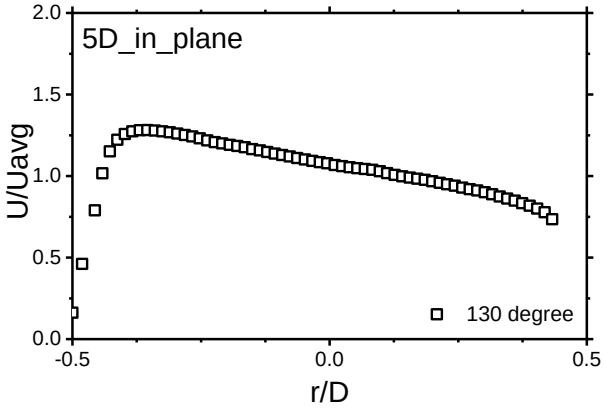

14) Velocity profile at 130 degree (5 D)

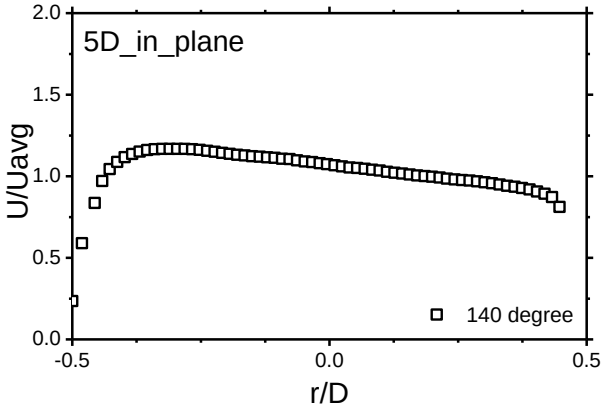

15) Velocity profile at 140 degree (5 D)

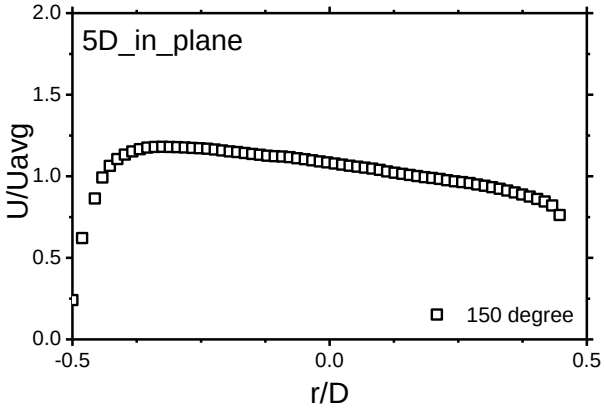

16) Velocity profile at 150 degree (5 D)

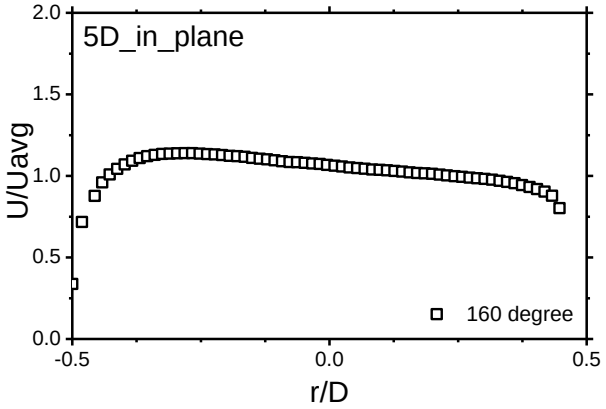

17) Velocity profile at 160 degree (5 D)

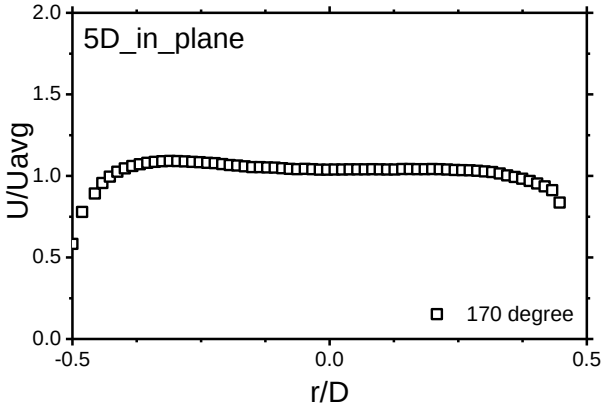

18) Velocity profile at 170 degree (5 D)

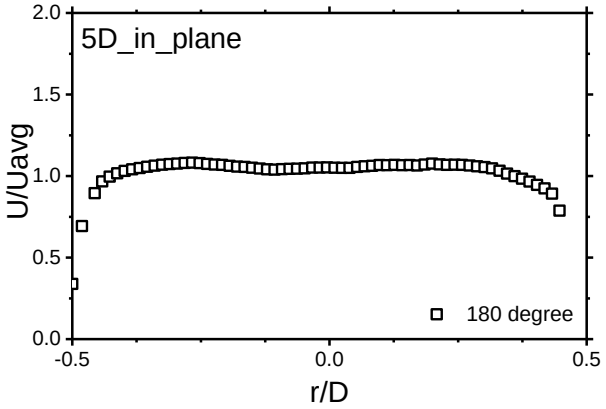

19) Velocity profile at 180 degree (5 D)

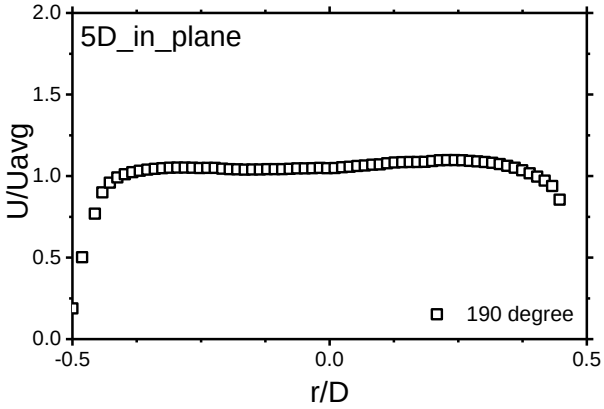

20) Velocity profile at 190 degree (5 D)

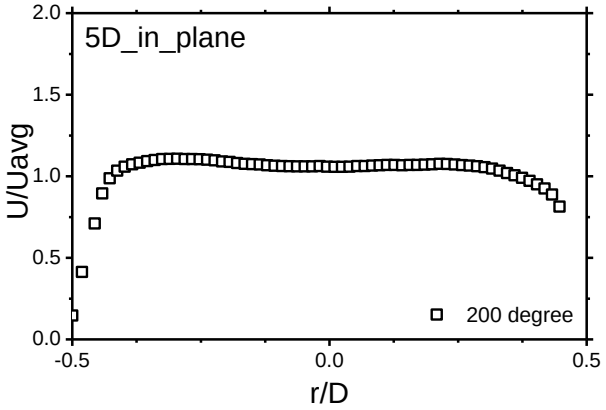

21) Velocity profile at 200 degree (5 D)

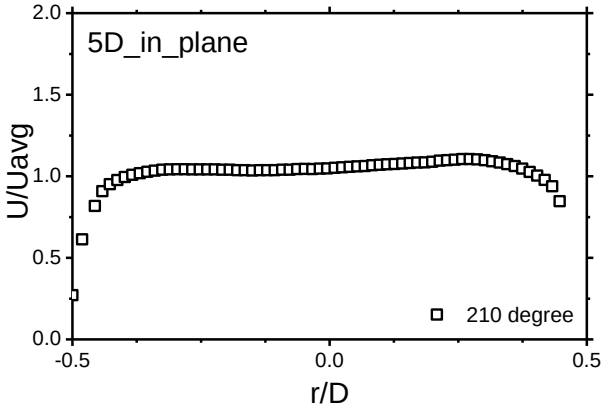

22) Velocity profile at 210 degree (5 D)

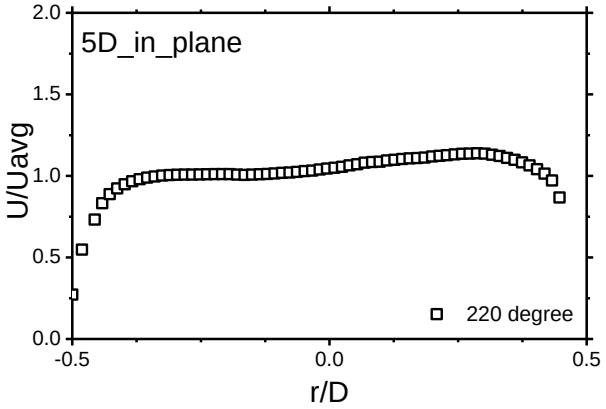

23) Velocity profile at 220 degree (5 D)

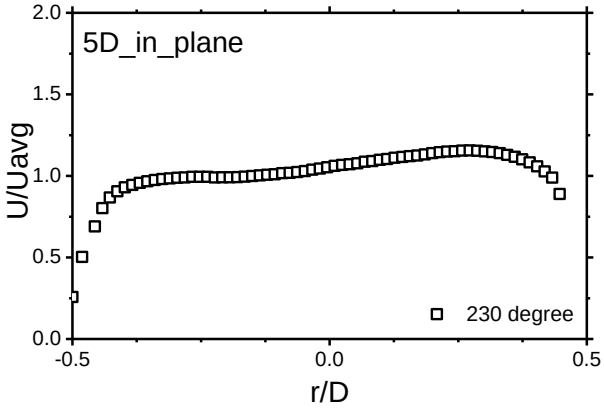

24) Velocity profile at 230 degree (5 D)

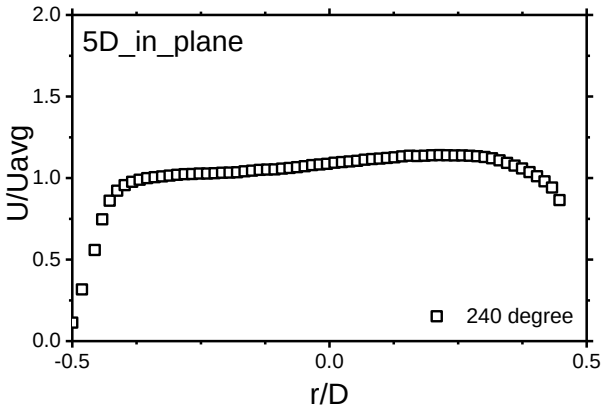

25) Velocity profile at 240 degree (5 D)

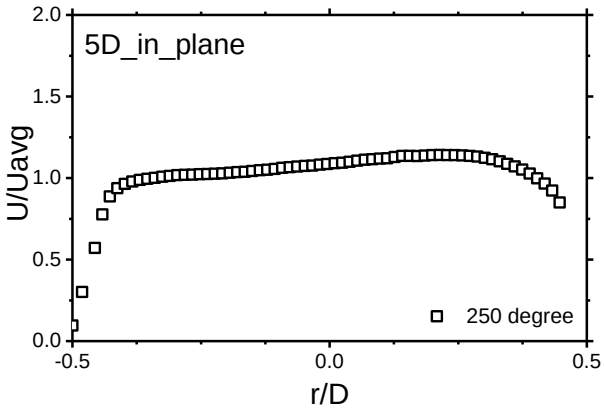

26) Velocity profile at 250 degree (5 D)

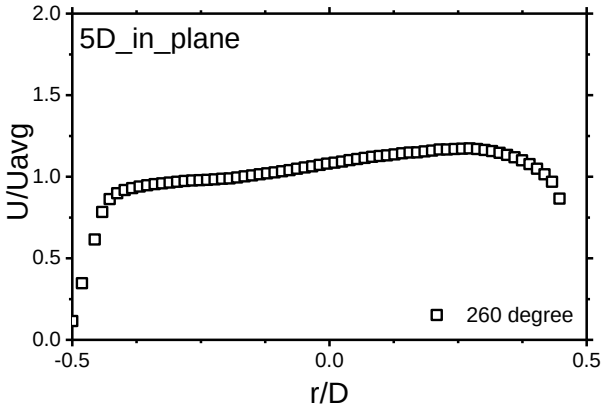

27) Velocity profile at 260 degree (5 D)

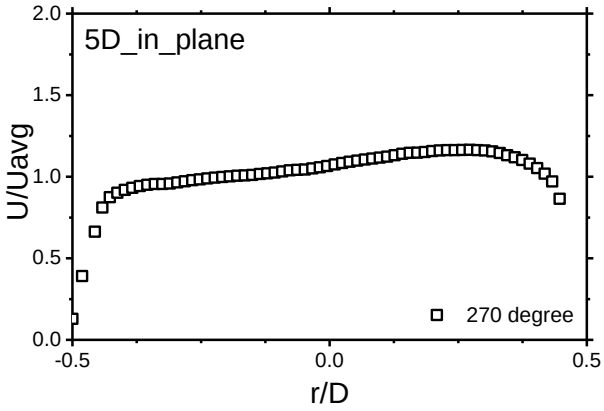

28) Velocity profile at 270 degree (5 D)

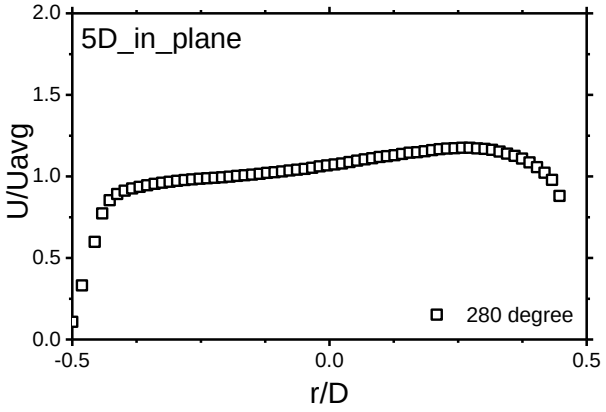

29) Velocity profile at 280 degree (5 D)

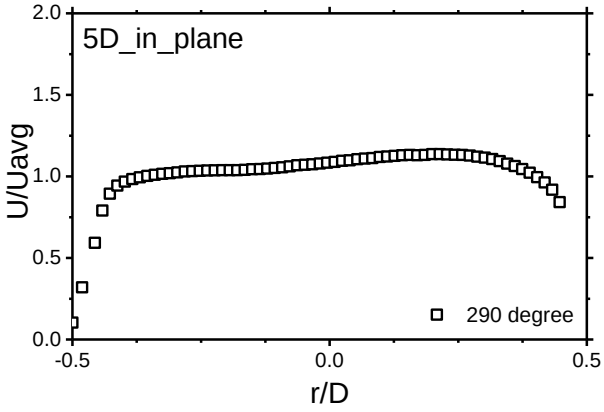

30) Velocity profile at 290 degree (5 D)

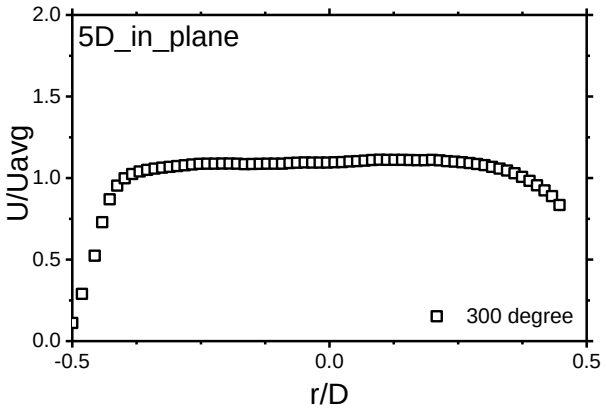

31) Velocity profile at 300 degree (5 D)

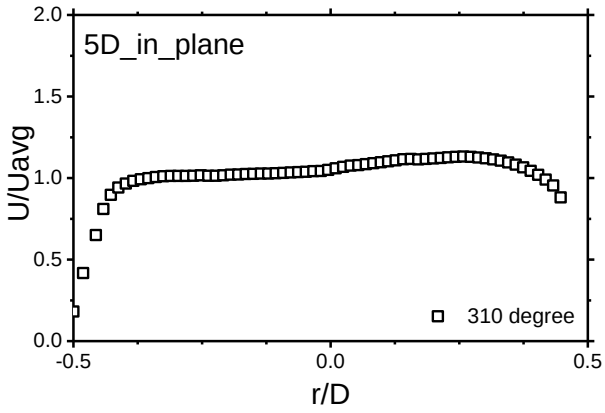

32) Velocity profile at 310 degree (5 D)

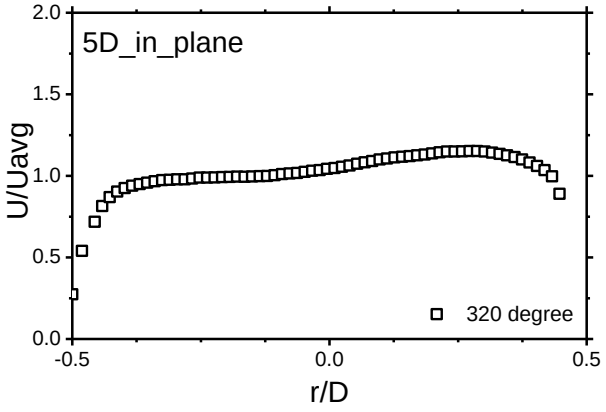

33) Velocity profile at 320 degree (5 D)

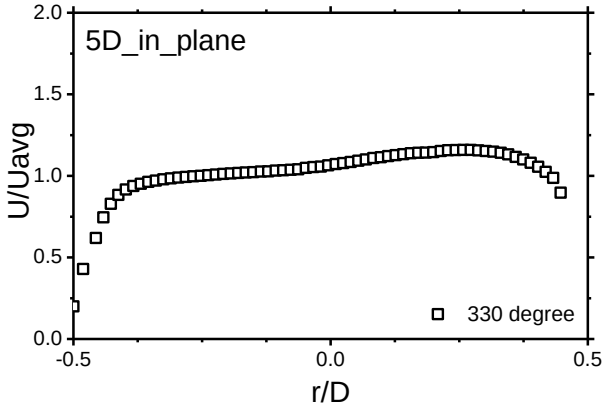

34) Velocity profile at 330 degree (5 D)

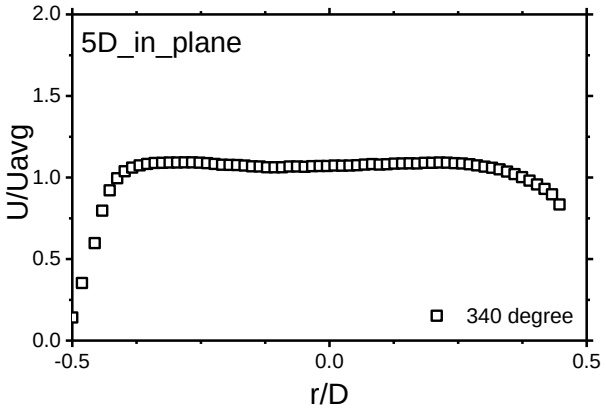

35) Velocity profile at 340 degree (5 D)

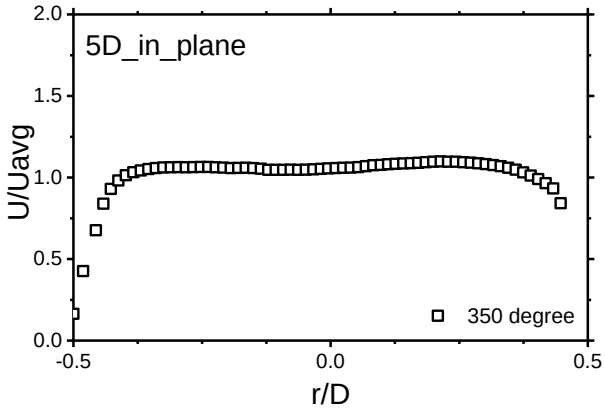

36) Velocity profile at 350 degree (5 D)

Fig. 5-21 Velocity profiles at 5D in plane double bent pipe

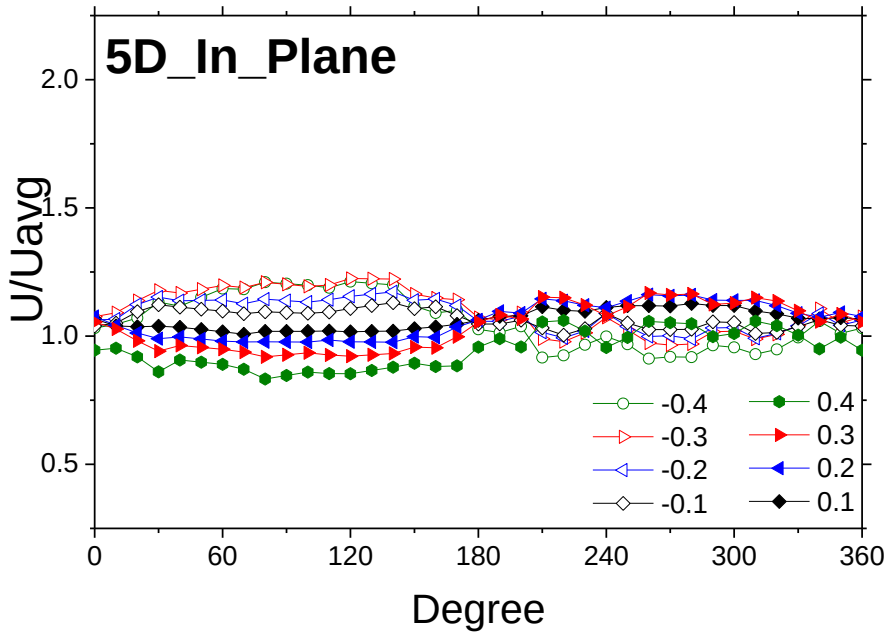

Fig. 5-22 Circumferential velocity profiles at 5D in plane double bent pipe

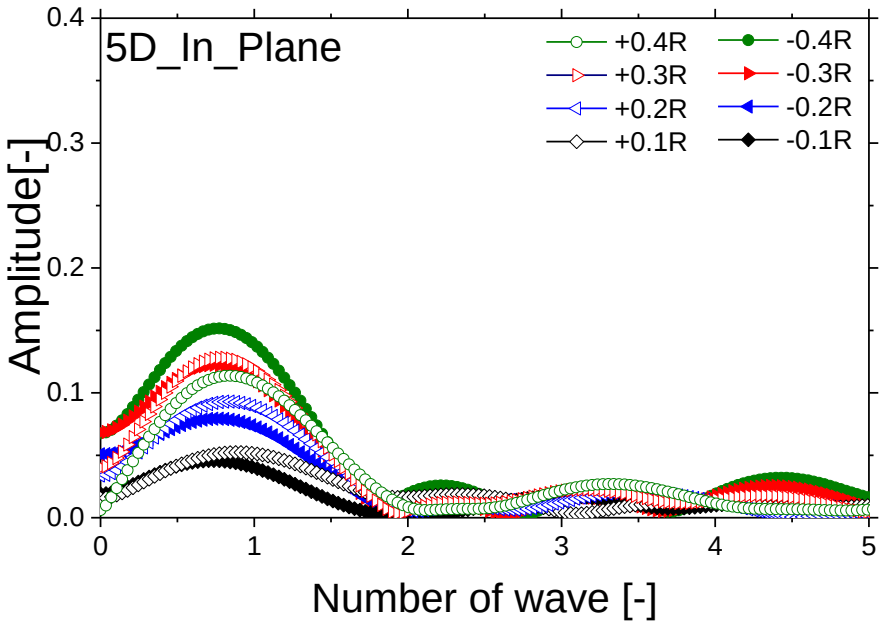

Fig. 5-23 FFT's results of circumferential velocity profiles at 5D in plane double bent pipe

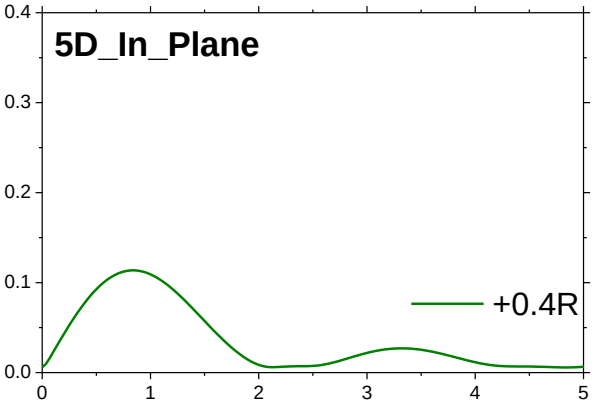

a) Number of waves from line -0.1 R (5 D)

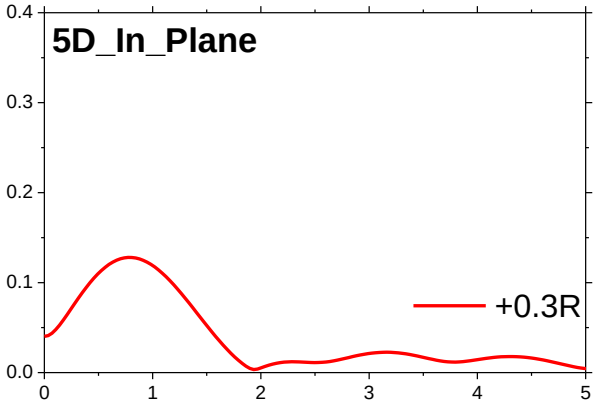

b) Number of waves from line -0.2 R (5 D)

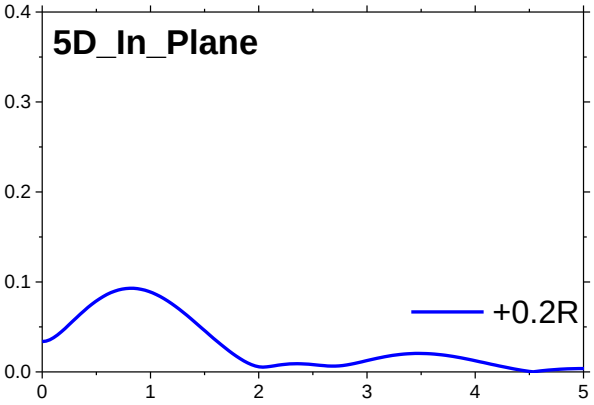

c) Number of waves from line -0.3 R (5 D)

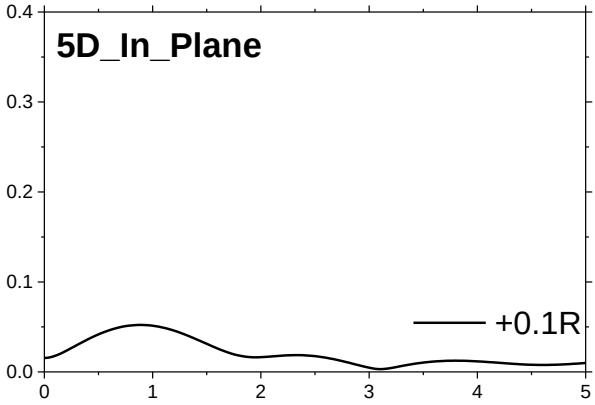

d) Number of waves from line -0.4 R (5 D)

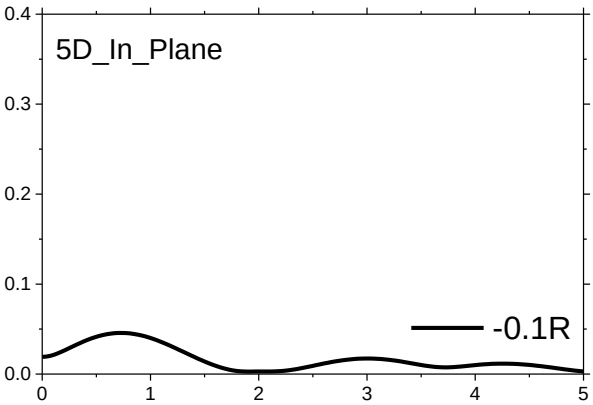

e) Number of waves from line -0.1 R (5 D)

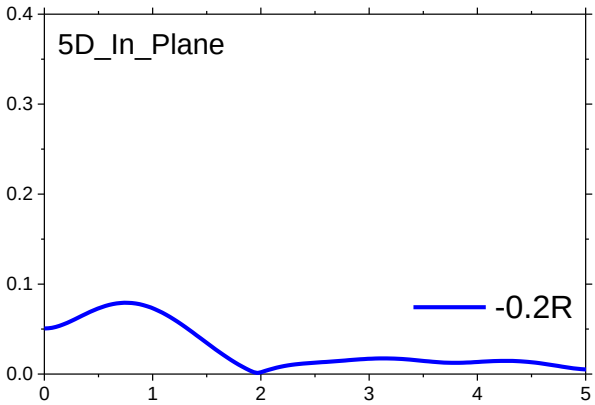

f) Number of waves from line -0.2 R (5 D)

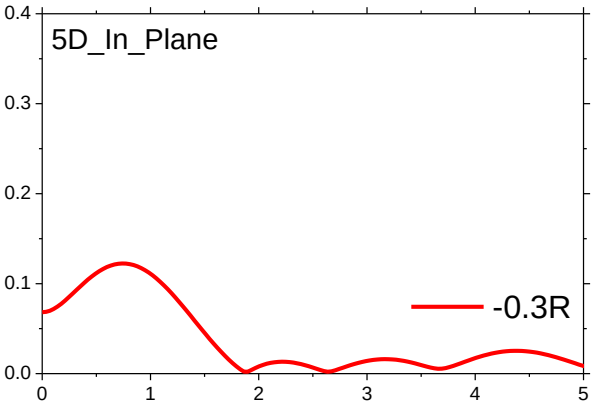

g) Number of waves from line -0.3 R (5 D)

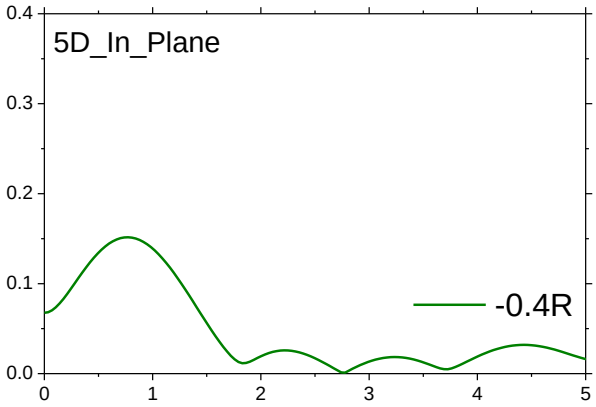

h) Number of waves from line -0.4 R (5 D)

Fig. 5-23 FFT results of circumferential velocity profiles at 5D

CHAPTER 6

ACCURATE FLOWRATE MEASUREMENT DOWNSTREAM OF THE DOUBLE BENT PIPE USING ESTIMATING METHOD

6.1 INTRODUCTION

The complicated flow as the pipe flow downstream of the double bent pipe which effects the accuracy of flowrate was studied by using multiple measurement lines. It is for making the two-dimensional velocity map. S. Wada et al. studied about the flowrate measurement after a single bent pipe of upward flow where just below a bent and sudden expansion pipe employing three measurement lines. They reported that the errors were less than 1% **[6-4]**. In addition, R. Kotze et al. studied about the flowrate measurement using UVP measurement with multiple measurement lines for the accurate flowrate measurement in the complex flow such as in the valve **[6-5]**. However, the errors in the case were quite high as more than 10% because of insufficient of the number of measurement lines. Nevertheless, the complex bent pipe systems are usually used in general plants. Not only the single bent pipes are installed, but also the double bent pipes are generally used. In my previous study, the double bent pipe was studied using multiple ultrasound transducers. The results of the experimental errors of the flowrate measurement were less than 1% using 3 measurement lines at the distance of inlet length 5 times of pipe diameter **[6-6]**. However, the other type of the complicated flow is the pipe flow downstream of the out of plane double bent pipe which more difficult to measure.

The out of plane double bent pipe system is determined in this study. The theoretical analysis to estimate the optimal number of measurement lines and the minimum inlet length or measurement position base on sampling rate theorem and Fast Fourier Transform (FFT) are applied to estimate the number of measurement lines at 3 various inlet lengths at 3 D, 4 D and 5 D.

Figure 6-1 a) shows the harmonic wave of velocity profile on circular measurement line of -0.4R at 3D. The horizontal axis means the transducer circumferential position of transducer, while the vertical axis means the time-average velocity was normalized by mean velocity. After the transformation of raw data with Fast Fourier Transform technique, the frequency and amplitude data can obtain as shown in **Fig. 6-1 b).**

6.2 THEORY

6.2.1 Signal processing

The data which able to generate in the term of time series we can analyze with the signal processing technique. In theory, signal processing is the mathematic method to understand the data. Mathematical methods applied in signal processing such as linear time-invariant system theory, and transform theory, System identification and classification and Calculus. Differential equations. For example in image processing, signal processing can analyze the data from digital cameras, computers and various imaging systems.

Signal processing is an area of systems engineering, electrical engineering and applied mathematics that deals with operations on or analysis of signals, or measurements of time-varying or spatially varying physical quantities. Signals of interest can include sound, electromagnetic radiation, images, and sensor data, for example biological data such as electrocardiograms, control system signals, telecommunication transmission signals, and many others. If we can transform the data to the wave form which formed in time domain sequence, we will also able to understand the characteristic of the waveform.

6.2.2 Sampling rate and Nyquist frequency

Aliasing is a common problem in digital media processing applications. Many readers have heard of "anti-aliasing" features in high-quality video cards. This page will explain what Aliasing is, and how it can by avoided. Aliasing is an effect of violating the Nyquist-Shannon sampling theory. During sampling the base band spectrum of the sampled signal is mirrored to every multifold of the sampling frequency. These mirrored spectra are called alias. If the signal spectrum reaches farther than half the sampling frequency base band spectrum and aliases touch each other and the base band spectrum gets superimposed by the first alias spectrum. The easiest way to prevent aliasing is the application of a steep sloped low-pass filter with half the sampling frequency before the conversion.

6.2.3 Fast Fourier transform

It is never possible to eliminate aliasing completely from measured data. As will be discussed below, this effect comes about from three sources: the infinite bandwidth induced by finite record length, and the spectrum replication caused by representation of the data by its discrete-time samples, and in the case of experimentally measured data, the finite attenuation provided by non-ideal anti-aliasing filters. It is impossible to experimentally record a signal of infinite duration. Therefore, all recorded signals must have frequency content that approaches infinity due to the convolution theorem. Observing a signal over finite time duration is equivalent to multiplication of that signal with a rectangular window function. According to the convolution theorem **[6-2]**, multiplication of the signal by the rectangular window function in the time domain is equivalent to the inverse transform of the convolution of the signal's transform with the transform of the window function. In this case, the transform of the window function is the sinc function, which is infinite in bandwidth **[6-2].** The Fourier transform of the finite-length signal is then given by

$$X_w(f) = X_c(f) * W(f)$$

where (*) denotes convolution. Since *W(f)* is infinite, the convolution of *W(f)* with a spectrum of finite length produces a spectrum of infinite length. The magnitude of the content may become small as frequency increases, but it persists nonetheless. Therefore, the act of observing an event over finite time duration induces infinite support in its Fourier spectrum.

Fourier analysis is a mathematical method used to break down and transform a periodic function i.e., a mathematical relationship between a quantity and a variable or variables whose relative values consistently repeat over some regular period of time into a set of simpler functions which can then be summed and transformed back into the original form. Today, it has been applied to a wider variety of problems in the physical and natural sciences. Improved, expanded upon, and the core of what has come to be known as the field of harmonic analysis, Fourier analysis has evolved and progressed to include the study of more abstract and general phenomena. Then, in this study, it was applied to estimate the largest number of waves, and necessary numbers of transducers for each position are indicated analytically by using sampling rate theorem.

In theory "The Nyquist Sampling Rate is the lowest sampling rate that can be used without having aliasing. The sampling rate for an analog signal must be at least two times the bandwidth of the signal. So, for example, an audio signal with a bandwidth of 20 kHz must be sampled at least at 40

kHz to avoid aliasing. The Nyquist sampling rule **[6-3]** provides a prescription for the nominal sampling interval required to avoid aliasing. Aliasing occurs when a signal is discretely sampled at a rate insufficient to capture the changes in the signal. Nyquist sampling theorem suggests that the sampling frequency should be higher than twice of the highest frequency contained in the signal. In theory, a Nyquist frequency just larger than the signal bandwidth is sufficient to allow perfect reconstruction of the signal from the samples. However, in practice, the perfect reconstruction is unattainable.

Figure 6-2 shows simple examples of the circumferential velocity profile with one sinuous wave. The number of waves is 1 in **Fig. 6-2 a)** and b), and 1.5 in **Fig. 6-2 c).** The necessary numbers of transducers for each is calculated as 2 for the case of a) and b), and 3 for the case of c), respectively, that is twice of the wave number. When two measurement lines are applied as shown in **Fig. 6-2 a)**, the transducers can capture both two peaks of the wave. However, two transducers cannot obtain any signal if the sensors are placed at the position of 0° and 180°. When the number of transducers (i.e. measurement lines) is 3 and 4 as shown in **Fig. 6-2 b)** and c), respectively, that is over twice of the wave number, the shape of the profile can be captured by the transducers. Accordingly, the suitable number of transducers is estimated by using sampling rate theorem, as just over twice of the wave number.

6.3 EXPERIMENTAL CONDITIONS

Experimental conditions of experimental apparatus, ultrasonic transducers, and method for determining the wall positions are the same as used in the experiments explained above.

Figure 6-3 illustrates the positions on the measuring line on the inner wall, the center of the pipe and on the farther pipe wall are indicated as the point of r/D = -0.5, 0 and +0.5, respectively. The area of r/D = -0.5 to 0 is named as ‘near field’, and the area of r/D = 0 to +0.5 as ‘far field’. The circle passing through the points of the same r/D for different circumferential position is named as ‘measuring circle’.

To evaluate the suitable number of transducers near the second bent where the accurate flowrate measurement is necessary, circumferential velocity profiles are necessary. Thus, multiple UVP measurements were applied. Measurement lines are changed circumferentially with angle of every

10° as shown in **Fig. 6-4**. Thus, 36 radial measurements of UVP method were repeated to obtain one circumferential velocity profile. **Figure 6-5** shows the schematic diagram around the measuring line.

Therefore, observed velocity magnitudes at the same *r/D* position among different circumferential positions are listed against the circumferential angle, and they converted into a circumferential velocity profile on the measurement circle. Velocity profile on the circle of *r/D* = -0.5 and 0.5 cannot be obtained because these points are on the wall surface, and also profile on the circle of *r/D* = 0 cannot be obtained because it indicates the same position, the center of the pipe. Thus, circumferential velocity profiles are obtained only for *r/D* = -0.4, -0.3, -0.2, -0.1, 0.1, 0.2, 0.3 and 0.4. The relationship of the locations of transducer, measurement lines, measurement circles, near field and far field are also summarized in **Fig. 6-6 , 6-7, 6-8**.

6.4 RESULTS AND DISCUSSIONS

Figure 6-5 shows converted velocity profiles along each measuring circle from radial profiles obtained using the UVP method. These **Fig. 6-5 a)-c)** indicates that velocity profiles vary with circumferential position and the measurement distance from the outlet of the second bent.

In the region of circumferential angle 0-180°, near field profiles (*r/D* = -0.4, -0.3, -0.2 and -0.1) are relatively larger and far field profiles (*r/D* = 0.1, 0.2, 0.3 and 0.4) smaller. This result indicates asymmetric flow at that point. Moreover, these results imply main flow inclination. If the flow is straight (see **Fig. 6-6 a)**), the circumferential velocity profile on a measurement circle becomes flat. However, if the flow is inclined, observed velocity magnitude by UVP is affected by the inclination. For example, in the case of **Fig. 6-6 b)**, transducer at the right side wall can observe velocity magnitude at the position P_α. The observed velocity magnitude V_{α_UVP} becomes larger by the inclination of the flow because V_{α_UVP} is a projection of V_α to the measurement line and the angle between the flow and measurement line becomes smaller due to the inclination. Calculated velocity to the pipe direction becomes larger if assumption that flow direction is same as pipe direction and no adjustment are applied. However, observation for the point P_γ is also executed in this case. P_α and P_γ exist at very close position however not the same position. Thus, V_{α_UVP} and V_{γ_UVP} should be similar due to their position. On the other hand, the effect of flow inclination to the right reduces V_{γ_UVP}. Accordingly, flow inclination is implied by the difference between V_{α_UVP} and V_{γ_UVP}. For the results of **Fig. 6-5 a)-c)**, the profiles of near field at circumferential angle 0°-180° should be compared with

far field profile at the angle 180°-360°. They don't show good agreement, and it implies the flow inclination at that point.

Figure 6-7 depicts the FFT results from the data of velocity profiles along the measuring circles. Near field area from transducer is shown as the thick lines. On the other hand, far field area is shown as the thin lines. Twice the wave number is theoretically defined as the required number of transducers.

The largest number of wave can be estimated using window magnitude responses **[6-4]**. For example, the largest number of wave (N_w) at 2 D (**Fig. 6-7 a)**) was approximately 2.7 (Dot line) as shown in the profile of r/D = -0.1. Considering the wave number and the sampling theorem, the required number of transducers was estimated as 5.4, and should be 6 for the real measurement. **Figure 6-7 b)** shows the FFT results calculated for the profiles at 3 D. The largest peak appeared in the profile of r/D = 0.3 and the required number of transducers is estimated as 4.8, and should be 5 in real, for this case. For the case at 5 D (**Fig. 6-7 c)**), the maximum peak of r/D = 0.1 appeared and the largest number of wave (N_w) was estimated as approximately 2, thus, the required number of transducers in real is estimated as 4.

Furthermore, the analytical technique can estimate the number of measurement lines which achieves to capture a peak of simple harmonic wave where the velocity in the profile shows highest fluctuation. The Number of wave which used for estimating the number of measurement lines can determine with the size of main lobe (peak lobe). However, it generally includes some sidelobes. These sidelobes affect the frequency of wave. From this reason, there are many types of window function can reduce the sidelobes amplitudes for example Hamming, Hanning, Rectangular or Triangular window function **[6-16]**. In this study, Hanning window function was used to estimate the largest number of wave as shown as the dot lines in **Fig. 6-7 a)-c)**.

The out of plane angle effects on the number of measurement lines for the accurate flowrate measurement which show at every distance downstream from the bent as shown in FFT results of b) figure from Fig.12 to Fig. 20. It is obvious that the number of measurement lines is increasing, when the out of plane angles are increasing at every inlet length from the bent pipe for example at 3 D. Figure 12 b), Figure 13 b) and Figure 14 b) show the number of measurement lines are 4.8, 5.2 and 5.4 in out of plane angle 0°, 8° and 16° respectively

The flowrate was calculated integration a velocity profile obtained along a measuring line. When using multiple transducers, these were located on a pipe wall with a constant circumferential interval, and the velocity profiles they obtained were used to interpolate between these profiles and calculate the flow rate. Additionally, to investigate the effect of circumferential transducer position on the flowrate measurement error, flowrates were calculated at each position varied by **Fig. 6-8 a)**, **Fig. 6-8 b)** and **Fig. 6-8 c)** show the standard deviation of flowrate errors for = 3D, 4D and 5 D versus the number of measurement lines, respectively.

The flowrate errors increased as increasing the out of plane angle for the same number of measurement lines, since the Fourier amplitude at large wave number increased as shown in **Fig. 15 b) Fig. 16 b)** and **Fig. 17 b)** which are the FFT results at 3 D. The estimation of number of measurement lines using the results of this method was plotted as the rectangle dot line in every figures. For every case, the errors were decreasing than 2 % when using the more of the measurement lines.

Furthermore, the analytical technique can estimate the number of measurement lines which achieves to capture a peak of simple harmonic wave where the velocity in the profile shows highest fluctuation. The Number of wave which used for estimating the number of measurement lines can determine with the size of main lobe (peak lobe). However, it generally includes some sidelobes. These sidelobes affect the frequency of wave. From this reason, there are many types of window function can reduce the sidelobes amplitudes for example Hamming, Hanning, Rectangular or Triangular window function. **[6-9]** In this study, Hanning window function was used to estimate the largest number of wave as shown as the dot lines in **Fig. 6-10 a)-c)**.

Figure 6-10 a) presents the results of FFT which from all 8 circumferential velocity profiles. The results of -0.1R has the largest frequency as 2.7. Then, we can calculate the sampling rate using Nyquist theory by multiplied 2 that is 5.4 measurement lines. Actually, the numbers of measurement lines have to be designed in the integer number. Therefore, the number of measurement lines at 2 D is 6 measurement lines.

In addition, **Fig. 6-10 b)** and **Fig. 6-10 c)** present the results of FFT which from all 8 circumferential velocity profiles at 3 D and 5D, respectively. The results of +0.3R has the largest frequency at 3 D as

2.4. The detail of FFT results are shown in **Fig. 6-13** and **Fig. 6-14**. After that, we can calculate the sampling rate using Nyquist theory by multiply by 2 that is 4.8 measurement lines that means 5 measurement lines. At the same time, the number of measurement lines at 5 D is designed as 4 measurement lines from the largest frequency on +0.1R which is 2 as shown in **Table 6-2.**

Figure 6-11 a) – c) show the arrangements of measurement lines in the cases of 4, 5 and 6 transducers. At 2 D, the setup of measurement lines of 6 measurement lines can be located the ϕ angle between measurement line each other at 90° such as line no.1 at ϕ angle at 30°, line no.2 at ϕ angle at 90°, line no.3 at ϕ angle at 150°, line no.4 at ϕ angle at 210°, line no.5 at ϕ angle at 270° and line no.6 at ϕ angle at 330° as shown in **Fig 6-11 c).** At 3D, the setup of measurement lines of 5 measurement lines can be located the ϕ angle between measurement line each other at 72.5° such as line no.1 at ϕ angle at 17.5°, line no.2 at ϕ angle at 90°, line no.3 at ϕ angle at 162.5°, line no.4 at ϕ angle at 235° and line no.5 at ϕ angle at 307.5° as shown in **Fig 6-11 b).** In the last case, at 5 D, the setup of measurement lines of 4 measurement lines can be located the ϕ angle between measurement line each other at 90° such as line no.1 at ϕ angle at 0°, line no.2 at ϕ angle at 90°, line no.3 at ϕ angle at 180° and line no.4 at ϕ angle at 270° as shown in **Fig 6-11 a).**

Figure 6-12 show the velocity profiles in every 10° of ϕ angle. The velocity profile measurement started at 0° as shown in **Fig. 6-6**. **Figure 6-12 1)** shows the first measurement line at 0° which cross the center of pipe in the horizontal direction. On the right haft of velocity profile (-0.5 to 0 r/D) is the near field of transducer and on the left side of velocity profile (0 to +0.5 r/D) is the far field of transducer. **Figure 6-12 1) - 10)** show the velocity at near field is increasing when the ϕ angle was also increasing from ϕ = 0° to ϕ = 90° because the direction of flow in this area is influenced of the 2 difference centrifugal force directions from vertical and horizontal directions. Each centrifugal force makes the high velocity opposite side of each force. The vertical centrifugal force is come from the vertical bent pipe and the horizontal centrifugal force is come from the out of plane angle of the second bent pipe. From this reason, the maximum velocity theoretically appears on the outer area from both centrifugal force. It changes the flow behavior downstream of out-of-plane pipe compare with the in-plane double bent pipe. It makes non-symmetry flow as non-symmetrical twin vortices.

Figure 6-12 11) - 28) show the velocity at near field is decreasing when the ϕ angle was increasing from ϕ = 100° to ϕ = 270° because the direction of flow in this area is influenced of the centrifugal

force in vertical directions from the center of bent pipe to the outer of bent pipe. From this reason, the maximum velocity appears at the outer area of outlet of the bent pipe. On the other hand, the far field of transducer is increasing when the when the ϕ angle was increasing from $\phi = 100°$ to $\phi = 270°$ same the case of near field of transducer at $\phi = 0°$ to $\phi = 90°$.

Figure 6-12 29) - 36) show the velocity at near field is increasing when the ϕ angle was increasing from $\phi = 280°$ to $\phi = 0°$ and from $\phi = 10°$ to $\phi = 90°$. This is same as the case of $\phi = 0°$ to $\phi = 90°$ because the direction of flow in this area is influenced of the centrifugal force in vertical directions from the center of bent pipe to the outer of bent pipe. In the case of double bent pipe in vertical direction piping system, the outer area of the bent pipe is on the top of the outlet. On the other hand, the minimum velocity in the pipe flow always appears at the bottom of the outlet or inner of the center of bent curve.

Figure 6-13 show circumferential velocity profiles totally 8 profiles such as 4 profiles at near field of transducer (r/D = -0.4, -0.3, -0.2 and -0.1) at 2 D. These near field circumferential velocity profiles are increasing when the ϕ angle was increasing from $\phi = 0°$ to $\phi = 90°$. In addition, the velocities are decreasing when $\phi = 100°$ to $\phi = 270°$. As the mention above, the direction of flow in this area is influenced of the centrifugal force in vertical directions from the center of bent pipe to the outer of bent pipe. On the other hand, at the far field of transducer (r/D = +0.4, +0.3, +0.2 and +0.1). These far field circumferential velocity profiles are decreasing when the ϕ angle was increasing from $\phi = 0°$ to $\phi = 90°$.

Figure 6-14 and fig. 6-15 show FFT results in detail from all circumferential velocity profiles totally 8 profiles such as 4 profiles at near field of transducer (r/D = -0.4, -0.3, -0.2 and -0.1) and 4 profiles at far field of transducer (r/D = +0.4, +0.3, +0.2 and +0.1) at 2 D. The results of -0.1R has the largest frequency as 2.7. Then, we can calculate the sampling rate using Nyquist theory by multiplied 2 that is 5.4 measurement lines. Actually, the numbers of measurement lines have to be designed in the integer number. Therefore, the number of measurement lines at 2 D is 6 measurement lines.

Figure 6-16 show the velocity profiles at 3D in every 10° of ϕ angle. The velocity profile measurement started at 0° as shown in **Fig. 6-6**. **Figure 6-12 1)** shows the first measurement line at

0° which cross the center of pipe in the horizontal direction. On the right haft of velocity profile (-0.5 to 0 r/D) is the near field of transducer and on the left side of velocity profile (0 to +0.5 r/D) is the far field of transducer. **Figure 6-16 1) - 10)** show the velocity at near field is increasing when the ϕ angle was also increasing from $\phi = 0°$ to $\phi = 90°$ same as the case of the velocity profile at 2 D as mention above.

Figure 6-16 11) - 28) show the velocity at near field is decreasing when the ϕ angle was increasing from $\phi = 100°$ to $\phi = 270°$ because the direction of flow in this area is influenced of the centrifugal force in vertical directions from the center of bent pipe to the outer of bent pipe. From this reason, the maximum velocity appears at the inner area of bent pipe. On the other hand, the far field of transducer is increasing when the when the ϕ angle was increasing from $\phi = 100°$ to $\phi = 270°$ same the case of near field of transducer at $\phi = 0°$ to $\phi = 90°$.

Figure 6-16 29) - 36) show the velocity at near field is increasing when the ϕ angle was increasing from $\phi = 280°$ to $\phi = 0°$ and from $\phi = 10°$ to $\phi = 90°$. This is same as the case of $\phi = 0°$ to $\phi = 90°$ because the direction of flow in this area is influenced of the centrifugal force in vertical directions from the center of bent pipe to the outer of bent pipe. In the case of double bent pipe in vertical direction piping system, the outer area of the bent pipe is on the top of the outlet. On the other hand, the minimum velocity in the pipe flow always at the bottom of the outlet or inner of the center of bent curve.

Figure 6-17 show circumferential velocity profiles totally 8 profiles such as 4 profiles at near field of transducer (r/D = -0.4, -0.3, -0.2 and -0.1) at 2 D. These near field circumferential velocity profiles are increasing when the ϕ angle was increasing from $\phi = 0°$ to $\phi = 90°$. In addition, the velocities are decreasing when $\phi = 100°$ to $\phi = 270°$. As the mention above, the direction of flow in this area is influenced of the centrifugal force in vertical directions from the center of bent pipe to the outer of bent pipe. On the other hand, at the far field of transducer (r/D = +0.4, +0.3, +0.2 and +0.1). These far field circumferential velocity profiles are decreasing when the ϕ angle was increasing from $\phi = 0°$ to $\phi = 90°$.

Figure 6-18 and fig. 6-19 show FFT results in detail from all circumferential velocity profiles totally 8 profiles such as 4 profiles at near field of transducer (r/D = -0.4, -0.3, -0.2 and -0.1) and 4

profiles at far field of transducer (r/D = +0.4, +0.3, +0.2 and +0.1) at 3 D. The results of r/D = +0.3 has the largest frequency as 2.4. Then, we can calculate the sampling rate using Nyquist theory by multiplied 2 that is 4.8 measurement lines. Actually, the numbers of measurement lines have to be designed in the integer number. Therefore, the number of measurement lines at 3 D is 5 measurement lines.

Figure 6-20 show the velocity profiles at 5D in every 10° of ϕ angle. The velocity profile measurement started at 0° as shown in **Fig. 6-6**. **Figure 6-20 1)** shows the first measurement line at 0° which cross the center of pipe in the horizontal direction. On the right haft of velocity profile (-0.5 to 0 r/D) is the near field of transducer and on the left side of velocity profile (0 to +0.5 r/D) is the far field of transducer. **Figure 6-20 1) - 10)** show the velocity at near field is increasing when the ϕ angle was also increasing from ϕ = 0° to ϕ = 90° same as the case of the velocity profile at 5 D as mention above.

Figure 6-20 11) - 28) show the velocity at near field is decreasing when the ϕ angle was increasing from ϕ = 100° to ϕ = 270° because the direction of flow in this area is influenced of the centrifugal force in vertical directions from the center of bent pipe to the outer of bent pipe. From this reason, the maximum velocity appears at the outer area of bent pipe. On the other hand, the far field of transducer the velocities are increasing when the when the ϕ angles were increasing from ϕ = 100° to ϕ = 270° same the case of near field of transducer at ϕ = 0° to ϕ = 90°.

Figure 6-20 29) - 36) show the velocity at near field is increasing when the ϕ angle was increasing from ϕ = 280° to ϕ = 0° and from ϕ = 10° to ϕ = 90°. This is same as the case of ϕ = 0° to ϕ = 90° because the direction of flow in this area is influenced of the centrifugal force in vertical directions from the center of bent pipe to the outer of bent pipe. In the case of double bent pipe in vertical direction piping system, the outer area of the bent pipe is on the top of the outlet. On the other hand, the minimum velocity in the pipe flow always appears at the bottom of the outlet or inner of the center of bent curve.

Figure 6-21 show circumferential velocity profiles totally 8 profiles such as 4 profiles at near field of transducer (r/D = -0.4, -0.3, -0.2 and -0.1) at 2 D. These near field circumferential velocity profiles are increasing when the ϕ angle was increasing from ϕ = 0° to ϕ = 90°. In addition, the

velocities are decreasing when ϕ = 100° to ϕ = 270°. As the mention above, the direction of flow in this area is influenced of the centrifugal force in vertical directions from the center of bent pipe to the outer of bent pipe. On the other hand, at the far field of transducer (r/D = +0.4, +0.3, +0.2 and +0.1). These far field circumferential velocity profiles are decreasing when the ϕ angle was increasing from ϕ = 0° to ϕ = 90°.

Figure 6-22 and Fig. 6-23 show FFT results in detail from all circumferential velocity profiles totally 8 profiles such as 4 profiles at near field of transducer (r/D = -0.4, -0.3, -0.2 and -0.1) and 4 profiles at far field of transducer (r/D = +0.4, +0.3, +0.2 and +0.1)at 5 D. The results of r/D = +0.1 has the largest frequency as 2. Then, we can calculate the sampling rate using Nyquist theory by multiplied 2 that is 4.0 measurement lines. Actually, the numbers of measurement lines have to be designed in the integer number. Therefore, the number of measurement lines at 5 D is 4 measurement lines.

Table 6-2 shows the number of measurement lines from the estimation analytical technique. The numbers of measurement lines are decreasing when the inlet length is farther. This is because when the fluid enters any pipe or channel, boundary layers keep on growing to be a stable flow condition after some distance downstream from the entrance region. Velocity in the core of the flow outside the boundary layer increases with increasing distance from entrance. This is due to the fact that through any cross section same amount of fluid flows, and boundary layer is growing. That means the stability of flow behavior will increase when the distance downstream from the inlet is increasing. It affects the number of measurement line directly such as the number of measurement lines are decreasing from 2 D, 3 D and 5 D as 6, 5 and 4 measurement lines, respectively.

6.5 CONCLUSIONS

This study investigated the effect of out of plane angle on the number of the optimal number of measurement lines and the inlet length downstream from the double bent pipe by using new analytical method. To estimate the number of ultrasound transducer as the number of measurement lines at various inlet lengths downstream of the out of plane double bent pipe. Velocity profiles on the measurement lines through the center of the pipe are transferred to velocity profiles along the circles which concentric center is as same as the pipe center. FFT analysis is performed to obtain

largest number of wave for circumferential direction, and optimized number of transducer for each position was calculated from the FFT results. The result indicates more transducers are necessary for very accurate flowrate measurement. However, enough accurate measurement can be realized with less transducer.

The position of maximum velocity in pipe flow downstream from the double bent pipe is changed affect from the out of plane angle such as at 3 D, the position of maximum velocity is 90°, 80° and 60°, on the out of plane angle are 0°, 8° and 16° respectively, at 4D, the position of maximum velocity is 90°, 80° and 70°, on the out of plane angle are 0°, 8° and 16° respectively, and , the position of maximum velocity is 90°, 85° and 80°, on the out of plane angle are 0°, 8° and 16° respectively. From this reason, it affects the number of measurement lines because it makes more complicated flow such as at 3 D, the number of measurement lines are increasing when the out of plane angles are increasing as 4.8, 5.2 and 5.4 at 0°, 8° and 16° respectively,. at 4 D, the number of measurement lines are increasing when the out of plane angles are increasing as 4.2, 4.4 and 4.8 at 0°, 8° and 16° respectively and at 5 D, the number of measurement lines are increasing when the out of plane angles are increasing as 4.0, 4.4 and 4.6 at 0°, 8° and 16° respectively In addition, it is more difficult to measure the velocity profile and also for flowrate measurement. However, more measurement lines can be applied to more accurate flowrate measurement. The optimal number of measurement lines at each position was investigated in this study.

REFERENCES

[6-1] A. Papoulis, The Fourier Integral and its Applications, McGraw-Hill, New York, USA, 1962

[6-2] Johan, L. and Driesen, J.: Wavelet-Based Power Quantification Approaches, IEEE T. Instrum. and Meas., 52-4, 2003

[6-3] Nyquist, H.: Certain Topics in Telegraph Transmission Theory, Trans. AIEE, 47, 617-644, 1928

[6-4] Lyons, R. G.: Understanding of Digital Signal Processing, 2nd ed. Bernard Goodwin, 2004

[6-5] A. Papoulis, The Fourier Integral and its Applications, McGraw-Hill, New York, USA, 1962

[6-6] Johan, L. and Driesen, J.: Wavelet-Based Power Quantification Approaches, IEEE T. Instrumentals and Measurements. 52-4, 2003

[6-7] Lyons, R. G.: Understanding of Digital Signal Processing, 2nd ed. Bernard Goodwin, 2004

Table 6-1 Experimental conditions

Testing conditions	Units	Values
Reynolds Number	-	40,000
Number of measuring point	-	74
Channel width	mm	0.74
Basic frequency	MHz	8
Incident angle	Degree	10
Out of plane angle	Degree	0, 8, 16

Table 6-2 Number of transducers versus the out-of-plane angle (α) of double bent pipe and inlet length

	Inlet length		
Out-of-plane angle (α) of double bent pipe	3 D	4 D	5 D
0°	4.8	4.2	4
8°	5.2	4.4	4.4
16°	5.4	4.8	4.6

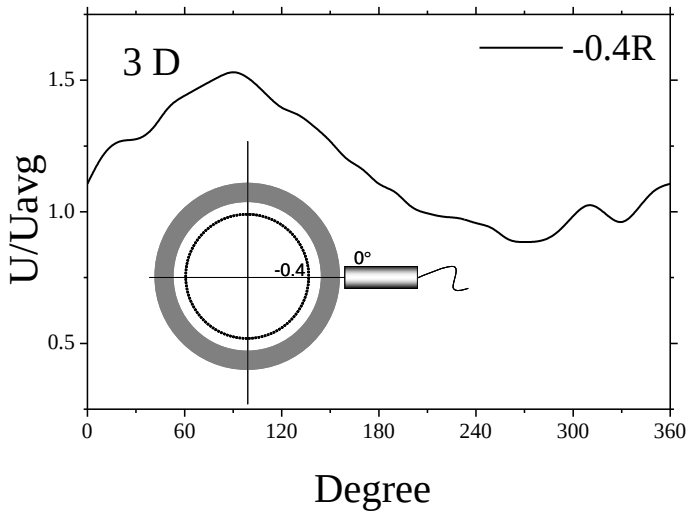

a) Velocity profile from circle measurement line.

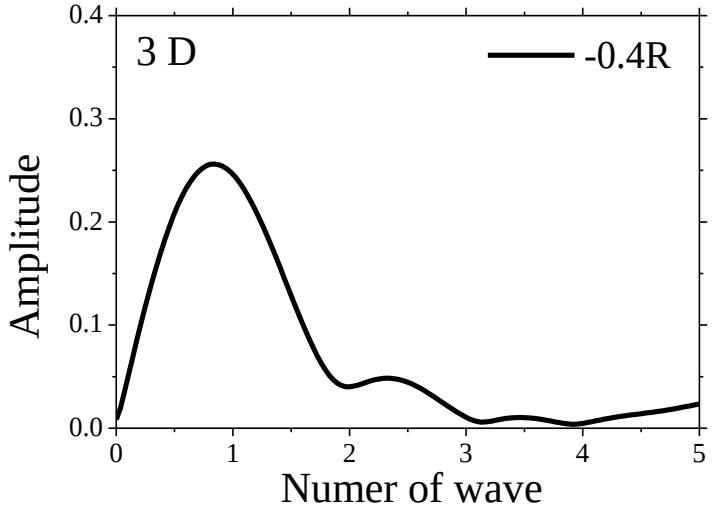

b) Frequency from FFT.

Fig.6-1 Velocity profile from circle measurement line -0.4R and the frequency data from Fast Fourier Transform.

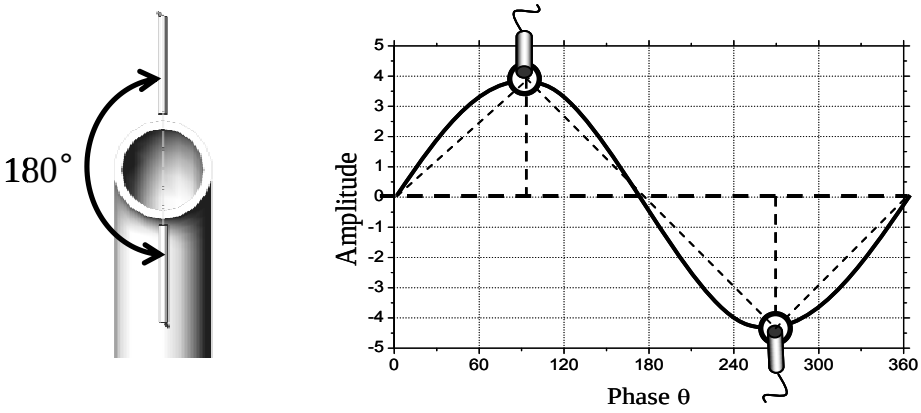

a) 2 Measurement lines

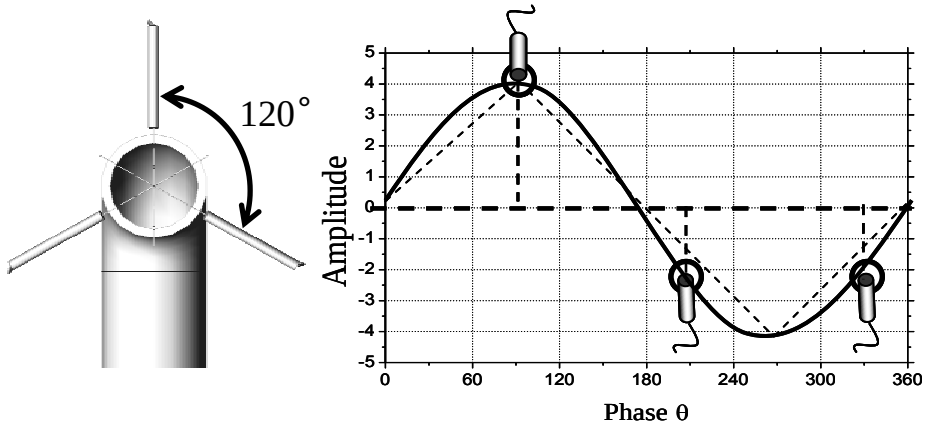

b) 3 Measurement lines

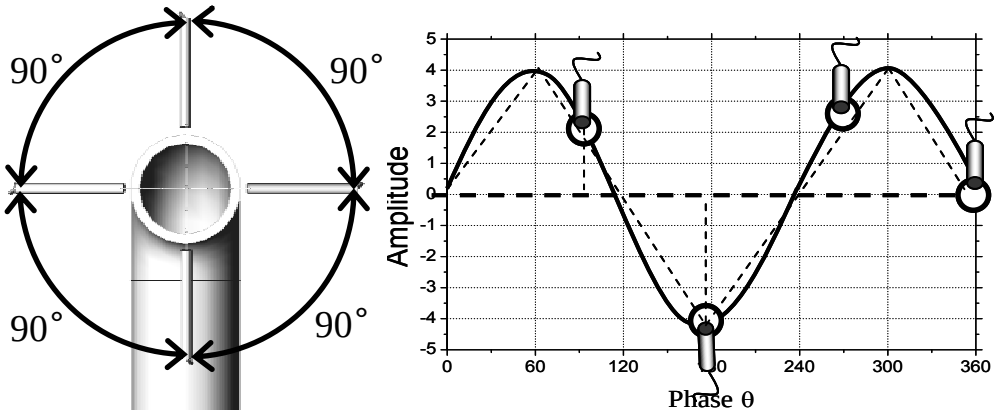

c) 4 Measurement lines

Fig.6-2 Measurement lines located and number of measurement lines related to phase of wave and sampling rate theorem to protect the error from aliasing.

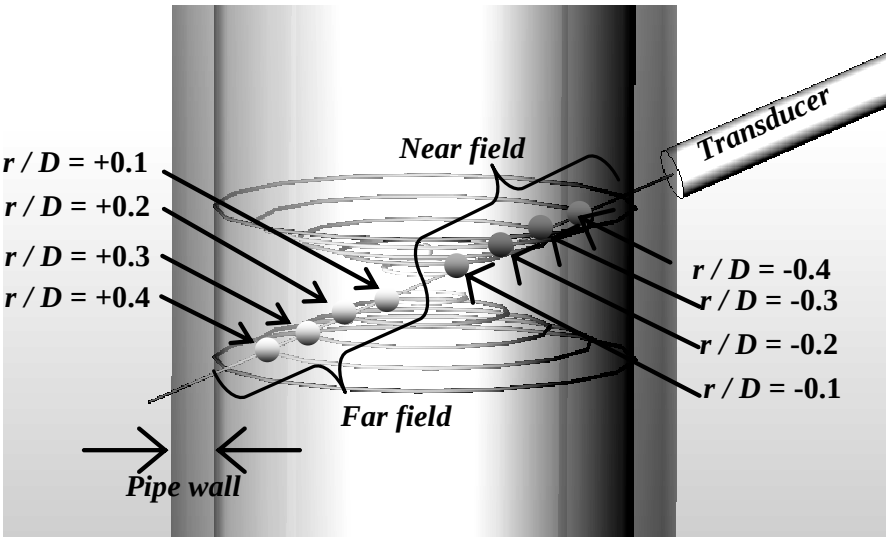

Fig.6-3 Measuring lines and circles of velocity profiles.

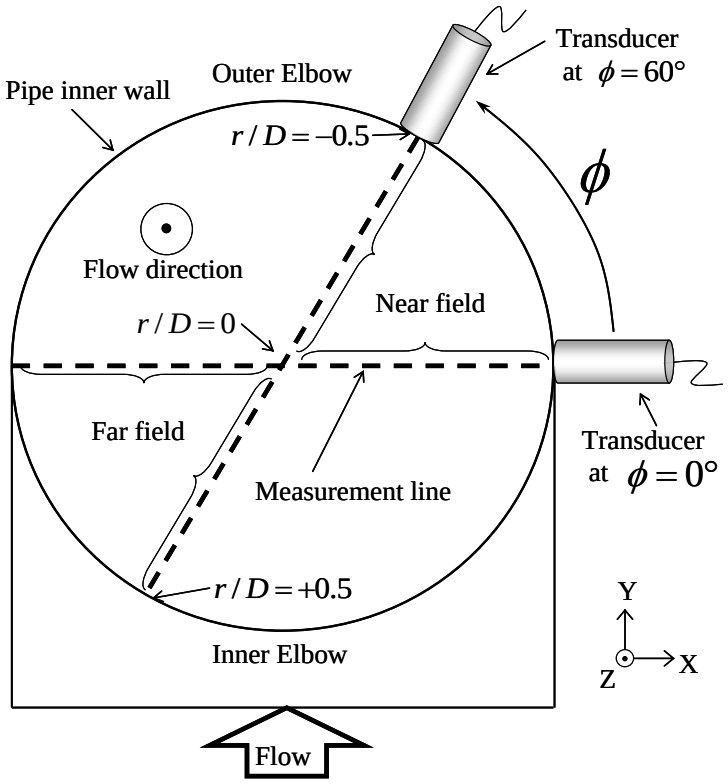

Fig.6-4 Circumferential transducer position ∅ around the pipe.

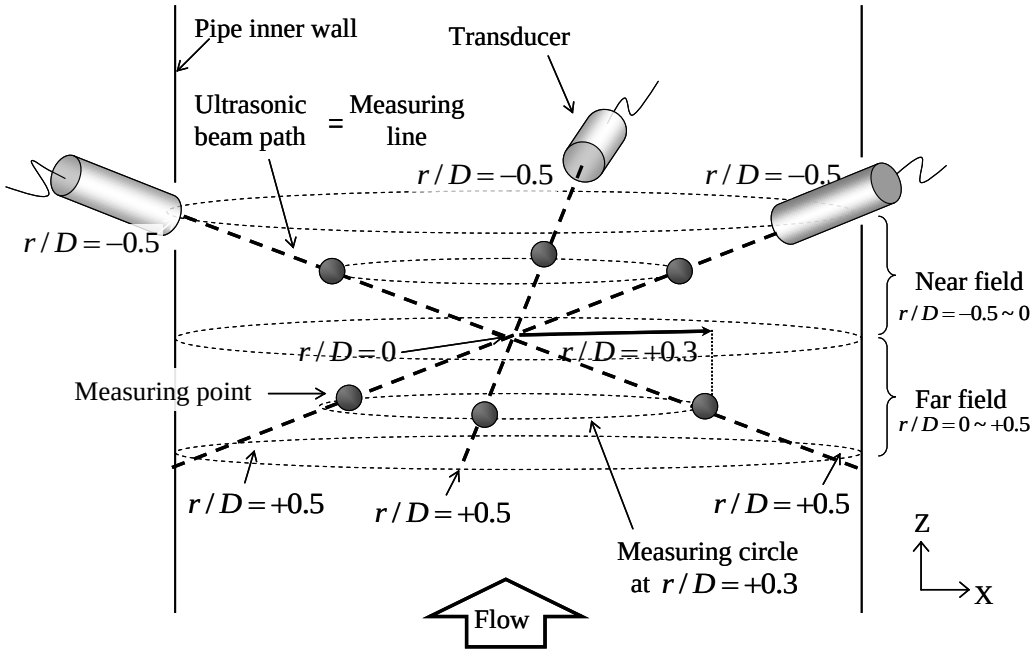

Fig.6-5 Measurement lines and circle of velocity profiles.

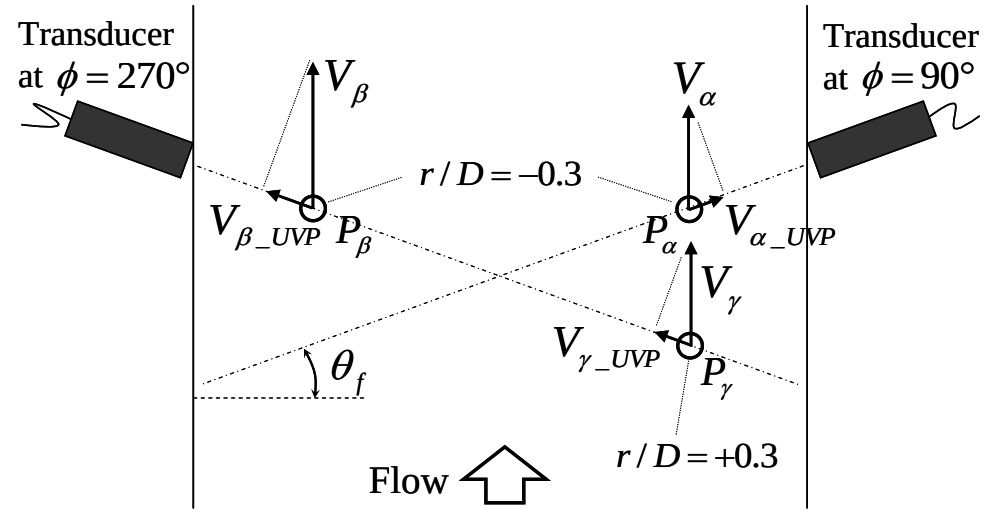

a) Straight flow

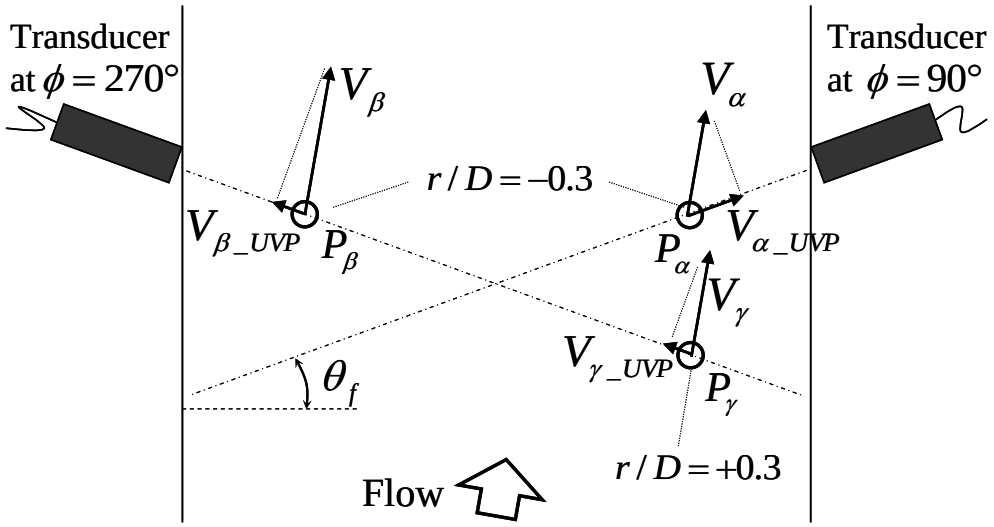

b) inclined flow

Fig.6-6 Schematic diagram of the velocity component measured by UVP method flow straight and inclined flow.

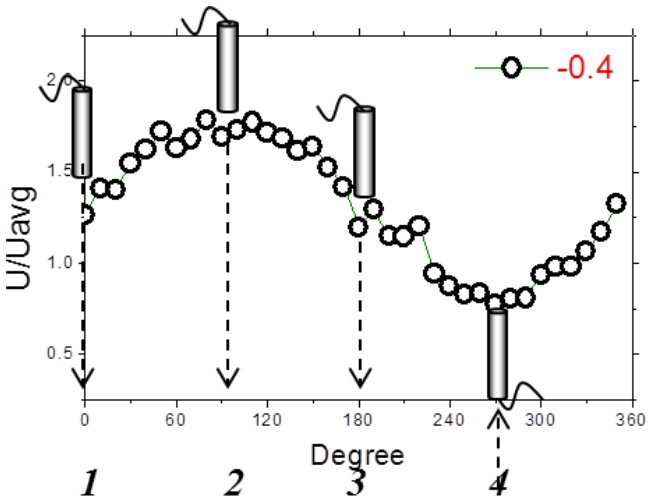

b) Frequency from FFT.

Fig.6-7 Velocity profile from circle measurement line -0.4R and the frequency data from Fast Fourier Transform.

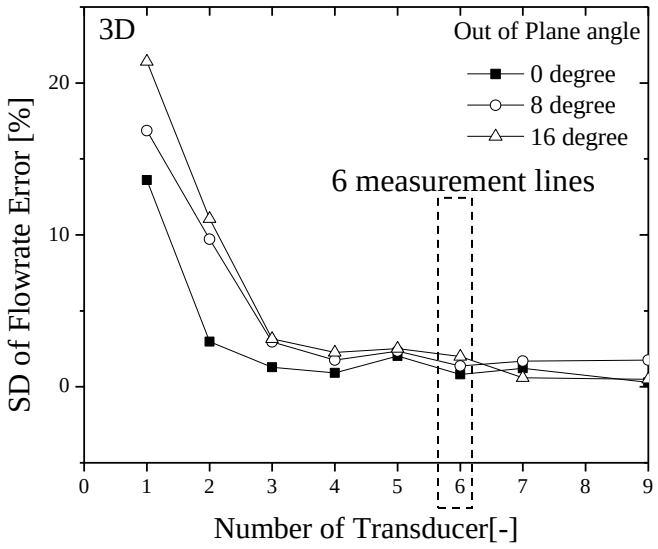
3D
Out of Plane angle
0 degree
8 degree
16 degree
6 measurement lines
SD of Flowrate Error [%]
Number of Transducer[-]

a) at 3D

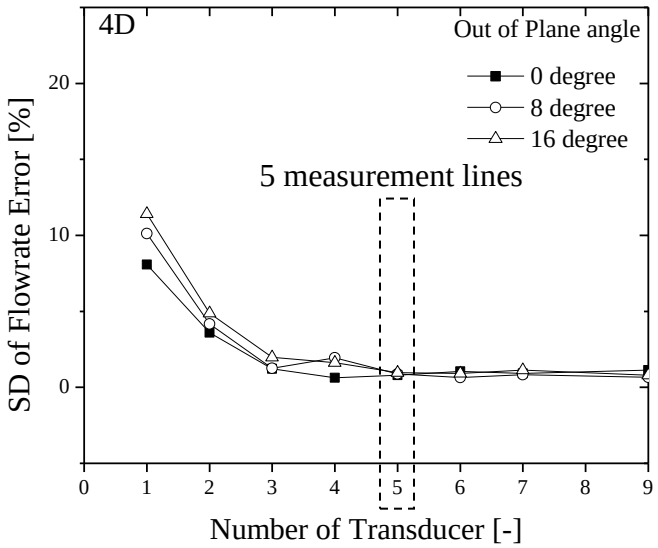
4D
Out of Plane angle
0 degree
8 degree
16 degree
5 measurement lines
SD of Flowrate Error [%]
Number of Transducer [-]

b) at 4D

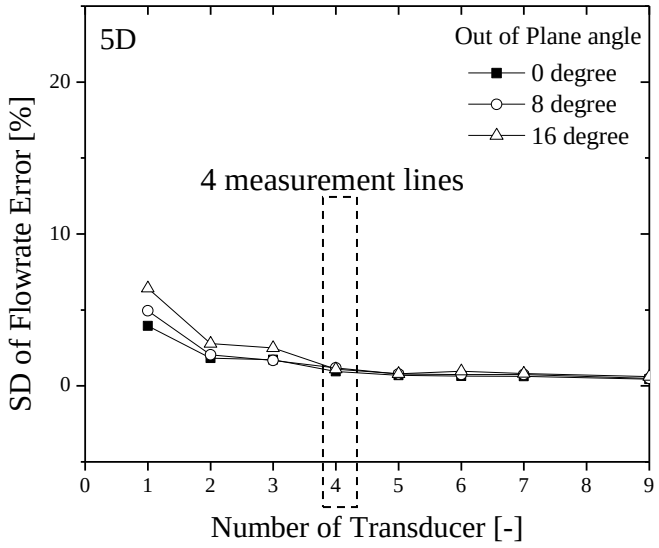

c) at 5D

Fig. 6-8 Standard deviation of flowrate error versus the number of measurement lines

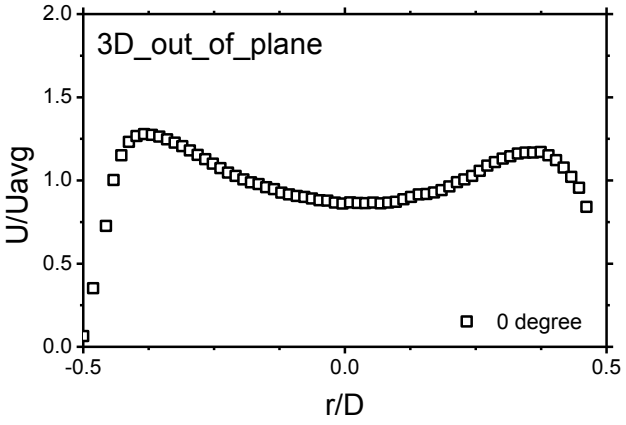

1) Velocity profile at 0 degree (3 D)

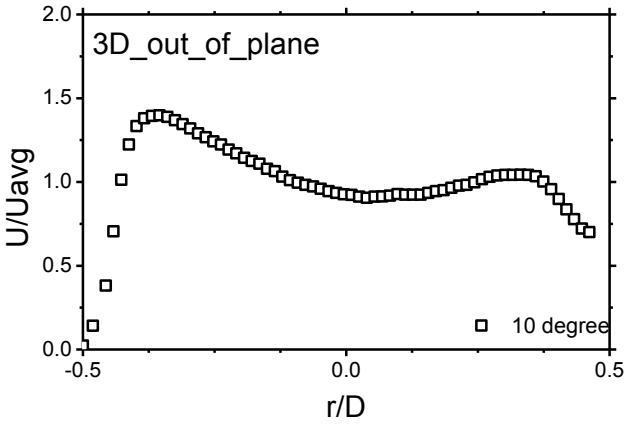

2) Velocity profile at 10 degree (3 D)

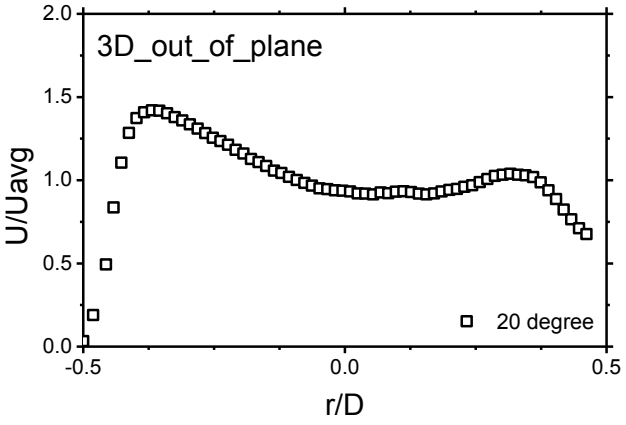

3) Velocity profile at 20 degree (3 D)

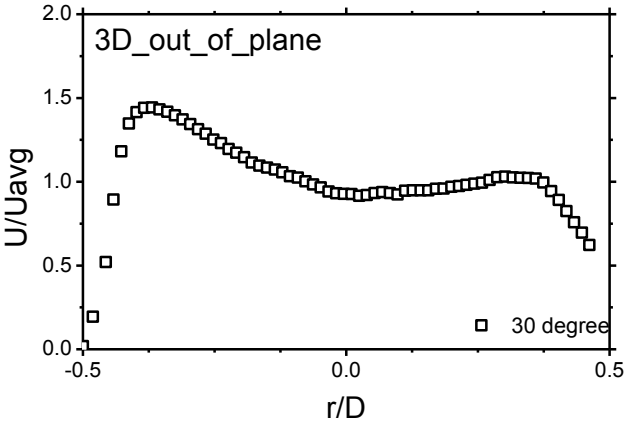

4) Velocity profile at 30 degree (3 D)

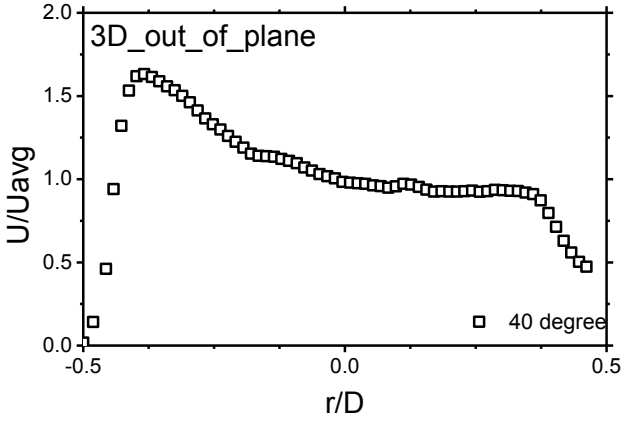

5) Velocity profile at 40 degree (3 D)

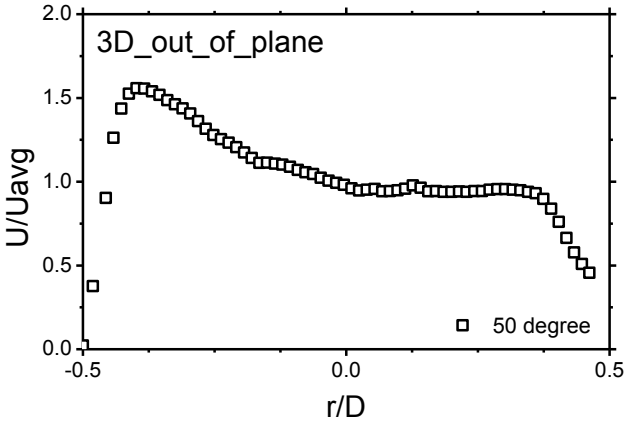

6) Velocity profile at 50 degree (3 D)

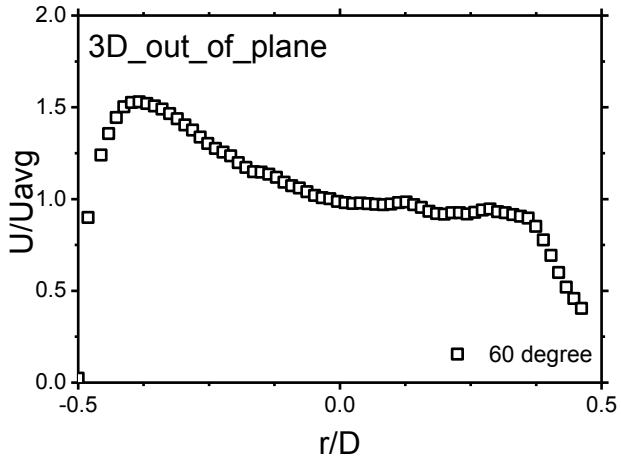

7) Velocity profile at 60 degree (3 D)

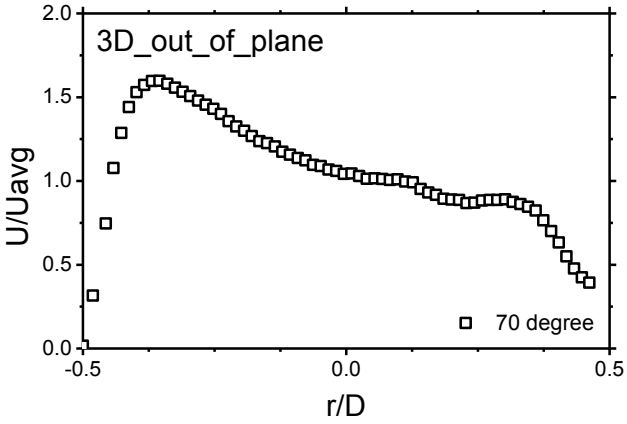

8) Velocity profile at 70 degree (3 D)

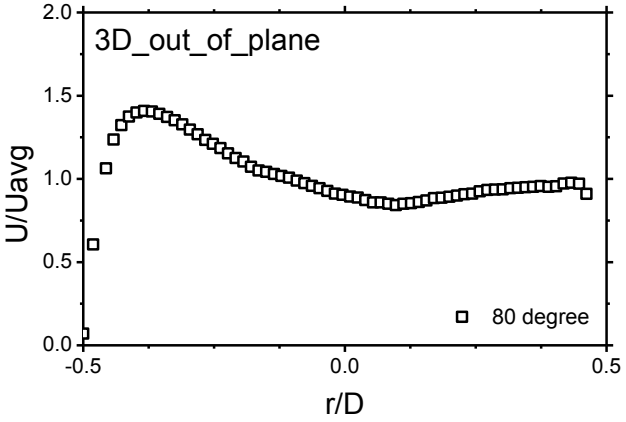

9) Velocity profile at 80 degree (3 D)

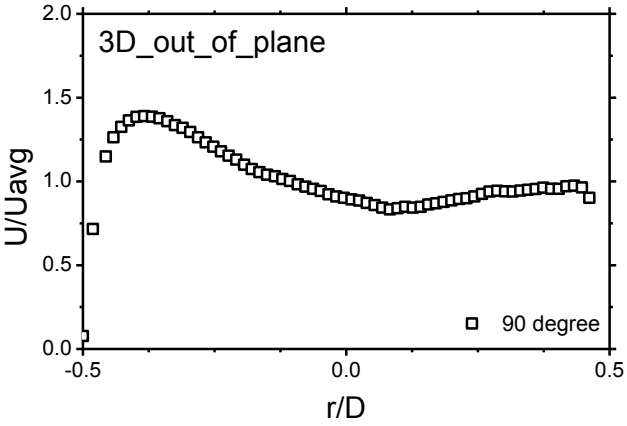

10) Velocity profile at 90 degree (3 D)

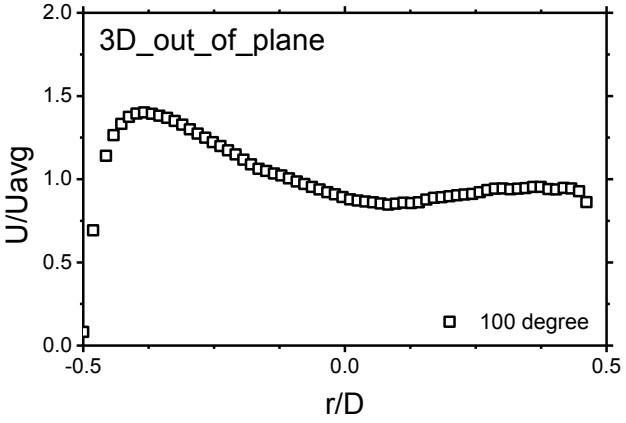

11) Velocity profile at 100 degree (3 D)

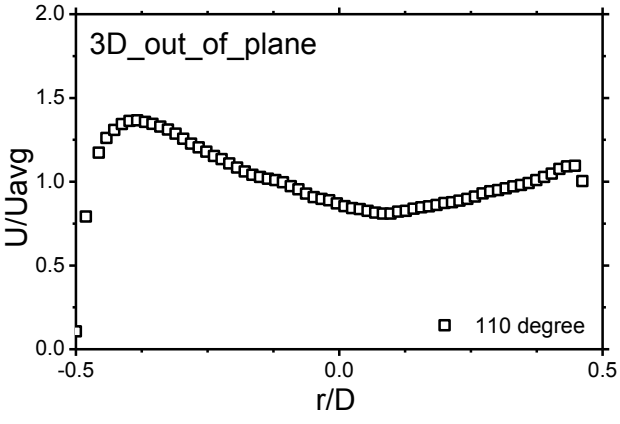

12) Velocity profile at 110 degree (3 D)

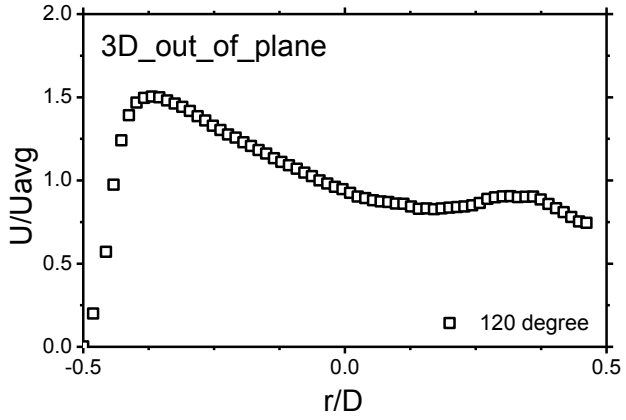

13) Velocity profile at 120 degree (3 D)

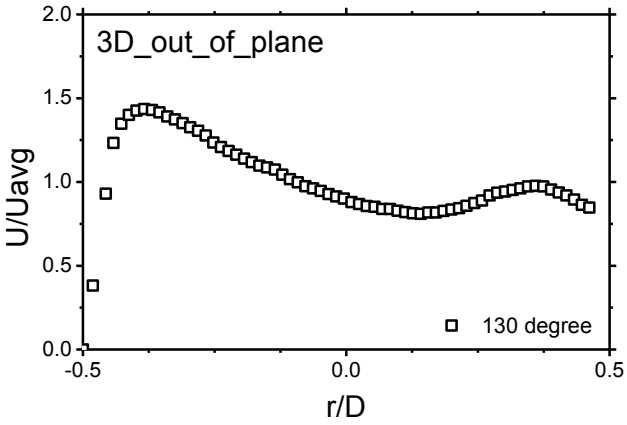

14) Velocity profile at 130 degree (3 D)

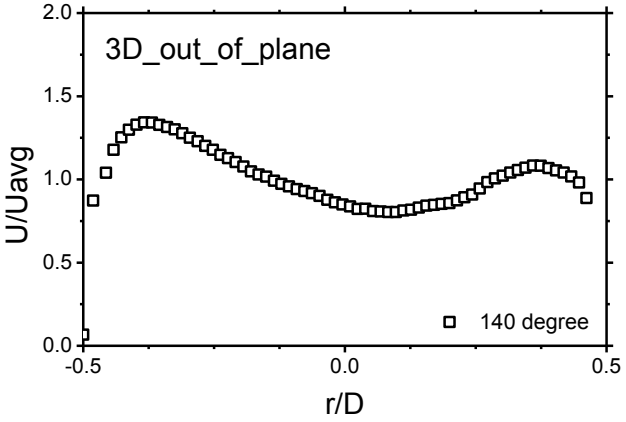

15). Velocity profile at 140 degree (3 D)

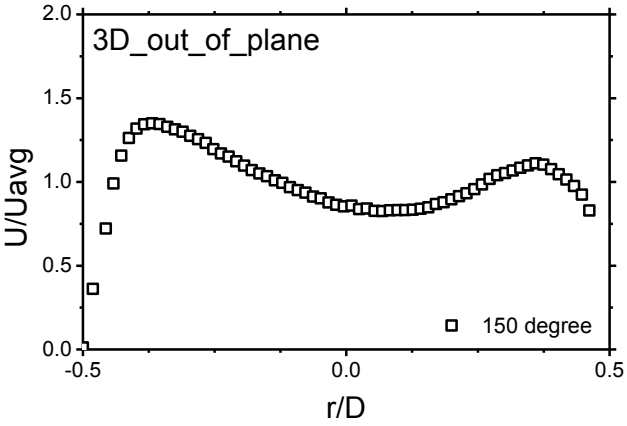

16) Velocity profile at 150 degree (3 D)

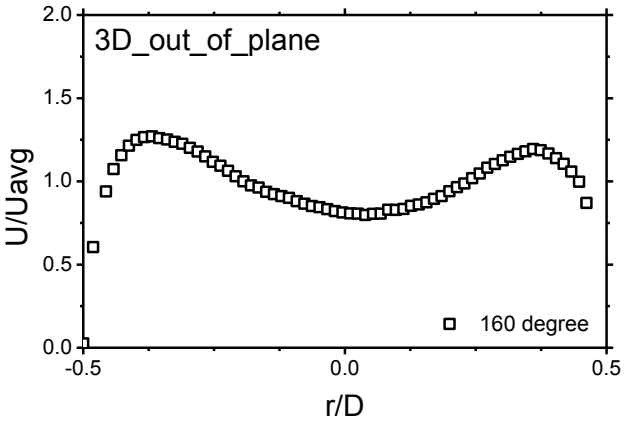

17) Velocity profile at 160 degree (3 D)

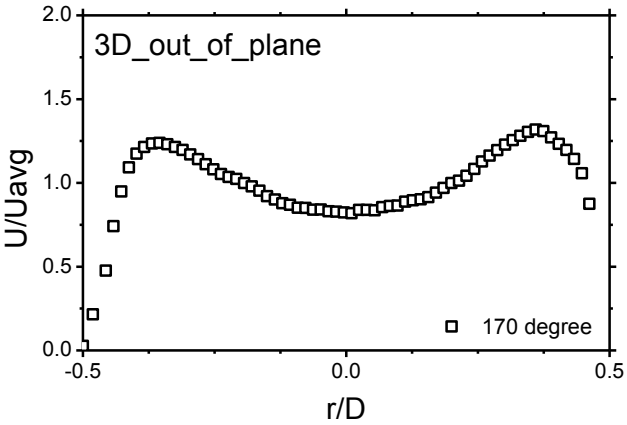

18) Velocity profile at 170 degree (3 D)

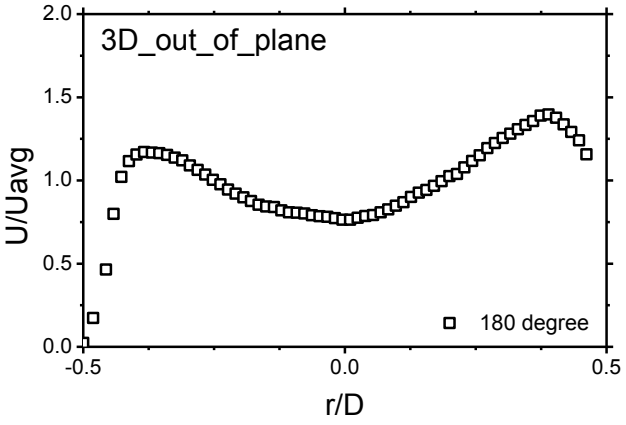

19) Velocity profile at 180 degree (3 D)

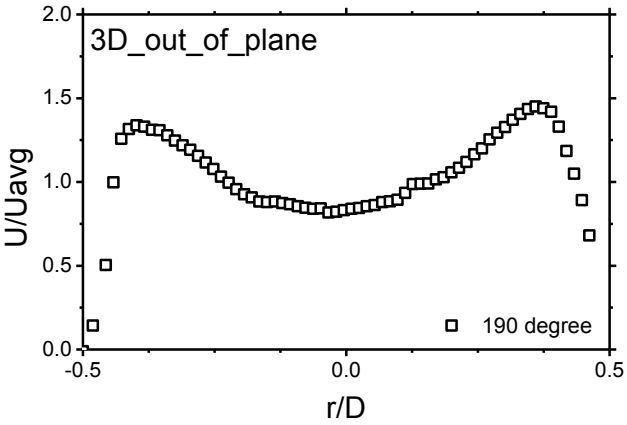

20) Velocity profile at 190 degree (3 D)

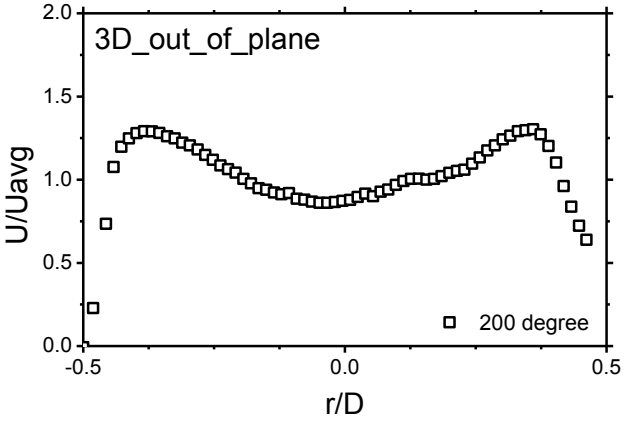

21) Velocity profile at 200 degree (3 D)

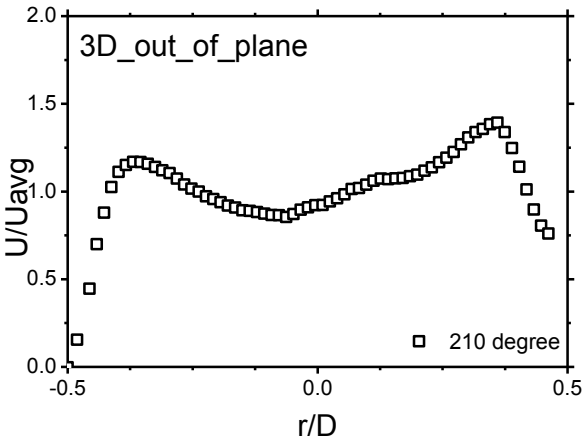

22) Velocity profile at 210 degree (3 D)

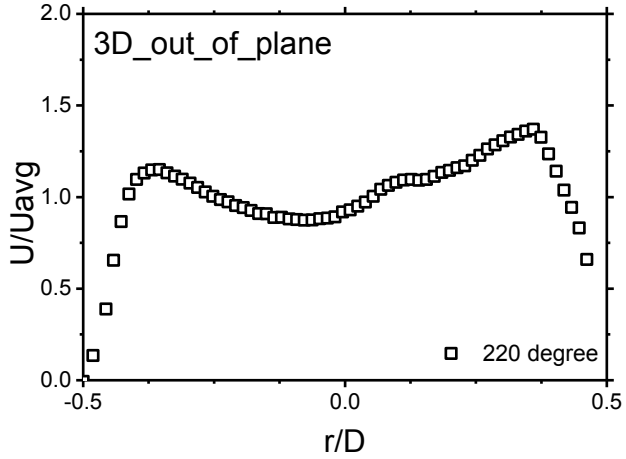

23) Velocity profile at 220 degree (3 D)

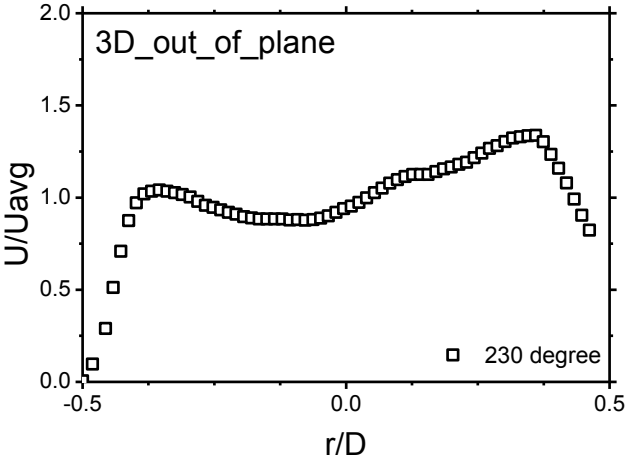

24) Velocity profile at 230 degree (3 D)

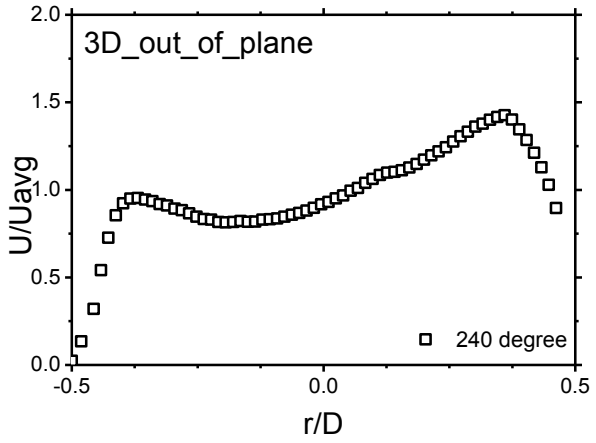

25) Velocity profile at 240 degree (3 D)

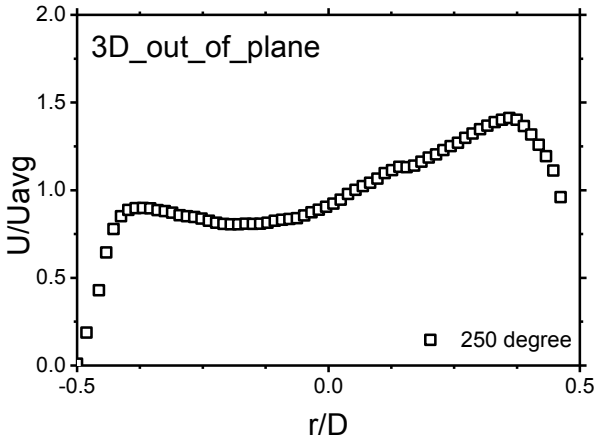

26) Velocity profile at 250 degree (3 D)

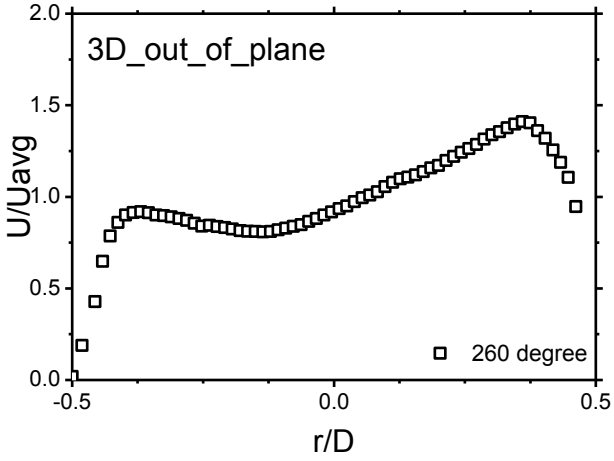

27) Velocity profile at 260 degree (3 D)

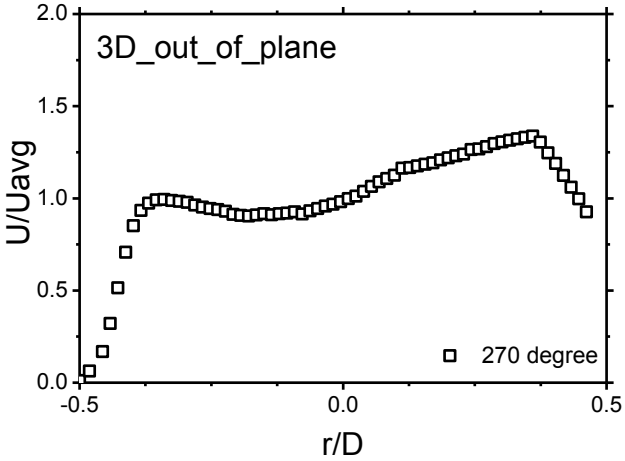

28) Velocity profile at 270 degree (3 D)

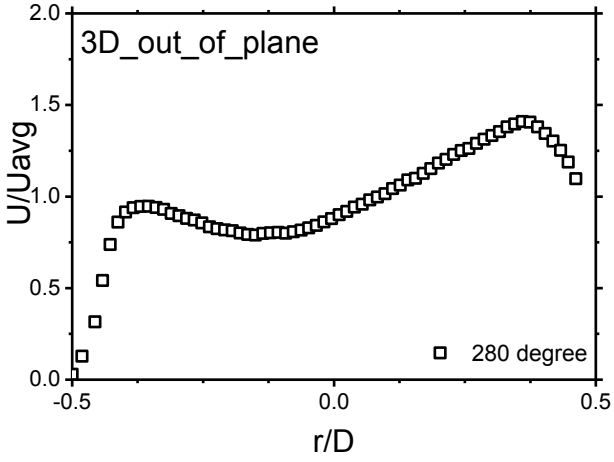

29) Velocity profile at 280 degree (3 D)

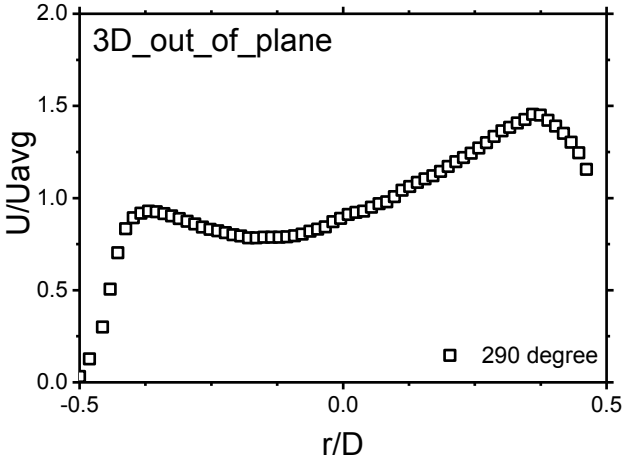

30) Velocity profile at 290 degree (3 D)

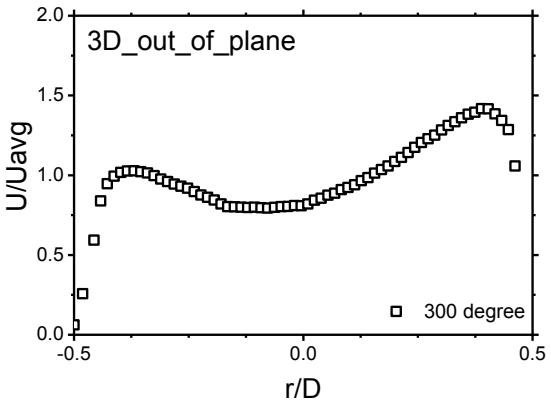

31) Velocity profile at 300 degree (3 D)

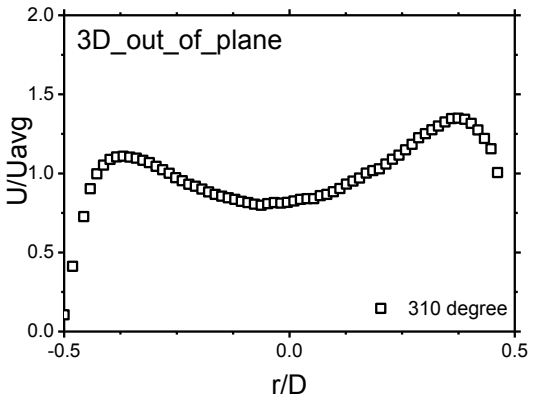

32) Velocity profile at 310 degree (3 D)

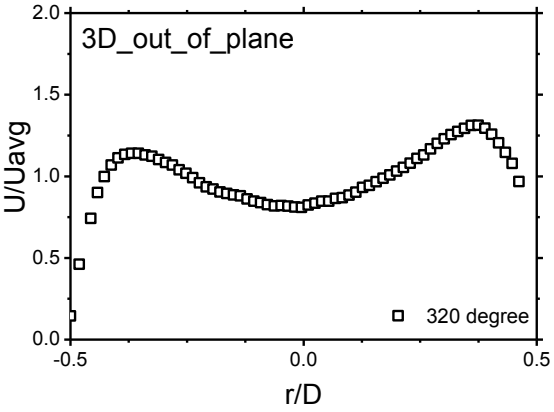

33) Velocity profile at 320 degree (3 D)

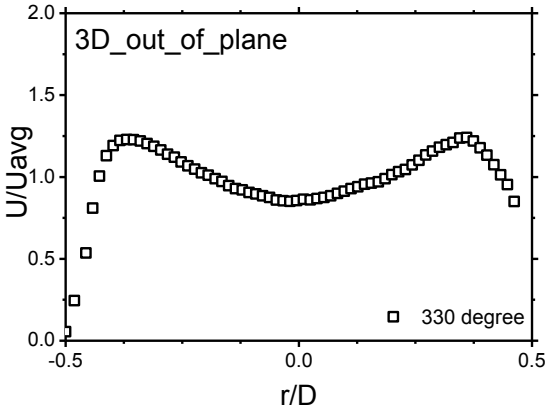

34) Velocity profile at 330 degree (3 D)

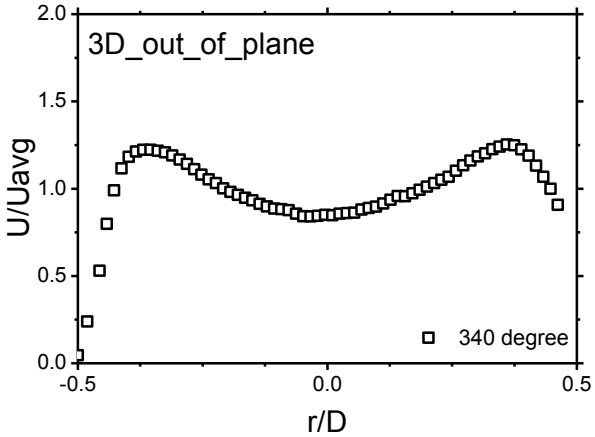

35) Velocity profile at 340 degree (3 D)

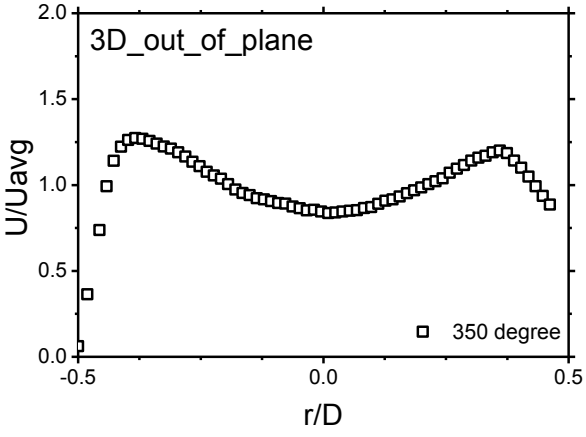

36) Velocity profile at 350 degree (3 D)

Fig. 6-9 Velocity profile at 3D

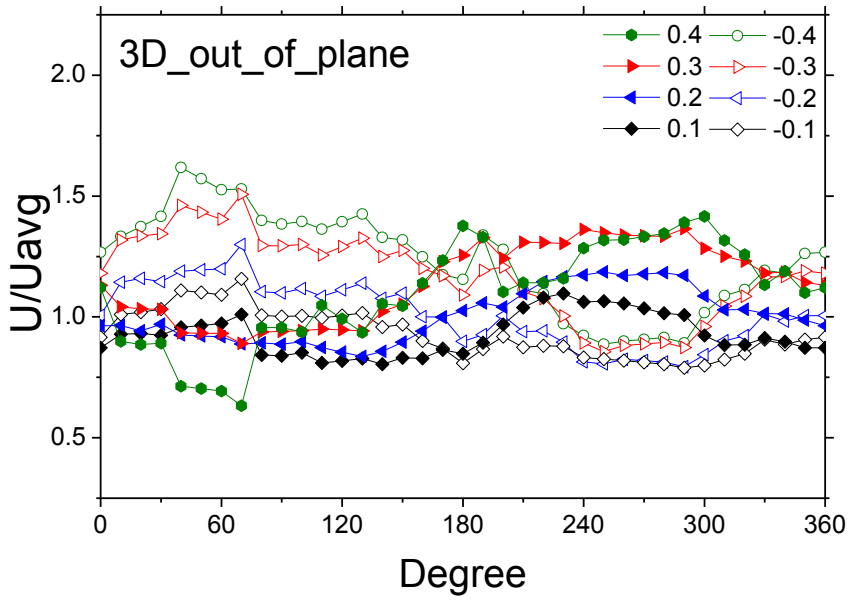

Fig.6-10 Circumferential velocity profiles at 3D

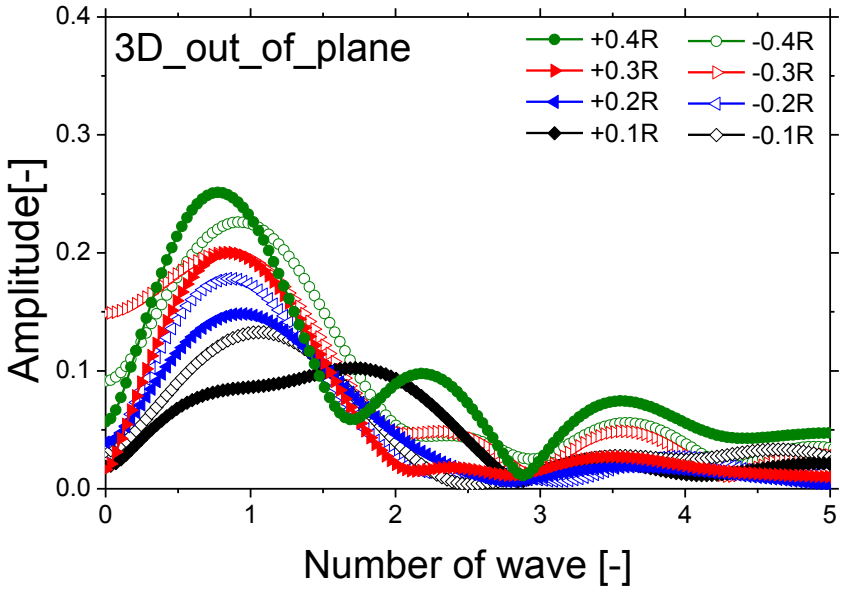

Fig. 6-11 FFT results

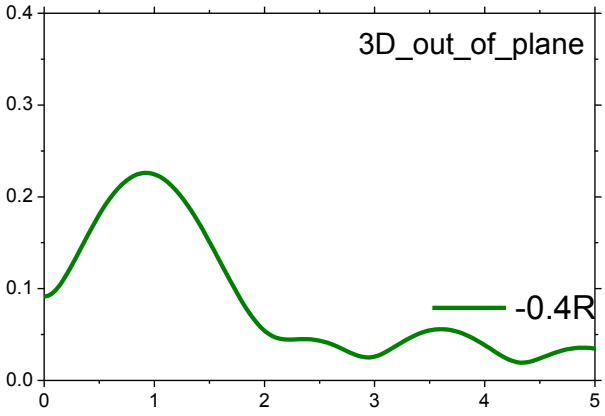

a) Number of waves from line -0.4 R (3 D)

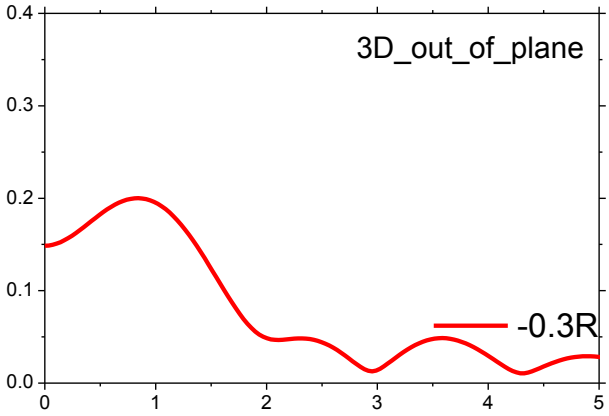

b) Number of waves from line -0.3 R (3 D)

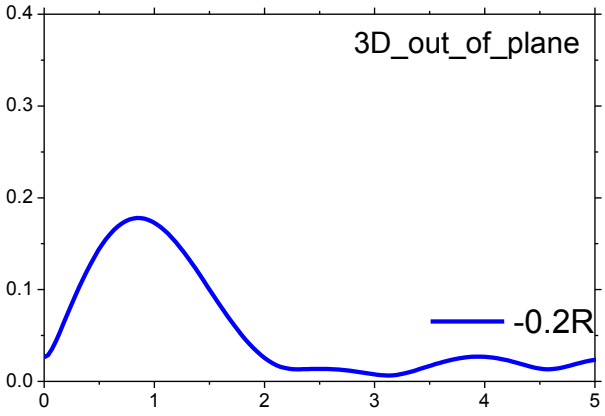

c) Number of waves from line -0.2 R (3 D)

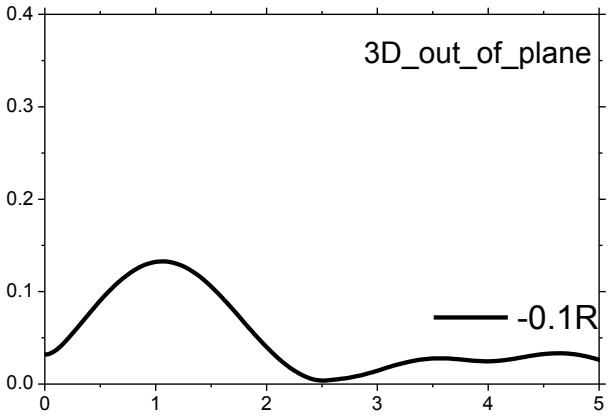

d) Number of waves from line -0.1 R (3 D)

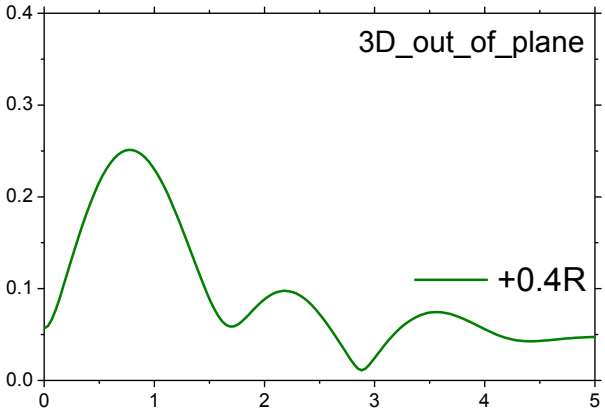

g) Number of waves from line +0.4 R (3 D)

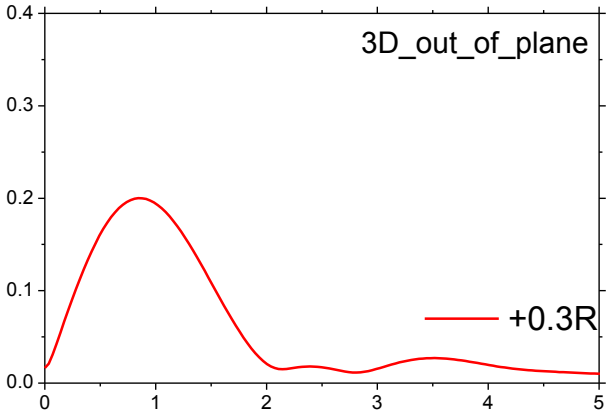

h) Number of waves from line +0.3 R (3 D)

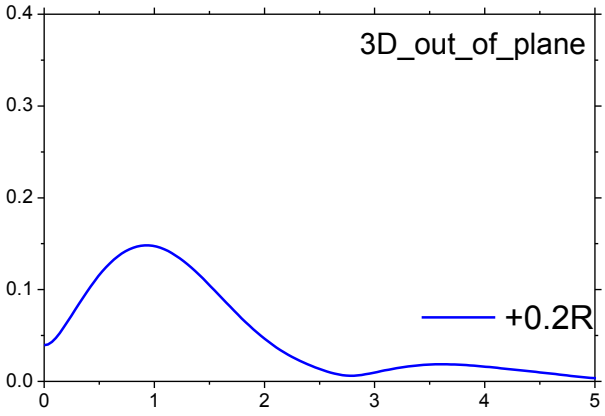

i) Number of waves from line +0.2 R (3 D)

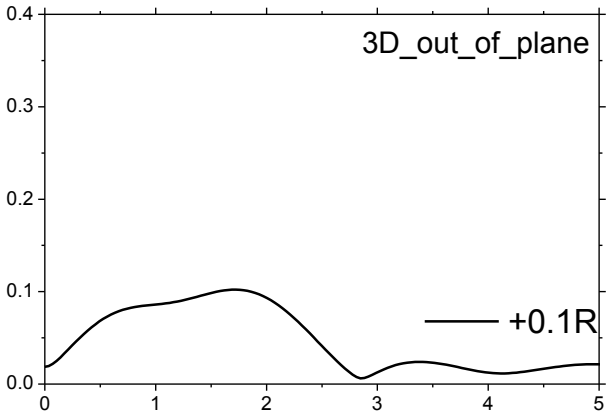

j) Number of waves from line +0.1 R (3 D)

Fig. 6-12 FFT results of circumferential velocity profiles at 3D

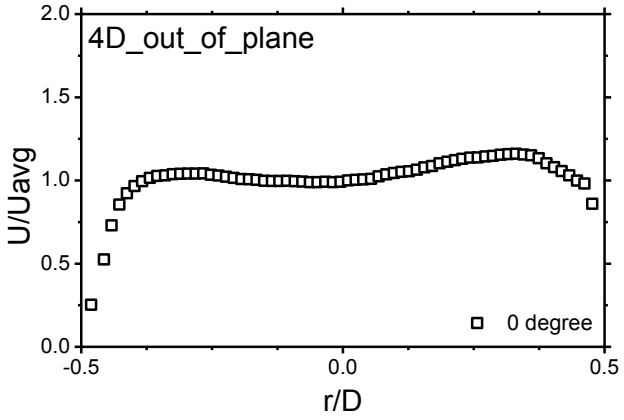

1) Velocity profile at 0 degree (4 D)

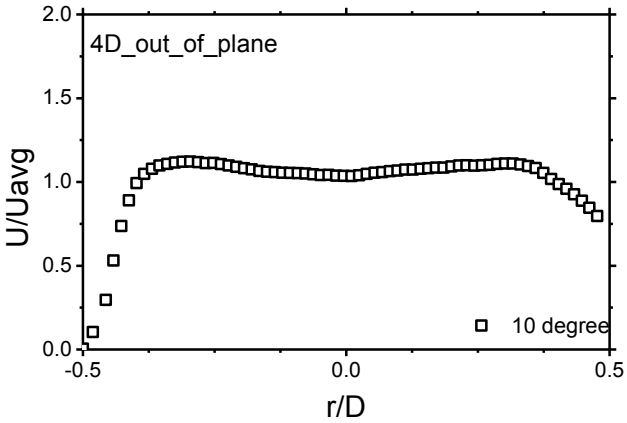

2) Velocity profile at 10 degree (4 D)

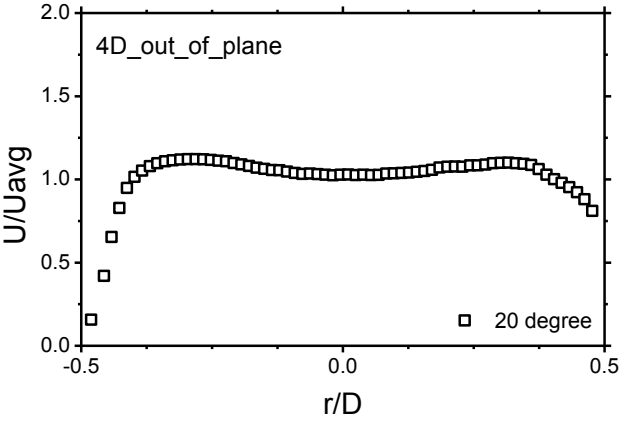

3) Velocity profile at 20 degree (4 D)

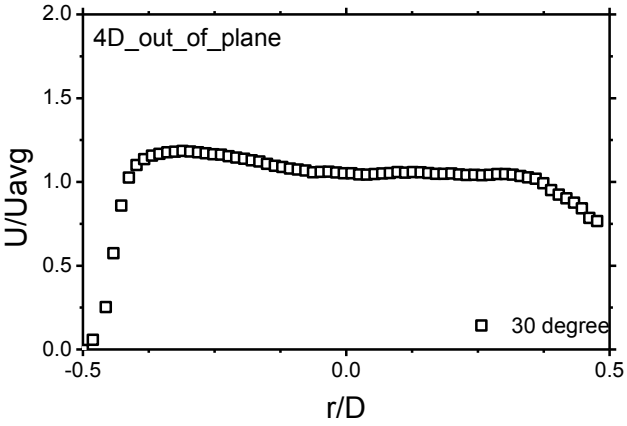

4) Velocity profile at 30 degree (4 D)

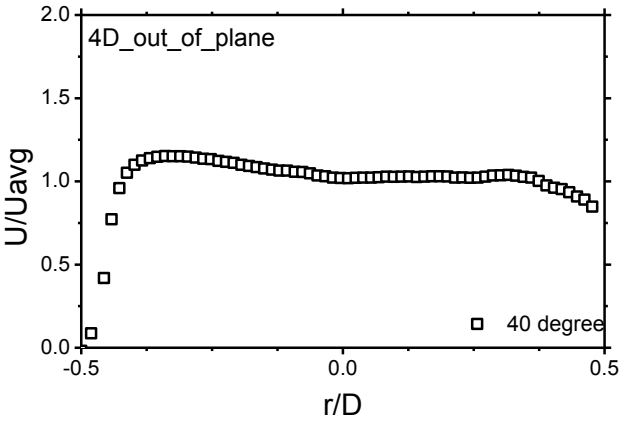

5) Velocity profile at 40 degree (4 D)

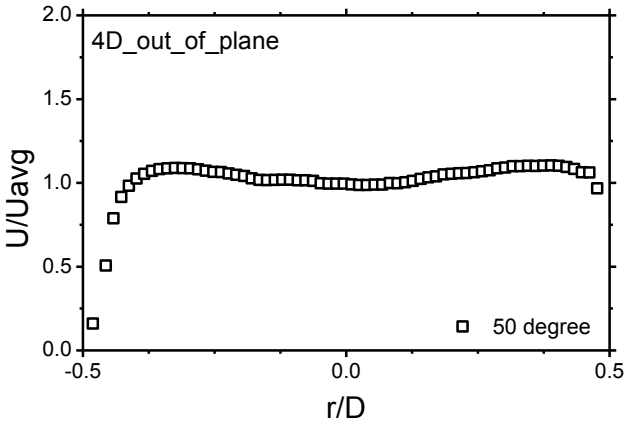

6) Velocity profile at 50 degree (4 D)

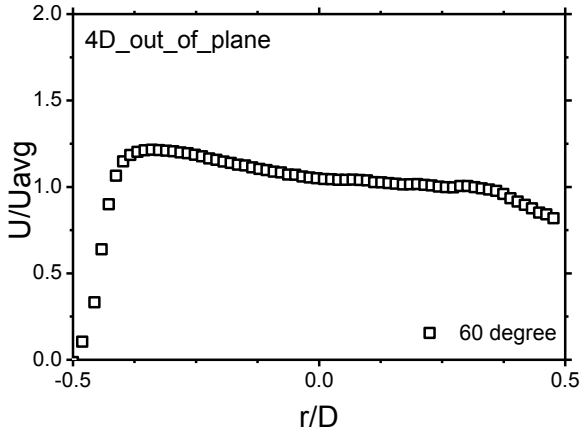

7) Velocity profile at 60 degree (4 D)

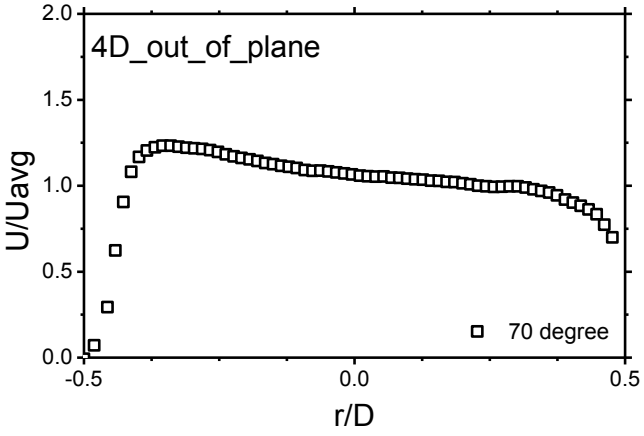

8) Velocity profile at 70 degree (4 D)

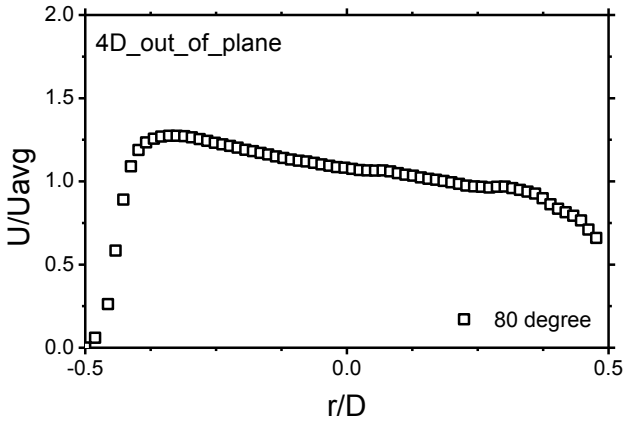

9) Velocity profile at 80 degree (4 D)

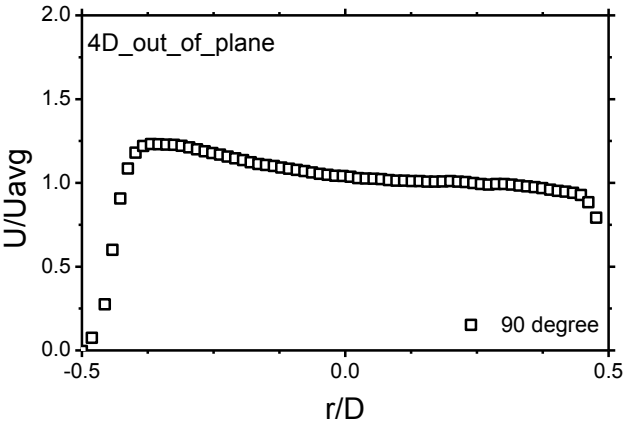

10) Velocity profile at 90 degree (4 D)

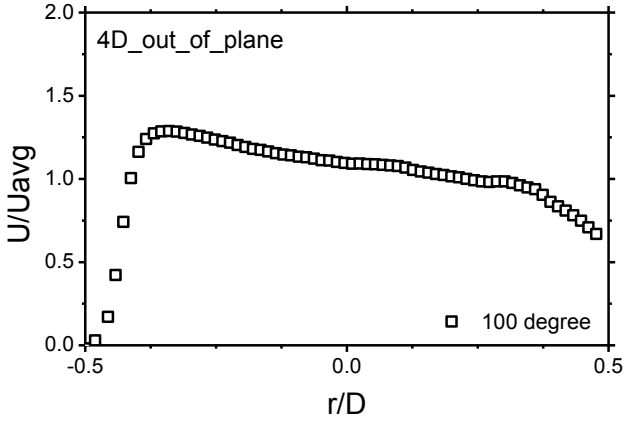

11) Velocity profile at 100 degree (4 D)

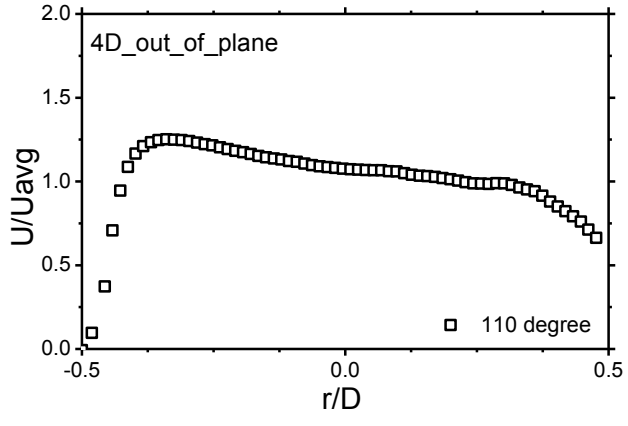

12) Velocity profile at 110 degree (4 D)

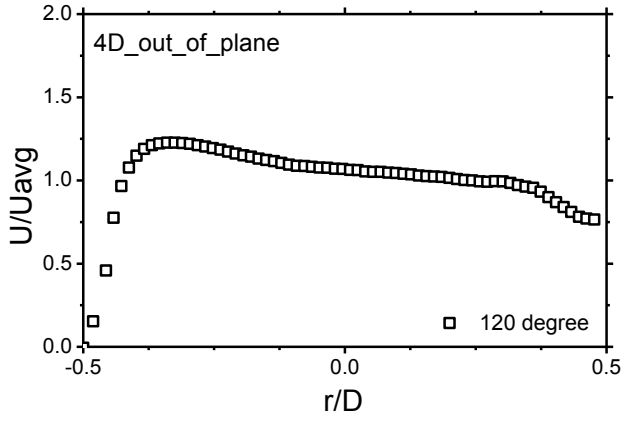

13) Velocity profile at 120 degree (4 D)

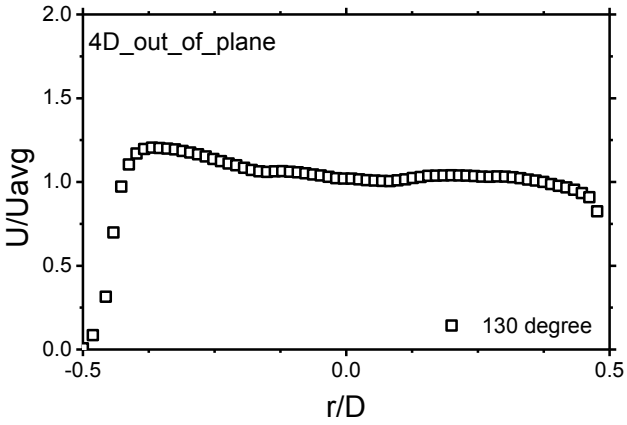

14) Velocity profile at 130 degree (4 D)

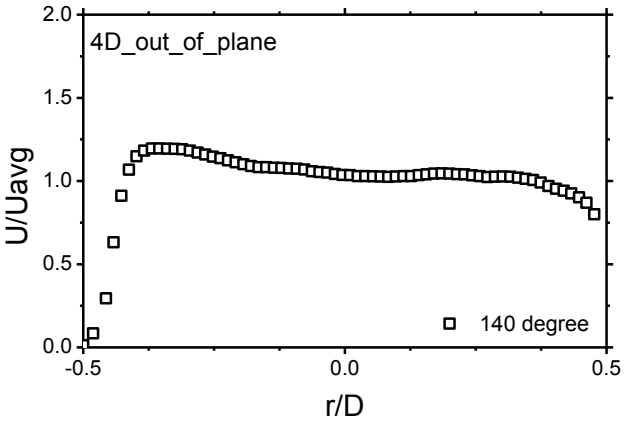

15) Velocity profile at 140 degree (4 D)

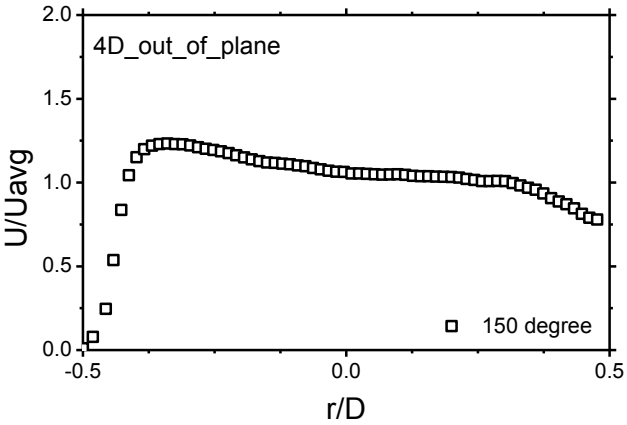

16) Velocity profile at 150 degree (4 D)

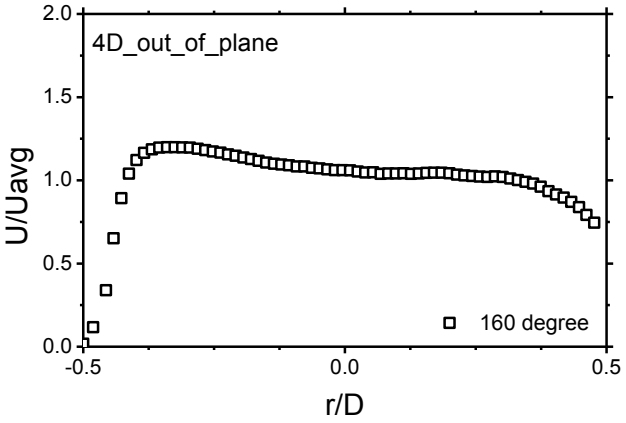

17). Velocity profile at 160 degree (4 D)

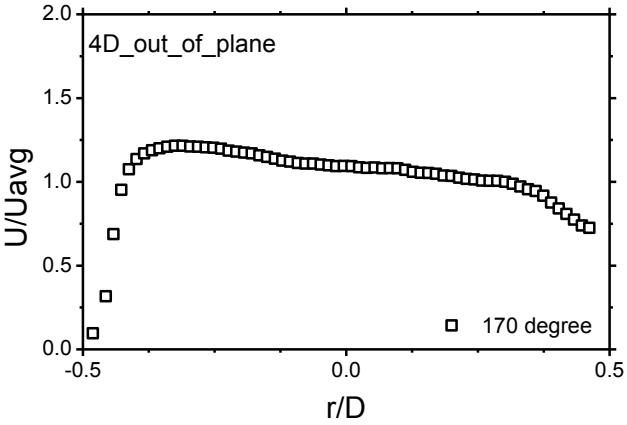

18) Velocity profile at 170 degree (4 D)

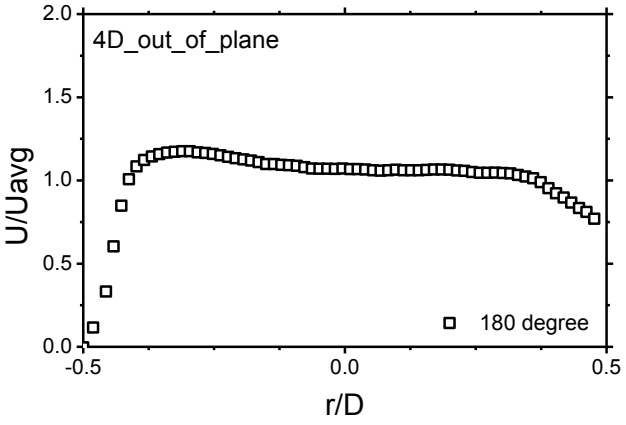

19) Velocity profile at 180 degree (4 D)

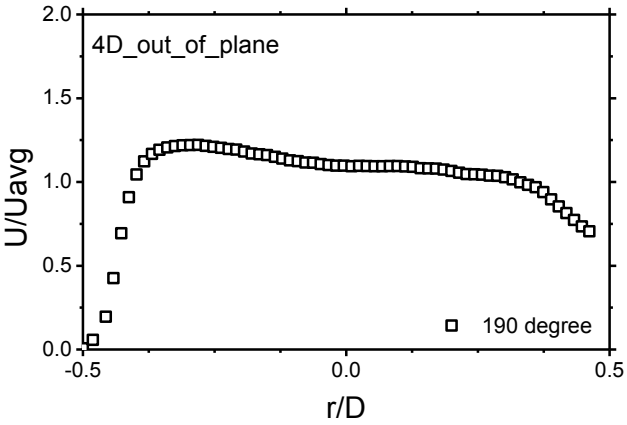

20) Velocity profile at 190 degree (4 D)

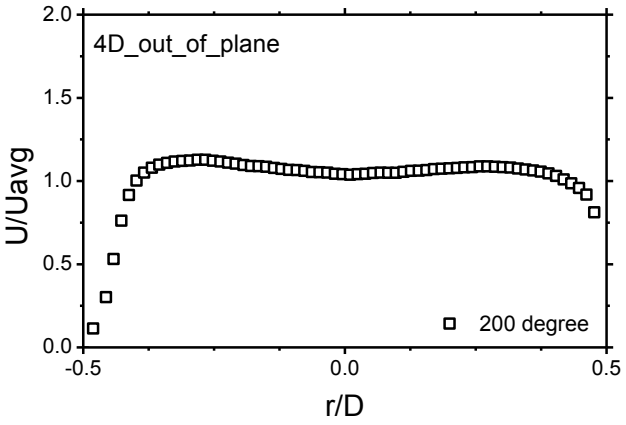

21) Velocity profile at 200 degree (4 D)

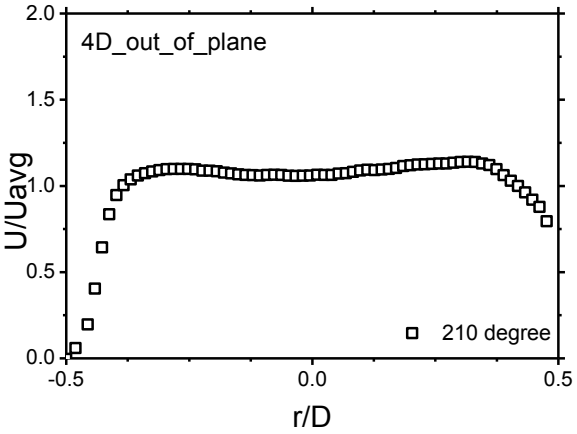

22) Velocity profile at 210 degree (4 D)

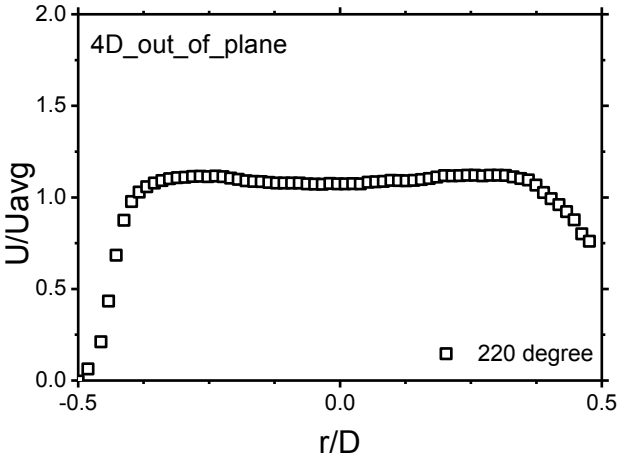

23) Velocity profile at 220 degree (4 D)

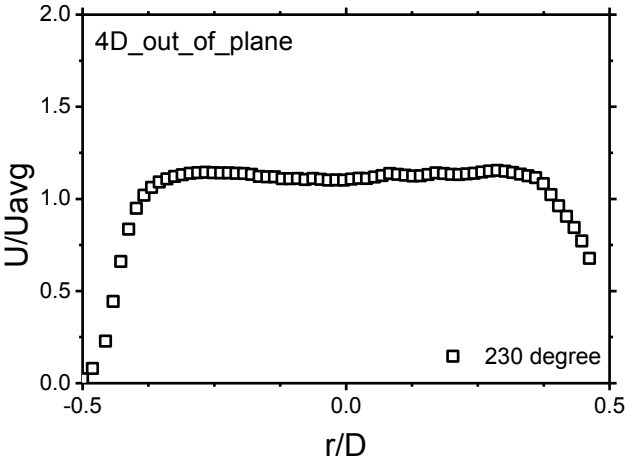

24) Velocity profile at 230 degree (4 D)

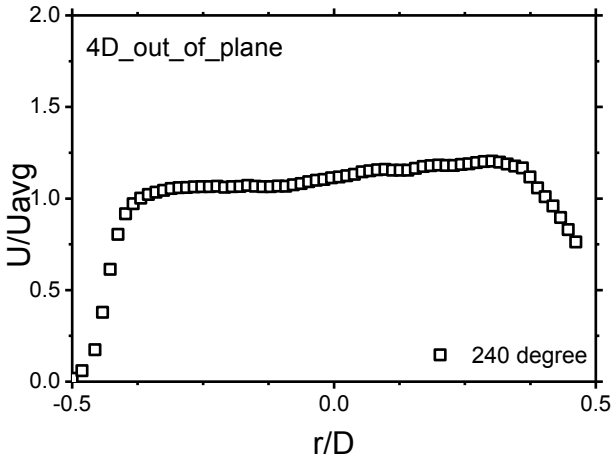

25) Velocity profile at 240 degree (4 D)

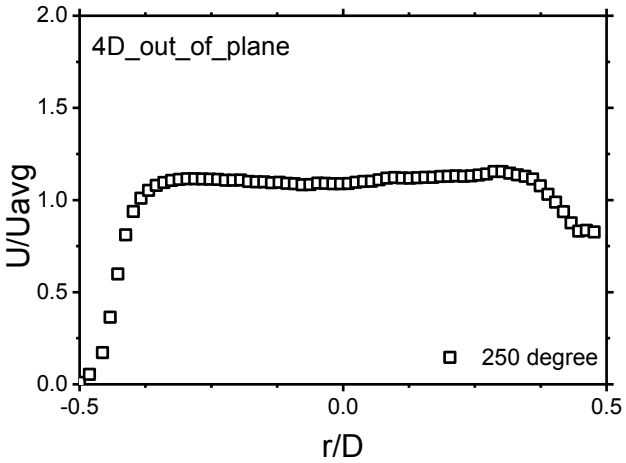

26) Velocity profile at 250 degree (4 D)

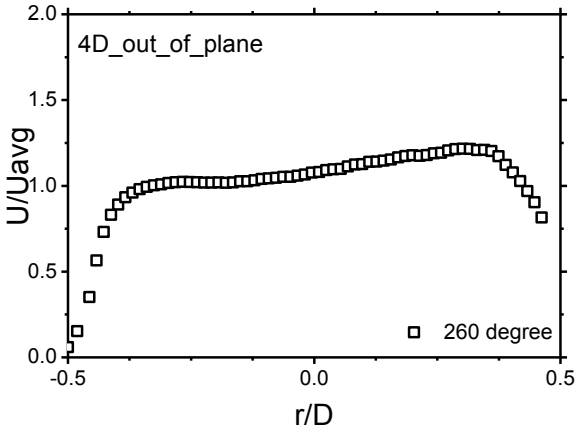

27) Velocity profile at 260 degree (4 D)

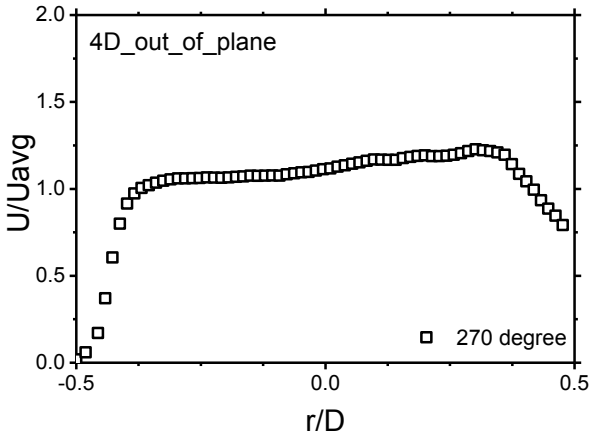

28) Velocity profile at 270 degree (4 D)

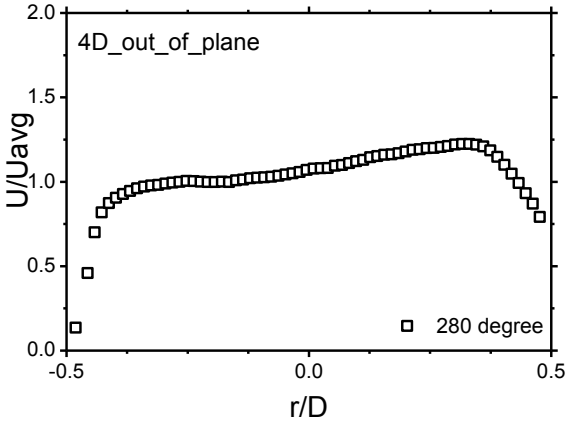

29) Velocity profile at 280 degree (4 D)

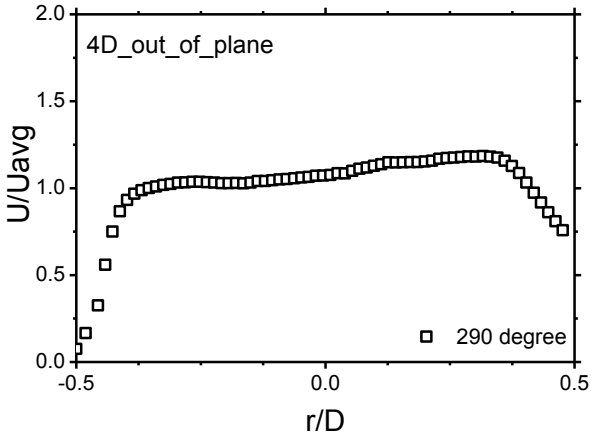

30) Velocity profile at 290 degree (4 D)

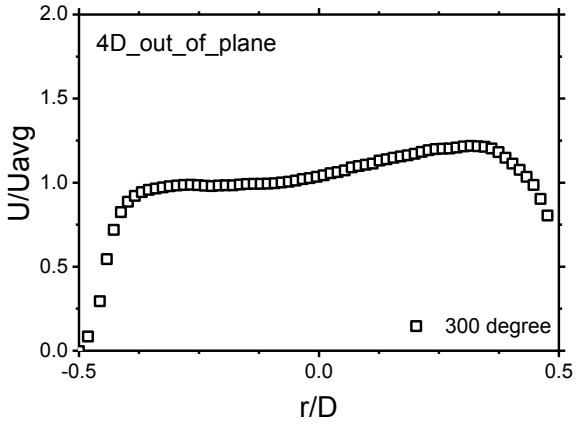

31) Velocity profile at 300 degree (4 D)

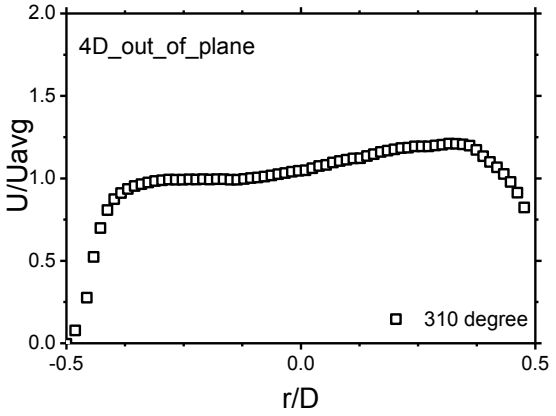

32) Velocity profile at 310 degree (4 D)

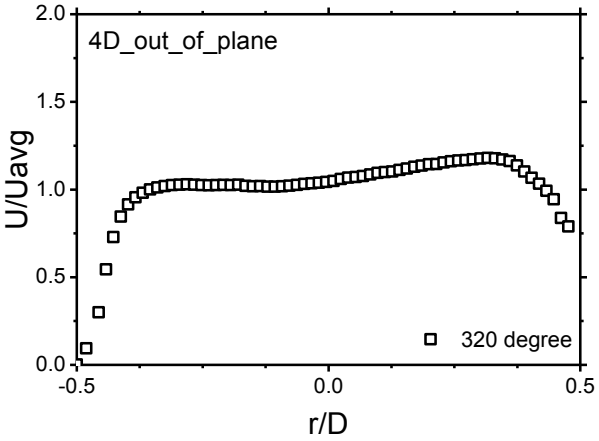

33) Velocity profile at 320 degree (4 D)

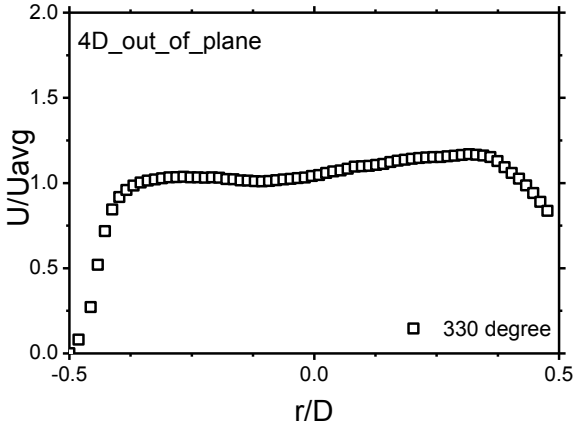

34) Velocity profile at 330 degree (4 D)

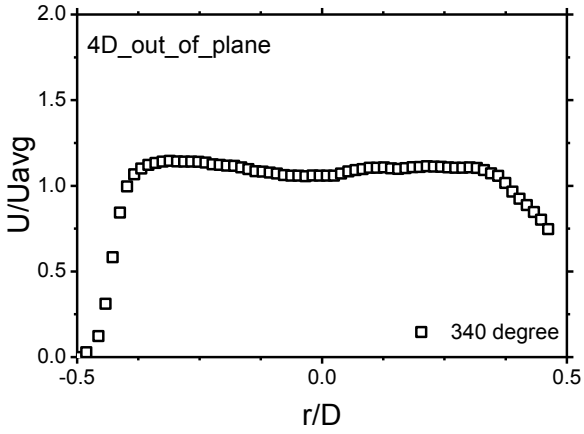

35) Velocity profile at 340 degree (4 D)

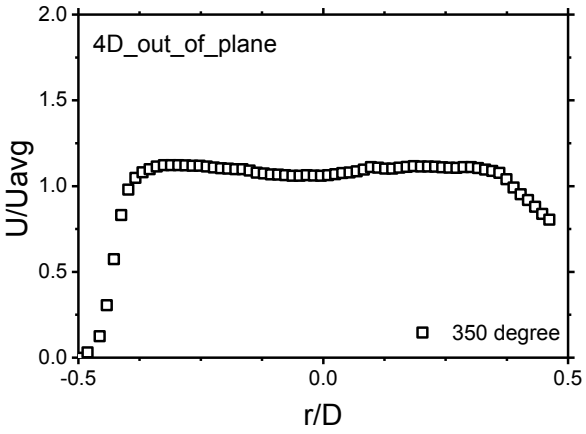

36) Velocity profile at 350 degree (4 D)

Fig. 6-13 Velocity profiles at 4D

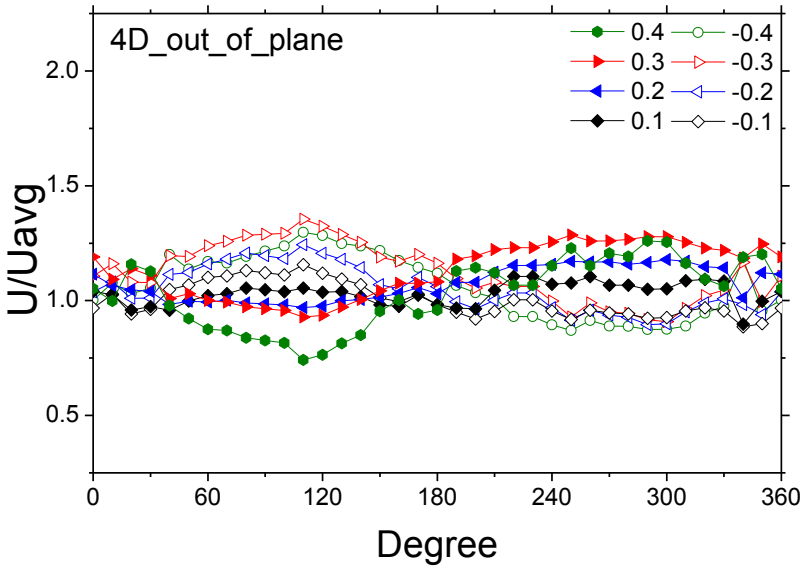

Fig. 6-14 Circumferential velocity profiles at 4D

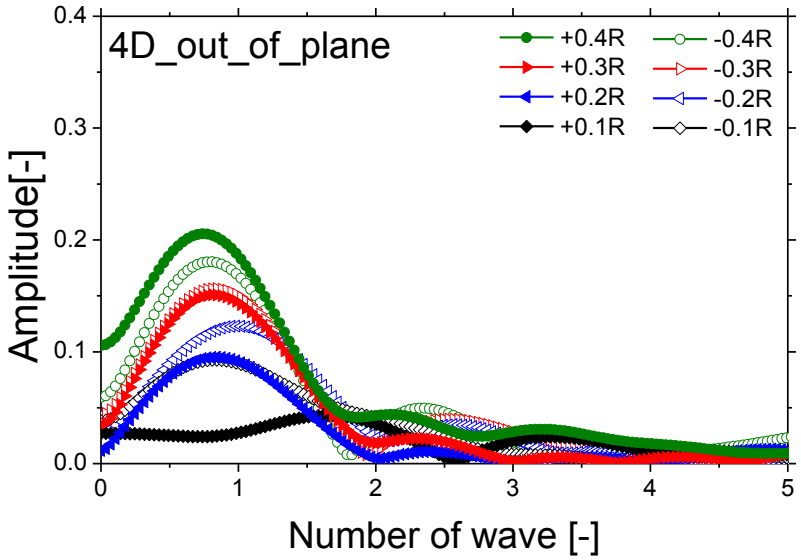

Fig. 6-15 Fast Fourier Transform (FFT) Circumferential velocity profiles at 4D

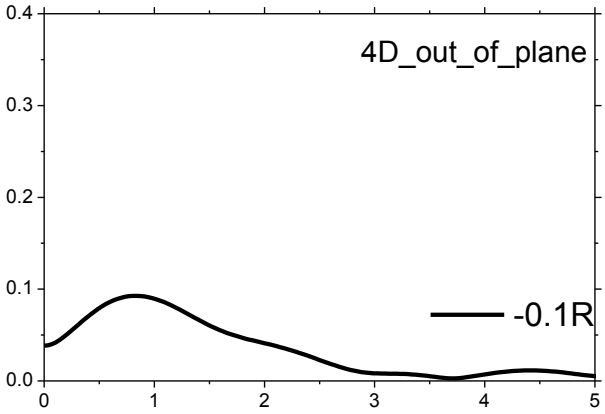

a) Number of waves from line -0.1 R (4 D)

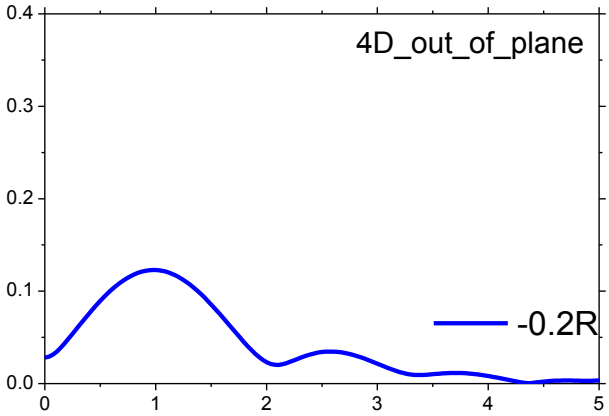

b) Number of waves from line -0.2 R (4 D)

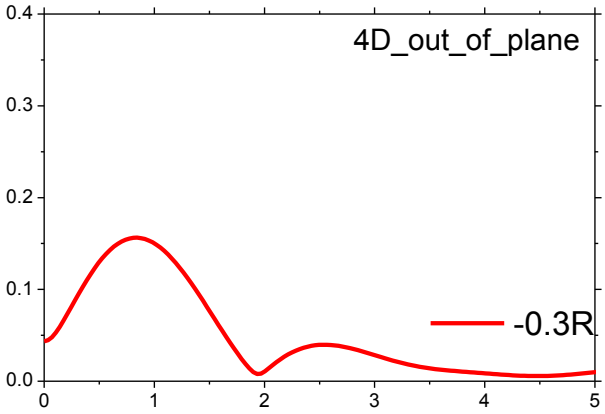

c) Number of waves from line -0.3 R (4 D)

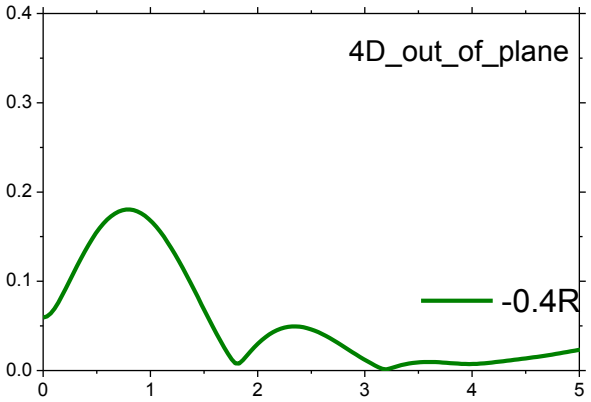

d) Number of waves from line -0.4 R (4 D)

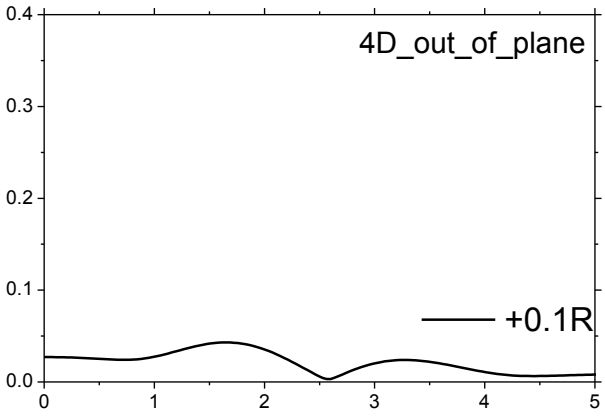

e) Number of waves from line +0.1 R (4 D)

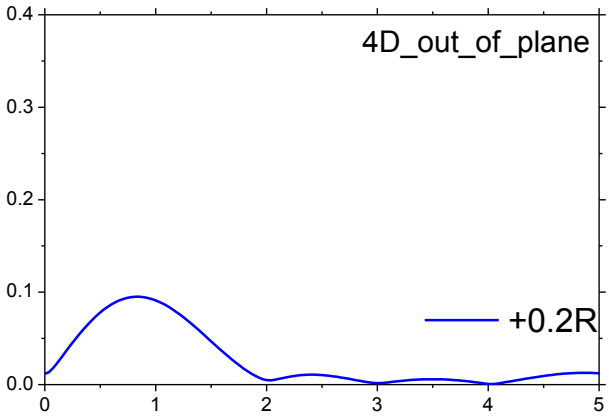

f) Number of waves from line +0.2 R (4 D)

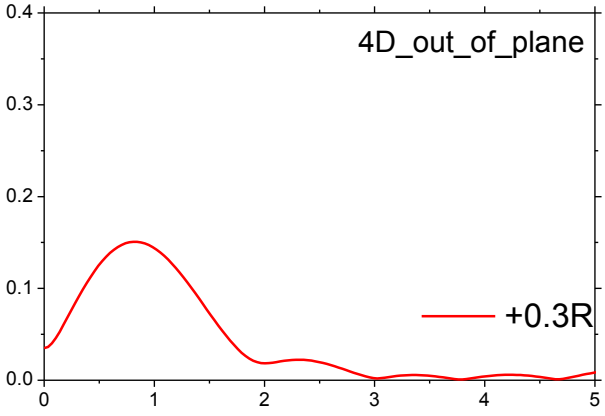

g) Number of waves from line +0.3 R (4 D)

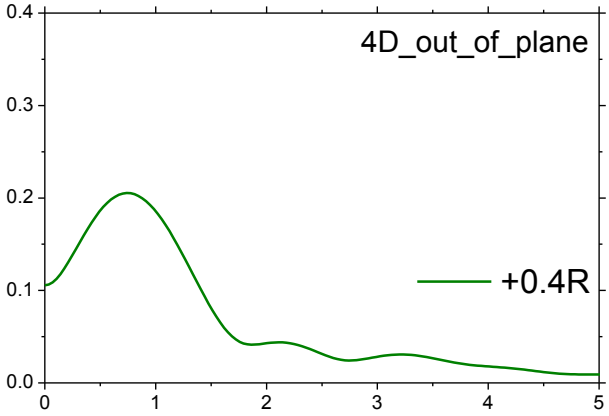

h) Number of waves from line +0.4 R (4 D)

Fig. 6-16 FFT results of Circumferential velocity profiles at 4D

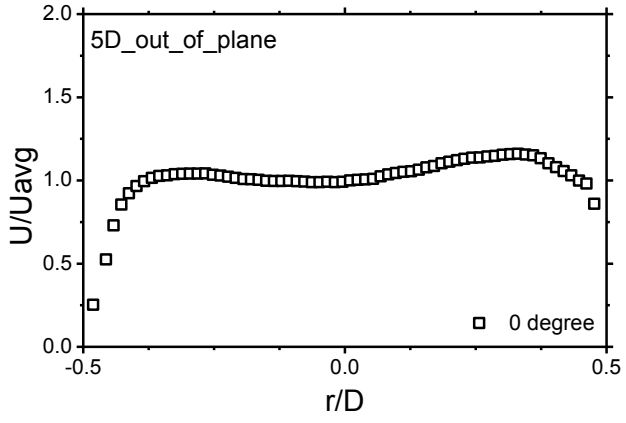

1) Velocity profile at 0 degree (5 D)

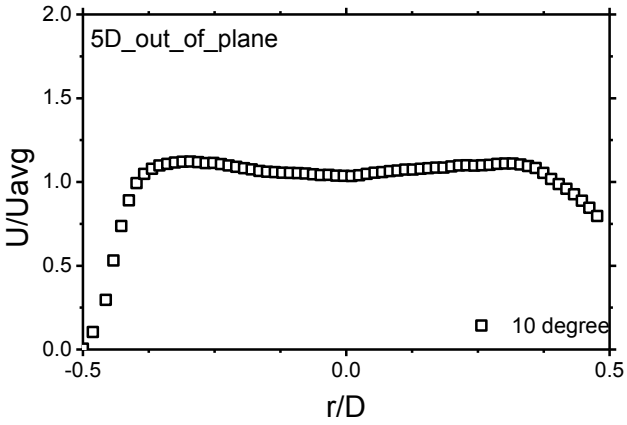

2) Velocity profile at 10 degree (5 D)

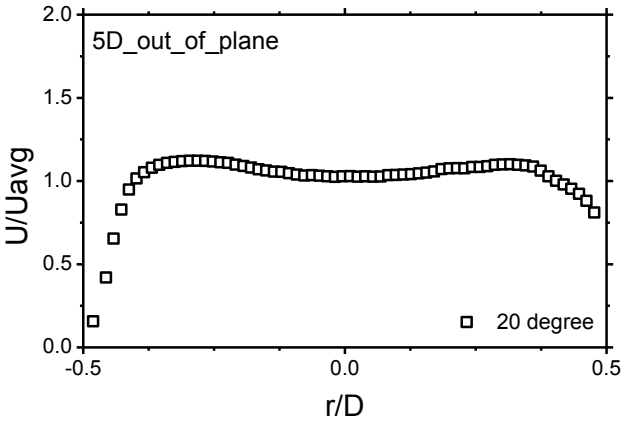

3) Velocity profile at 20 degree (5 D)

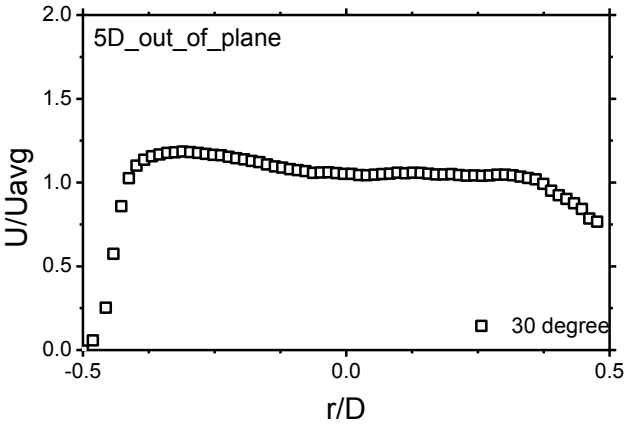

4) Velocity profile at 30 degree (5 D)

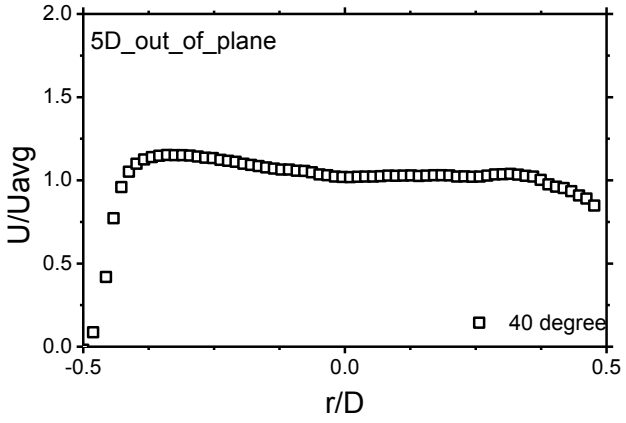

5) Velocity profile at 40 degree (5 D)

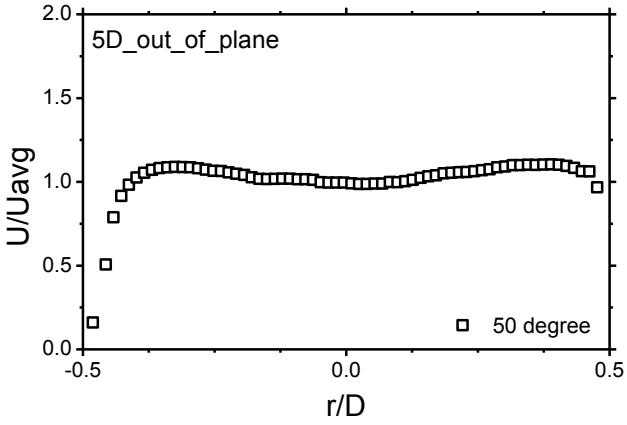

6) Velocity profile at 50 degree (5 D)

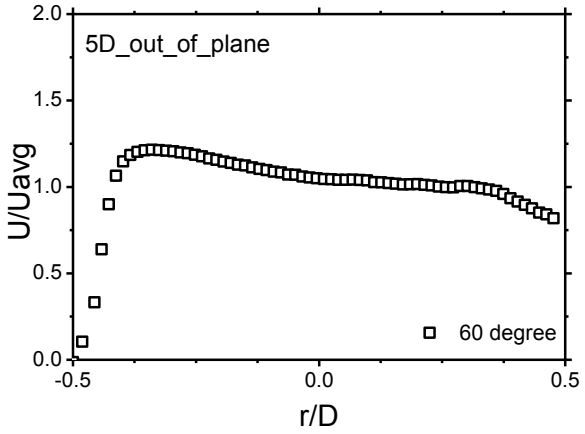

7) Velocity profile at 60 degree (5 D)

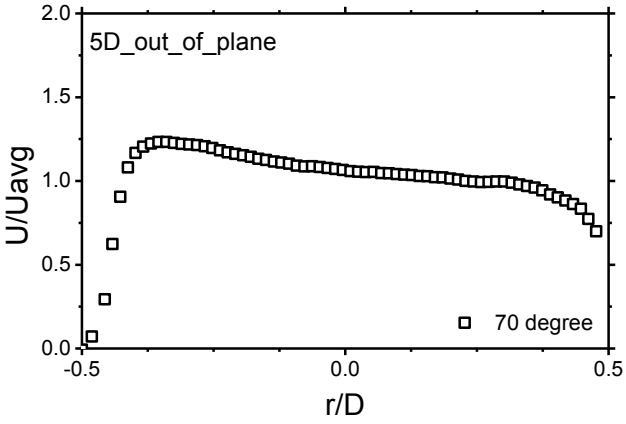

8) Velocity profile at 70 degree (5 D)

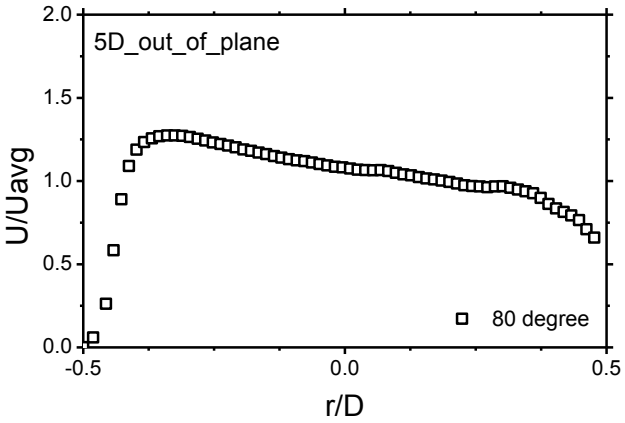

9) Velocity profile at 80 degree (5 D)

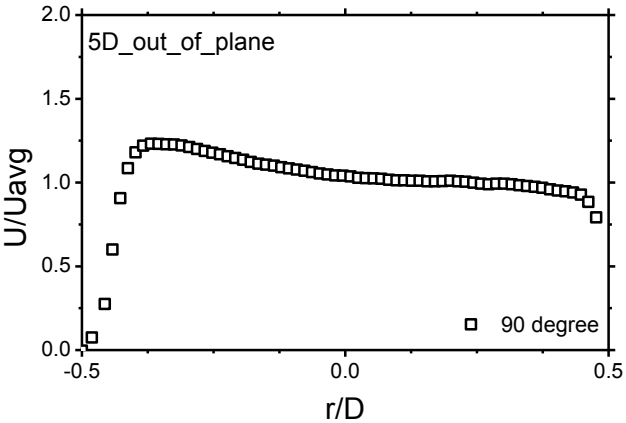

10) Velocity profile at 90 degree (5 D)

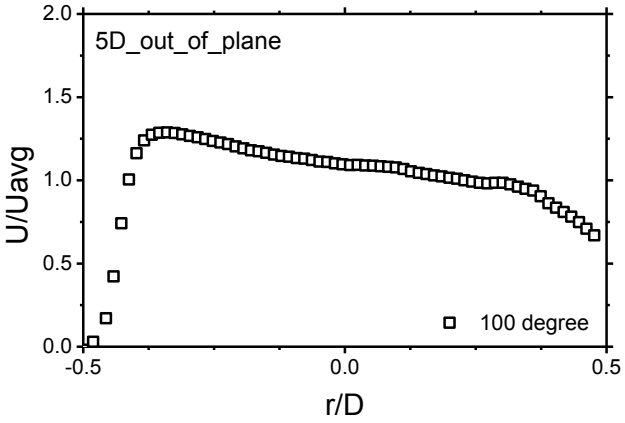

11) Velocity profile at 100 degree (5 D)

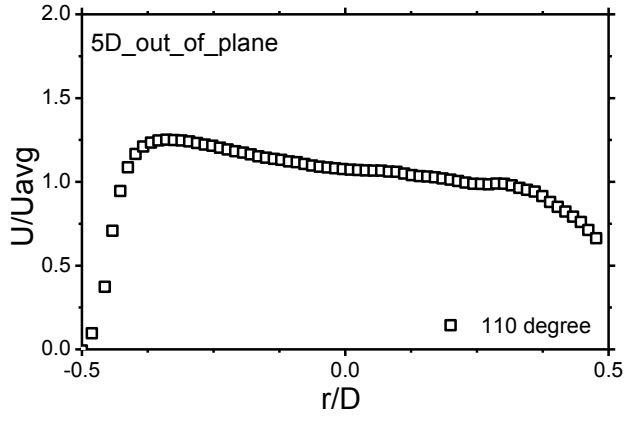

12) Velocity profile at 110 degree (5 D)

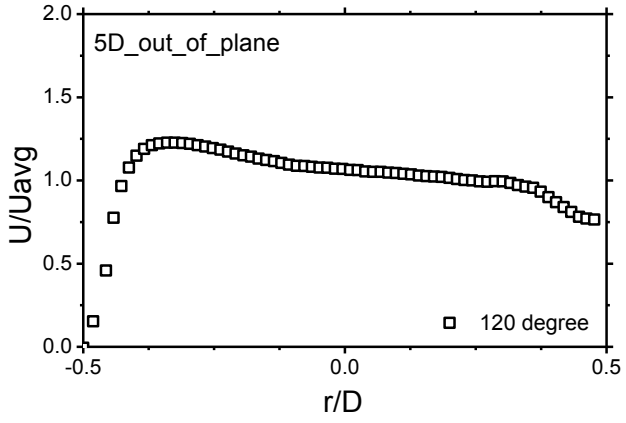

13) Velocity profile at 120 degree (5 D)

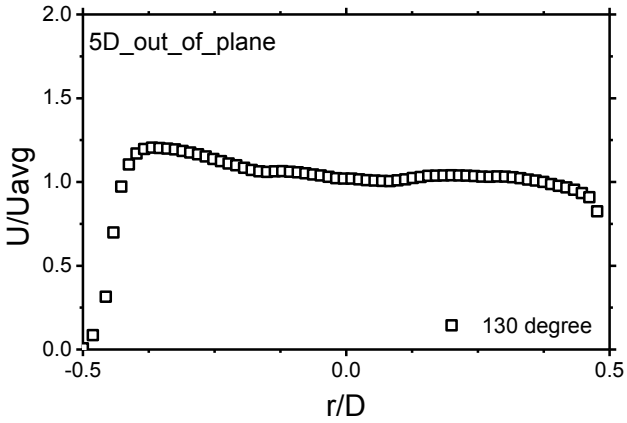

14) Velocity profile at 130 degree (5 D)

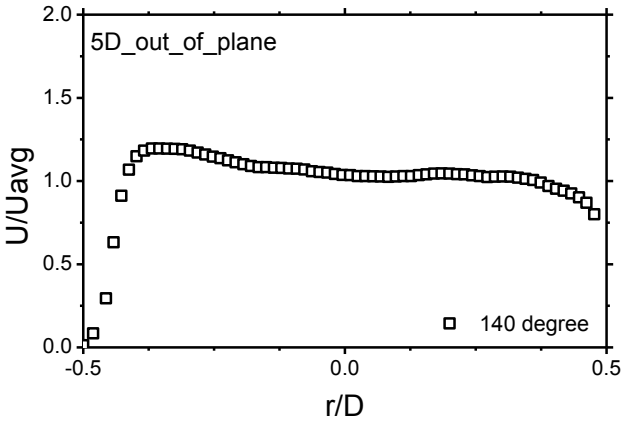

15) Velocity profile at 140 degree (5 D)

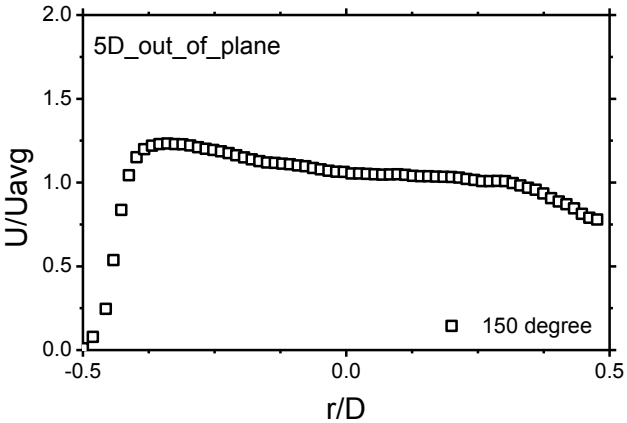

16) Velocity profile at 150 degree (5 D)

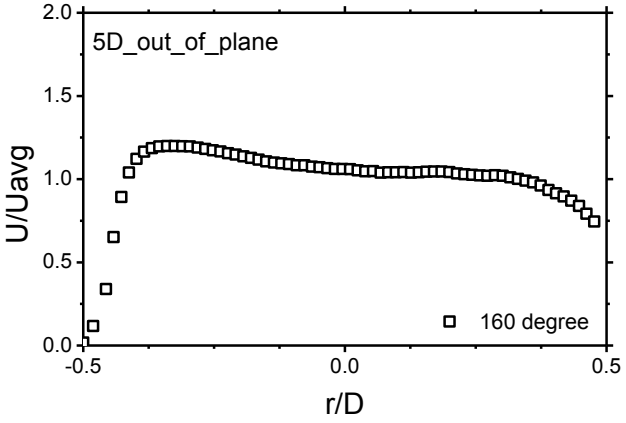

17) Velocity profile at 160 degree (5 D)

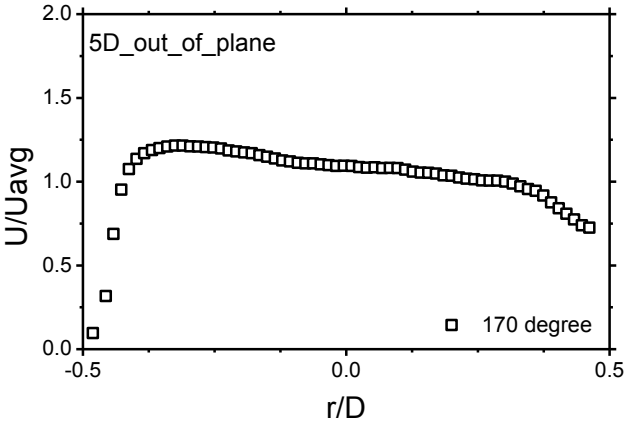

18) Velocity profile at 170 degree (5 D)

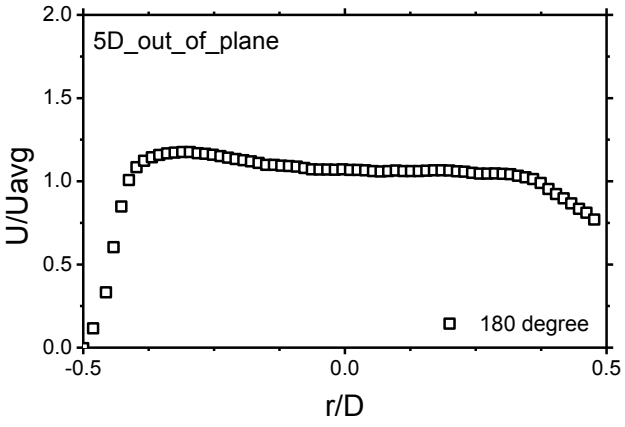

19) Velocity profile at 180 degree (5 D)

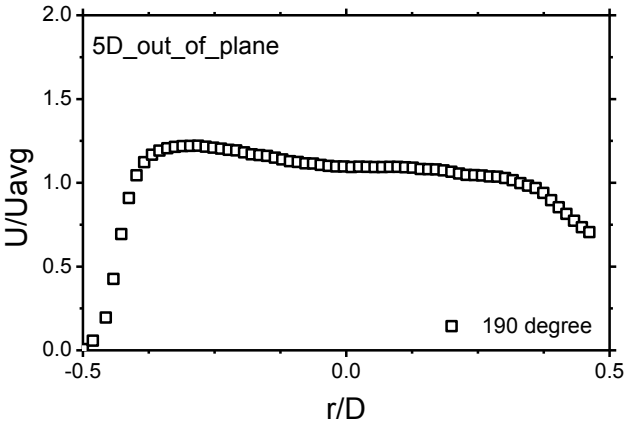

20) Velocity profile at 190 degree (5 D)

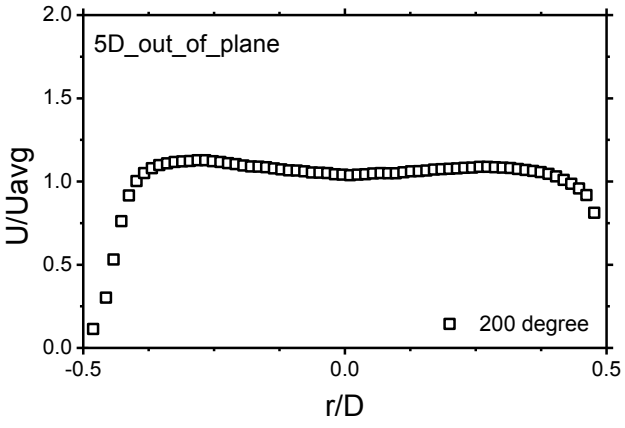

21) Velocity profile at 200 degree (5 D)

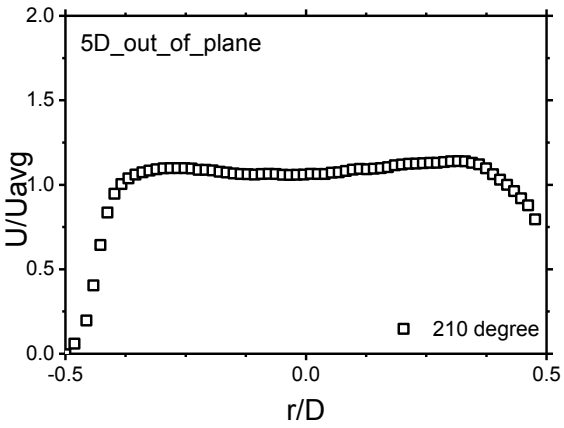

22) Velocity profile at 210 degree (5 D)

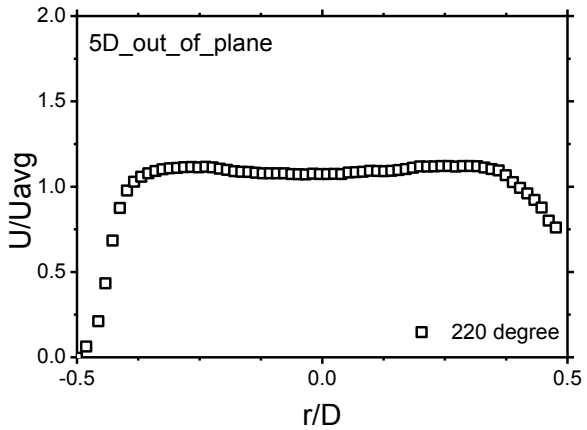

23) Velocity profile at 220 degree (5 D)

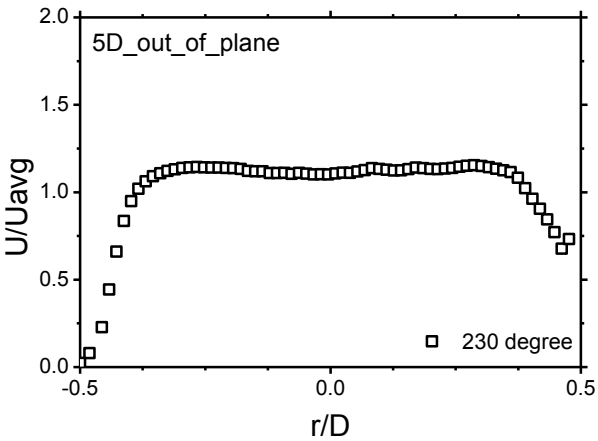

24) Velocity profile at 230 degree (5 D)

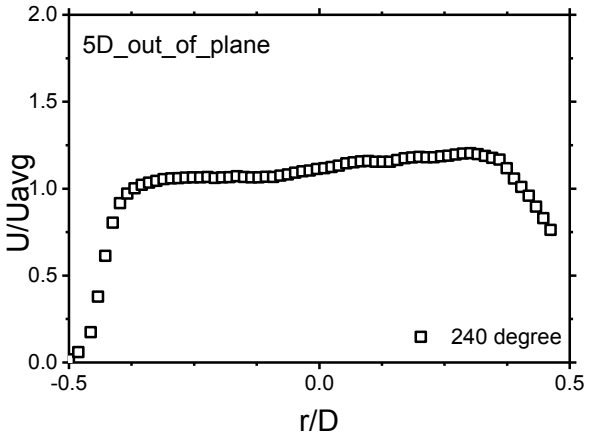

25) Velocity profile at 240 degree (5 D)

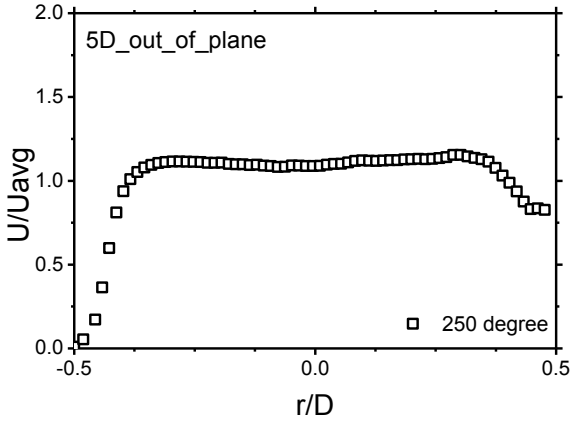

26) Velocity profile at 250 degree (5 D)

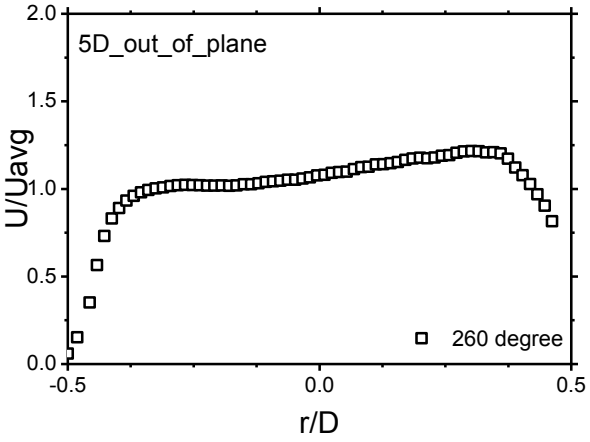

27) Velocity profile at 260 degree (5 D)

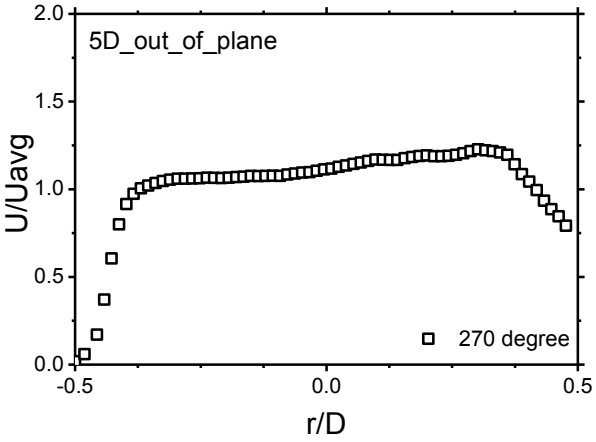

28) Velocity profile at 270 degree (5 D)

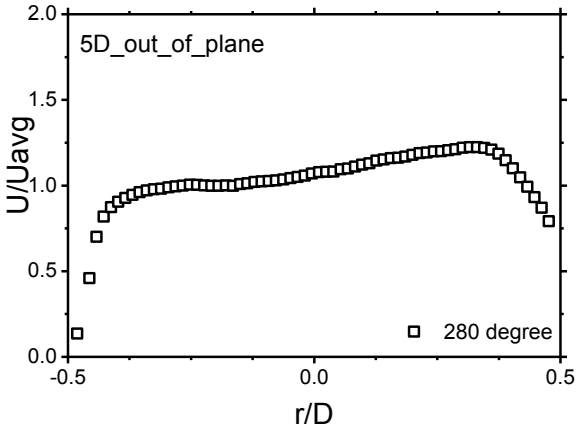

29) Velocity profile at 280 degree (5 D)

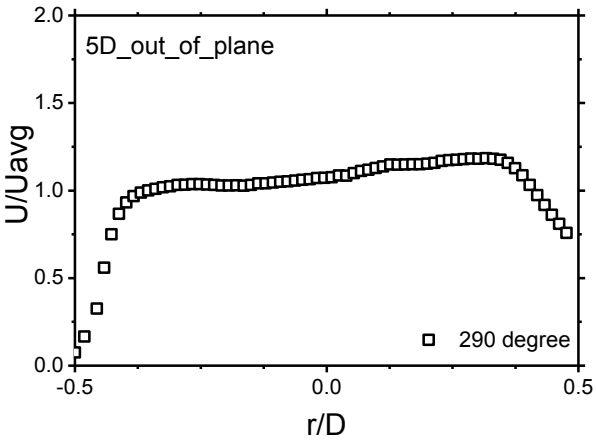

30) Velocity profile at 290 degree (5 D)

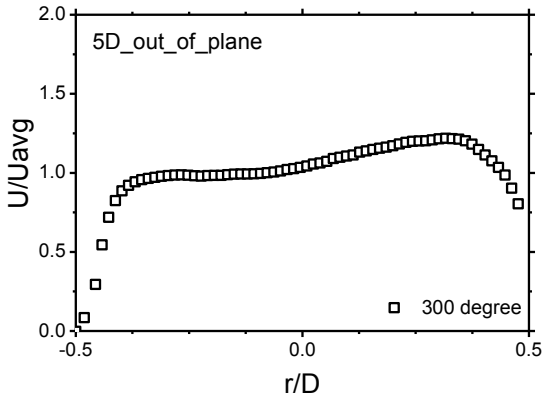

31) Velocity profile at 300 degree (5 D)

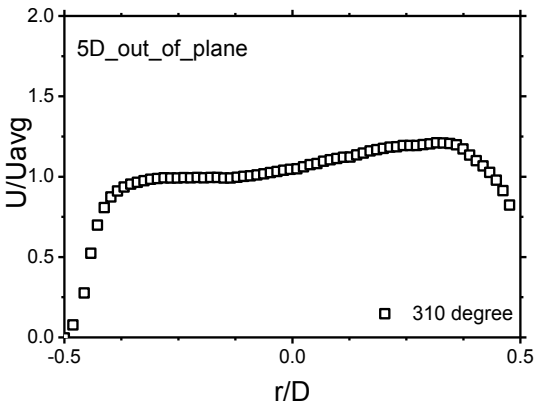

32) Velocity profile at 310 degree (5 D)

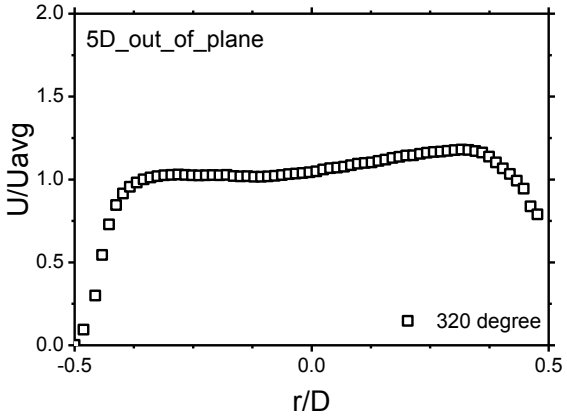

33) Velocity profile at 320 degree (5 D)

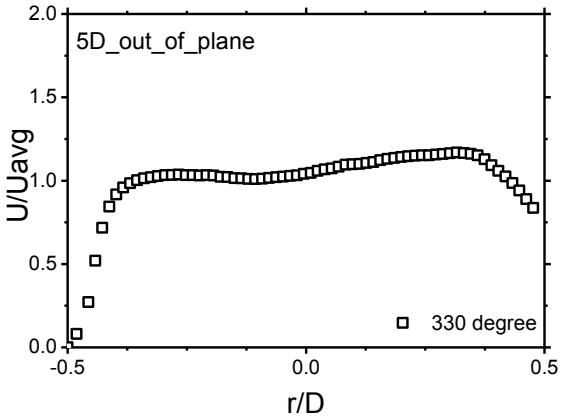

34) Velocity profile at 330 degree (5 D)

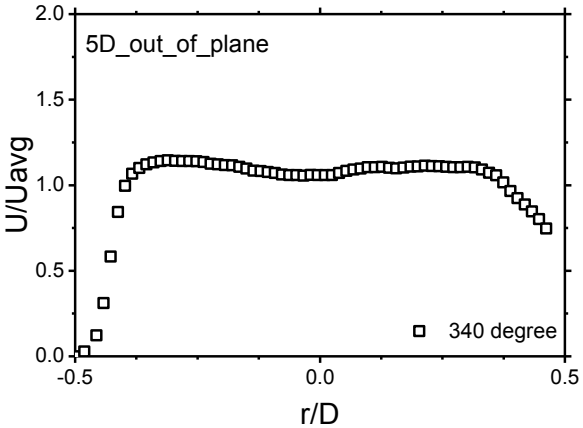

35) Velocity profile at 340 degree (5 D)

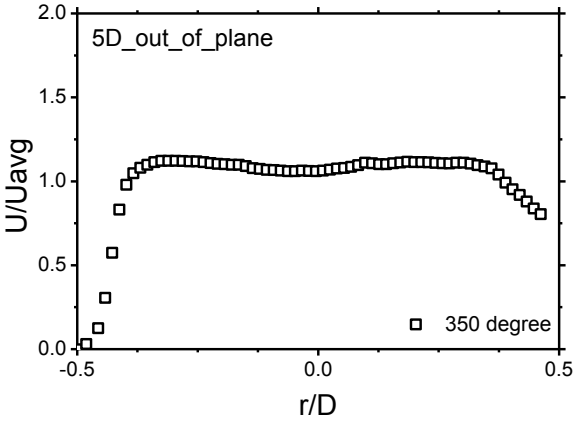

36) Velocity profile at 350 degree (5 D)

Fig. 6-17 Velocity profiles at 5D of out of plane double bent pipe 8 degree.

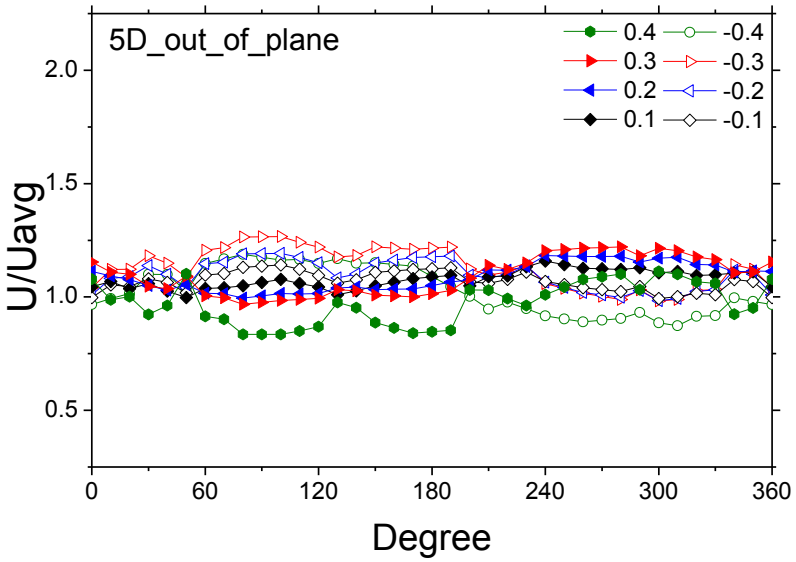

Fig. 6-18 Circumferential velocity profiles at 5D of out of plane double bent pipe 8 degree.

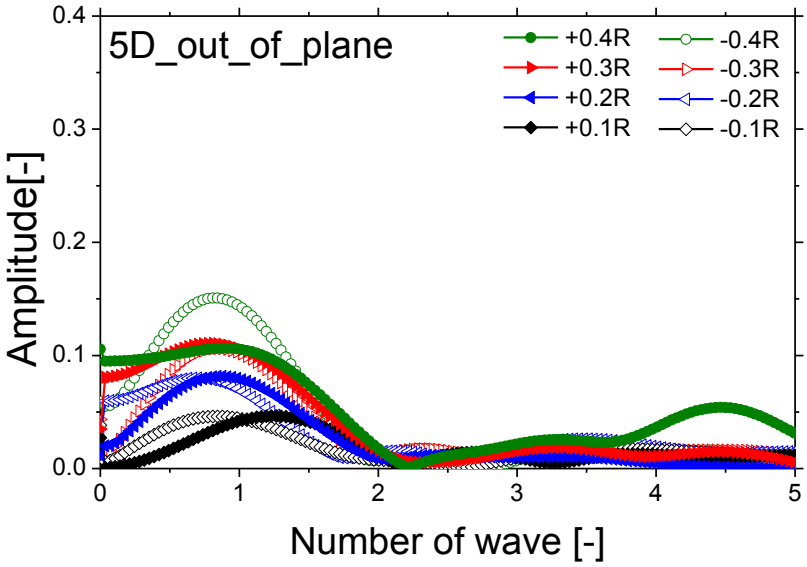

Fig. 6-19 FFT's results of circumferential velocity profiles at 5D out of plane angle 8 degree double bent pipe

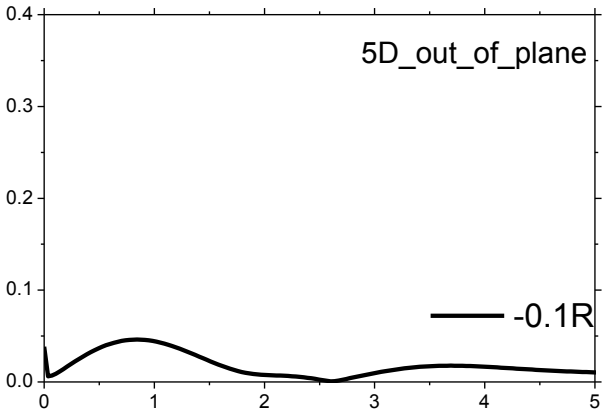

a) Number of waves from line -0.1 R (5 D)

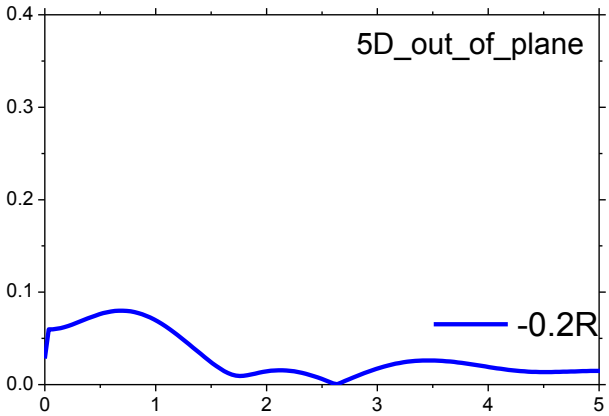

b) Number of waves from line -0.2 R (5 D)

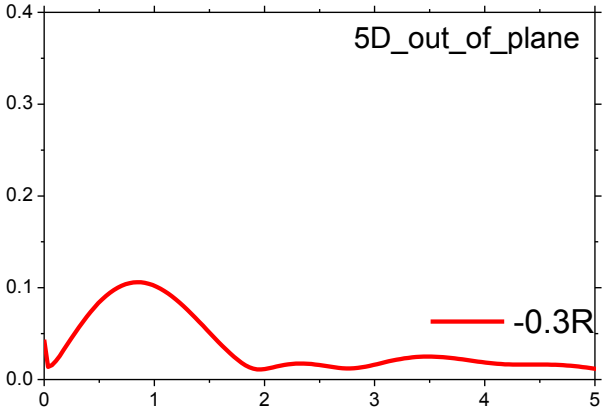

c) Number of waves from line -0.3 R (5 D)

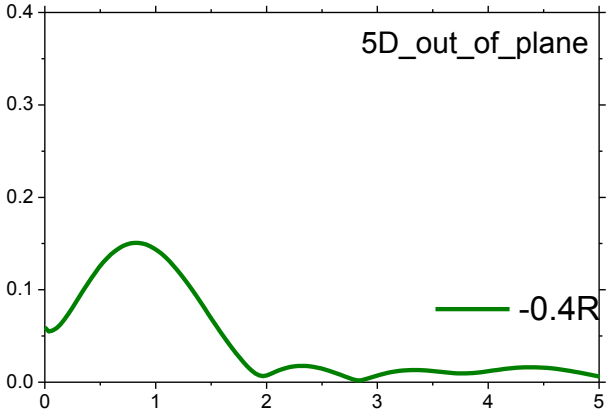

d) Number of waves from line -0.4 R (5 D)

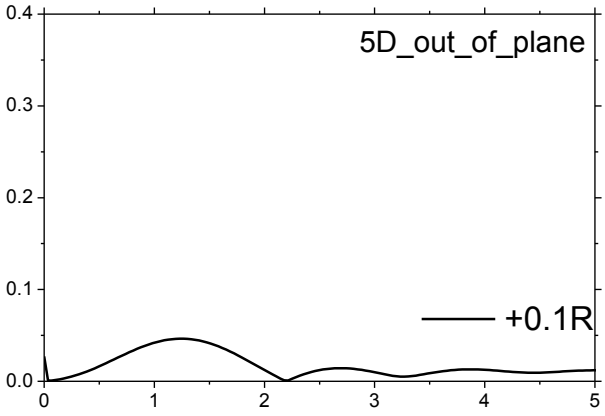

e) Number of waves from line +0.1 R (5 D)

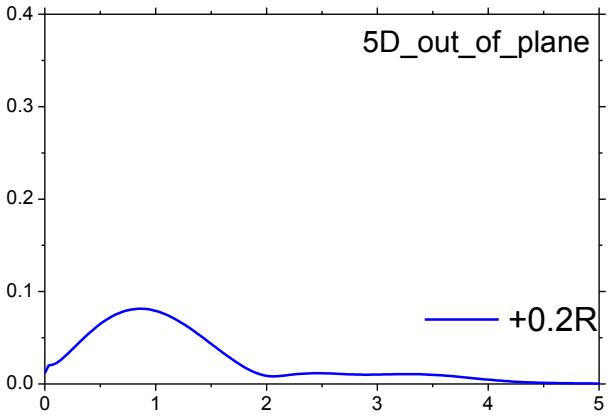

f) Number of waves from line +0.2 R (5 D)

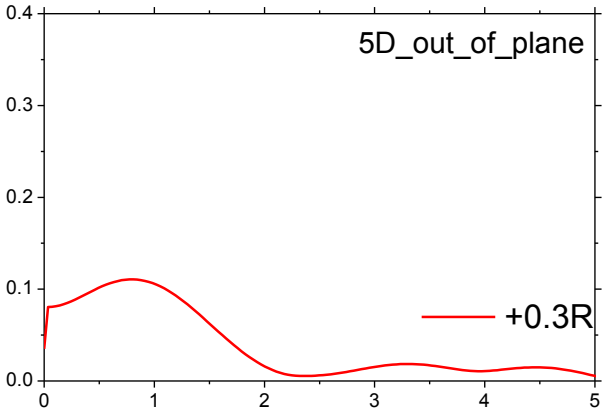

g) Number of waves from line +0.3 R (5 D)

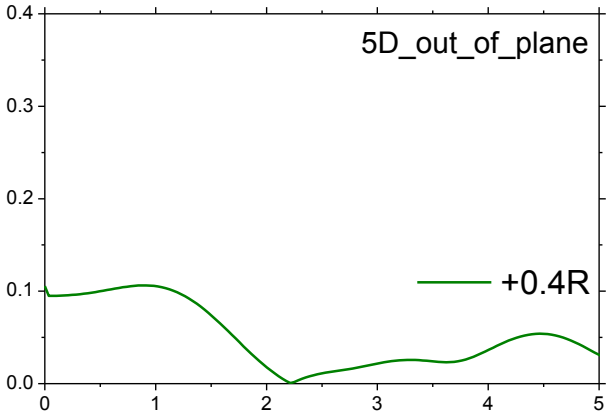

h) Number of waves from line +0.4 R (5 D)

At 3 D out of plane angle 16°

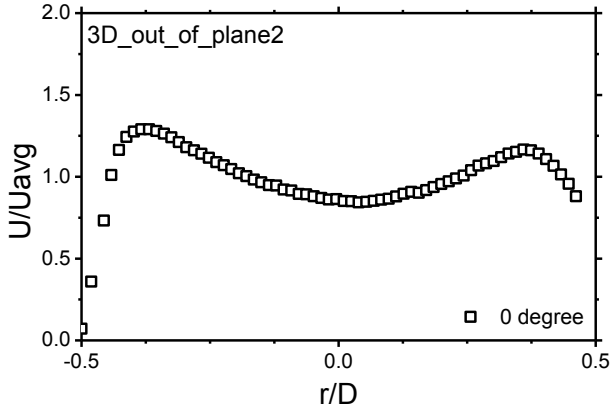

1) Velocity profile at 0 degree (3 D)

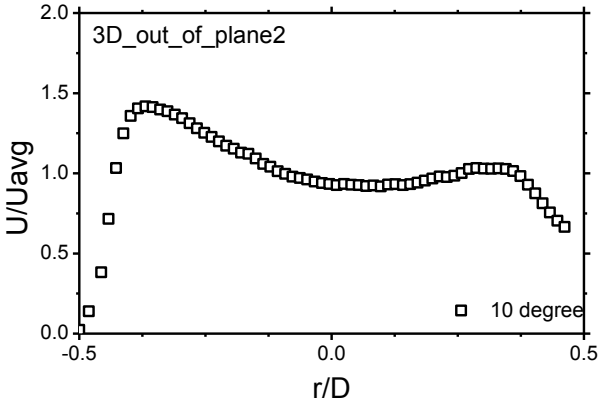

2) Velocity profile at 10 degree (3 D)

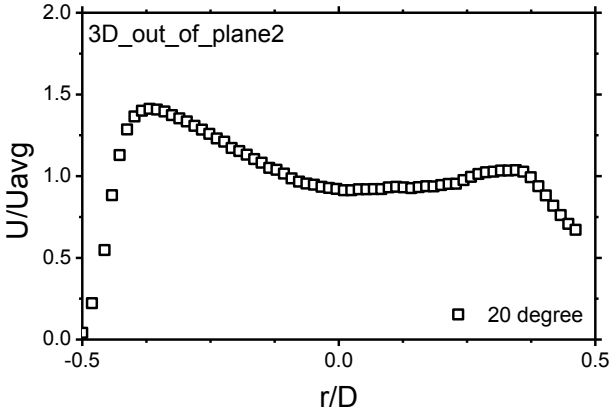

3) Velocity profile at 20 degree (3 D)

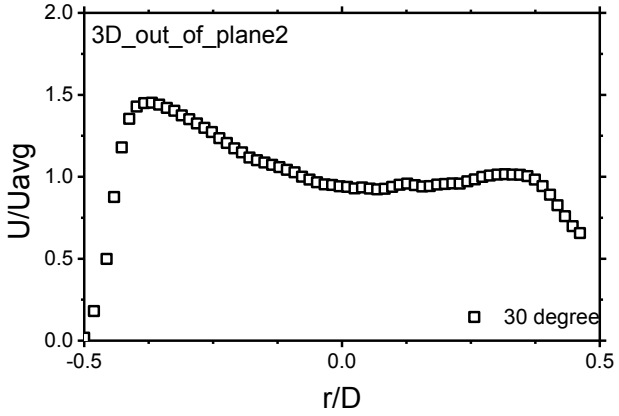

4) Velocity profile at 30 degree (3 D)

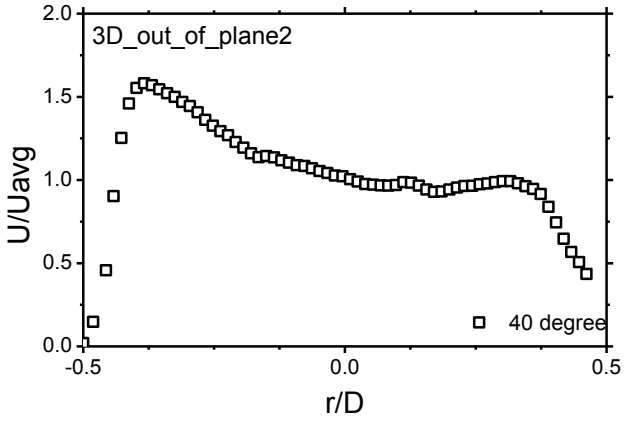

5) Velocity profile at 40 degree (3 D)

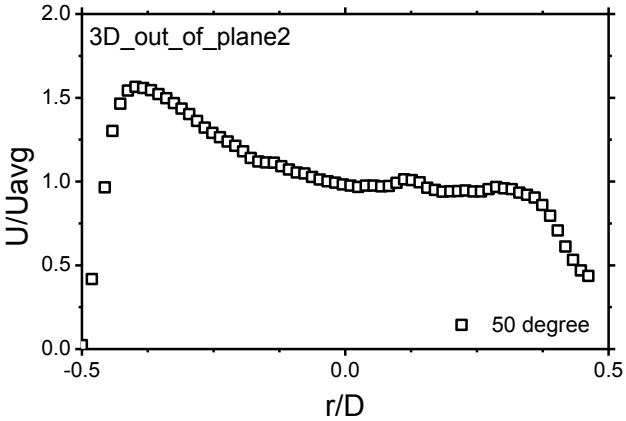

6) Velocity profile at 50 degree (3 D)

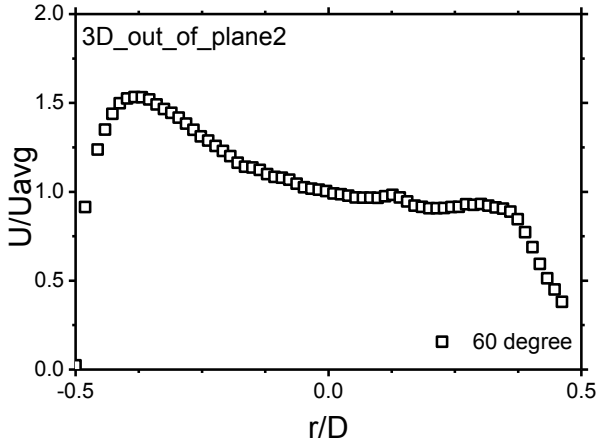

7) Velocity profile at 60 degree (3 D)

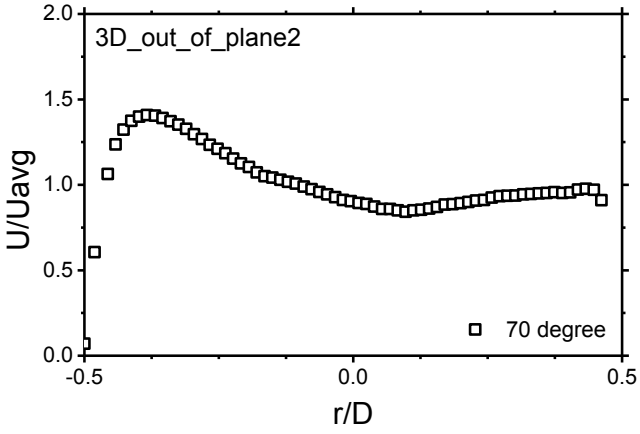

8) Velocity profile at 70 degree (3 D)

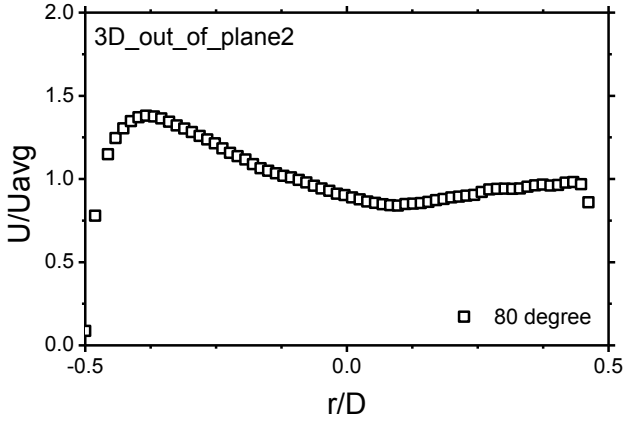

9) Velocity profile at 80 degree (3 D)

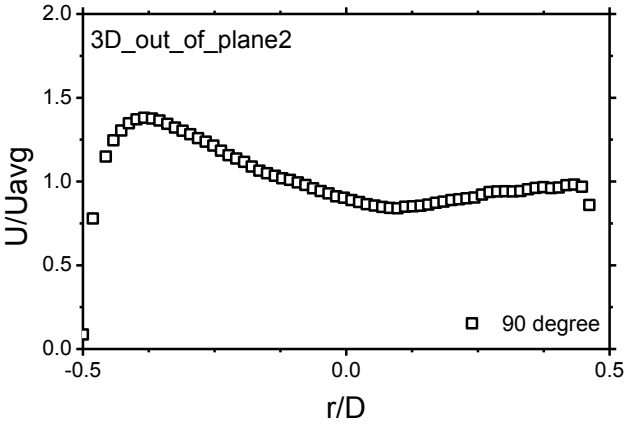

10) Velocity profile at 90 degree (3 D)

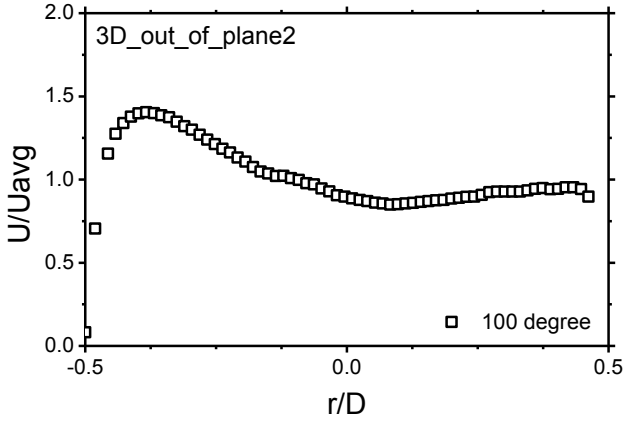

11) Velocity profile at 100 degree (3 D)

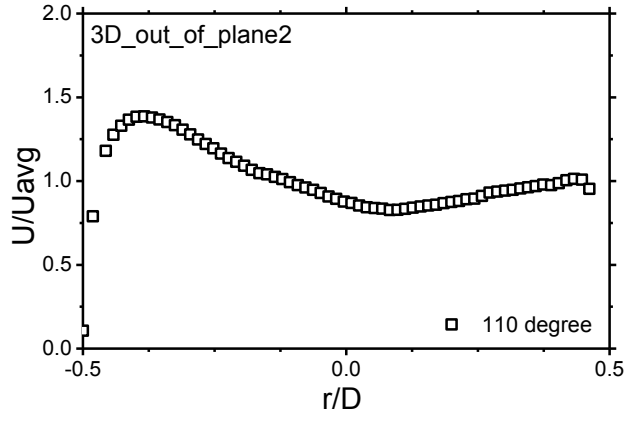

12) Velocity profile at 110 degree (3 D)

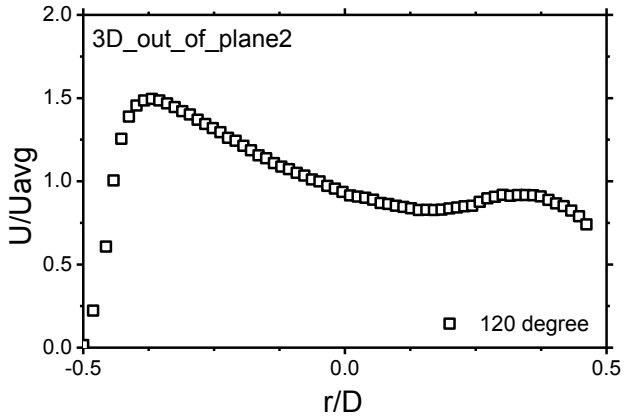

13) Velocity profile at 120 degree (3 D)

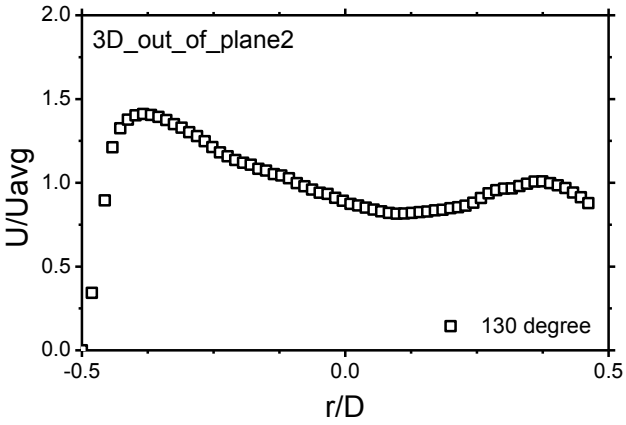

14) Velocity profile at 130 degree (3 D)

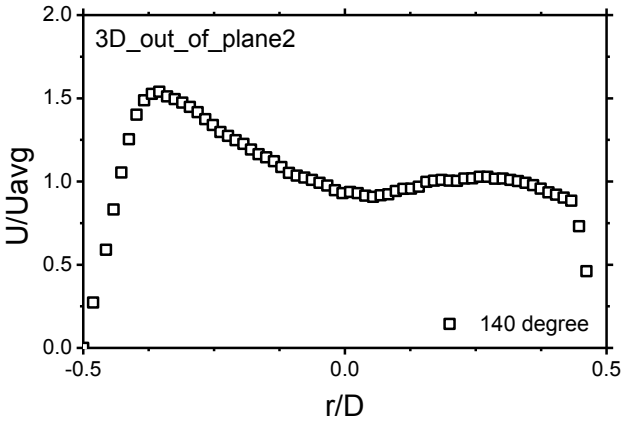

15) Velocity profile at 140 degree (3 D)

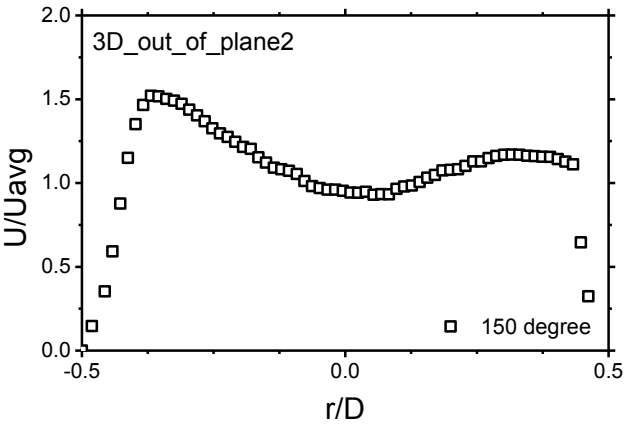

16) Velocity profile at 150 degree (3 D)

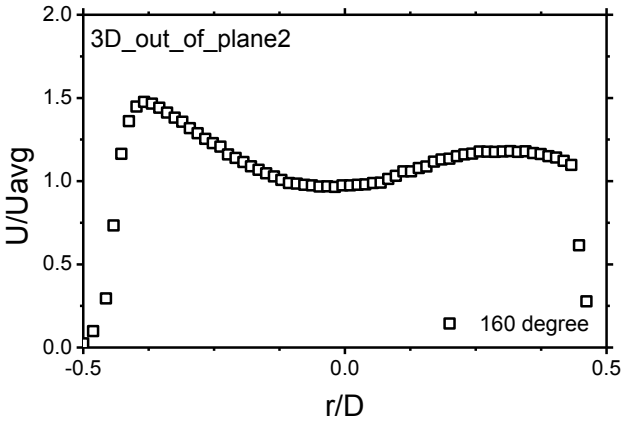

17) Velocity profile at 160 degree (3 D)

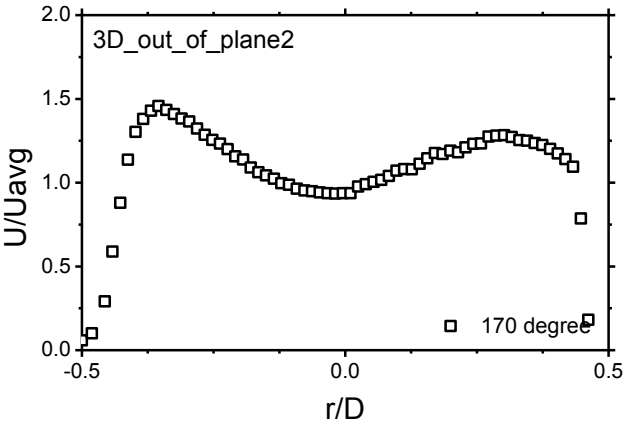

18) Velocity profile at 170 degree (3 D)

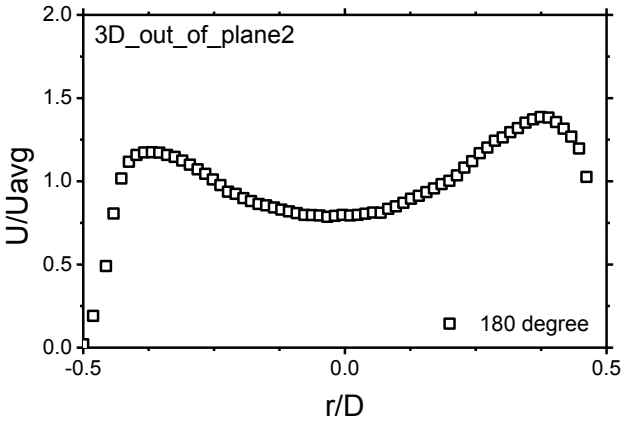

19) Velocity profile at 180 degree (3 D)

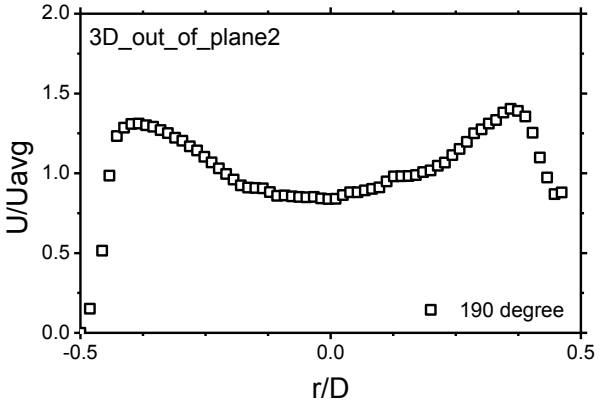

20) Velocity profile at 190 degree (3 D)

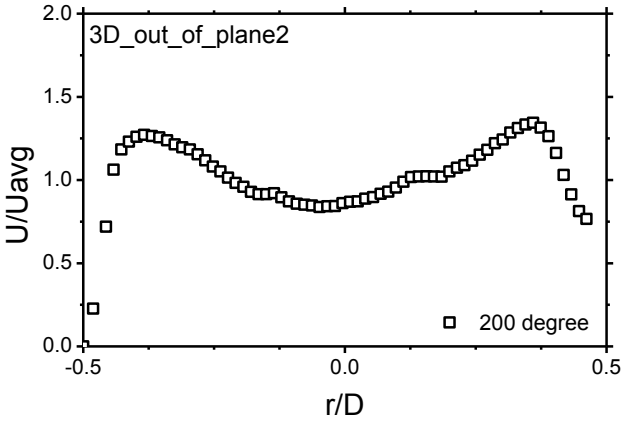

21) Velocity profile at 200 degree (3 D)

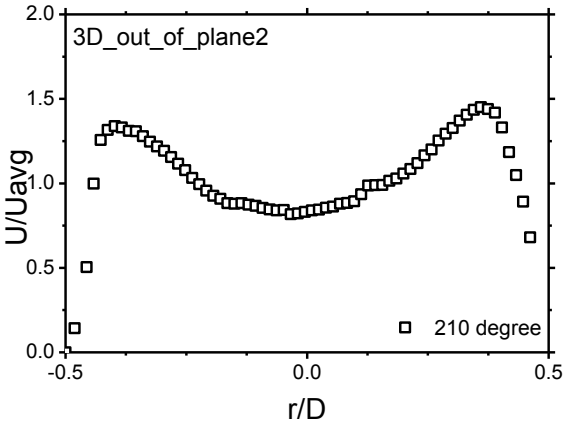

22) Velocity profile at 210 degree (3 D)

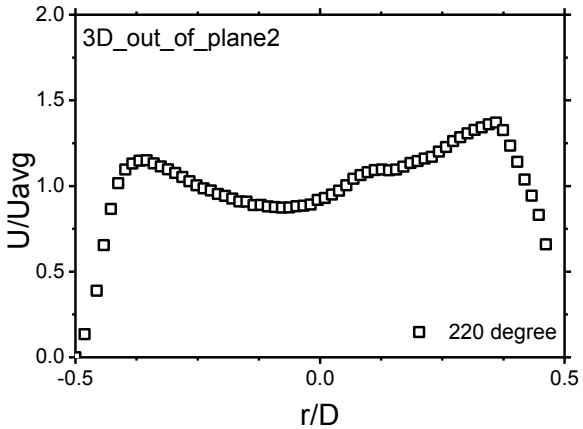

23) Velocity profile at 220 degree (3 D)

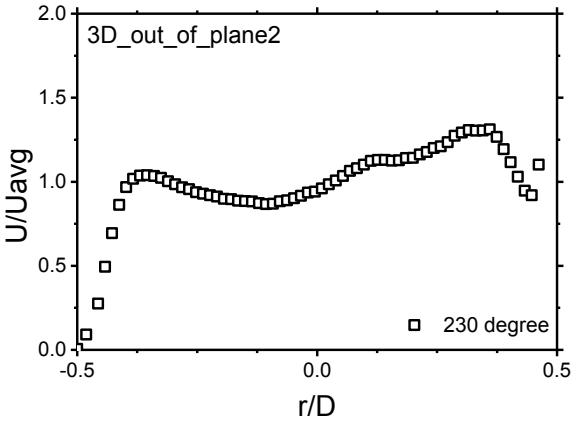

24) Velocity profile at 230 degree (3 D)

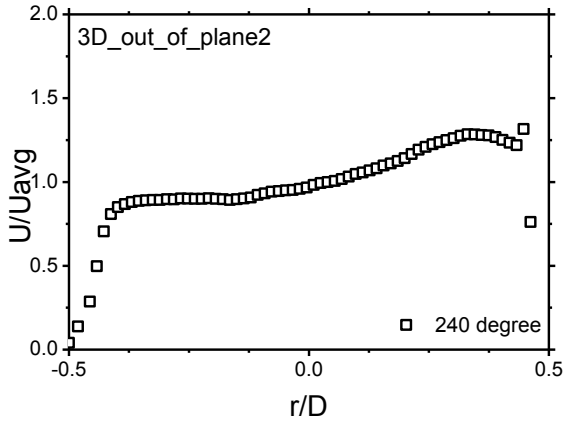

25) Velocity profile at 240 degree (3 D)

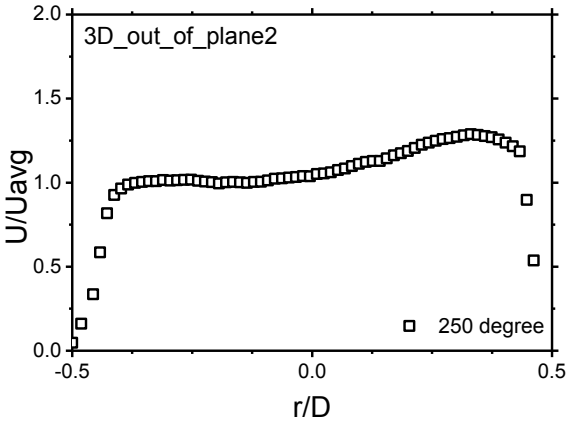

26) Velocity profile at 250 degree (3 D)

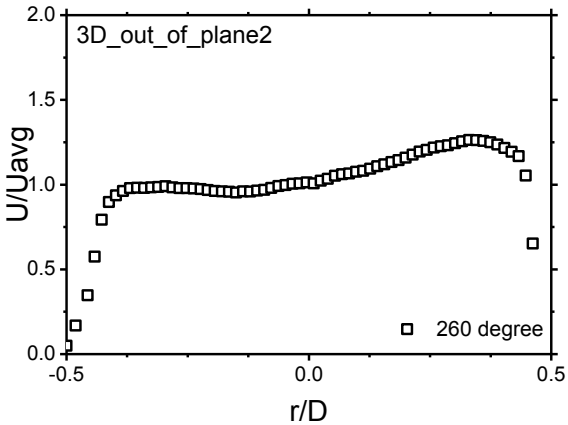

27) Velocity profile at 260 degree (3 D)

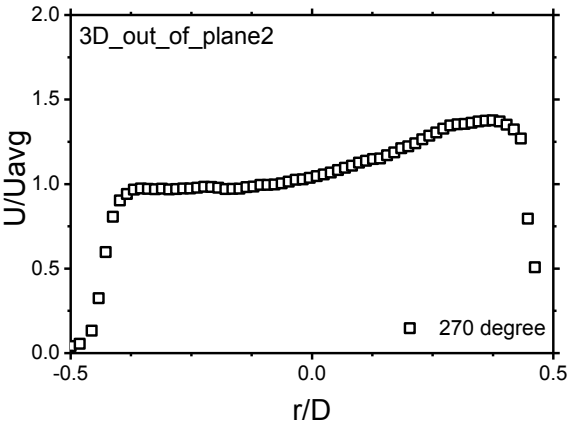

28) Velocity profile at 270 degree (3 D)

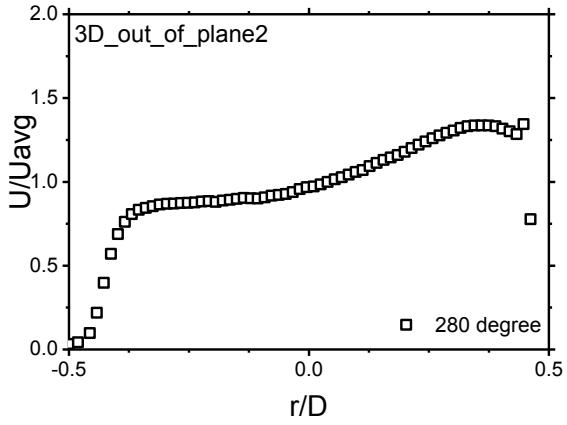

29) Velocity profile at 280 degree (3 D)

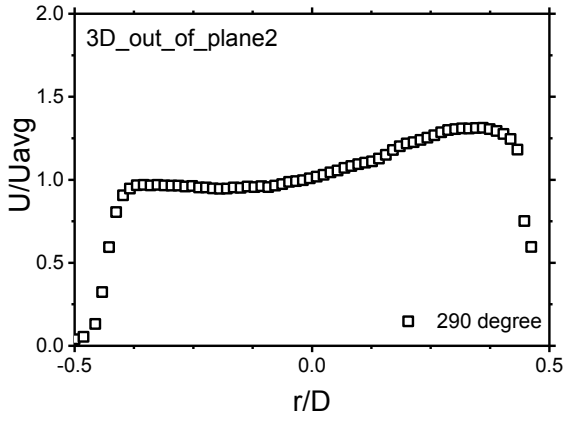

30) Velocity profile at 290 degree (3 D)

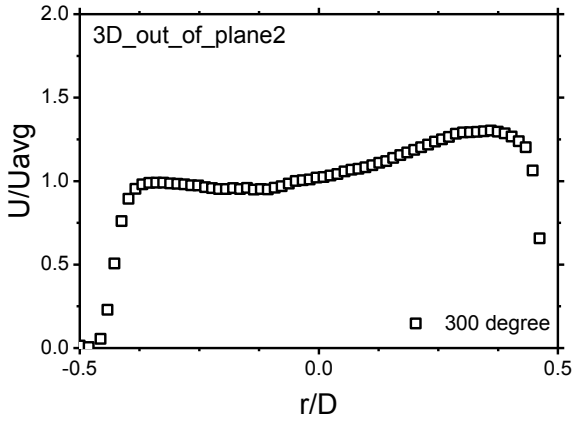

31) Velocity profile at 300 degree (3 D)

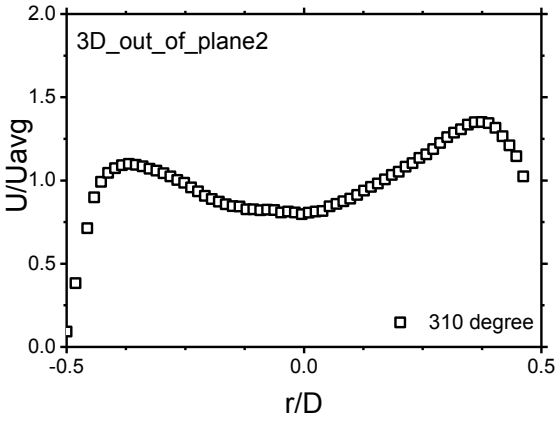

32) Velocity profile at 310 degree (3 D)

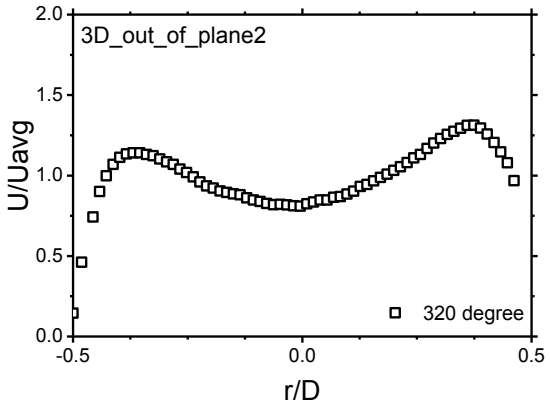

33) Velocity profile at 320 degree (3 D)

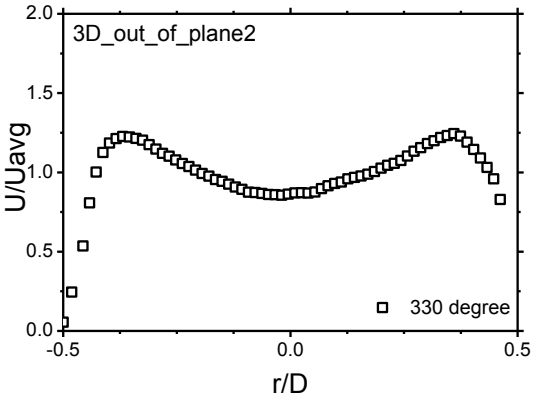

34) Velocity profile at 330 degree (3 D)

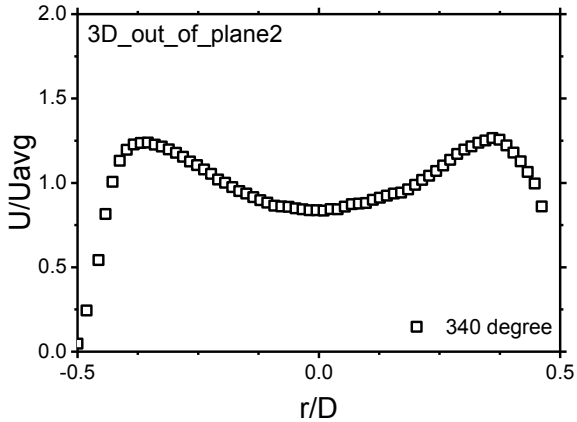

35) Velocity profile at 340 degree (3 D)

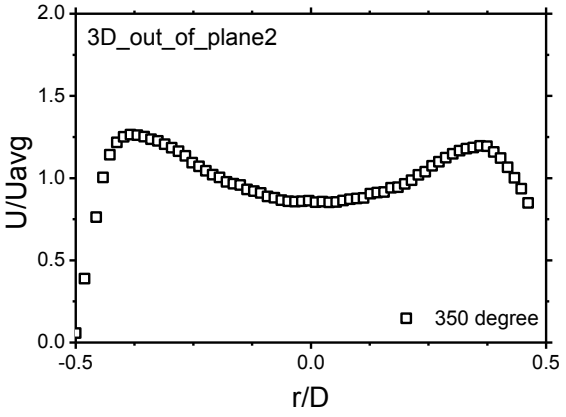

36) Velocity profile at 350 degree (3 D)

Fig. 6-20 Velocity profile at 3D of out of plane angle 16 degree double bent pipe.

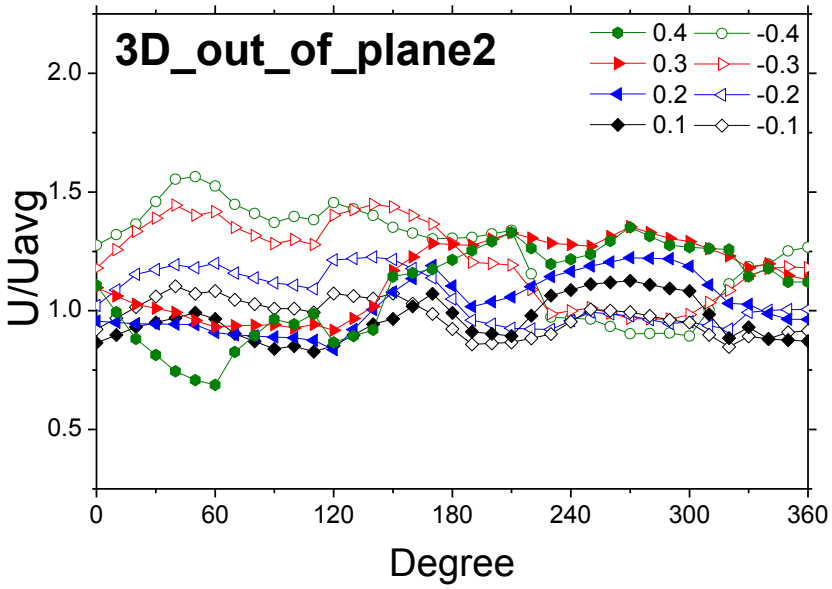

Fig. 6-21 Circumferential velocity profile at 3D of out of plane angle 16 degree double bent pipe.

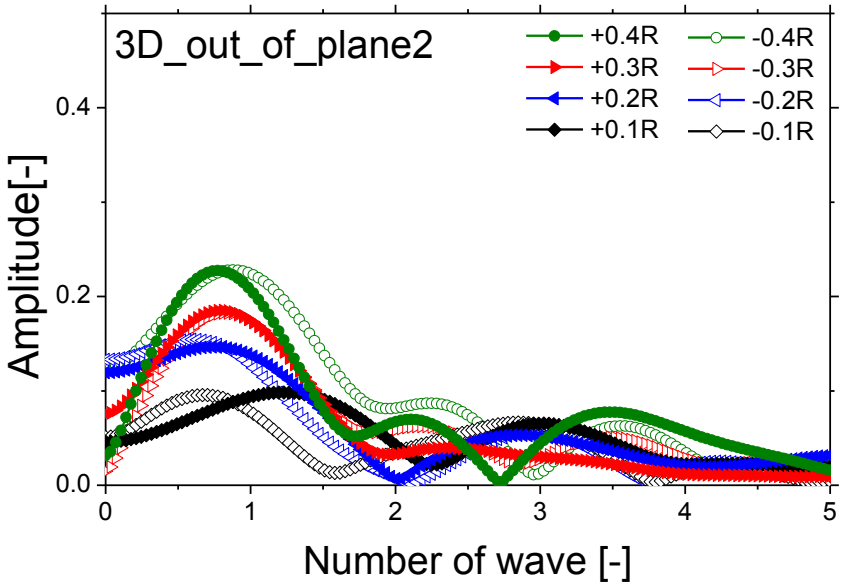

Fig. 6-22 FFT's results of Circumferential velocity profile at 3D of out of plane angle 16 degree double bent pipe.

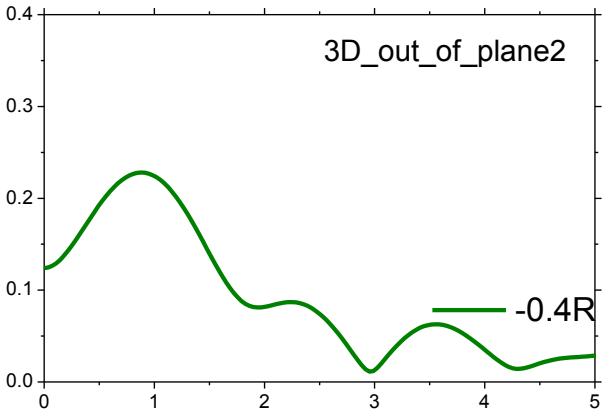

a) Number of waves from line -0.4 R (3 D)

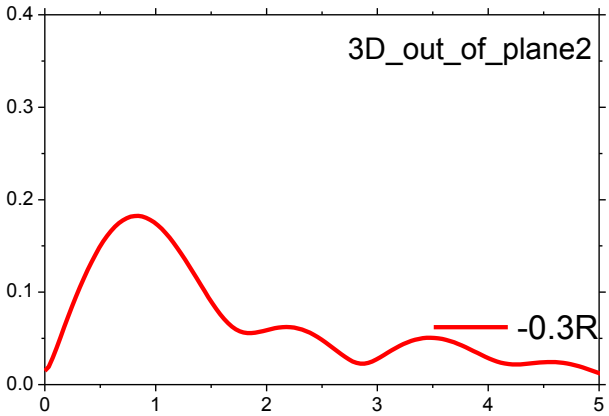

b) Number of waves from line -0.3 R (3 D)

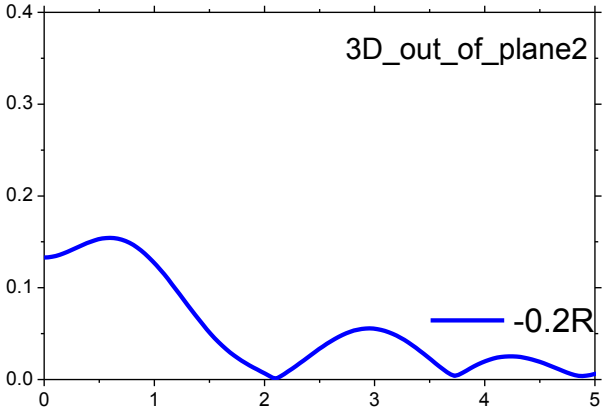

c) Number of waves from line -0.2 R (3 D)

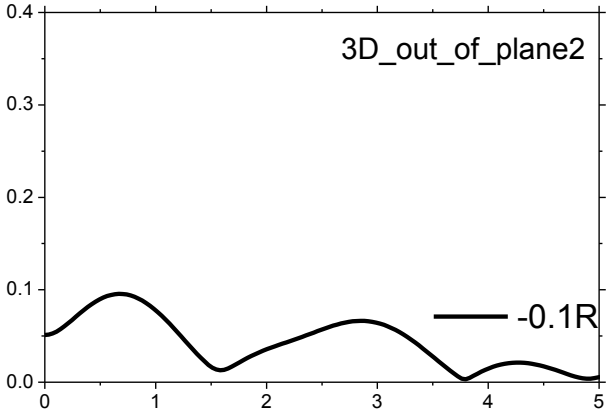

d) Number of waves from line -0.1 R (3 D)

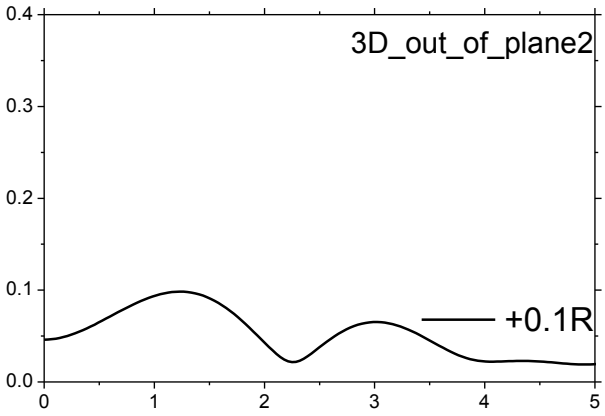

e) Number of waves from line +0.1 R (3 D)

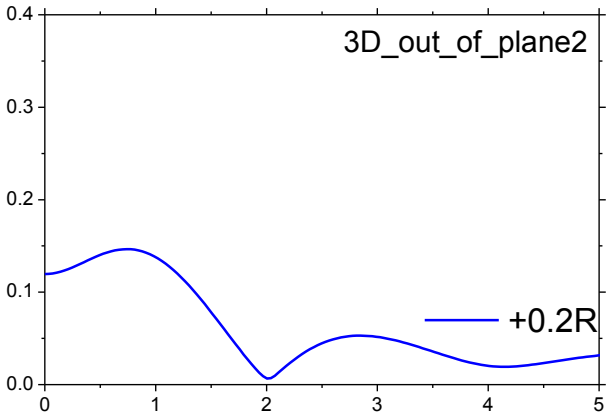

f) Number of waves from line +0.2 R (3 D)

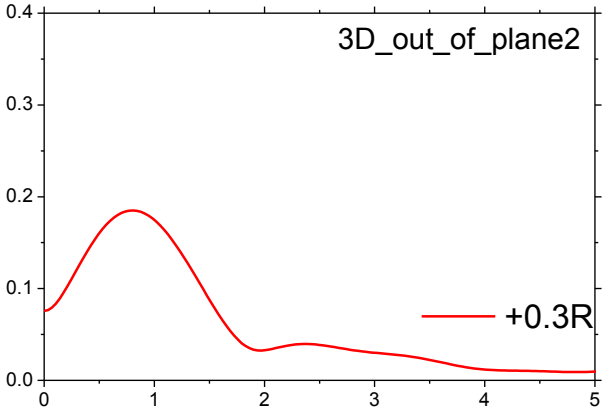

i) Number of waves from line +0.3 R (3 D)

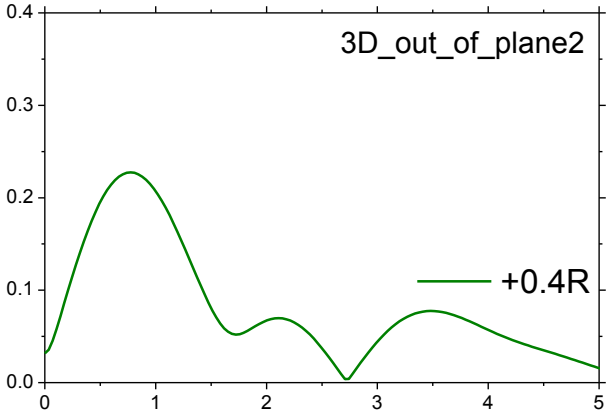

j) Number of waves from line +0.4 R (3 D)

At 4 D out of plane angle is 16°

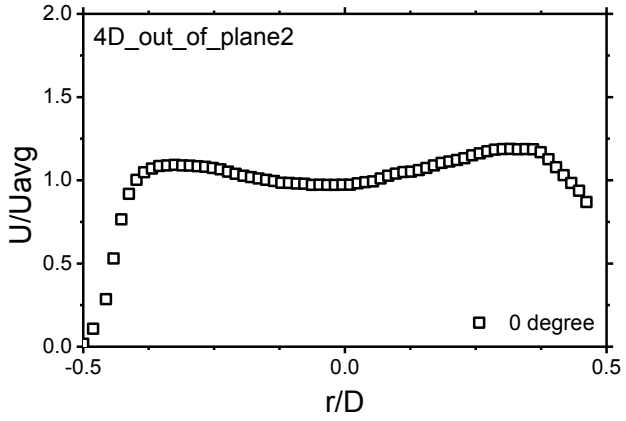

1) Velocity profile at 0 degree (4 D)

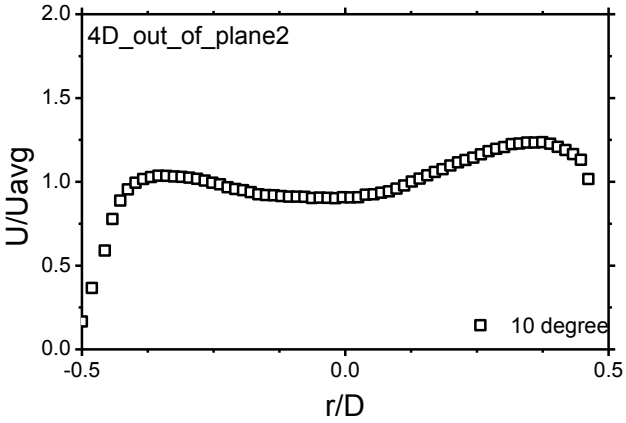

2) Velocity profile at 10 degree (4 D)

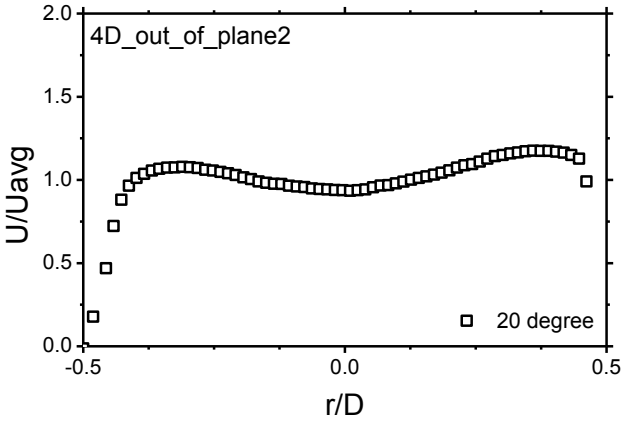

3) Velocity profile at 20 degree (4 D)

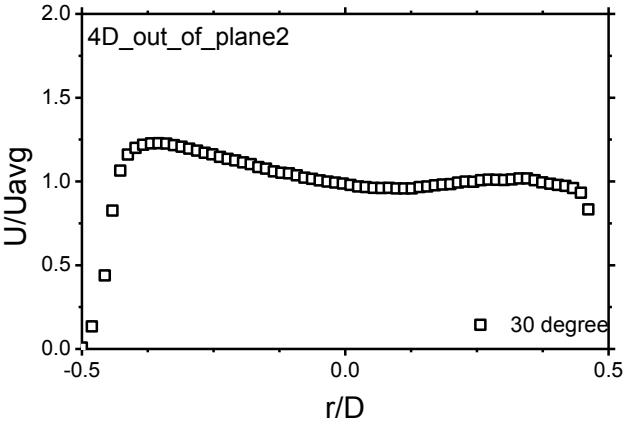

4) Velocity profile at 30 degree (4 D)

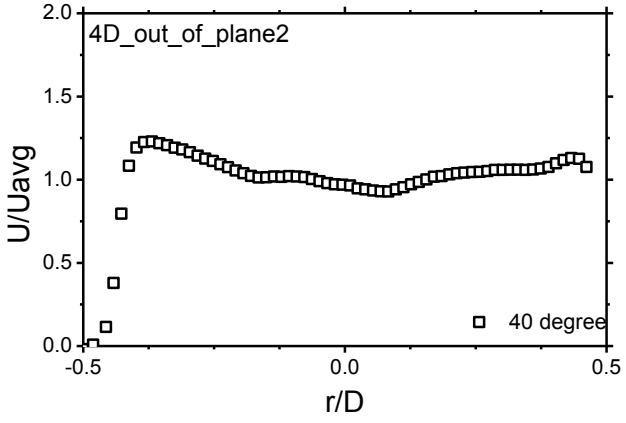

5) Velocity profile at 40 degree (4 D)

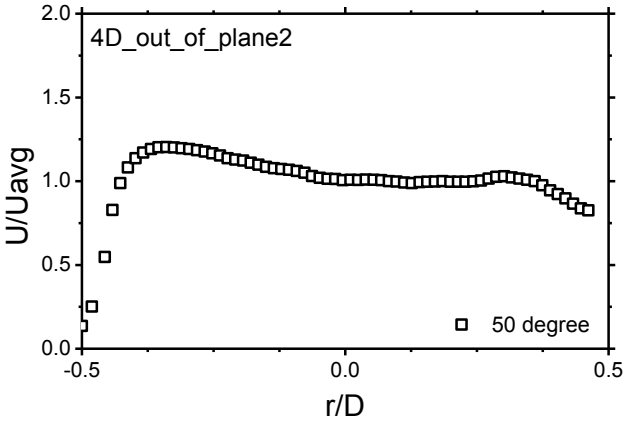

6) Velocity profile at 50 degree (4 D)

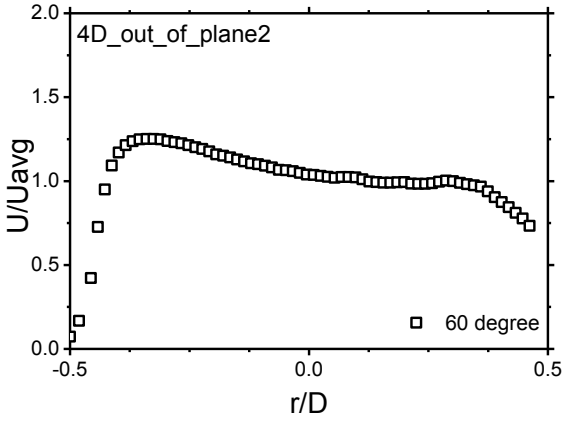

7) Velocity profile at 60 degree (4 D)

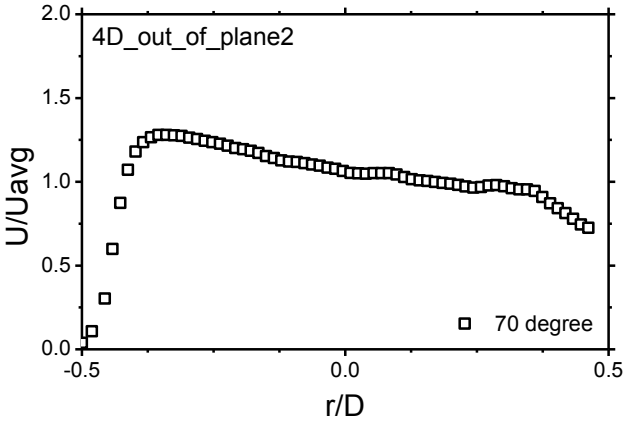

8) Velocity profile at 70 degree (4 D)

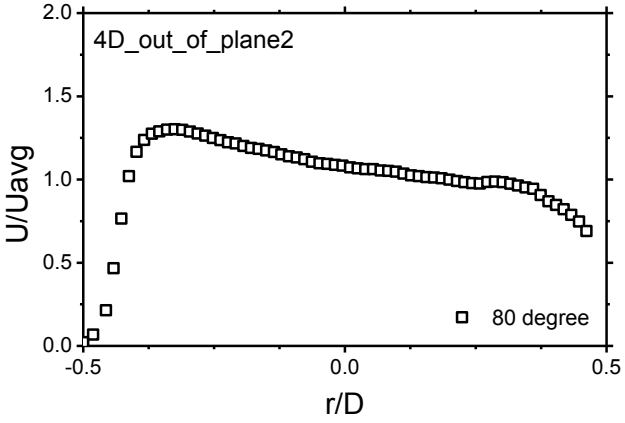

9) Velocity profile at 80 degree (4 D)

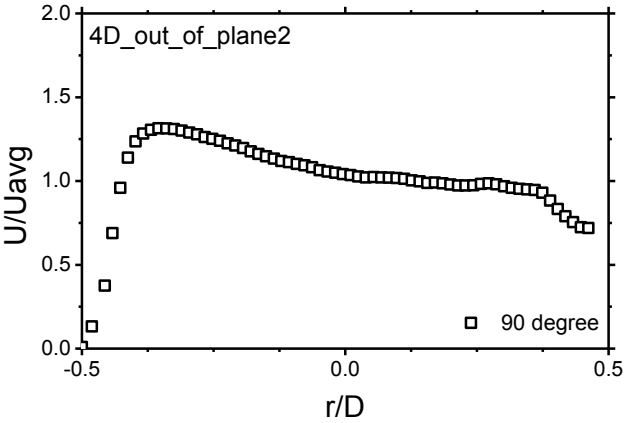

10) Velocity profile at 90 degree (4 D)

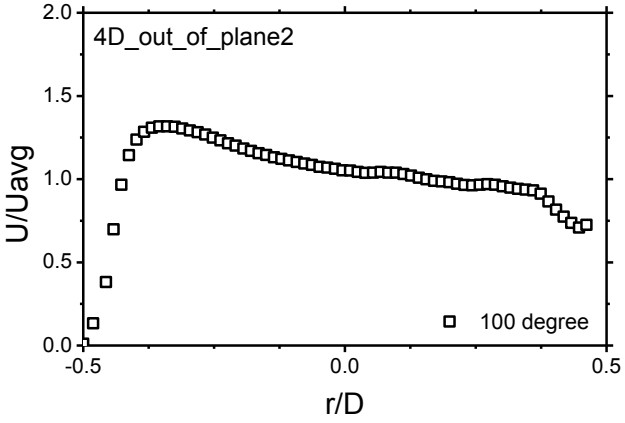

11) Velocity profile at 100 degree (4 D)

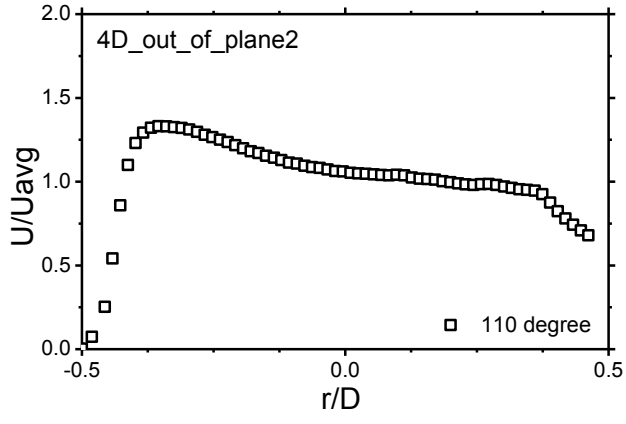

12) Velocity profile at 110 degree (4 D)

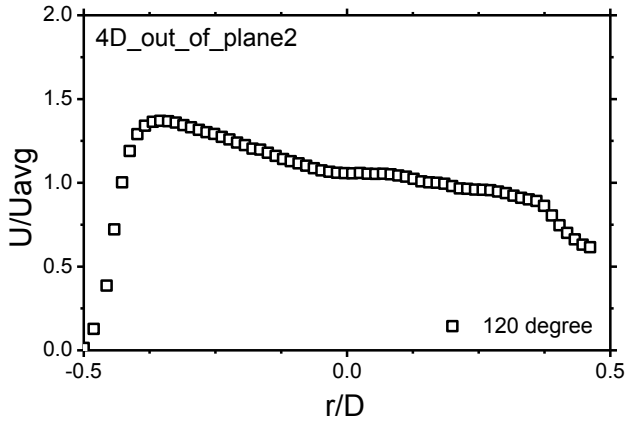

13) Velocity profile at 120 degree (4 D)

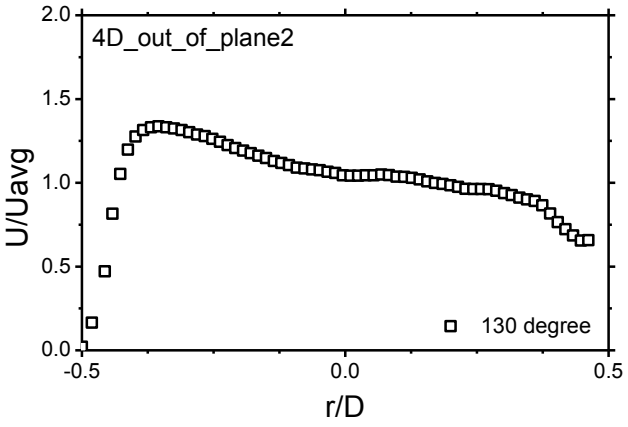

14) Velocity profile at 130 degree (4 D)

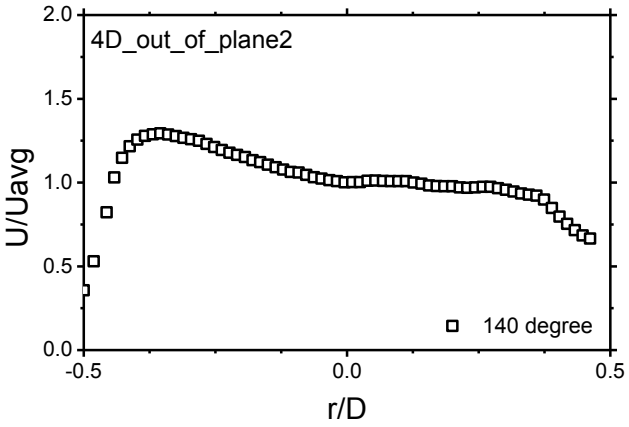

15) Velocity profile at 140 degree (4 D)

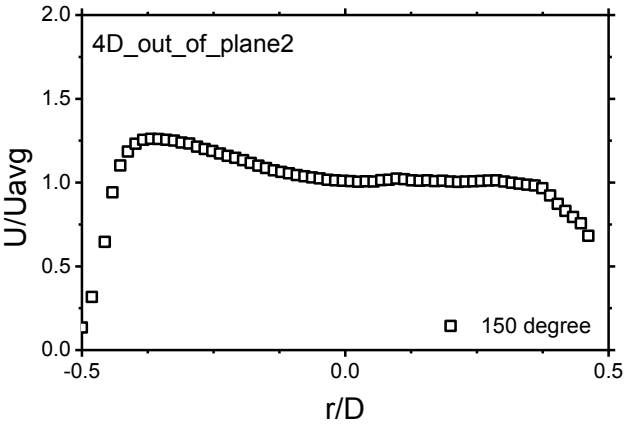

16) Velocity profile at 150 degree (4 D)

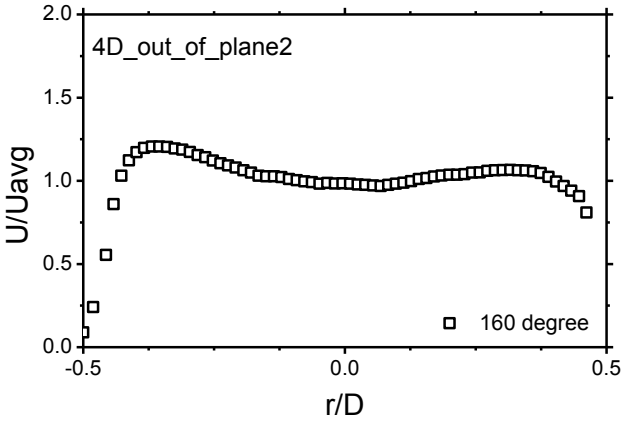

17) Velocity profile at 160 degree (4 D)

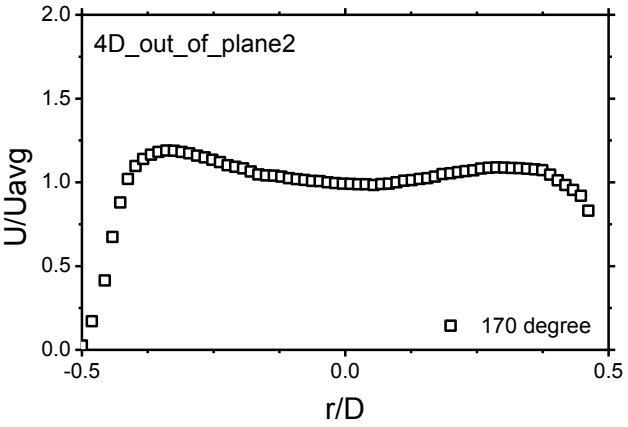

18) Velocity profile at 170 degree (4 D)

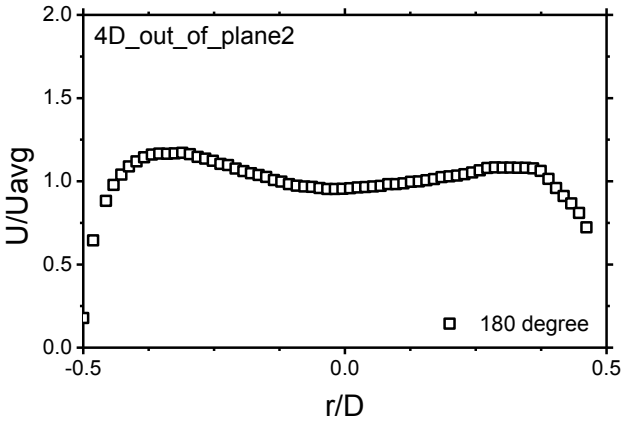

19) Velocity profile at 180 degree (4 D)

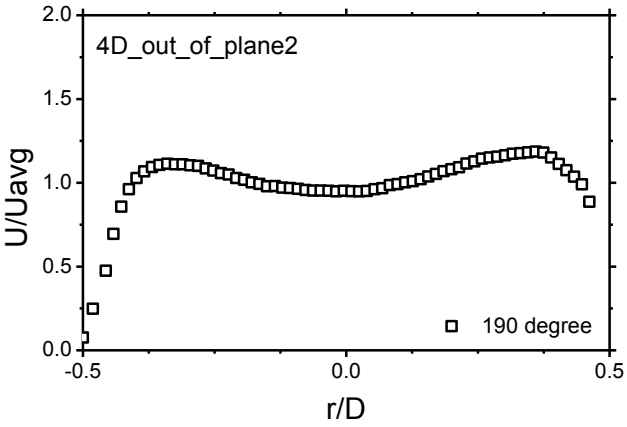

20) Velocity profile at 190 degree (4 D)

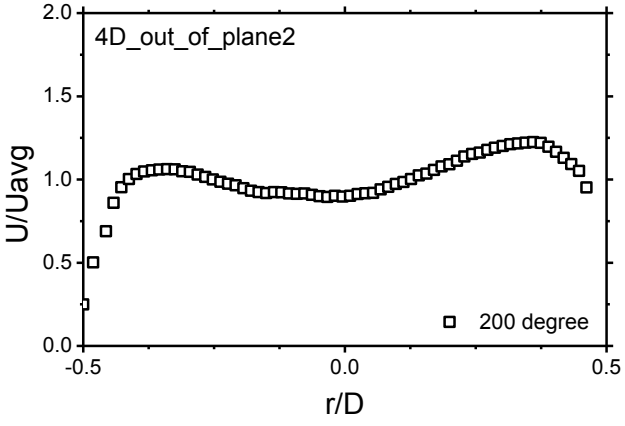

21) Velocity profile at 200 degree (4 D)

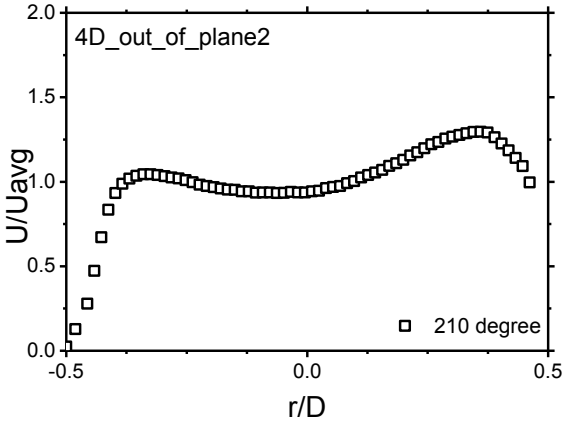

22) Velocity profile at 210 degree (4 D)

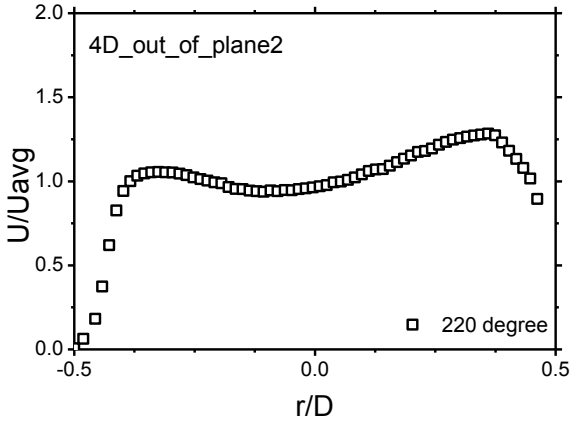

23) Velocity profile at 220 degree (4 D)

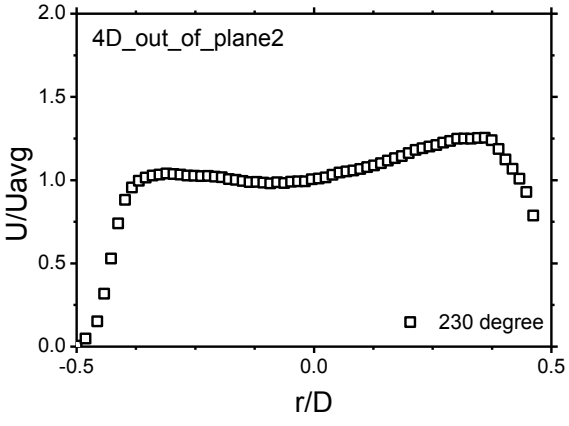

24) Velocity profile at 230 degree (4 D)

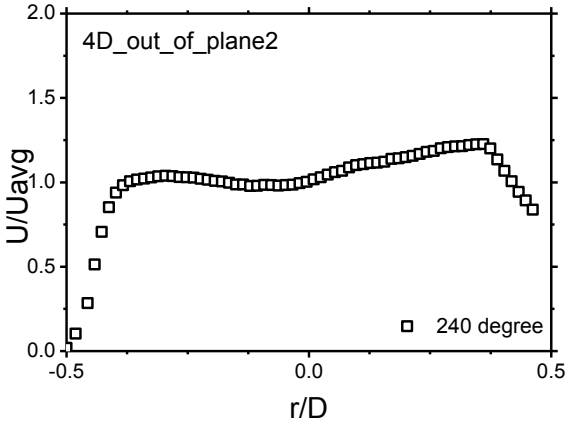

25) Velocity profile at 240 degree (4 D)

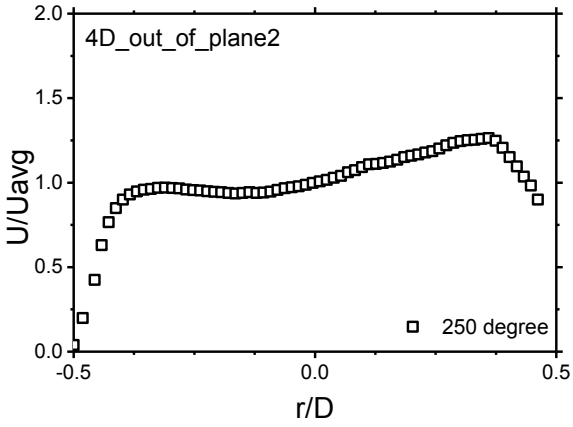

26) Velocity profile at 250 degree (4 D)

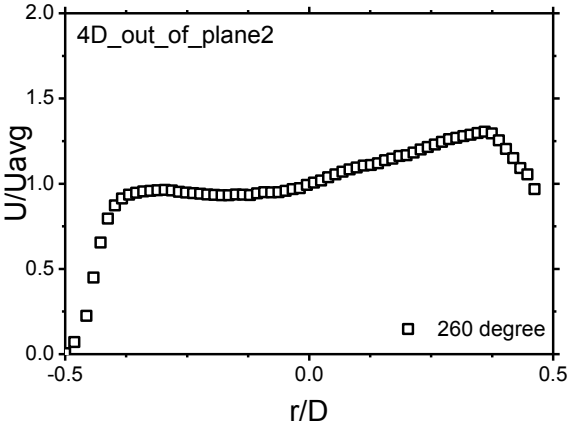

27) Velocity profile at 260 degree (4 D)

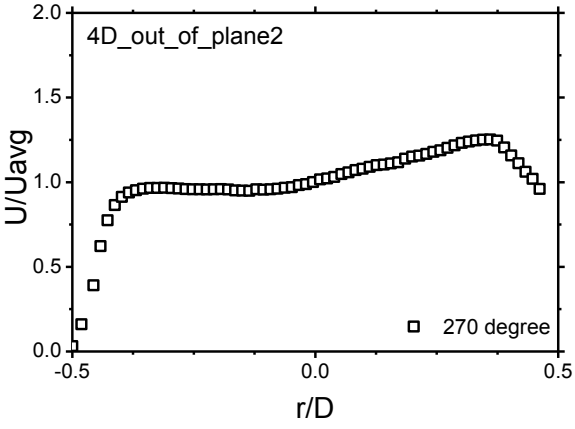

28) Velocity profile at 270 degree (4 D)

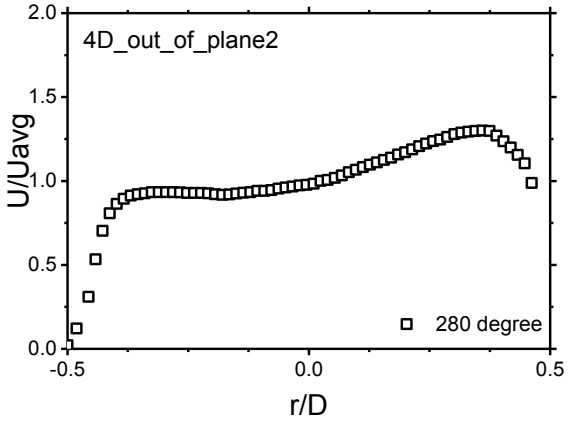

29) Velocity profile at 280 degree (4 D)

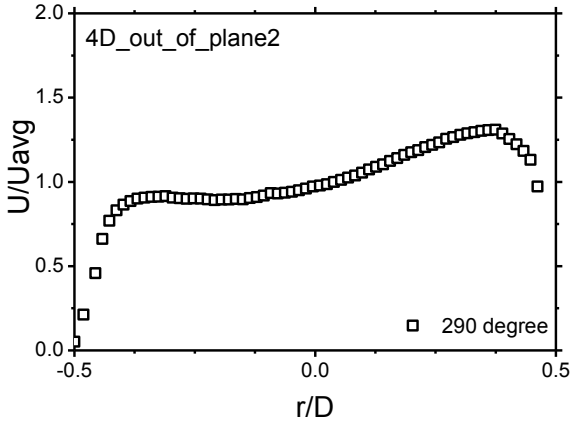

30) Velocity profile at 290 degree (4 D)

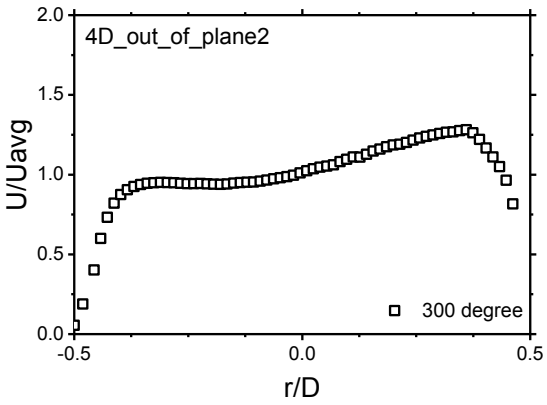

31) Velocity profile at 300 degree (4 D)

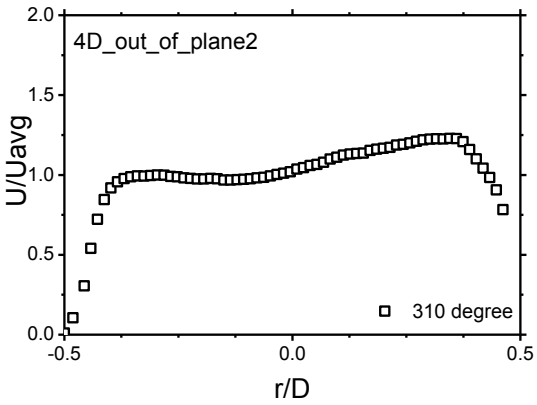

32) Velocity profile at 310 degree (4 D)

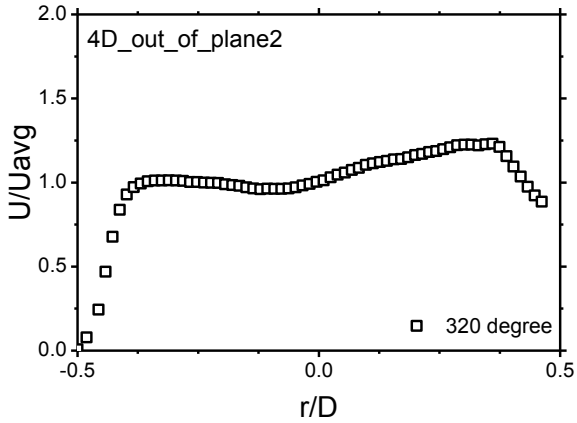

33) Velocity profile at 320 degree (4 D)

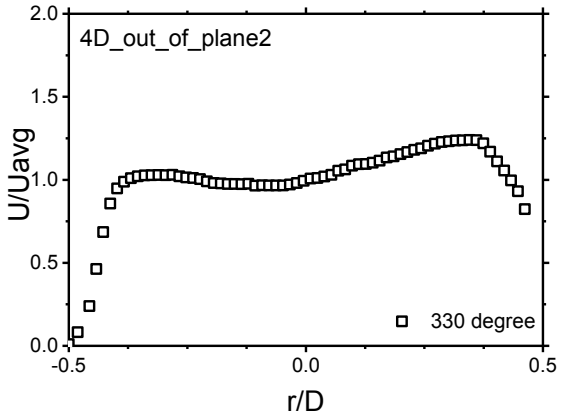

34) Velocity profile at 330 degree (4 D)

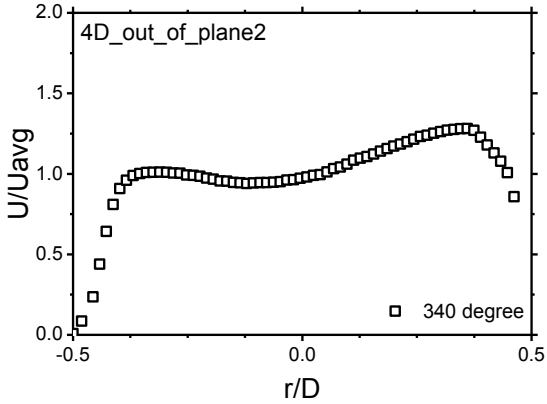

35) Velocity profile at 340 degree (4 D)

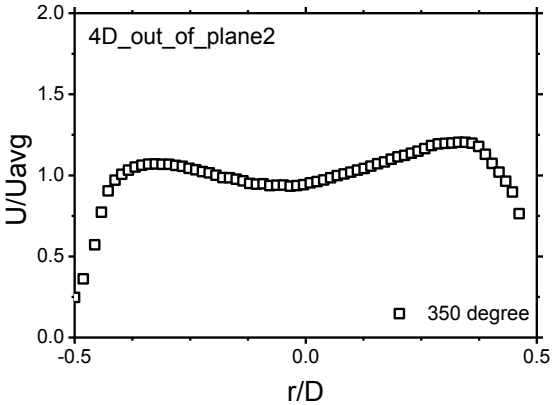

36) Velocity profile at 350 degree (4 D)

Fig. 6-23 Velocity profile at 4D of out of plane angle 16 degree double bent pipe.

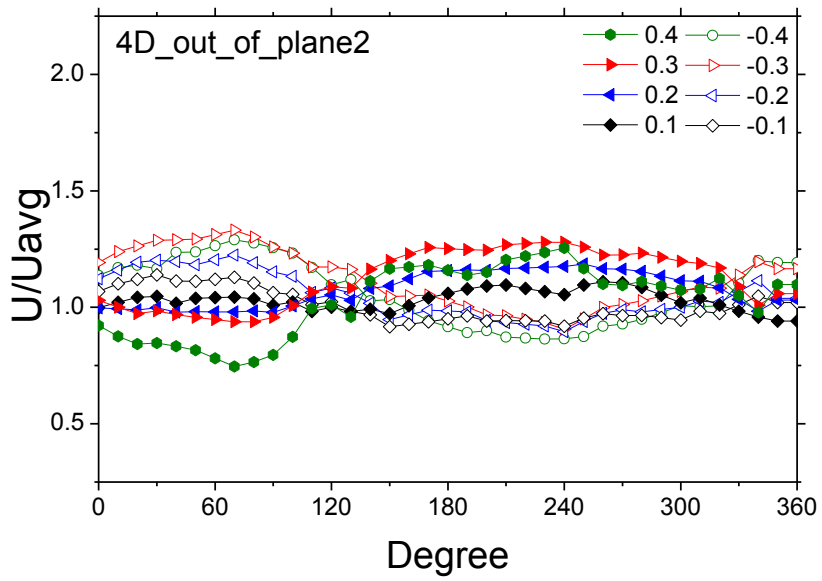

Fig. 6-24 Circumferential velocity profile at 4D of out of plane angle 16 degree double bent pipe.

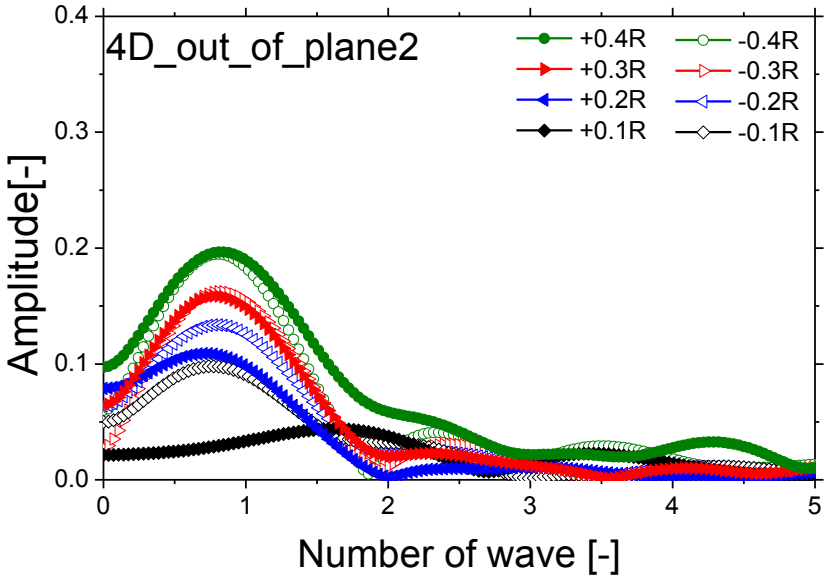

Fig. 6-25 FFT's results of circumferential velocity profile at 4D of out of plane angle 16 degree double bent pipe.

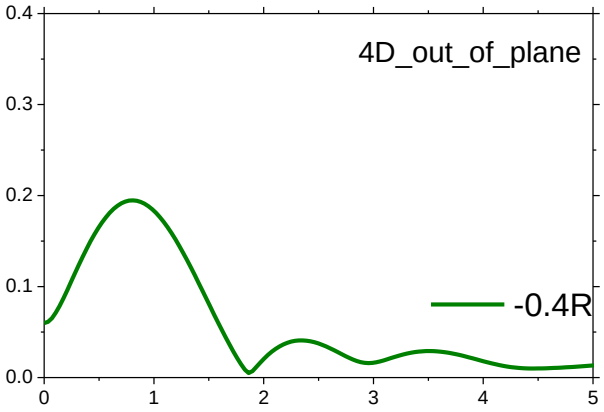

a) Number of waves from line -0.4 R (4 D)

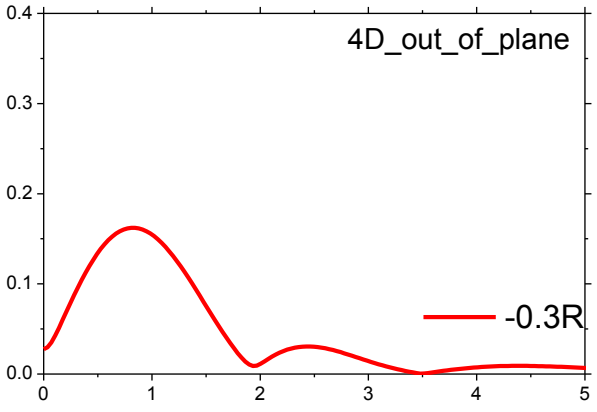

b) Number of waves from line -0.3 R (4 D)

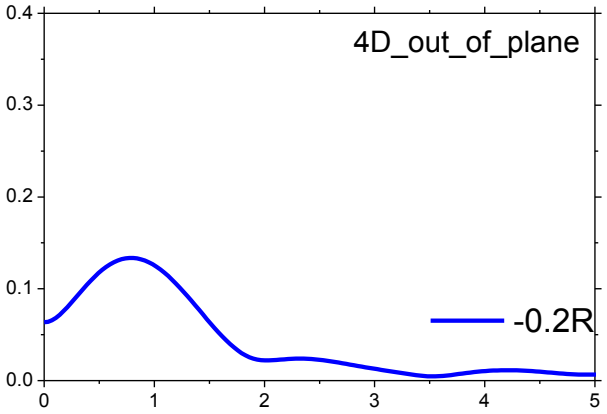

c) Number of waves from line -0.2 R (4 D)

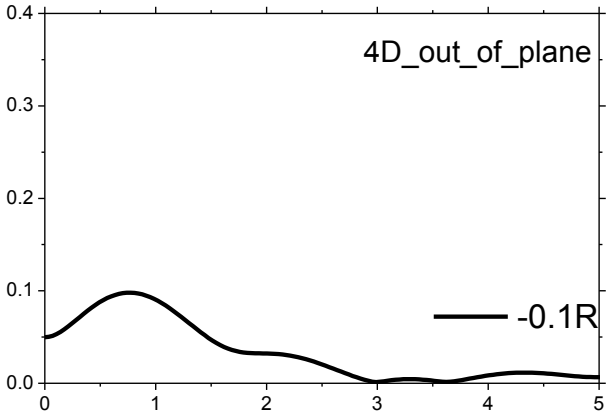

d) Number of waves from line -0.1 R (4 D)

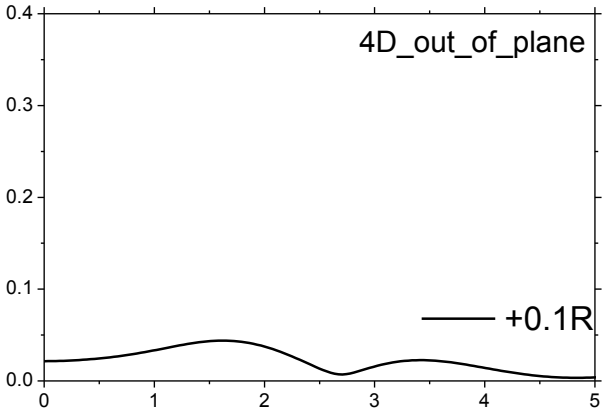

e) Number of waves from line +0.1 R (4 D)

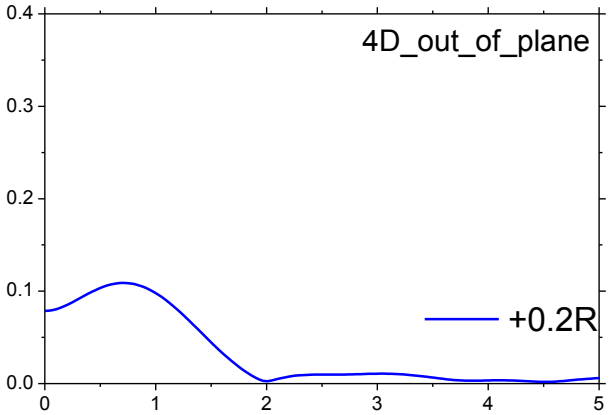

f) Number of waves from line +0.2 R (4 D)

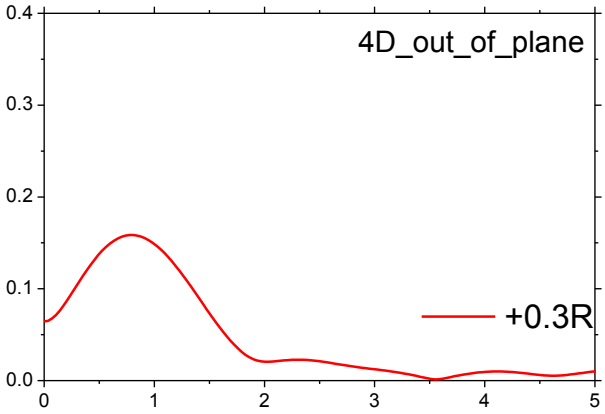

g) Number of waves from line +0.3 R (4 D)

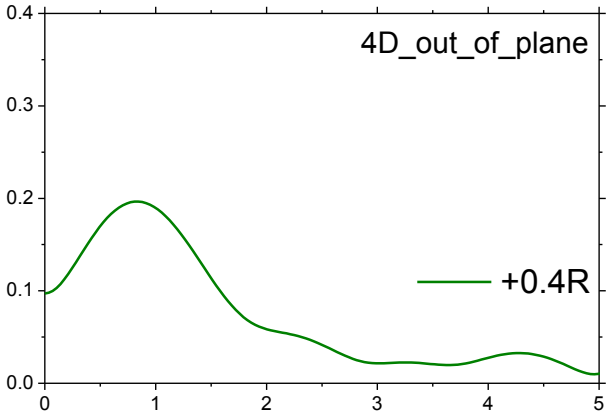

h) Number of waves from line +0.4 R (4 D)

Fig. 6-26 FFT's results of circumferential velocity profile at 4D of out of plane angle 16 degree double bent pipe.

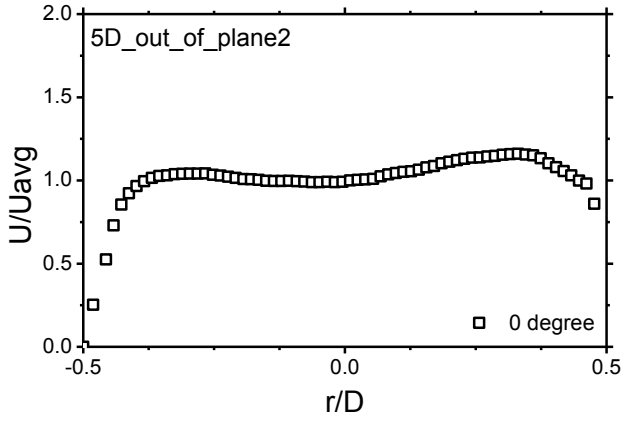

1) Velocity profile at 0 degree (5 D)

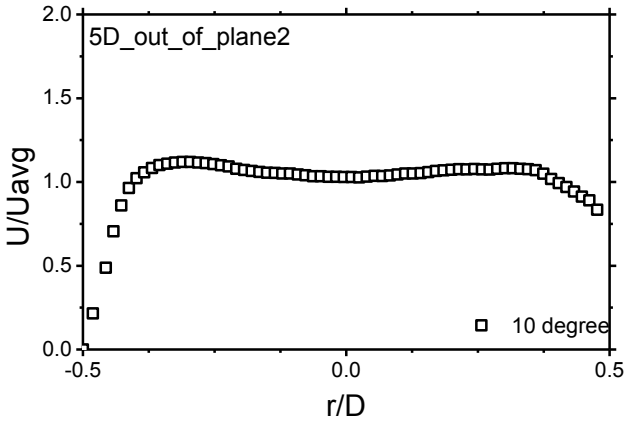

2) Velocity profile at 10 degree (5 D)

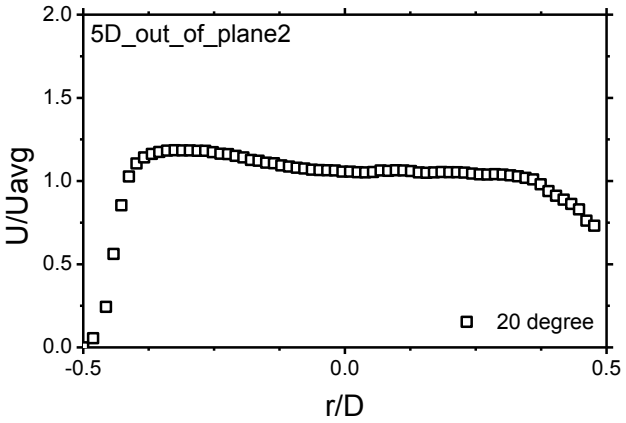

3) Velocity profile at 20 degree (5 D)

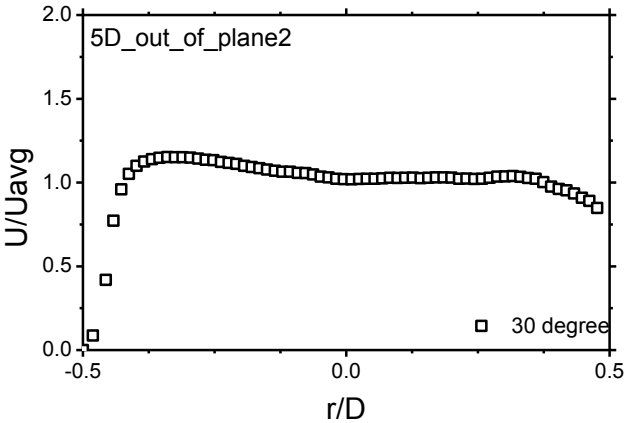

4) Velocity profile at 30 degree (5 D)

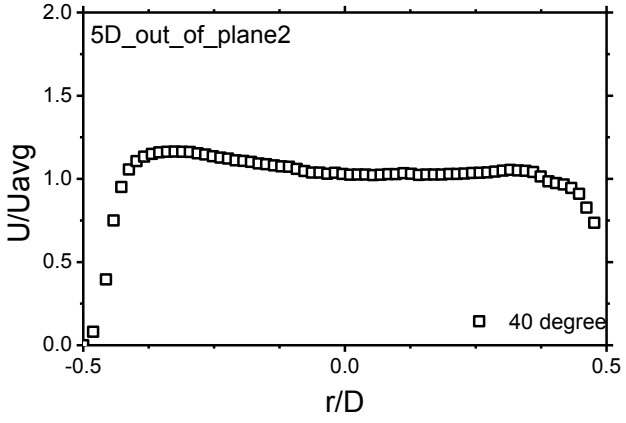

5) Velocity profile at 40 degree (5 D)

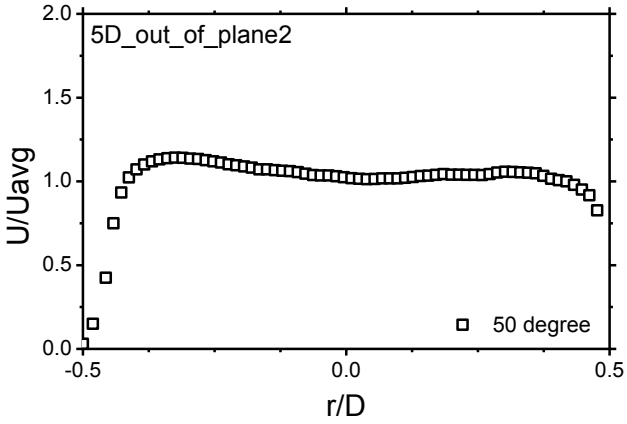

6) Velocity profile at 50 degree (5 D)

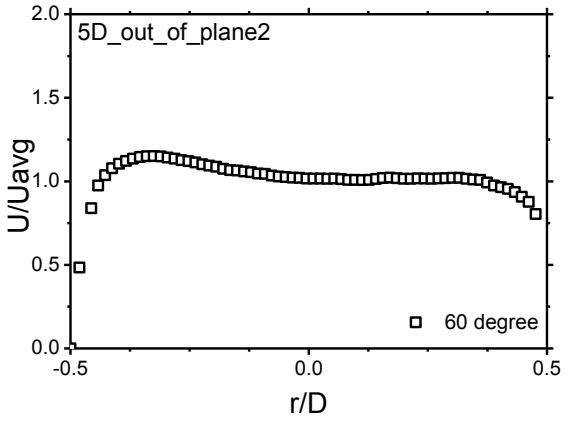

7) Velocity profile at 60 degree (5 D)

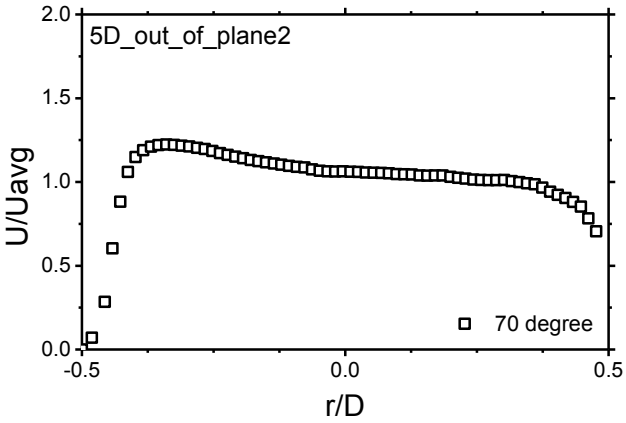

8) Velocity profile at 70 degree (5 D)

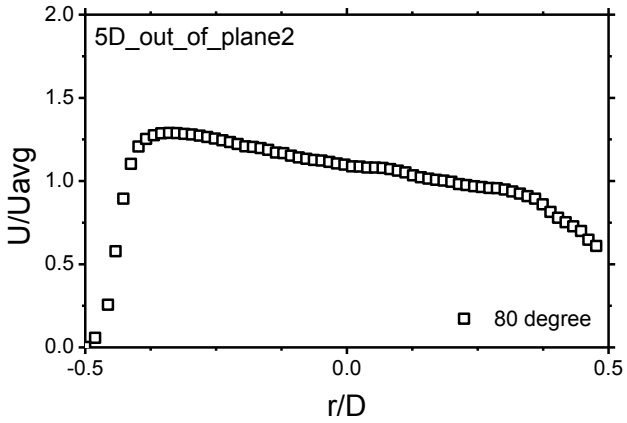

9) Velocity profile at 80 degree (5 D)

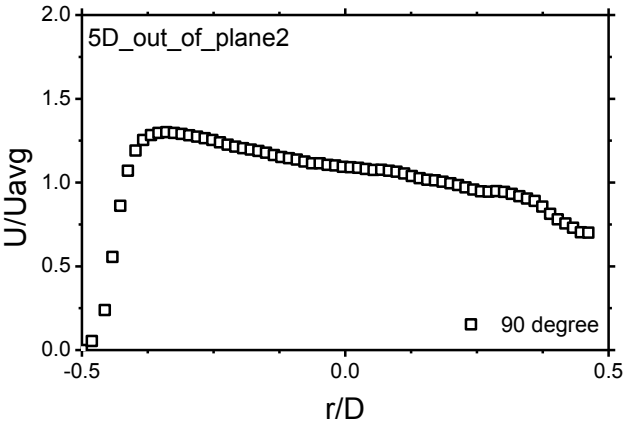

10) Velocity profile at 90 degree (5 D)

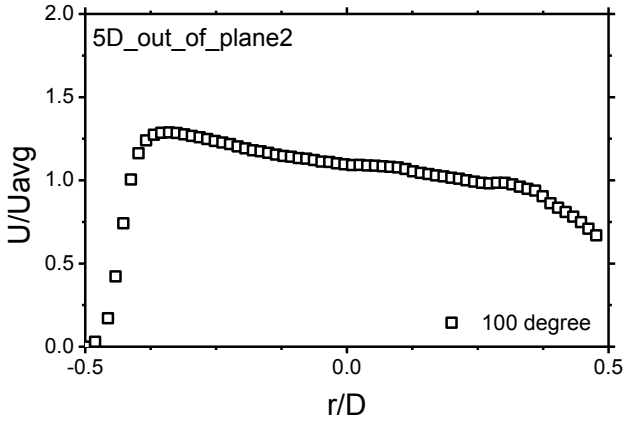

11) Velocity profile at 100 degree (5 D)

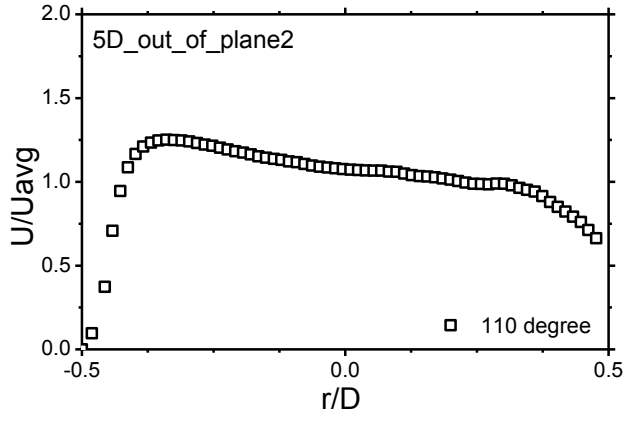

12) Velocity profile at 110 degree (5 D)

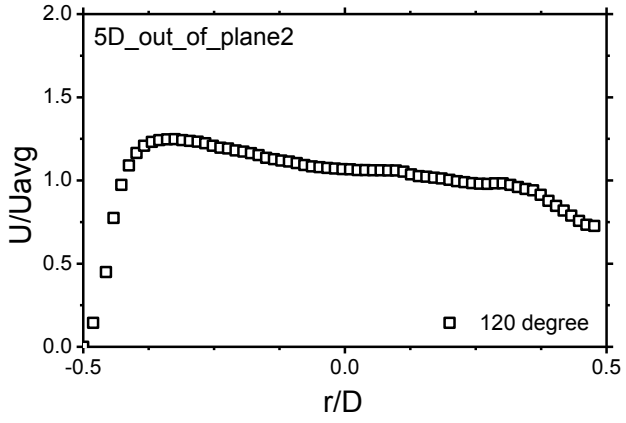

13) Velocity profile at 120 degree (5 D)

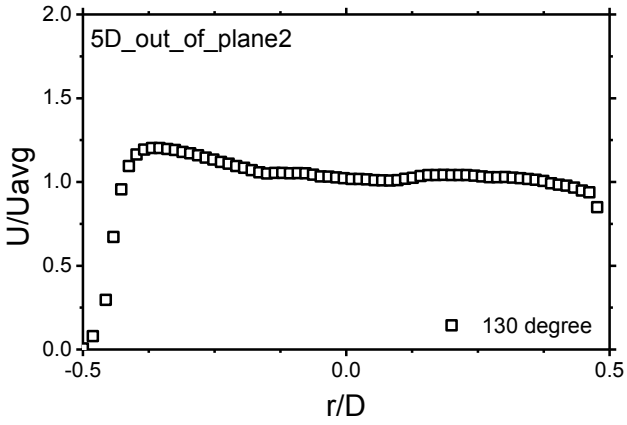

14) Velocity profile at 130 degree (5 D)

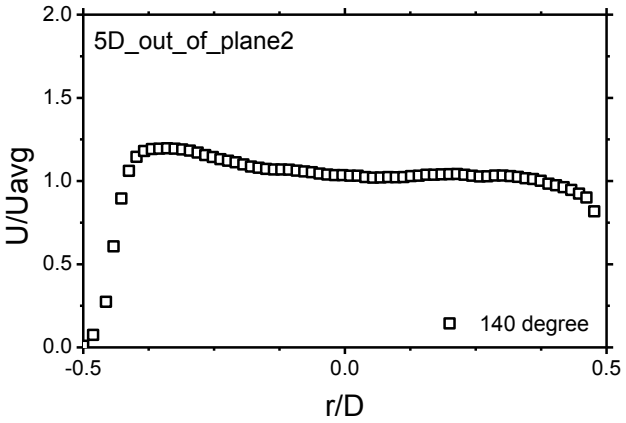

15) Velocity profile at 140 degree (5 D)

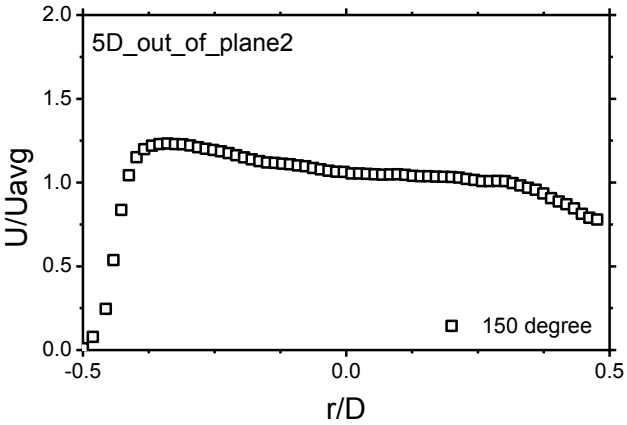

16) Velocity profile at 150 degree (5 D)

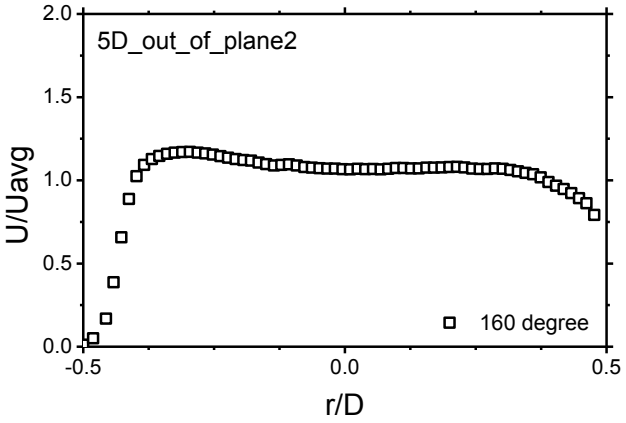

17) Velocity profile at 160 degree (5 D)

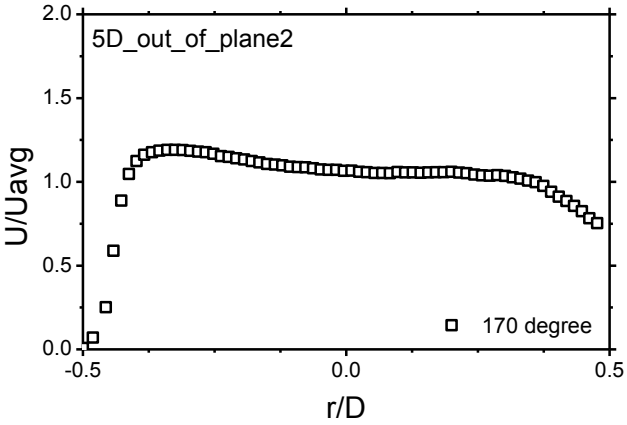

18) Velocity profile at 170 degree (5 D)

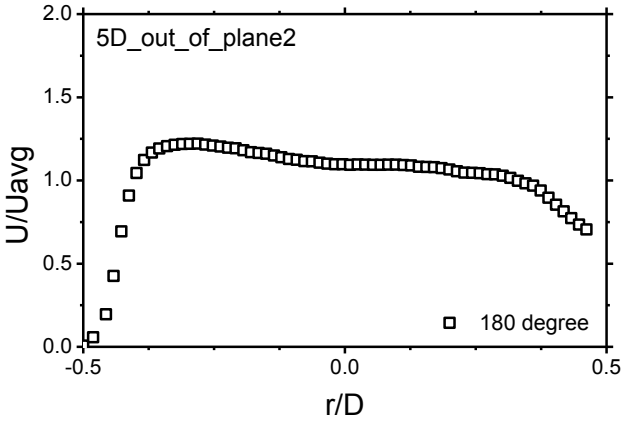

19) Velocity profile at 180 degree (5 D)

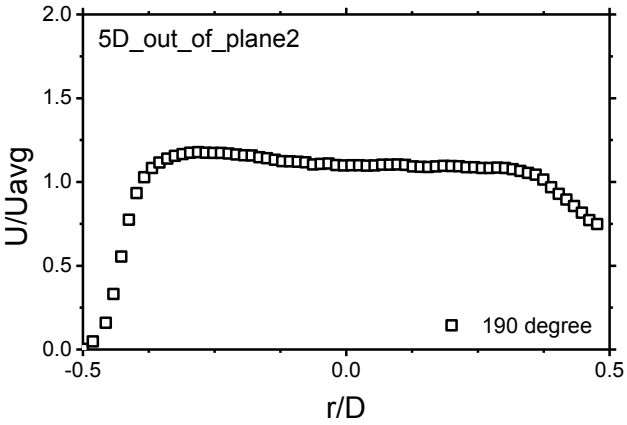

20) Velocity profile at 190 degree (5 D)

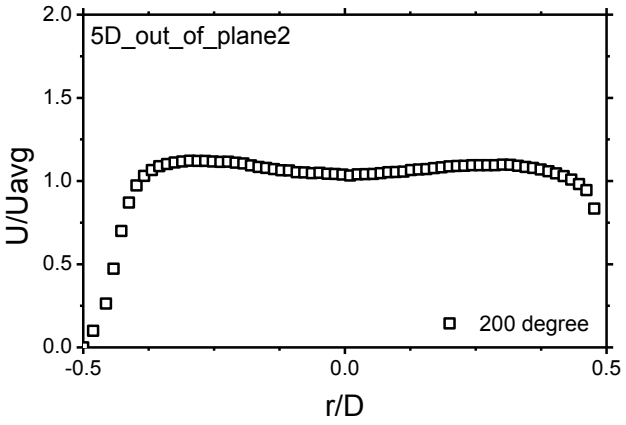

21) Velocity profile at 200 degree (5 D)

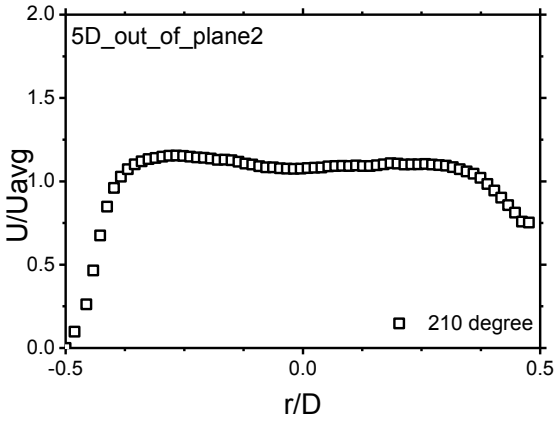

22) Velocity profile at 210 degree (5 D)

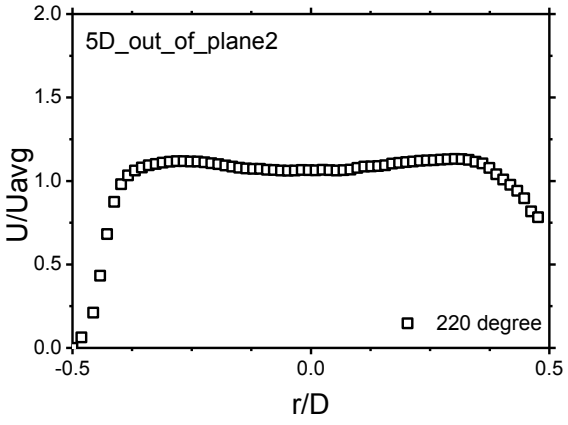

23) Velocity profile at 220 degree (5 D)

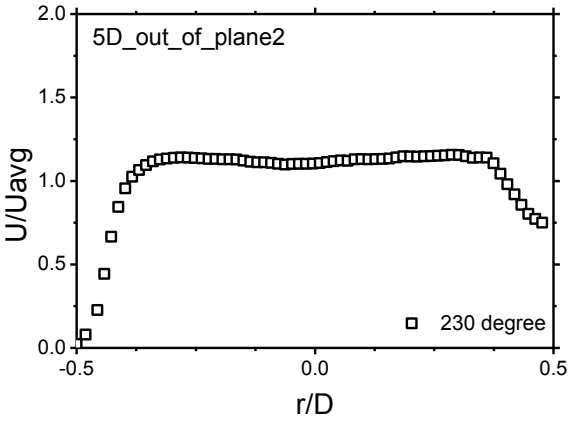

24) Velocity profile at 230 degree (5 D)

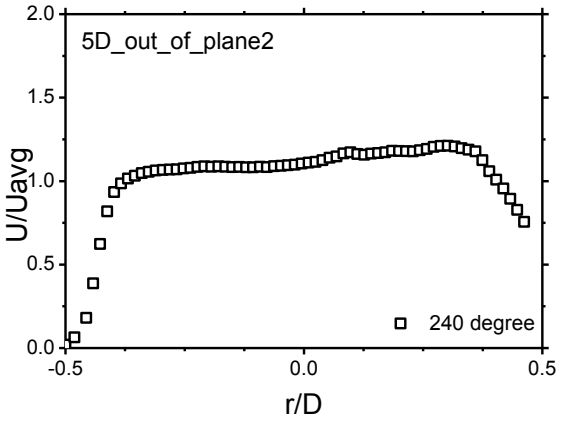

25) Velocity profile at 240 degree (5 D)

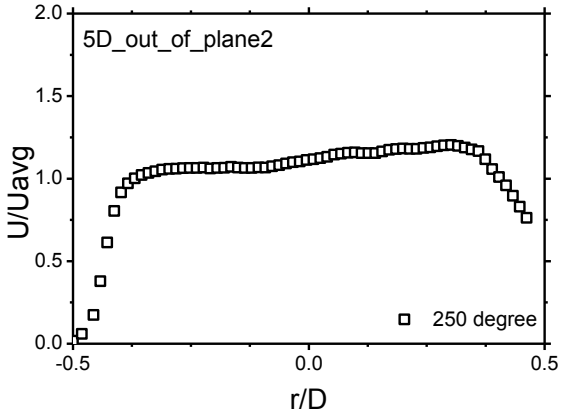

26) Velocity profile at 250 degree (5 D)

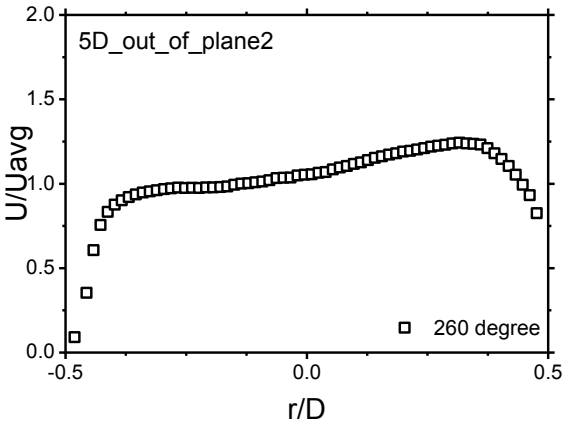

27) Velocity profile at 260 degree (5 D)

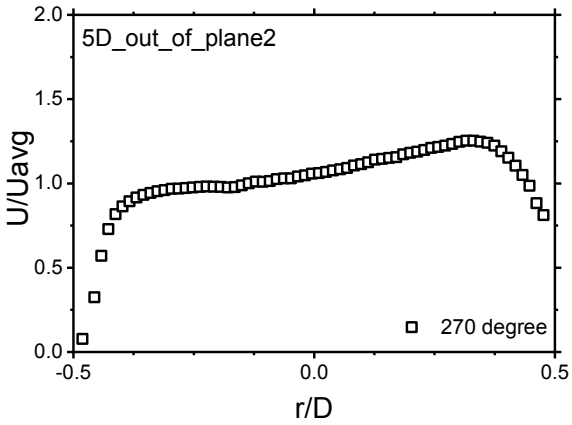

28) Velocity profile at 270 degree (5 D)

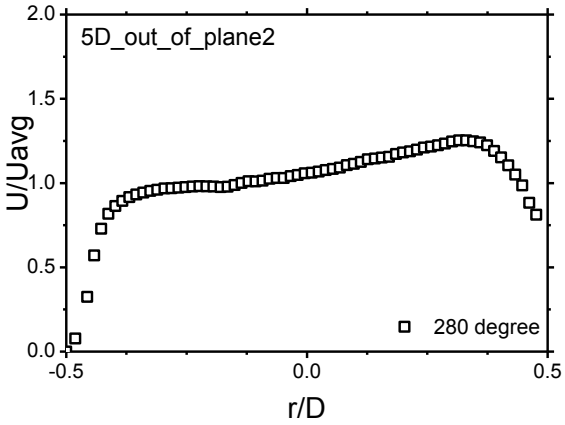

29) Velocity profile at 280 degree (5 D)

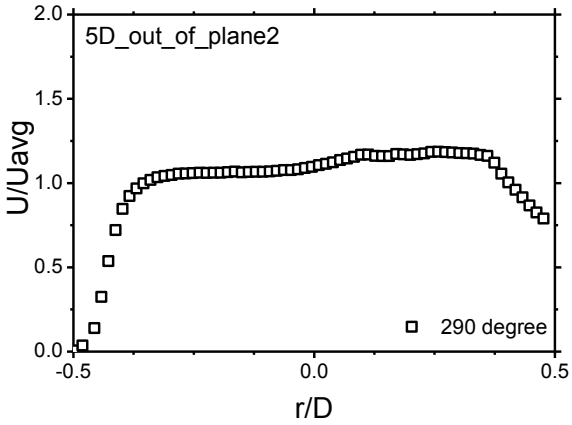

30) Velocity profile at 290 degree (5 D)

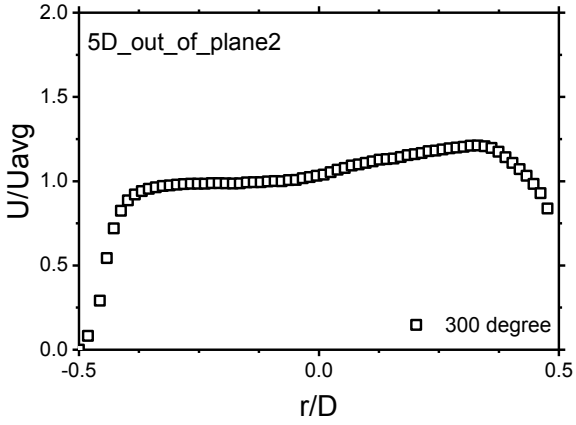

31) Velocity profile at 300 degree (5 D)

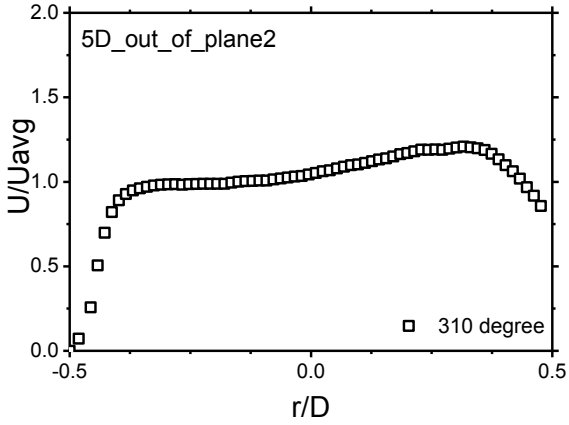

32) Velocity profile at 310 degree (5 D)

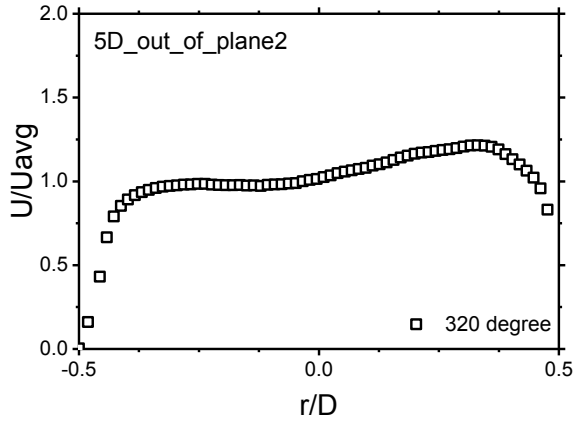

33) Velocity profile at 320 degree (5 D)

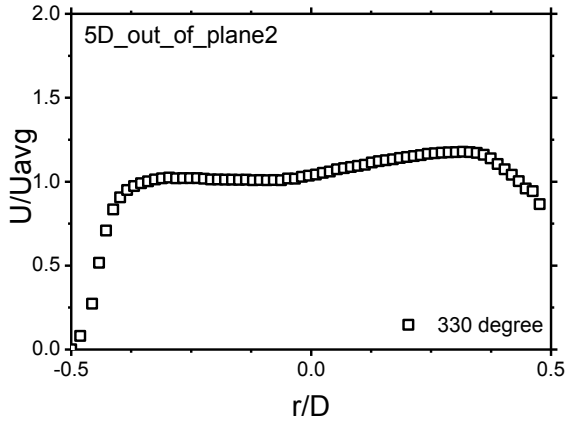

34) Velocity profile at 330 degree (5 D)

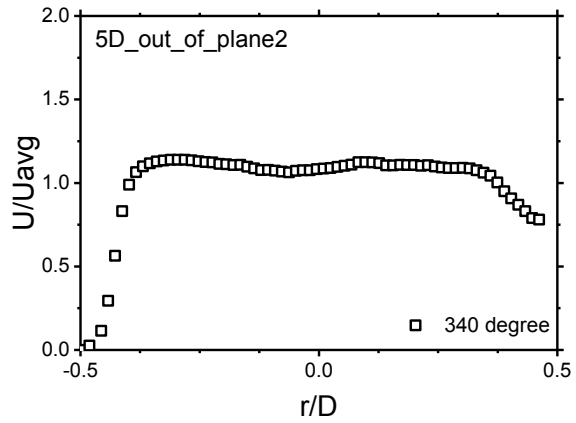

35) Velocity profile at 340 degree (5 D)

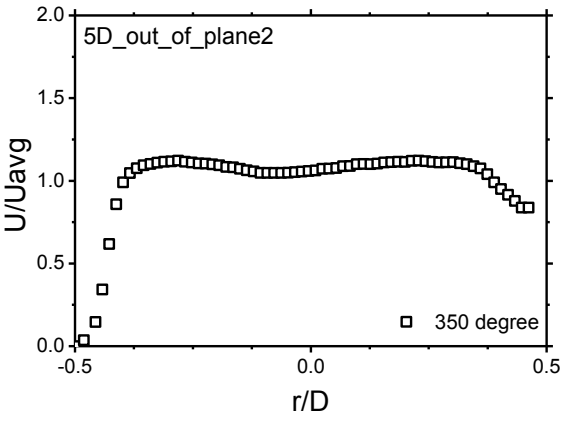

36) Velocity profile at 350 degree (5 D)

Fig. 6-27 Velocity profile at 5D of out of plane angle 16 degree double bent pipe.

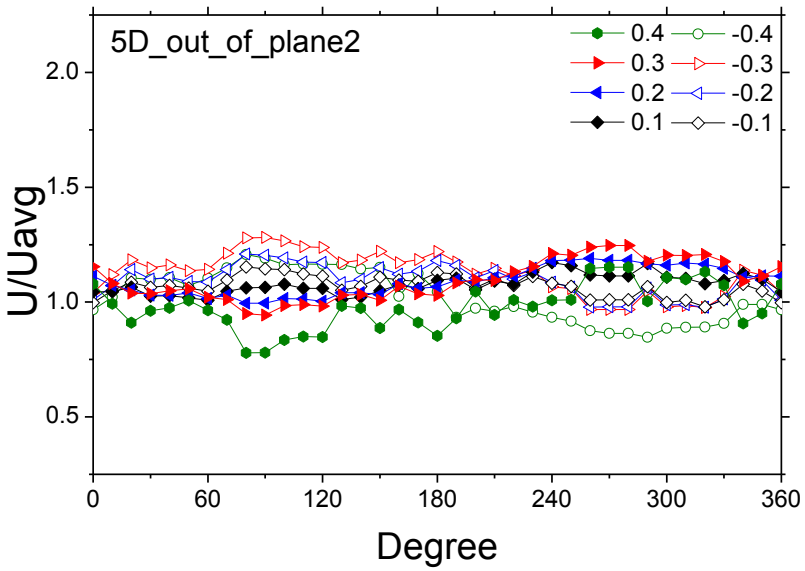

Fig. 6-28 Circumferential velocity profile at 5D of out of plane angle 16 degree double bent pipe.

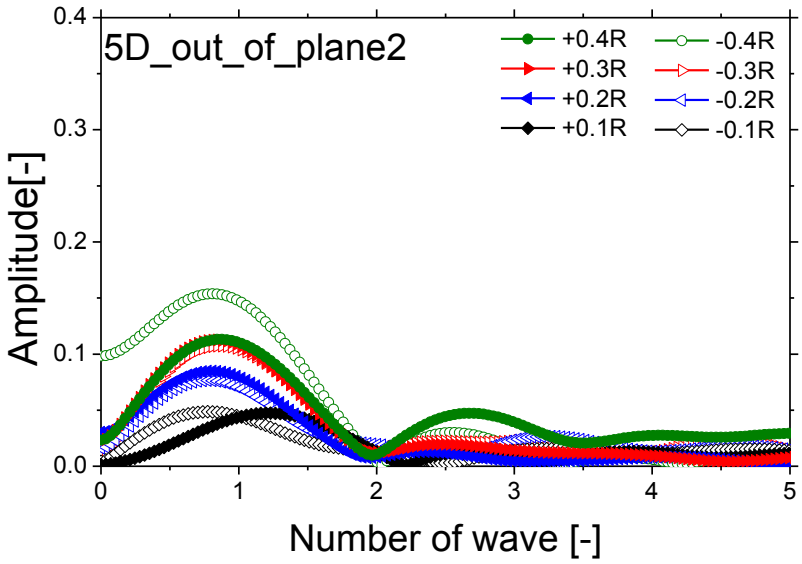

Fig. 6-29 FFT's results of Circumferential velocity profile at 5D of out of plane angle 16 degree double bent pipe.

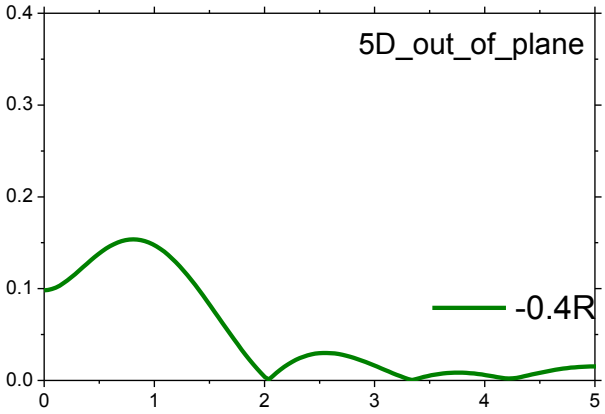

a) Number of waves from line -0.4 R (5 D)

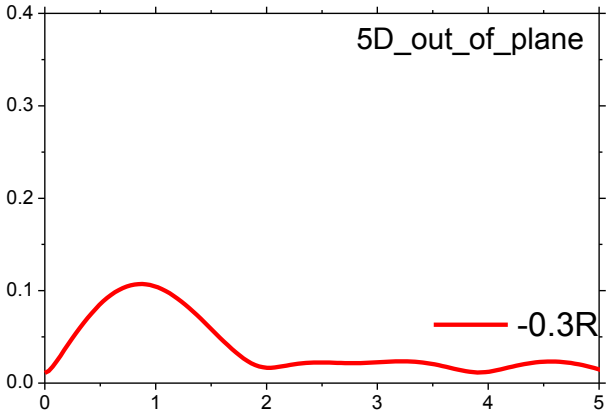

b) Number of waves from line -0.3 R (5 D)

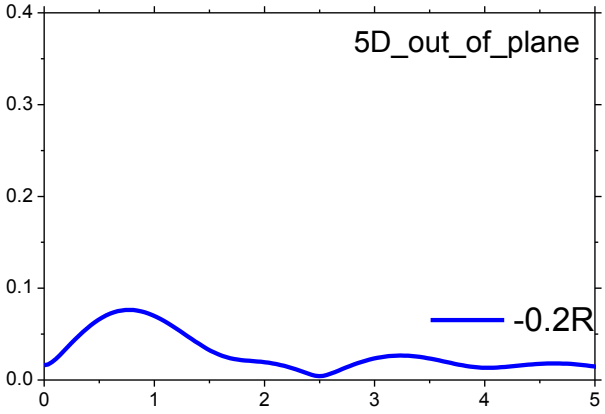

c) Number of waves from line -0.2 R (5 D)

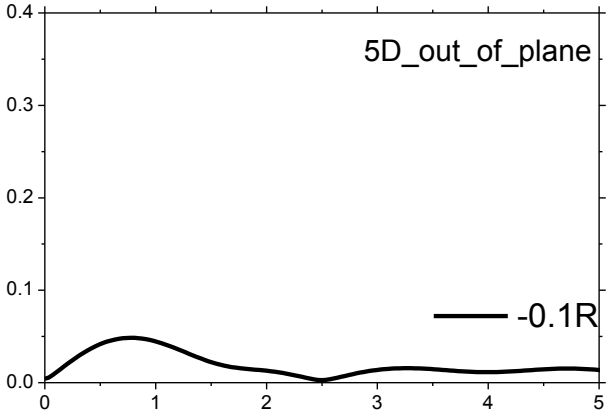

d) Number of waves from line -0.1 R (5 D)

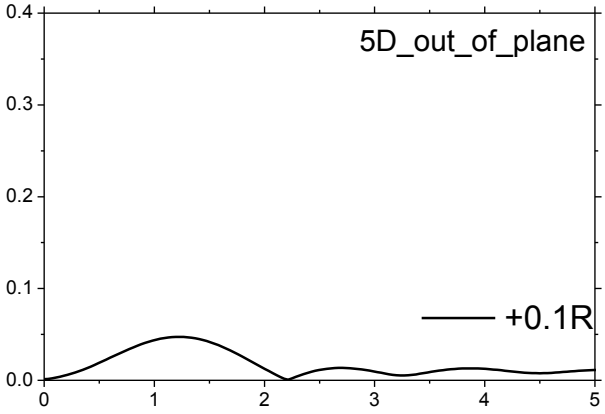

e) Number of waves from line +0.1 R (5 D)

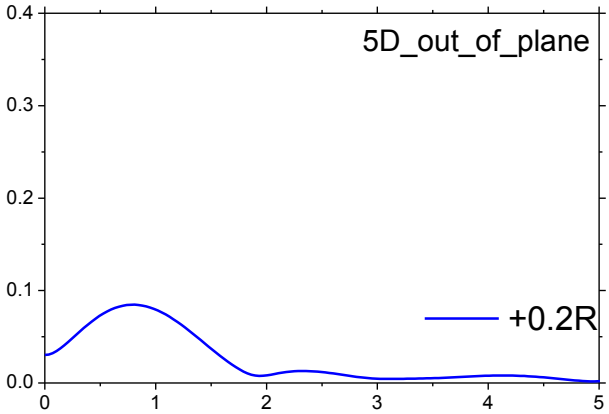

f) Number of waves from line +0.2 R (5 D)

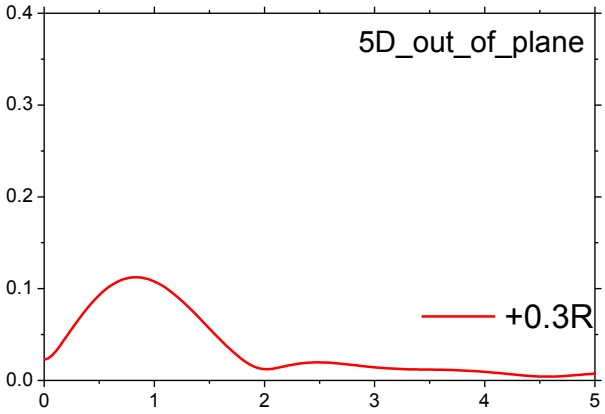

g) Number of waves from line +0.3 R (5 D)

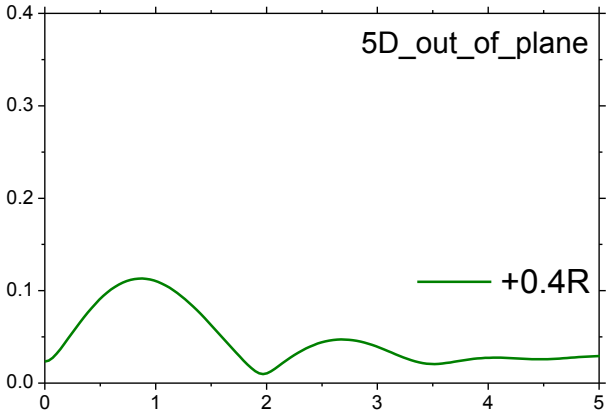

h) Number of waves from line +0.4 R (5 D)

Fig. 6-30 FFT's results of Circumferential velocity profile at 5D of out of plane angle 16 degree double bent pipe.

CHAPTER 7

CONCLUSIONS

This thesis presents a study on ultrasonic measurement technique for the complicated flow as downstream of the double bent pipe. The main purposes are development of ultrasonic velocity profile (UVP) method with multiple ultrasound transducers.

To achieve this, methodology is designed start from the fundamental of UVP. Firstly, the ultrasonic characteristics are investigated. Ultrasonic velocity profiles (UVP) utilize a pulse ultrasonic beam and the scattering of ultrasonic waves on tracer particles to obtain instantaneous velocity profiles.

Chapter 2 To design the conditions which appreciate for the experiment, we consider the incident angle and the accurate velocity profile from the effect of beam spread property. The results of sound transmission show the suitable setup angle which has a good transmission ratio at 30° with 0.7 % of error. However, the condition for the large pipe diameter the small angle is good for good transmission. When a sound wave is incident on an interface between two interfaces, part of it is reflected back into the original medium as the reflection wave. Its' amplitude will decrease when pass thought the interface of different medium. The amount of energy reflected back depends on impedance. When a sound wave is incident on an interface between two interfaces, part of it is reflected back into the original medium as the reflection wave. Its' amplitude will decrease when pass thought the interface of different medium. The amount of energy reflected back depends on impedance. For complicated flow which is the target of this study a small incident angle of 10° is applied for the experiments. The percentage of error at 10° is enough less as -0.97% and -1.2% for Reynolds number 40,000 and 60,000 respectively. In addition, a longer measurement line demands a longer maximum depth for UVP measurement, which decreases spatial and temporal resolution of UVP method. This is another reason of the application of the small incident angle 10°.

Chapter 3. Flowrate measurement on the double bent pipe. Flow rate in the transient conditions downstream of double 90º bent was measured to investigate the accuracy of the flow rate measurement using this multi-lines method. Many ultrasonic transducers can be used when more accurate flowrate is desired or the flow is asymmetric flow. Flowrate using multiple flow profiles can be calculated by using the interpolation of each velocity profile. When flowrate near the bent pipe is measured by UVP method, many measurement lines are necessary to make two- or three-dimensional velocity profile mapping due to its asymmetric flow.

Chapter 4. UVP measurement can obtain only velocity profiles in line. Usual Particle Image

Velocimetry (PIV) gives two-dimensional velocity mapping; however, PIV cannot obtain the flow distribution instantaneously. Hence, it is difficult to obtain fully three-dimensional velocity profile experimentally. To evaluate this limitation of experimental method, the numerical simulations using Computational Fluid Dynamics (CFD) were conducted. Numerical simulation calculation can give fully three-dimensional velocity profiles. In these days, computers are well developed, and numerical simulation becomes very popular and useful method to obtain velocity profiles because of its costs compare to the real experimental. Thus, simulation calculation was performed for the experimental condition, and the numerical result was compared with the experimental one as velocity profiles along the measuring lines. It can confirm both experimental and numerical results.

Chapter 5. Development of accurate flowrate measurement for a complicated flow is executed using UVP measurement. Double bent pipe system is used to realize the complicated flow. Experimental flowrate measurements on the system were executed for Re ~ 40,000. The velocity profiles were obtained at the distance 2 D, 3 D and 5 D from the bent where the flow is complicated due to existence of vortices. From experimental results using 1-3 transducers, flowrate for each distance is calculated using integration and interpolation. The accuracy of this method is evaluated by comparison with the flowrate value of electro-magnetic flowmeter installed in the experimental loop. It is concluded that accurate flowrate will be calculated in the condition of using three transducers and the distance is over 3 D within 4% error.

To confirm the optimization, the velocity profiles are also obtained changing the circumferential measuring angle by 10°. Velocity profiles on the measurement lines through the center of the pipe are transferred to velocity profiles along the circles which concentric center is as same as the pipe center. FFT analysis is performed to obtain largest number of wave for circumferential direction, and optimized number of transducer for each position is calculated from the FFT results. The result indicates more transducers are necessary for very accurate flowrate measurement. However, enough accurate measurement can be realized with less transducer.

Chapter 6. The estimation of measurement lines is important to measure accurate flowrate effectively as mention above. From this aspect, the number of velocity profiles was optimized experimentally to calculate the flowrate in former chapter. However, necessary number of sensors can be calculated analytically by regarding velocity profiles as a kind of wave. Sampling rate theorem for waves can indicate the necessary number of the sensors. In additions, the application of

this method can be applied in this chapter in case of circulation water loop system in nuclear power plant as the similar conditions for instance, the out-of-plane angle of the double bent pipe, the distance between first bent and second bent pipe, Reynolds number and so on. From the results of this method, this study can apply the estimating method for the number of measurement lines using UVP method.

The accuracy of flowrate measurements for the complicated flow downstream of the double bent pipe system had been applied to the conditions of the circulation water loop in Nuclear power plant. The experimental result from UVP measurement was used to the estimating the number of measurement lines in general piping system downstream of the bent pipe as a complicated flow with the effects of vortex and recirculation area close to the bent pipe not only in nuclear power plant.

ACKNOWLEDGEMENTS

I would like to express my utmost gratitude to many people who have been helping my study and encouraging me in many occasions. The all my study and this dissertation could not have been completed without the great helps from the following persons:

I would like to express my deepest gratitude and appreciate to **Miss Areerak Rueanngoen,** nuclear scientist of the Office of Atom for Peace, Thailand**, Prof. Nares Chankow,** the faculty of nuclear engineering, Chulalongkorn University, Thailand and **Prof. Takatoshi Takemoto** of Tokyo Institute of Technology, who gave me the important opportunity to study in Tokyo Institute of Technology.

I would like to express my deepest gratitude and appreciate to me who is my advisor: **Prof. Hiroshige Kikura** who has a very helpful training not only the study but also the attitude of researcher. The technical is not enough to be a good researcher. It should be started with the idea and question of ourselves and try to find out the correct answer (s) and finally improve and develop it by ourselves. He have never give up to try and teach the student, even though it's difficult to change someone. I cannot say anything that is completely word of my thought about his kindness for me. Without his educate and training, I would not be succeeded.

I also would like to express my appreciation to **Prof. Masaki Saito, Prof. Minoru Takahashi, Prof. Yasuyoshi Kato and Prof. Hiroshi Akatsuka.** They are examining committee of this doctoral dissertation. They have given me valuable advices and critical review to this thesis.

Dr. Nobuyoshi Tsuzuki, researcher in Kikura Laboratory. He has given me grateful suggestion in solving many difficult technical problems not only about the simulations but also he give me many solutions of the experiment problems. I have a good knowledge about writing journal paper from his recommendation and his training. He teach me how to write the journal paper with the attitude of the scientific paper. I would like to acknowledge **Dr. Sanehiro Wada** and **Dr. Kenichi Tezuka** who suggest me and give me about the information of the operation conditions of nuclear power plant and the discussion about the research objective and finally how to develop ultrasonic velocity profile method applied the real nuclear power plant.

I would like to express my gratitude to all students in Kikura Laboratory. **Nguyen Tat Thang** taught me the first step of research about UVP method and how to live in Japan. Maasaki Tachi taught me how to live in Japan and Japanese style. **Mr.Ihara Tomonori** taught and advise me about how to analyze the experiment data. **Mr.Tsukada Keisuke** and **Mr.Fukumoto Takuya** helped during my experiments of UVP. **Mr.Duong Thang Tung and Mr. Ari Hamdani** improved my English skill in speaking and listening. In addition, I would like to express Thai student for the discussion of study and gave the knowledge about signal processing technique such as **Mr.Natee Thongoun**, **Mr.Pracha Khamphakdi.**

MARCH, 2014

Weerachon TREENUSON

LIST OF PUBLICATIONS

I. JOURNALS

1. W. Treenuson, N. Tsuzuki, H. Kikura, M. Aritomi, S., Wada and K. Tezuka, Accurate Flowrate Measurement on the Double Bent Pipe using Ultrasonic Velocity Profile Method, the Japanese Society for Experimental Mechanics, Vol. 13, No.2, (2013), pp. 200-211,
2. W. Treenuson, N. Tsuzuki, H. Kikura and S. Wada, Out of plane effect of double bent pipe on ultrasonic flow metering, The Ultrasonic Technology, (2014-1) 投稿済.

II. INTERNATIONAL CONFERENCES (WITH REVIEW)

1. W. Treenuson, N. Tsuzuki, H. Kikura, M., Aritomi, S. Wada and K. Tezuka, Development of flow rate measurement in the bent pipe using ultrasonic velocity profile method, "The 9th International Topical Meeting on Nuclear Thermal Hydraulic, Operation and Safety (NUTHOS-9)", 9-13, September, Kouhsiung, Taiwan(2012), Paper No. N9P0293, pp.1-15.
2. W. Treenuson, N. Tsuzuki, H. Kikura, M. Aritomi, S. Wada and K. Tezuka, Development of flow rate measurement at bent pipe using comparison between ultrasonic velocity profile (UVP) method and computational fluid dynamics (CFD), The 3rd International Forum on Heat Transfer (IFHT2012), 12-15, November, Nagasaki, Japan(2012), Paper No.82, pp.1-6

II. INTERNATIONAL CONFERENCE (WITHOUT REVIEW)

1. W. Treenuson, N. Tsuzuki, H. Kikura, M. Aritomi, S. Wada and K. Tezuka, Out of plane effect of double bent pipe on ultrasonic flow metering, The International Conference on Experimental Mechanics 2013 (ICEM 2013) and the 12th Asian Conference on Experimental Mechanics (ACEM12), 25-27, November, Bangkok, Thailand (2013), Paper No. EFO-124, pp.1-12.

III. JAPANESE CONFERENCES

1. W. Treenuson, N. Tsuzuki, H. Kikura, M. Aritomi, S. Wada and K. Tezuka, Development of flow rate measurement in the bent pipe using ultrasonic velocity profile method, The 17th National Symposium on Power and Energy Symposium (SPES 2012), 21-22, June, Fukuoka, Japan(2012), pp.291-294.

2. W. Treenuson, N. Tsuzuki, H. Kikura, M. Aritomi, S. Wada and K. Tezuka, Verification of Flow Rate Measurement at Bent Pipe Comparing between Experiment and Numerical Calculation, The 31st annual Meeting of Japanese Society for Multiphase Flow (JSMF) Symposium on Multiphase Flow, 9-11, August, Kashiwa Campus (Kashiwanoha, Kashiwa)(2012), pp.76-77.
3. W. Treenuson, N. Tsuzuki, H. Kikura, M. Aritomi, S. Wada and K. Tezuka, High accurate flow measurement at the bent pipe by using ultrasonic velocity profile method, The 11th Young Research debate presentation, Kanto Branch of the Atomic Energy Society of Japan, 14, November, Tokyo, Japan (2012), S3-9, p.9.
4. W. Treenuson, N. Tsuzuki, H. Kikura, M. Aritomi, S. Wada and K. Tezuka, Estimation of the optimal number of ultrasound transducers for accurate flowrate downstream of inclination bent pipe, Conference for younger researcher Joint session between INES-4 & AESJ, 11, November, Tokyo, Japan(2013), A-18.

VI. RELATED JOURNALS

1. S. Wada, K. Tezuka, W. Treenuson, N. Tsuzuki, and H. Kikura, Study on the optimal number of transducers or pipe flow rate measurement downstream of a single elbow using the ultrasonic velocity profile Method, Sci. Technol. Nucl. Install, (2012), ID 464113, pp.1-12.
2. S. Wada, K. Tezuka, W. Treenuson, N. Tsuzuki and H. Kikura, Estimating the number of transducers for flow rate measurement using the UVP method downstream of double elbows, Flow measurement and Instrumentation, 32 (2013), pp.51-62.